NHC-stabilized Rh Nanoparticles as eficient catalysts for the hydrogenation of aromàtics and selective H/D exchange in P-based ligands

Francisco Martinez Espinar

Francisco Martinez Espinar

NHC-stabilized Rh Nanoparticles as efficient catalysts for the hydrogenation of aromatics and selective H/D exchange in P-based ligands

DOCTORAL THESIS

Supervised by

Dr. Cyril Godard, Dr. Sergio Castillón and

Dr. Bruno Chaudret

Departament de Química Física i Inorgànica

UNIVERSITAT ROVIRA i VIRGILI

Tarragona, 2017

UNIVERSITAT ROVIRA i VIRGILI

Departament de Química Física i Inorgànica
Campus Sescelades
C/Marcel·lí Domingo s/n, 43007, Tarragona
Tel. 977559575; Fax. 977559563

Els sota signants Cyril Godard, Professor agregat interí del Departament de Química Física i Inorgànica de la Universitat Rovira i Virgili, Sergio Castillón Miranda, catedràtic d'universitat del Departament de Química Analítica i Química Orgànica de la mateixa universitat i Bruno Chaudret, director d'investigació del CNRS.

FEM CONSTAR que aquest treball, titulat "*NHC-stabilized Rh Nanoparticles as efficient catalysts for the hydrogenation of aromatics and selective H/D exchange in P-based ligands*", que presenta Francisco Martinez Espinar per a l'obtenció del títol de Doctor, ha estat realitzat sota la nostra direcció al Departament de Química Física i Inorgànica d'aquesta universitat, i que compleix els requeriments per poder optar a la Menció Europea.

Tarragona, 18 de Maig de 2017

Dr. Cyril Godard Dr. Sergio Castillón Dr. Bruno Chaudret

El present treball ha estat desenvolupat amb una beca Martí Franquès finançada per la Universitat Rovira i Virgili (2013PMF-PIPF-90). El treball descrit en aquesta tesi ha estat finançat pels següents projectes:

CTQ2013-43438-R
CTQ2016-75016-R
NANOSONWINGS 246763

Agraïments

Arribem sens dubte a la part més difícil de la tesis. Dur a terme aquesta tesis ha estat per mi una etapa molt important que m'ha permès aprendre i adquirir diverses competències útils per la meva formació. Aquesta etapa també m'ha permès conèixer gran nombre de persones amb les que he conviscut i de les que he après també moltes coses i m'emporto grans records. És per això que m'agradaria dedicar unes línies i agrair a tots aquells que han estat al meu costat durant la realització d'aquesta tesis. Intentaré ser breu.

En primer lloc m'agradaria agrair als meus directors de tesis Prof. Cyril Godard i al Prof. Sergio Castillón per donar-me l'oportunitat de poder realitzar el treball de doctorat. Gracias Cyril por guiar y dirigir mi proyecto. Gracias por tus consejos, ideas, en ocasiones paciencia y por transmitirme tu pasión por la química. Es de agradecer el poder trabajar con alguien que siempre tendrá un momento para ayudar a resolver una duda o dar su punto de vista sobre un problema surgido en el laboratorio. Gracias Sergio por tus consejos, por dar siempre tu opinión y por aportar tus conocimientos con el fin de buscar solución a algunos de los problemas con los que nos hemos ido encontrando a lo largo de estos años. Gracias Carmen Claver por hacer posible que pudiera realizar la tesis en el grupo, siempre dando tu opinión cuando ha sido necesario y por mostrarnos tu entusiasmo por la química del que todos hemos aprendido mucho. Siempre recordaré las excursiones por Benasque. Thanks Bruno for giving me the opportunity to stay in Toulouse and to work in your lab. It has been an opportunity for me to visit such a nice city. Thanks for your knowledge in the world of NPs. I learnt so much during these years.

Finalment, gràcies a la resta dels grups d'investigació del departament. Gràcies a Aurora Ruiz i Anna Masdeu pels vostres consells i comentaris a les reunions de grup, gràcies Oscar Pàmies, Montserrat Diéguez i Elena Fernández per la vostra simpatia i per compartir algun que altre reactiu químic quan ha sigut necessari. Y finalmente gracias Pascal Blondeau por tener siempre un hueco para el análisis de mis muestras.

En aquesta tesis també han tingut un paper molt important els tècnics. Del Servei de Recursos Científics: gràcies Ramon, Francesc, Rita, Mercè, Mariana i Lukas pel vostre interès en el bon ús de les tècniques necessàries per l'estudi de caracterització presentat en aquesta tesis. També agrair als tècnics del departament: gràcies Raquel per la teva feina, sent tant eficient i estant sempre disposada a ajudar en tot el que ha calgut i per la teva paciència amb els problemes de la caixa seca. Gràcies Josep per la teva cordialitat i ajudar-nos sempre a l'enviament i rebuda de paquets i en la comanda de solvents. Agrair als tècnics de Toulouse el treball realitzat per la caracterització de les NPs. Thanks Pier-Francesco Fazzini and Pierre Lecante for the HRTEM and WAXS analysis; and Yannick Coppel and Christian Bijani for the NMR experiments. Finally, thanks Elisabeth Lance for helping me with contract and bank account issues when I arrived to Toulouse for the first time.

Dedicar també unes línies als companys de laboratori o gent amb la que he anat coincidint per la universitat durant tots aquests anys. Als companys de cristal·lografia i computacional: Josu, Marc Medina, Irina, Nicole, Agustí i Laura. Gràcies per les estones passades a l'office, esmorzant/berenant, prenent un cafè o simplement xerrant

pels passadissos. Agraeixo tots aquests moments de desconnexió, sense els que el dia a dia a la universitat no hagués sigut el mateix. Són molts els records que m'emporto, amb alguns ja des de la carrera. Espero que seguim coincidint fora de la universitat.

A tots els del Departament de Química Orgànica: Macarena, Jordi, Irene, Adrià Cardona, Collado, Margarita, Míriam, Joan Guasch, Sebas, Isma, Adrià Moreno i Emma per estar sempre disposats a deixar-nos algun que altre reactiu o material de laboratori quan l'hem necessitat. Amb alguns de vosaltres hem compartit grans moments de festa, congressos i discussions de química. Per tot això gràcies.

Gracias a Juan Miguel y Israel por acogerme en el laboratorio del LPCNO durante mi estancia en Toulouse. Gracias a ambos por vuestros consejos, ayuda en la preparación de las muestras y darme la opción de utilizar el equipamiento necesario para la correcta manipulación de mis muestras.

Gràcies a tots els companys del grup del CTQC amb els que tot i ser a l'altra banda del carrer hem compartit molts moments i molta química i sempre han estat disposats a donar-me un cop de mà. A Bianca y Mónica por vuestros consejos y por dejarme poner reacciones en vuestra vitrina cuando fue necesario. A la Dolores i la Míriam per les vostres preguntes i idees a les reunions de grup. Al Stefano, l'italià amb el millor català que he conegut. A Jorge y Olivia por vuestra experiencia con las NPs y por ayudarme con el GC cuando ha habido problemas o ha sido necesario. Al Jordi per les teves visites al nostre laboratori, sempre disposat a fer una mica de broma i entretenir-nos amb les teves llistes de reproducció. A Itziar por tu simpatía, tu experiencia y por traernos aquí a Tarragona algo

de temperamento vasco. A Sara por tu cordialidad y ayuda cuando ha sido necesario. Són molts els moments que hem passat plegats al laboratori, reunions de grup, congressos, sopars d'estiu/nadal i viatges a Benasque. M'emporto molts bons records de tots vosaltres.

A tots els que heu passat pel lab 218: Laia, Xavi Castilla, Rui i Claudia. Agrair-vos les vostres participacions en les reunions de grup, aportant sempre idees noves en relació al món de les NPs. Gràcies Laia per la teva simpatia i cordialitat, ha estat un plaer haver compartit seminari i dinars a l'office plegats. Espero que tot et vagi molt bé.

Agrair també a tots els companys del laboratori veí, el 217 i també als que tot i haver passat poc temps entre nosaltres hem anat coincidint pels rotavapors: Albert Cabré i Lutz. A la Mercè, la veterana del grup i amant dels animals amb la que ja vam coincidir al laboratori de pràctiques. A la Carlota, la reusenca per excel·lència amb la que he sigut company de taula quasi fins a l'últim moment. Gràcies per totes les estones viscudes, viatges a Sapeira inclosos, i molta sort amb el que et queda de doctorat. Al Marc Magre, l'únic noi del laboratori que ha entès la importància d'Instagram a les nostres vides. Molta sort en aquesta nova etapa per Alemanya que fa poc has començat. A la Jèssica, la tarragonina vinguda des del Perelló. Et desitjo molta sort per Suècia. A la Maria, la noia amb més art del laboratori i també la més tranquil·la i callada. Gràcies per convidar-nos a l'Ametlla per temporada de calçots. To Zahra for your support in terms related to the thesis. You have almost finished. I wish you the best of luck for your future. I als nouvinguts Efrem i Joan, molta

sort amb el doctorat, espero que us porti pocs problemes i moltes alegries.

També volia agrair als companys de laboratori, que no per treballar en metal-free conditions són menys importants: Cristina Pubill, Cristy, Jèssica Cid, Xavi, Gerard, Henrik, Ana, Enrico, Thierry, Marc Garcia, Núria, Jordi Royes i Albert; i als que han format part del grup durant les seves estades: Maikel and Christy i Erik. A la Cristy, la nostre iron girl personal. Gràcies per la teva energia al laboratori i pels bons moments de voleibol a la platja llarga. Al Gerard, el poliglota del laboratori amant dels astres. Al Xavi pels moments que hem passat plegats ja fins i tot abans de coincidir al laboratori. Espero que ens veiem aviat per Reus. A Ana por tu sabiduria y por ayudarnos en ésto de la química siempre que hemos tenido alguna duda. Las excedrinas se agradecen. Al Thierry pel teu tardà sentit de l'humor. Tu ara imaginat que has de fer un agraïment...peeeerooo.....que faries? Queda pendent un karting.
A Enrico por tu sentido del humor italiano y tus lecciones de salsa cerca de los rotavapores. Te deseo mucha suerte por Inglaterra. Al Marc García, el monitor de caus, esplais, voluntari, etc. Sort amb la recta final de la tesis. A la Núria, la targarina del laboratori. Gràcies per la teva simpatia i rialles dins i fora del laboratori. Arribarem molt lluny amb això del pàdel! Al Jordi, per animar l'esperit del laboratori sempre que ha estat necesari amb els seus "ieppaaaa!" S'ha de dir que per ser de Fraga no colpeges gens malament de revés. A l'Albert amb qui tot i haver conviscut relativament poc temps al laboratori hem passat molt bons moments. Et desitjo molta sort per Suïssa i si mai baixes per aquí a fer una visita no dubtis en avisar-me, que he de passar per Bacelona a fer unes coses...

Arriba el moment d'agrair als companys del grup. A l'Eli per estar-me sempre al darrere quan vaig arribar al grup i per ensenyar-me a treballar com cal en un laboratori. Se't troba a faltar pel seminari. A la Jessi per mostrar-me tot el que sabia en relació al món de les NPs. Gràcies per la teva ajuda, sense tu l'arribada al nanomón no hagués sigut el mateix. A Jamin por tu experiencia y por echarme una mano con los carbenos cuando fue necesario. A l'Alberto, veí de vitrina durant molts anys. Les hores al laboratori no haguessin sigut el mateix sense un company tan divertit. Me quedo con tu frase: "La vida es larga, y la tesis más". Al Toni, omnipresent a la vitrina del darrere, el noi de les columnes, el dels memes d'en Caaaarrrrlll. Et passo el relleu del grup, espero que hi posis ordre. Et desitjo molta sort per Dinamarca. To Nanette for all the moments we spent together. You are also almost finishing the thesis, so I hope it will go well. If someday I visit Denmark I will let you know. Al Jordi, per la teva cordialitat i per haver-me acollit a casa teva durant la meva estància a Toulouse. T'estaré sempre agraït. To Myriam, I wish you all the best in the thesis. If you keep working this hard you won't have any problem. I finalment també agrair a Aaron, Fàtima, Laura, Luís i Hector, gent que tot i haver realitzat estades curtes al nostre grup m'emporto molt bons records. A l'Aaron, el metalero del laboratori. Com oblidar 'la lechuga está pocha'? A la Fàtima, l'apassionada del sushi. Gràcies pels moments de companyía i les xerrades al laboratori. Espero que tot vagi molt bé per Holanda/Alemanya. A la Laura i el Lluís, els germans Montiel, amb els que vam compartir vitrina i passadís. I finalment a l'Héctor, l'última incorporació del nostre laboratori. Molta sort amb el treball de màster, saps que si treballes de valent ho aconseguiràs. Ens veiem

a l'Ogura. En definitiva, ha sigut un plaer conviure al laboratori amb tots vosaltres.

No querría acabar sin agradecer a mi gran familia el soporte recibido durante todos estos años. Todos ellos han sido una parte fundamental durante toda mi vida. A mis padres por educarme y enseñarme todo lo que he aprendido durante todos estos años. Por darme la oportunidad de realizar mis estudios. Por mimarme siempre y desear siempre lo mejor para mí, por aguantarme día tras día y por ayudarme siempre en todo lo que he necesitado. Sin vosotros no podría haber llegado hasta aquí. Y a mi hermana por apoyarme también en los buenos y malos momentos. Sé que siempre podré contar contigo. Sin olvidar a mi gato Tesla, quien me ha hecho mucha compañía durante la escritura de esta tesis.

I finalment a la Marta, gràcies per creuar-te en el meu camí i entrar a la meva vida. Per tots els moments que hem viscut junts i per recolzar-me en aquests darrers anys. La vida és molt més maca si tens algú amb qui compartir-la.

En definitiva, gràcies a tots, ha estat un plaer haver-vos tingut al meu costat durant el transcurs d'aquest treball.

"Remember to look up at the stars and not down at your feet. Try to make sense of what you see and wonder about what makes the universe exist. Be curious."

-Stephen Hawking

Table of contents

Abbreviations and acronyms

A	
Ac	acetyl
acac	acetylacetonate
atm	atmosphere
B	
bp	boiling point
bs	broad signal
C	
ca	approximately
CD	cyclodextrin
CNT	carbon nanotube
conv.	conversion
CP-MAS	Cross Polarization Magic Angle Spinning
D	
d	doublet
dba	dibenzylideneacetone
DHQ	decahydroquinoline
DMAP	dimethylaminopyridine
dppb	1,2-bis(diphenylphosphino)butane
dppe	1,2-bis(diphenylphosphino)ethane
dppm	1,2-bis(diphenylphosphino)methane
E	
EA	elemental analysis
ee	enantiomeric excess
equiv.	equivalent(s)
F	
FTS	Fischer-Tropsch Synthesis
FT	Fourier transform
G	
g	gram
GC-MS	Gas Chromatography-Mass Spectrometry
H	
h	hour(s)

HAP	hydroxyapatite
hcp	hexagonal close packing
HDA	1,6-hexanediamine
HPNMR	High Pressure Nuclear Magnetic Resonance
HPS	Hypercrosslinked polystyrene
HRTEM	High Resolution Transmission Electron Microscopy
Hz	Hertz(s)

I

IL*s*	ionic liquids
IPr	1,3-Bis(2,6-diisopropylphenyl)-1,3-dihydro-2*H*-imidazol-2-ylidene
*i*Pr	isopropyl
IR	Infra-red
I*t*Bu	*N,N*-di(*tert*-butyl)imidazol-2-ylidene

J

J	coupling constant

L

L	ligand

M

m (in NMR)	multiplet
M	metal
ml	millilitres
MOF	metal organic framework
MS	Mass Spectrometry
MWCNT	multi-walled carbon nanotubes
m/z	mass over charge

N

NHC	N-Heterocyclic Carbene
NMR	Nuclear Magnetic Resonance
nm	nanometer(s)
NPs	nanoparticles
NP	nanoparticle
Ns	total umber of atoms on the surface
Nt	total number of atoms

P	
PAA	polyacrylic acid
PEG	polyethylene glycol
PFIL	phosphorus-functionalised ionic liquids
ppm	parts per million
PVP	poly(N-vinyl-2-pyrrolidone)
PVPy	poly(4-vinylpyridine)
Q	
Q	quinoline
R	
r.t	room temperature
RDF	Radial Distribution Function
S	
SB3-12	*n*-dodecyl-*N,N*-dimethyl-3-ammonio-1-propanesulfonate
SEM	Scanning Electron Microscopy
T	
T	temperature
t	triplet
t-BHP	*tert*-butylhydroperoxide
td	triplet of doublet
TEM	Transmission Electron Microscopy
TGA	Thermogravimetric Analysis
THF	tetrahydrofuran
THQ	tetrahydroquinoline
THS	tetrabutylammonium hydrogen sulfate
TOF	turn over frequency
TON	turn over number
U	
UHV	Ultra High Vacuum
V	
VHH	Van Hardevel Hartod
vs.	versus
W	
WAXS	Wide-Angle X-ray Scattering

X

XRD	X-Ray Diffraction
XPS	X-Ray Photoelectron Spectroscopy

Summary of the thesis

Transition metal nanoparticles (M-NPs) have gained significant interest in catalysis during the recent years and have been considered at the frontier between homogeneous and heterogeneous catalysis, potentially combining the advantage of both. Because of their small size, and consequently high surface to volume ratio, they have exhibited high activities, even under mild reaction conditions. They are soluble in a wide range of organic solvents that are commonly used as reaction media in catalysis. For their preparation, the use of stabilizers is required to avoid the formation of bulk metal, which is the thermodynamically favoured product during the aggregation of metal atoms. In this context, the utilization of small molecules such as ligands for NPs stabilization is of special interest since parameters such as their steric and electronic properties have been extensively studied in homogeneous catalysis and allows the tuning of the final metallic catalyst performance. In the field of ligand-stablized M-NPs, N-heterocyclic carbenes (NHCs) have demonstrated to be efficient compounds for the formation of stable M-NPs due to their high σ-donor properties. For these reasons, M-NPs have been considered promising catalysts for different processes such as selective hydrogenation and C-H activation reactions, among others.

The final goal of this thesis was the synthesis and characterization of Rh NPs stabilized by N-heterocyclic carbene (NHC) ligands for their application in the hydrogenation of compounds bearing aromatic rings such as aromatic ketones, phenols and pyridines. Besides, the

catalytic performance of these Rh NPs towards the selective deuteration of P-containing molecules such as phosphines and phosphine oxides has also been explored to get insights into the coordination mode of these P-ligands at metal surfaces.

In Chapter 1 a general introduction on the synthesis and application of M-NPs in catalytic reactions will be exposed. In this part, some examples on the use of M-NPs in reactions such as oxidation of alkanes and alkenes, Fischer-Tropsch, hydrosilylation of alkenes and akynes, C-C coupling (Heck and Suzuky-Miyaura), hydroformylation of alkenes, transfer hydrogenation of ketones, olefins, nitroarenes and α,β-unsaturated carbonyl compounds hydrogenation and H/D exchange of N- and P-based compounds will be described.

Chapter 2 sets out the general objectives of the thesis.

The synthesis of Rh NPs formed by the utilization of different stabilizing agents will be exposed in the introduction part of Chapter 3, with special emphasis on the methods previously reported for the formation of M-NPs stabilized by NHC ligands. Results regarding the synthesis and characterization of Rh NPs stabilized by 1,3-Bis(2,6-diisopropylphenyl)-1,3-dihydro-2*H*-imidazol-2-ylidene (IPr) will be exposed in this chapter. The effect of the amount of ligand used on the Rh NPs formation will be investigated and the availability of sites on the NPs surface where catalytic reactions can take place will be examined by CO adsorption experiments.

The research in Chapter 4 deals with the application of these Rh NPs stabilized by IPr in the selective hydrogenation of aromatic ketones, phenols and N-heteroaromatic compounds as such as pyridines and

quinoline. A review of the previously reported results regarding these catalytic reactions using M-NPs will be described, followed by the catalytic results obtained using these NHC-stabilized Rh NPs.

In the case of aromatic ketones, the preferential reduction of the arene ring over the ketone moiety will be investigated. Parameters such as the arene-ketone distance and the presence of different substituents close to the ketone group and in an aromatic position will also be examined.

In the case of phenols, the selective formation of cyclohexanones by partial reduction of the arene ring will be examined, studying the effect of the presence of different substituents in *ortho* and *para* positions of the arene ring.

Finally, in the case of N-heteroaromatic substrates such as pyridine derivatives, the catalytic activity of these Rh NPs will be examined. The selective reduction of substituted pyridines bearing phenyl and ketone moieties will also be investigated. The complete reduction of quinoline was also aimed at during this study.

Chapter 5 describes the application of Rh and Ru NPs stabilized by IPr and poly(N-vinyl-2-pyrrolidone) (PVP) in the selective H/D exchange of P-containing substrates. The catalytic application of M-NPs in this reaction provided valuable information on the coordination mode of these substrates at the surface of these NPs. In this context, a detailed review exposing the reported results concerning the application of M-NPs in the selective H/D exchange reaction of N- and P-containing molecules will be presented in the introduction of this chapter. The research in this chapter explores

the difference in catalytic activity and selectivity of Rh and Ru NPs formed by stabilization of IPr and PVP in the selective deuteration of various phosphines and diphosphines bearing aryl/alkyl positions and phosphine oxides. Indeed, coordination mode for these substrates at the surface of these NPs will be proposed based on the results obtained for these selective deuteration reactions.

The final remarks and conclusions extracted from the results obtained in this thesis will be described in Chapter 6.

Resum de la tesis

Les nanopartícules metàl·liques de metalls de transició (M-NPs) han guanyat significant interès en catàlisis en els darrers anys i han estat considerades a la frontera entre la catàlisi homogènia i heterogènia, potencialment combinant avantatges de totes dues. A causa de la seva petita grandària, i en conseqüència la seva elevada relació superfície/volum, han demostrat exhibir elevades activitats, inclús sota condicions suaus de reacció. Són solubles en una àmplia gamma de dissolvents orgànics comunament utilitzats com a medis de reacció en catàlisi. Per la seva preparació, l'ús d'estabilitzants és requerit per evitar la formació de massa metàl·lica, la qual és el producte termodinàmicament afavorit durant l'agregació d'àtoms metàl·lics. En aquest context, l'ús de molècules petites com ara lligands per l'estabilització de NPs és d'especial interès ja que paràmetres tals com ara les seves propietats estèriques i electròniques han estat extensament estudiats en catàlisi homogènia i permeten l'afinació del rendiment del catalitzador metàl·lic final. En el camp de NPs metàl·liques estabilitzades per lligands, els carbens N-heterocíclics (NHCs) han demostrat ser compostos eficients per la formació de NPs metàl·liques estables a causa de les seves altes propietats σ-donadores. Per aquestes raons, les NPs metàl·liques han estat considerades prometedors catalitzadors per a diferents processos com ara reaccions d'hidrogenació selectiva i d'activació C-H, entre d'altres.

L'objectiu final d'aquesta tesis era la síntesi i la caracterització de NPs de Rh estabilitzades amb lligands carbens N-heterocíclics (NHC)

per la seva aplicació a la hidrogenació de compostos portadors d'anells aromàtics com ara cetones aromàtiques, fenols i piridines. Per altra banda, el rendiment catalític d'aquestes NPs de Rh cap a la deuteració selectiva de molècules que contenen àtoms de P com ara fosfines i òxids de fosfines han estat també explorades per tal d'obtenir coneixements sobre el mode de coordinació d'aquests lligands amb fòsfor sobre superfícies metàl·liques.

Al Capítol 1, una introducció general sobre la síntesis i aplicació de M-NPs en reaccions catalítiques serà exposada. En aquesta part, alguns exemples sobre l'ús de NPs metàl·liques en reaccions com ara oxidació d'alcans i alquens, Fischer-Tropsch, hidrosililació d'alquens i alquins, acoblament C-C (Heck i Suzuky-Miyaura), hidroformilació d'alquens, hidrogenació per transferència de cetones, olefines, nitroarens i compostos carbonílics α,β-insaturats, hidrogenació d'alquens, aromàtics, nitroarens i compostos carbonílics i intercanvi H/D de compostos basats en N i P seran descrits.

El Capítol 2 estableix els objectius generals de la tesis.

La síntesi de NPs de Rh formades per l'ús de diferents agents estabilitzants serà exposada en la introducció del Capítol 3, donant especial èmfasis als mètodes prèviament reportats per la formació de M-NPs estabilitzades amb lligands NHC. Resultats pel que fa a la síntesis i la caracterització de NPs de Rh estabilitzades amb 1,3-Bis(2,6-diisopropilphenil)-1,3-dihydro-2*H*-imidazol-2-yliden (IPr) seran exposats en aquest capítol. L'efecte de la quantitat de lligand utilitzat a la formació de les NPs de Rh serà investigada i la disponibilitat de llocs a la superfície de les NPs on reaccions

catalítiques es puguin produir seran examinades a través d'experiments d'adsorció de CO.

La investigació al Capítol 4 tracta sobre l'aplicació d'aquestes NPs de Rh estabilitzades amb IPr en la hidrogenació selectiva de cetones aromàtiques, fenols i compostos N-heteroaromàtics com ara piridines i quinolina. Una revisió de previs resultats reportats pel que fa aquestes reaccions catalítiques utilitzant M-NPs serà exposada, seguit pels resultats catalítics obtinguts utilitzant aquestes NPs de Rh estabilitzades amb lligands NHC.

En el cas de cetones aromàtiques, la preferencial reducció de l'anell aromàtic sobre la cetona serà investigada. Paràmetres com ara la distància anell aromàtic-cetona i la presència de diferent grups propers as grup cetona i en una posició aromàtica seran també examinats.

En el cas dels fenols, la formació selectiva de ciclohexanones per reducció parcial de l'anell aromàtic serà examinada, estudiant l'efecte de la presència de diferents substituents a les posicions *ortho* i *para* de l'anell aromàtic.

En el cas de substrats N-heteroaromàtics com ara derivats de piridina, l'activitat catalítica d'aquestes NPs de Rh serà examinada. La reducció selectiva de piridines substituïdes portant grups fenil i cetona serà també investigada. La completa reducció de quinolina també es va tractar durant aquest estudi.

El Capítol 5 descriu l'aplicació de NPs de Rh i Ru estabilitzades per IPr i poly(N-vinyl-2-pyrrolidona) (PVP) en l'intercanvi H/D selectiu de substrats portant àtoms de P. L'aplicació catalítica de M-NPs en

aquesta reacció proporcionó informació valuosa sobre el mode de coordinació d'aquests substrats a la superfície d'aquestes NPs. En aquest context, una revisió detallada exposant els resultats reportats referents a l'aplicació de M-NPs en l'intercanvi H/D selectiu de molècules que contenen àtoms de N i P serà presentada en la part introductòria d'aquest capítol. La investigació en aquest capítol explora la diferència en l'activitat i la selectivitat catalítica de NPs de Ru i Rh formades per estabilització per IPr i PVP en la deuteració selectiva de varies fosfines i difosfines amb posicions aril/alquil i òxids de fosfina. El mode de coordinació d'aquests substrats a la superfície de aquestes NPs serà proposada en base als resultats obtinguts en aquestes reaccions de deuteració selectiva.

Les observacions finals i les conclusions extretes dels resultats obtinguts en aquesta tesi seran descrits al Capítol 6.

Chapter 1

Introduction

1.1. Introduction to metal nanoparticles

Nanochemistry has been a field of intense scientific research during the last decades due to the wide variety of potential applications of metal nanoparticles in different areas such as biomedicine, optics, electronics and catalysis.[1,2]

Transition metal nanoparticles (M-NPs) are formed by the combination of several metallic atoms, usually in the zero oxidation state. They possess a nanometric dimension, between 1 and 100 nm in diameter. In this nanoscale regime, between metallic bulk and molecular complexes, atoms and molecules work differently, providing surprising and unique properties.

Soluble M-NPs have been considered at the frontier between homogeneous and heterogeneous catalysis, potentially combining the advantage of both. They are soluble in a wide range of organic solvents that are commonly used as reaction media in catalysis and where the substrate is also soluble. They have exhibited activity even under mild reaction conditions and high selectivity via the modulation of their surface. Because of their small size, and consequently high surface to volume ratio, they have exhibited high activities [3] and the fact that they can be easily recovered, in contrast to homogeneous systems, has been considered to be of extreme importance. In addition, these systems are freely rotational and three-dimensional when used in catalytic reaction, which increases the accessibility of the surface active sites and thus enhance their activity.[4] The main disadvantage of the use of M-NPs as catalysts is their instability in solution, particularly at high temperatures.[5]

1.2. Synthesis and stabilization of M-NPs

The formation of M-NPs can be achieved following two main general methodologies: the physical method and the chemical method (Figure 1. 1).[6] The physical method (Figure 1. 1a), also known as "top-down" approach, is based on lithography to pattern nanoscale structures. This method can be used for the formation of large NPs of >10nm in size. However, poor reproducibility and broad size distributions are usually obtained. On the other hand, the chemical method (Figure 1. 1b), known as "bottom-top" approach, uses interactions between colloidal particles to assemble discrete nanoobjects and is generally considered the most convenient procedure for the formation of small isolable NPs with a well-defined surface composition.

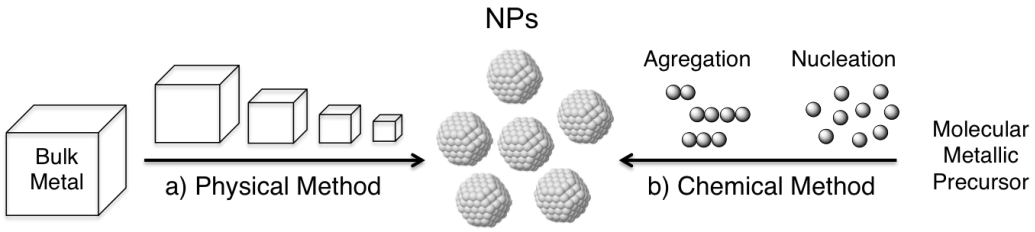

Figure 1. 1. Methods for the synthesis of metal nanoparticles

Within the chemical method, several synthetic procedures have been reported for the synthesis of M-NPs such as the reduction of transition metal salts, electrochemical synthesis and metal vapour synthesis.[7] More recently, other chemical methods used for the formation of M-NPs such as the organometallic approach, reported by Chaudret and co-workers, showed to be suitable for obtaining

NPs with narrow size distribution and clean surfaces in a reproducible manner.[8]

1.2.1. Electrostatic and steric stabilization

During the NPs formation, the formation of bulk metal is the thermodynamically favoured product during the aggregation of metal atoms. For this reason, colloidal suspensions need to be stabilized by protecting agents to avoid agglomeration. In the absence of repulsive interactions, the Van der Waals forces will attract two metallic particles to each other causing agglomeration and thus leading to the loss of properties associated with the colloidal state of M-NPs. In this topic, different types of M-NPs stabilization can be envisaged: electrostatic stabilization and steric stabilization.[9]

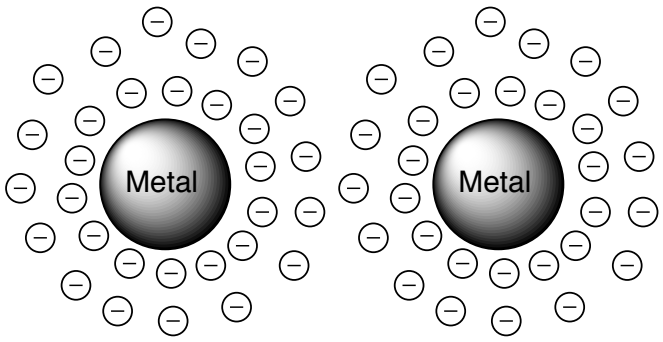

Figure 1. 2. Schematic representation of electrostatic stabilization of metal colloid particles

The electrostatic stabilization is based on the creation of an ionic environment at the surface of the particles (Figure 1. 2). The adsorption of ionic species such as halides, carboxylates or polyoxoanions (dissolved in aqueous media) at the surface of the

particles will generate an electrical double-layer around the particles. If the electric potential associated with the double layer is strong enough, then the electrostatic repulsion will prevent particle agglomeration.

The steric stabilization is based on the repulsion of molecules located at the surface of the particles (Figure 1. 3). Such repulsion can be induced by organic compounds such as polymers or small molecules such as ligands bearing coordinating groups in their structure. These species will prevent agglomeration of NPs by providing a protecting layer at the metallic surface. In contrast with the electrostatic stabilization, which is mainly used in aqueous phase, steric stabilization can be used in both organic and aqueous solvents.

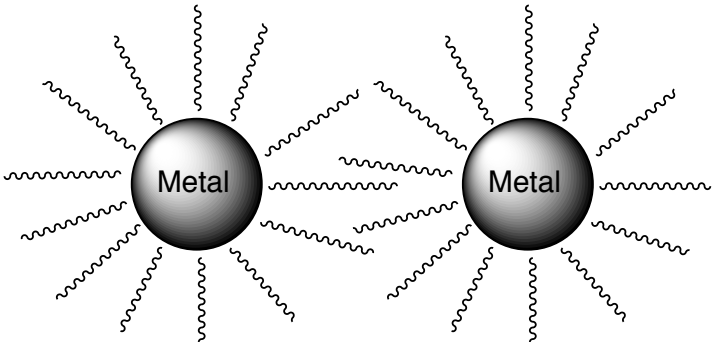

Figure 1. 3. Schematic representation of steric stabilization of metal colloid particles

1.2.2. Stabilizing agents

In terms of stabilizing agents, compounds such as polymers, surfactants, ionic liquids (ILs) and small molecules such as ligands, have been reported to efficiently stabilize soluble M-NPs (Figure 1. 4).[10]

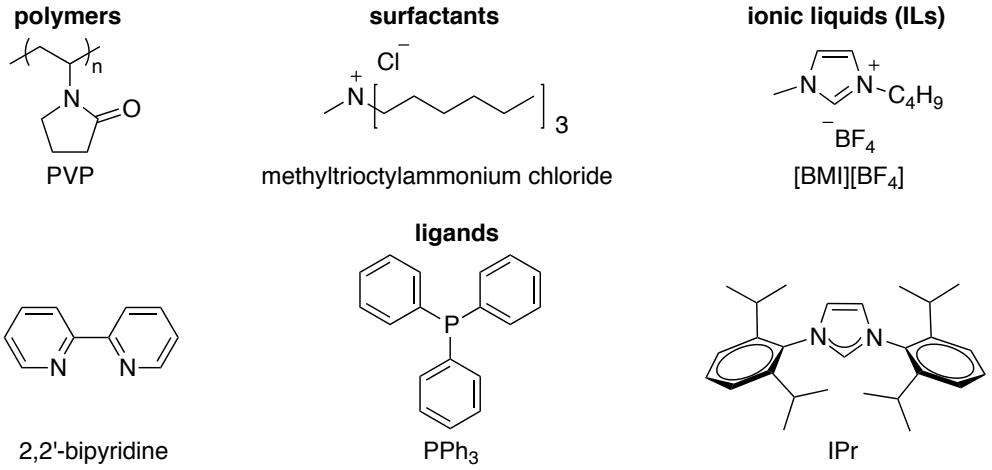

Figure 1. 4. Examples of stabilizing agents used for the formation of metal nanoparticles

Polymers

Polymers provide stabilization for M-NPs through the steric bulk of their framework, but also by binding weakly to the NPs surface via heteroatoms present in their structure. Poly(*N*-vinyl-2-pyrrolidone (PVP) (Figure 1. 4) is the most used polymer for NPs stabilization because it fulfils both steric and coordinating requirements.[10] The fact that it is soluble in water and other organic polar solvents such as methanol and ethanol has made PVP a versatile polymer to be used in M-NPs formation.

Surfactants, micelles and microemulsions

These stabilizing agents prevent agglomeration via the formation of a monomolecular layer around the particles core. Lipophilic surfactants of cationic type such as tetraalkylammonium halides ($R_4N^+X^-$) can lead to the formation of stable M-NPs.[11] Micelles has also been used as micro-reactors for the growth of particles, forming a confined environment able to control the size and distribution of the final M-NPs.

Ionic Liquids (ILs)

Ionic liquids have been reported to be valuable stabilizing agents for the formation of M-NPs.[12,13,14] The sterically hindered substituted imidazolium cation favours the electrosteric stabilization of particles. The size of the imidazolium cation can be modulated by the choice of the desired *N*-alkyl substituents. This tuning has an important role regarding the size and the solubility of M-NPs, which are parameters that have an effect on catalysis. Another interesting feature of these compounds is the possibility to use them as both solvent and stabilizer.[15] The fact that they display interesting physicochemical properties such as ionic mobility, hydrophobicity, low vapour pressure, non-flammability and miscibility with organic and inorganic solvents made them an alternative and complementary medium to classical organic solvents and water in many applications.[16]

Ligands

The utilisation of small molecules such as ligands for NPs stabilization is of special interest since parameters such as their

steric and electronic properties directly affect the performance of the final metallic catalyst. In this field, stabilization by N-, S- and Si-containing ligands, phosphines, phosphites and, more recently, N-heterocyclic carbenes (NHCs) has been reported.[17] This stabilization strategy potentially allows the fine tuning of the parameters that govern the catalytic performance of the final particles. Besides, the application of chiral ligands is also considered to be an effective technique for increasing the enantioselective efficiency of these M-NPs.

1.3. Heterogeneous nature of M-NPs

As previously mentioned, the application of M-NPs has been widely studied due to their potential high activity and selectivity when used as catalysts. However, leaching of molecular species from nanocatalysts can take place during the catalytic experiments. For this reason, it is crucial to demonstrate if the active catalyst is homogeneous or heterogeneous in nature and several studies based on the application of precise techniques aiming at the identification of the real active species in catalytic reaction were reported.

One of the most commonly used methods to assess whether a catalytic reaction goes through a homogeneous or heterogeneous mechanism is the poisoning of the catalyst surface by reagents that bind to the heterogeneous catalysts and inhibit their catalytic activity.[18] The selective poisoning of colloids using Hg is well known.[19]

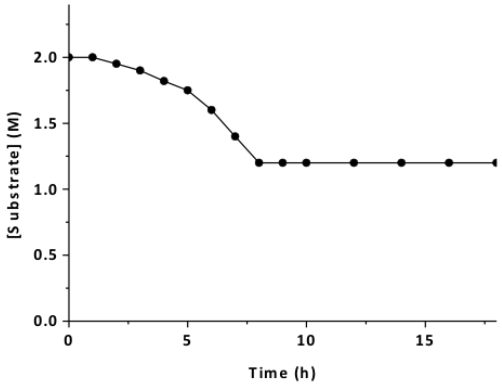

Figure 1. 5. Example of Hg^0 poisoning study using heterogeneous catalysts in a hydrogenation reaction

In a typical study, the catalyst activity and selectivity towards a certain reaction is studied in the absence and presence of Hg.[18] If the activity of the catalyst remains unchanged, then it is most likely homogeneous, while a decrease in the activity strongly suggests the existence of a colloidal catalyst (Figure 1. 5).

On the other hand, the utilization of other capping agents such as CO has also been published to be employed as poisoning in specific reactions such as catalytic hydrogenation reactions in mild reaction conditions.[20] Under these conditions, CO can bind to the metallic surface of NPs and perform its deactivation. Preliminary studies based on the quantification of surface hydrides on Ru NPs stabilized by PVP and 1,4-(diphenylphosphino)butane (dppb) demonstrated their complete removal upon exposure of to low pressures of CO.[21] More recently, further studies showed that saturation of the surface of these Ru NPs with CO groups could also have an effect on the catalyst performance towards styrene hydrogenation by fully inhibiting the catalyst activity.[20]

The application of Lewis bases as such as CS_2, PPh_3 or thiols as poisons represent an important tool to identify homogeneous catalysts.[22] The fact that the catalyst activity is inhibited when less than 1 equivalent of ligand is added to the catalytic mixture suggests the presence of a heterogeneous catalyst. As an example, surface-poisoning studies using PVP-stabilized Ru NPs by addition of sulfonated phosphine ligands evidenced a decrease in the catalytic activity towards the reduction of aromatic substrates such as phenol (Figure 1. 6) and thus demonstrated the heterogeneous character of this Ru catalyst.[23]

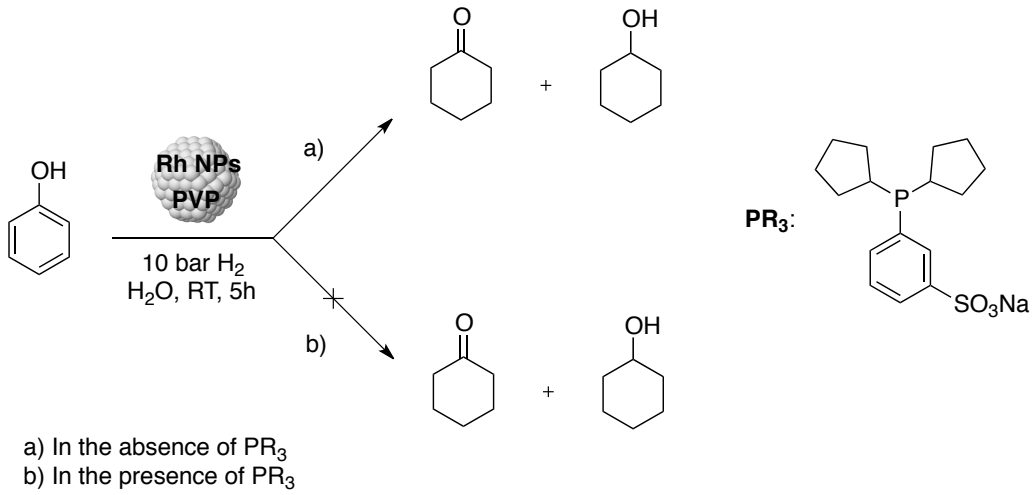

Figure 1. 6. Results reported by Dyson and co-workers in the hydrogenation of phenol using PVP-stabilized Rh NPs (a) in the absence and (b) the presence of PR_3[23]

In some specific cases, the reactivity observed in a catalytic reaction can also give information about the real active species in a catalytic reaction. For instance, the fact that hydrogenolysis of the C-O bond, which is characteristic of a surface metal catalyst, took place when the hydrogenation of acetophenone and anisole was performed

using Ir NPs stabilized by ILs, suggested that these NPs behave preferentially as heterogeneous catalysts. This behaviour was more recently observed using PPh_3-stabilized Rh NPs[24] and PVP-stabilized Rh NPs with NiO_x surface decoration[25] in the hydrogenation of substrates bearing arene moieties.

The study of the reaction kinetics also provides information on the real nature of the active catalytic species. In the case of heterogeneous catalysts, no induction period is expected, with the observation of an exponential decay aspect curve.[26] However, if NPs are formed *in situ* from a homogeneous compound, an incubation period is usually observed, as reported for the hydrogenation of benzene using Rh NPs.[27]

1.4. Application of colloidal M-NPs in catalysis

In view of their unique properties, M-NPs have been applied in several catalytic processes such as oxidation of alkanes and alkenes, Fischer-Tropsch Synthesis (FTS), hydrosilylation of alkenes and alkynes, C-C coupling, hydroformylation of alkenes, transfer hydrogenation of ketones, olefins, nitroarenes and α,β-unsaturated carbonyl compounds, hydrogenation and deuteration reactions.[28,29,30] A brief presentation of the application of M-NPs in these reactions is described below.

1.4.1. Colloidal M-NPs in oxidation reactions

In oxidation reactions, only a few examples of application of colloidal M-NPs as catalysts have been published to date. For instance, Fe[31] and Ru[32] NPs have showed to be active in the oxidation

of cyclooctane and cyclohexane[33] using *tert*-butylhydroperoxide (*t*-BHP) as oxidizing agent for the formation of cyclic aliphatic ketones. In the case of Ru NPs formed from $RuCl_3 \cdot 3H_2O$ in neat water, a conversion of 97% together with 90% selectivity to the ketone product were achieved, which constitutes a high-value-added intermediate for polymer or fine chemistry (Figure 1. 7).[33]

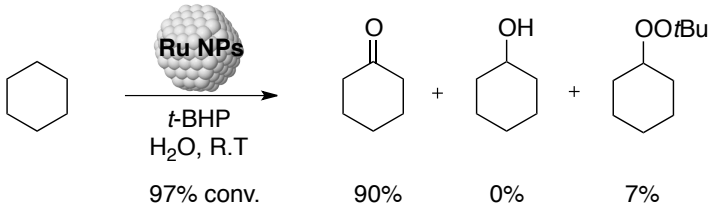

Figure 1. 7. Results reported by Roucoux and co-workers for the oxidation of cyclohexane using Ru NPs[33]

Besides, the oxidation of ethene has also been reported, in this case using Ag NPs in the presence of O_2, producing ethylene oxide as the reaction product. [34] The application of Ag NPs stabilized by polyacrylate under an oxygen atmosphere at 170°C provided higher catalytic activity than a commercial Ag catalyst. In addition, the presence of alkali metal ions such as Cs(I) or Ru(VII) remarkably increased the catalytic activity of these M-NPs.

1.4.2. Colloidal M-NPs in Fischer-Tropsch Synthesis reactions

From an industrial point of view, the production of liquid hydrocarbons from syngas (CO + H_2) by Fischer-Tropsch synthesis (FTS) is also of great interest.[35] Reaction schemes for the formation of paraffins and olefins are shown in Figure 1. 8.

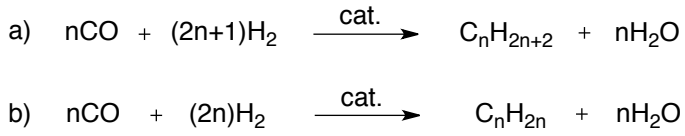

Figure 1. 8. Fischer Tropsch reaction scheme for the production of (a) paraffins and (b) olefins.

Concerning this reaction, the application of soluble M-NPs as catalyst is of special importance as they provide high levels of activity and selectivity using a wide range of solvents such as water, ionic liquids and high boiling point organic solvents. In this context, mainly Ru, Fe and Co based nanocatalysts formed in the presence of various stabilizing agents such as polymers, surfactants, ILs and small ligands have been investigated.[29] On the other hand, based on the high industrial interest of FTS, considerable efforts have been done concerning the synthesis and application of supported M-NPs.[36,37,38]

For instance, in 2010 Kou and co-workers published the application of Fe NPs dispersed in Polyethylene glycol (PEG) in the liquid-phase FTS under mild reaction conditions.[39] The fact that the FT reaction products were insoluble in PEG made them very easily separable from the reaction mixture. Some years later, the same research group described the application of Co NPs towards the aqueous-phase FTS.[40] These Co NPs, synthesised by reduction of $CoCl_2$ by $LiBEt_3H$ in the presence of *n*-dodecyl-*N,N*-dimethyl-3-ammonio-1-propanesulfonate (SB3-12), showed high catalytic activity and recycling ability with a high selectivity of 40% towards C_{5+} products.

More recently, our group reported the application of colloidal Co NPs stabilized by PVP in the aqueous FTS, evaluating their catalytic

performances at various pH values[41] and solvent compositions[42], parameters. The pH of the catalytic solution showed to affect both the activity and selectivity of the reaction since side reactions such as the Water Gas Shift reaction (WGS) and formation of formate from CO_2 were favoured at basic pH and in terms of solvent composition, the catalytic results revealed that both activity and selectivity was strongly dependent on the nature and composition of the solvent mixture.

1.4.3. Colloidal M-NPs in hydrosilylation reactions

Regarding the hydrosilylation reactions, colloidal Rh[43,44], Pd[45,46], Pt[47,48] and bimetallic RuRh and RuPt NPs[49] were reported. For instance, BINAP-stabilized Pd NPs were found to be more active and stable than previously reported homogeneous Pd complexes for the asymmetric hydrosilylation of styrene with trichlorosilane.[45] This work pointed towards a new direction in the design of chiral M-NPs catalyst for asymmetric transformations.

In a recent report, Shafir and co-workers reported the use of flower-like Rh NPs stabilized by a nitrogen-rich PEG tagged substrate for the stereoselective hydrosilylation reaction.[44] These Rh NPs showed to be very efficient catalysts towards the hydrosilylation of symmetric internal alkynes, achieving in almost all cases (*E*)-vinylsilanes in quantitative yields for a large variety of diaryl alkynes in solvent-free conditions.

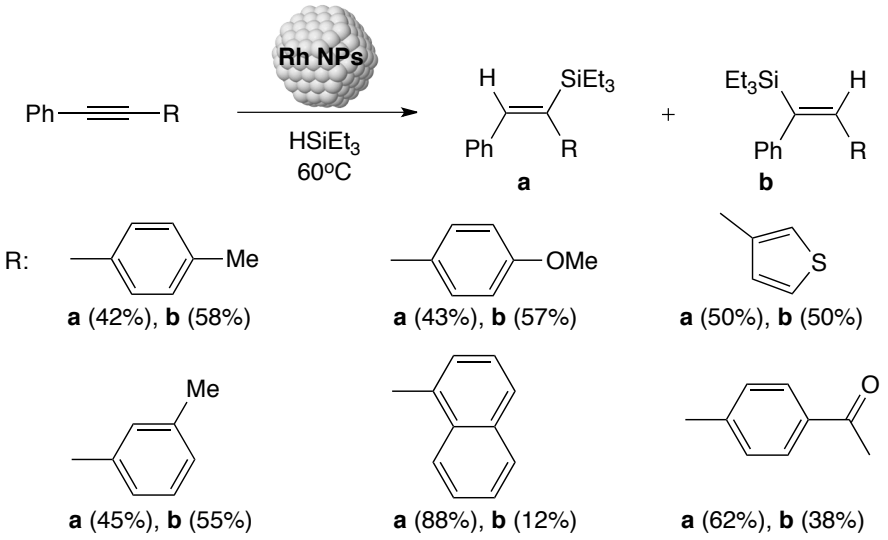

Figure 1. 9. Results reported by Shafir and co-workers for the stereoselective hydrosilylation of diaryl alkynes using Rh NPs[44]

1.4.4. Colloidal M-NPs in C-C coupling reactions

The use of transition metal catalysts for the formation of new C-C bonds is one of the most important reactions in organic synthesis. In this field C-C coupling reactions such as Heck and Suzuki-Miyaura have been widely described using Pd NPs.[50,51,52] In 1996, the first example of the use of Pd NPs to catalyse the Heck coupling reaction was reported by Herrmann and co-workers.[53] Since then, several examples have been described.[54,55,56,57]

However, when Pd NPs were prepared and isolated to be used as catalyst, the possibility of leaching and formation of catalytically active molecular species should be considered. Several mechanisms were proposed and are summarized in Figure 1. 10: (a) Pd NPs are the true heterogeneous catalyst and (b) Pd NPs act as a reservoir of molecular species.[50] In this latter case, either "naked Pd atoms" could

leach from the NPs or the first step of the reaction, namely the oxidative addition, could occur at the NPs surface followed by leaching of the [Pd(Ar)X] species which can initiate an homogeneous catalytic cycle. Moreover, it has been shown that the leaching can be reversible and that Pd NPs can be formed during the reactions from homogeneous metal complexes and thus, acting these NPs as a reservoir of molecular species.

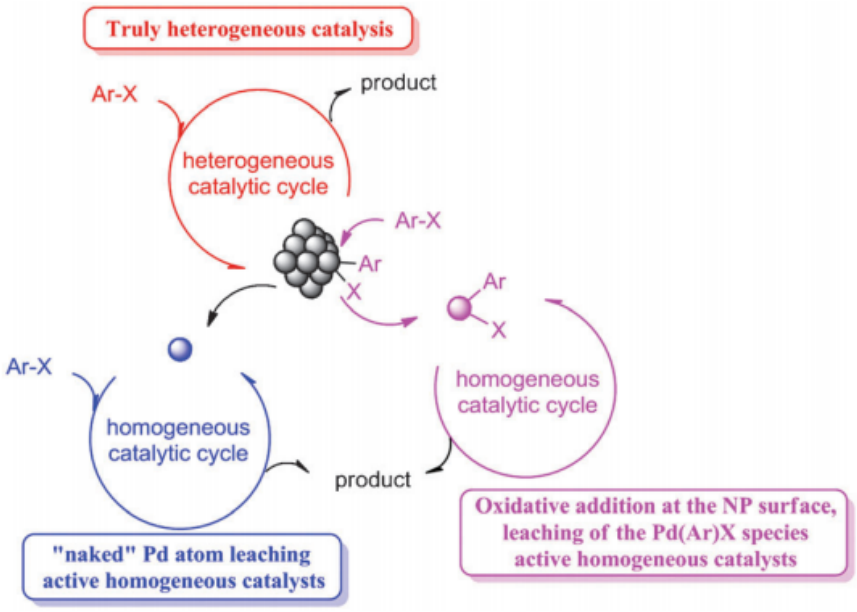

Figure 1. 10. Proposed mechanisms for the Pd NPs catalysed C-CO coupling reactions.[50]

The application of mainly Pd NPs[11,58,59,60,61,62,63] but also Ru NPs[64] in Suzuki-Miyaura C-C coupling reactions has also been studied. However, as in the case of Heck reactions, in most cases the catalytic activity was attributed to a homogeneous complex formed by leaching from M-NPs during the reaction.[65,66]

1.4.5. Colloidal M-NPs in hydroformylation reactions

The formation of C-C bonds through catalytic hydroformylation reactions in the presence of Rh NPs has also been studied. For instance, the hydroformylation of 1-alkenes was carried out using ILs-stabilized Rh NPs, achieving linear to branched ratios up to 25 for the linear/branched aldehyde product when xantphos-modified Rh NPs were used.[67] Nevertheless, an induction period detected in all reactions starting from NPs was indicative of NPs degradation under the reaction conditions into soluble mononuclear Rh-carbonyl species. This fact suggested the homogeneous nature of the real catalytic species in the reaction. The application of (*R*)-BINAP-[68] and chiral-diphosphite-[69] stabilised Rh NPs has also been reported for the asymmetric hydroformylation of styrene (Figure 1. 11). High regioselectivities with from low to moderate enantiomeric excesses (*ee*) were obtained in these cases.

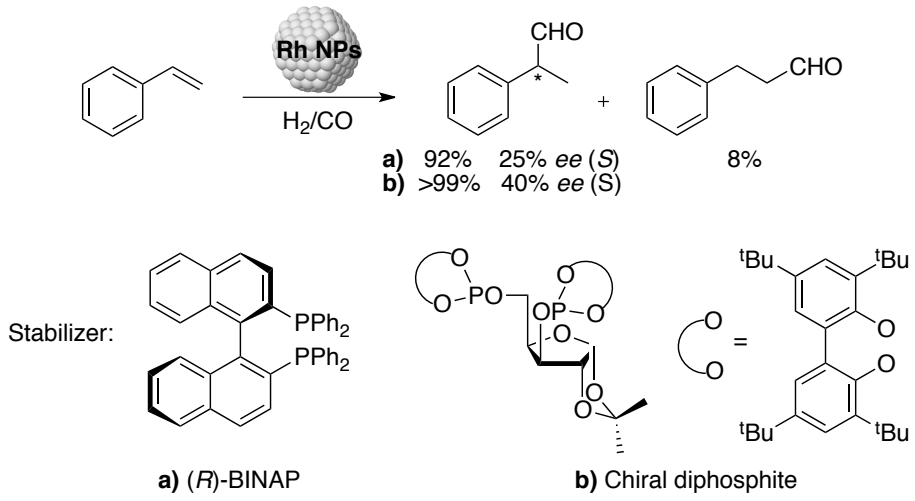

Figure 1. 11. Results reported for the asymmetric hydroformylation of styrene using Rh NPs stabilized by (a) (*R*)-BINAP[68] and (b) a chiral diphosphite[69]

Nevertheless, in both studies the formation of active homogeneous catalysts was detected. More recently, Rh NPs stabilized by hypercross-linked polystyrene (HPS) showed to be en efficient catalyst towards the hydroformylation of a variety of olefins in $scCO_2$.[70] The catalyst could be reused up to six times without any noticeable decrease in activity or regioselectivity.

To summarize, while Rh-based homogeneous complexes are well-known as highly active species in hydroformylation reactions, it appears that only a few examples deal with the application of Rh NPs.[71] This probably results from a lack of robustness of Rh NPs under hydroformylation reaction conditions, involving the formation of monometallic Rh(I)-species. This fact questions the real active species in this catalytic reaction, namely M-NPs or homogeneous complex due to the metal leaching.

1.4.6. Colloidal M-NPs in transfer hydrogenation reactions

Transfer hydrogenation of organic compounds is a much safer and more environmentally benign process compared to reduction reactions using molecular hydrogen, metal hydrides or dissolving metals and does not require elaborate experimental setups.[72] Furthermore, 2-propanol, which is one of the most used sources of hydrogen in this reaction, is readily available, cheap, easy to handle and environmentally friendly.

In this area, the application of Ni NPs have been widely investigated by Yus and co-workers[73] for the reduction of ketones (Figure 1. 12)[74,75] and olefins.[76] The same catalysts were also active in the

hydrogen-transfer reductive amination of aldehydes using isopropanol as the hydrogen source for the formation of secondary amines[77].

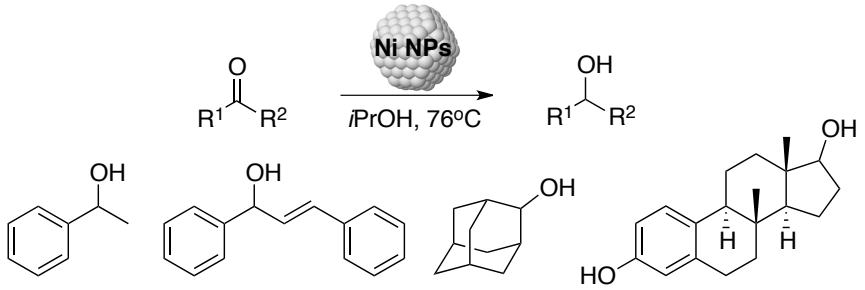

Figure 1. 12. Results reported by Yus and co-workers for the transfer hydrogenation of ketones using Ni NPs.[74]

The application of M-NPs based on Fe, Pd, Ir, Rh, Ni and bimetallic Ni-Co, in transfer hydrogenation reactions of nitroarenes[78,79,80] and α,β-unsaturated carbonyl compounds[81,82] was also reported. It is interesting to highlight the application of Fe[83] and, more recently, Rh[84] NPs stabilized by chiral ligands in the asymmetric hydrogenation of acetophenone, achieving up to 70 and 69% *ee* respectively.

1.4.7. Colloidal M-NPs in hydrogenation reactions

The catalytic hydrogenation reaction is one of the fields where the application of M-NPs has received much attention. The catalytic reduction of arenes has attracted much interest from both academic and industrial point of view due to the high activities of these systems when used under mild reaction conditions.[85] The application of heterogeneous catalysts was previously reported in this kind of transformations. However, colloidal M-NPs provided

higher selectivities compared to those obtained by classical heterogeneous systems. This feature made them of great interest for their application as catalysts in hydrogenation reactions of substrates bearing aromatic rings.

In this context, the hydrogenation of substrates such as benzene [86,87], mono- and di-substituted arenes [88, 89, 90], polyarenes [91], phenols, pyridines[92, 93], among others, using M-NPs have been described. The specific case of phenol is of commercial and environmental interest due to the application of one of its reduction products, namely cyclohexanone, in the production of Nylon 6 and Nylon 66 (Figure 1. 13).[94,95] Reported results regarding the application of M-NPs in the hydrogenation of phenols and pyridines are presented in Chapter 4 of this thesis.

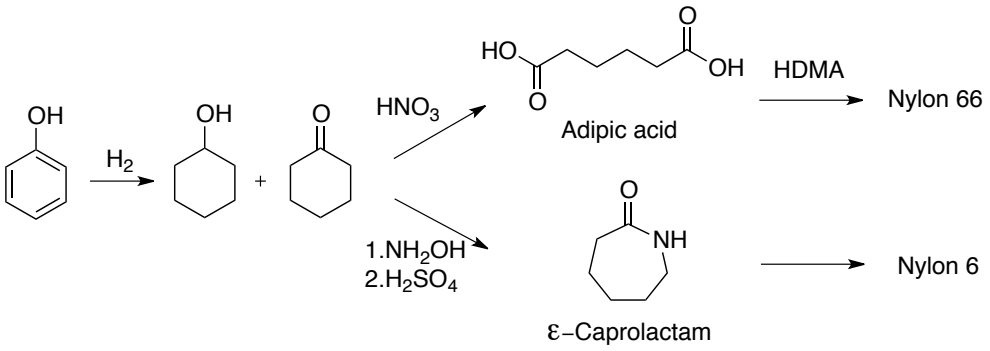

Figure 1. 13. Schematic synthesis of Nylon 6 and Nylon 66 using cyclohexanone produced by phenol reduction

The use of styrene as substrate has become of great importance due to the presence of an extra C=C double bond unit, which can lead to the formation of ethylbenzene, vinylciclohexane, or ethylcyclohexane, depending on the chemoselectivity of the reaction (Figure 1. 14). For this reason, this reaction was considered key to

evaluate the selective reduction of an aromatic ring and/or vinylic C=C bonds and although mainly Ru[96,97,98,99] and Rh[89,100,101,102] NPs have been used for this transformation; the application of Pd NPs[103] has also been reported.

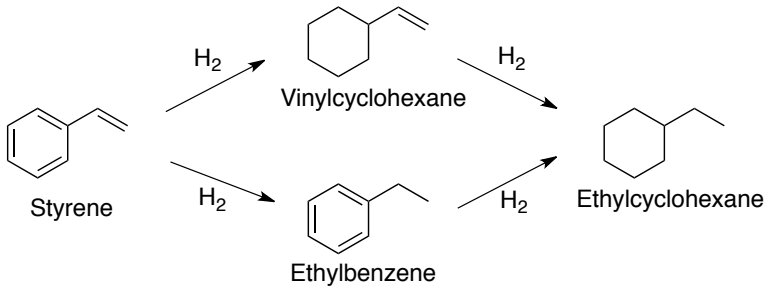

Figure 1. 14. Expected products for the selective hydrogenation of styrene

For instance, Philippot and co-workers reported the application of water soluble Ru NPs stabilized by different alkyl-sulphonated diphosphines for the selective reduction of styrene.[97] While mixtures of ethylbenzene and ethylcyclohexane were obtained in most cases, an increase in the steric hindrance at the NPs surface by an increment on the [L]/[Ru] molar ratio resulted in 84% of selectivity towards the formation of ethylbenzene (Figure 1. 15).

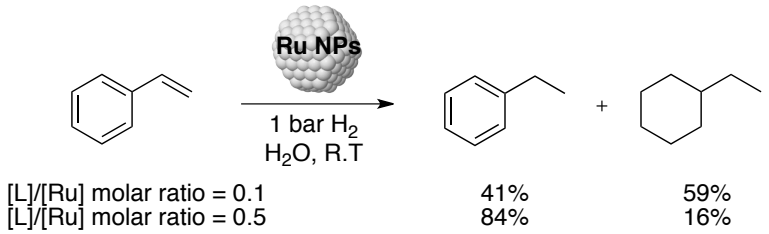

Figure 1. 15. Results reported by Philippot and co-workers for the selective hydrogenation of styrene using Ru NPs[97]

One year later, our research group investigated the application of Rh NPs stabilized by mono- and di-phosphine and phosphite ligands towards the hydrogenation of styrene.[89] In this case, selective reduction of the vinylic C=C bond over the arene ring was achieved at full conversion after short reaction times.

Reduction of other functionalities like nitro groups has also been investigated using M-NPs.[104] In this context, the application of Ni[105,106], Pd,[107] Rh[108,109], Ru[110], Ir[111,112], Pt[113,114] and bimetallic RuPt[115] NPs for the reduction of nitrobenzenes were reported.

As an example, Rh NPs stabilized by ILs functionalized by sulfonated phosphines were used in the reduction of different *m*-, *o*- and *p*-substituted nitrobenzenes and almost all substrates were efficiently converted into the corresponding aniline under mild reaction conditions.[109] In the case of chloro- and methyl-substituted nitrobenzenes, the corresponding aniline products could be afforded with comparable reaction rates with that of unsubstituted nitrobenzene.

The chemoselective reduction of nitroarenes bearing other reducible functional groups such as aldehydes, ketones, esters, amides or nitriles was also investigated using M-NPs. For instance, PVP-stabilized Ir NPs revealed efficient catalysts for the selective reduction of the nitro group in the presence of aldehyde, ketone or nitrile group (Figure 1. 16).[111]

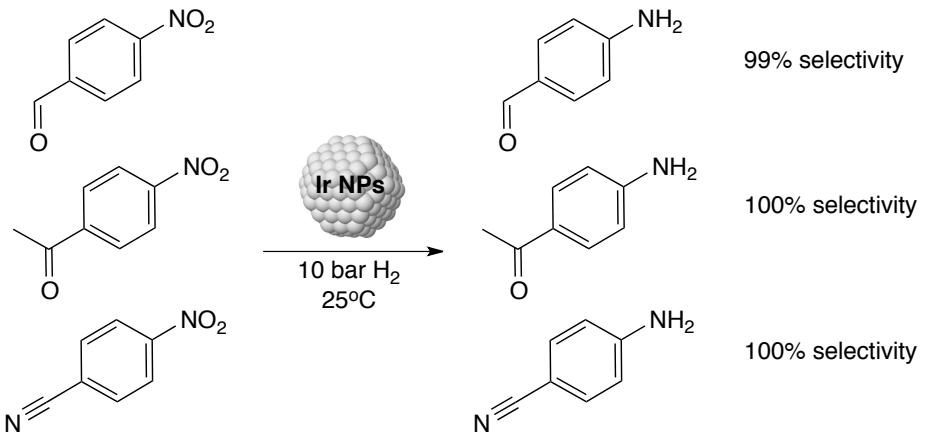

Figure 1. 16. Results reported by Tsukuda and co-workers for the selective hydrogenation of nitroarenes using Ir NPs[111]

In contrast, a distinct behavior in terms of selectivity was recently reported in the chemoselective reduction of 4-nitrobenzaldehyde using Ir NPs formed by decomposition of $[Ir(COD)(OMe)]_2$ under H_2 in the presence of a secondary phosphine oxide.[112] In this case, the hydrogenation of both reducible functionalities led to a selectivity of 95% at full conversion towards the formation of the aminobenzyl alcohol derivative after 18h of reaction under 20 bar of H_2.

The application of NHC-stabilized M-NPs for the hydrogenation of this type of compounds has also been reported.[107,110,114] Indeed, the high donor properties of such ligands result in an increase in the robustness of these nanocatalysts compared to other ligand-stabilized M-NPs. It is noteworthy that Pt NPs stabilized by NHC ligands exhibited high levels of activity and selectivity in the chemoselective reduction of diverse functionalized nitroarenes carrying amide, ester, ketone, aldehyde, nitrile, and α,β–unsaturated esters groups to the corresponding aniline derivative, leaving the

second reducible moiety untouched under mild conditions (Figure 1. 17).[114]

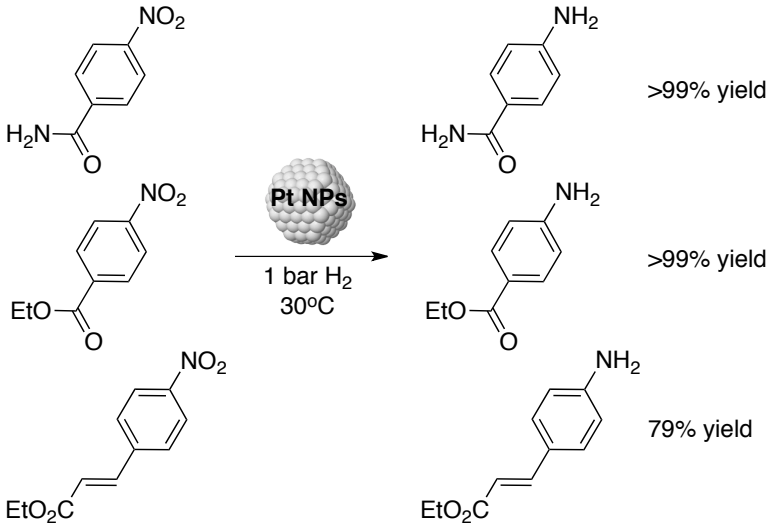

Figure 1. 17. Results reported by Chaudret and co-workers for the selective hydrogenation of nitroarenes using NHC-stabilized Pt NPs[114]

The hydrogenation of aromatic ketones has also been studied using M-NPs with acetophenone as the benchmark substrate. In this case, the selective reduction of the arene ring or a ketone group is of interest (Figure 1. 18).[99,114,116,117] A more detailed review of the literature regarding the reduction of aromatic ketones using colloidal M-NPs is presented in Chapter 4 of this thesis.

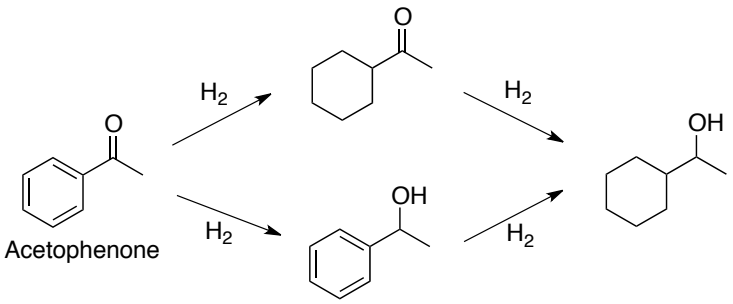

Figure 1. 18. Expected products for the selective hydrogenation of acetophenone

On the other hand, the reduction of aromatic substrates bearing other carbonyl functionalities as such as esters,[118,119,116h] amides[120], aldehydes[112, 121 , 122 , 123 , 124 , 125] and α,β-unsaturated carbonyl compounds[126] using colloidal M-NPs have also been reported.

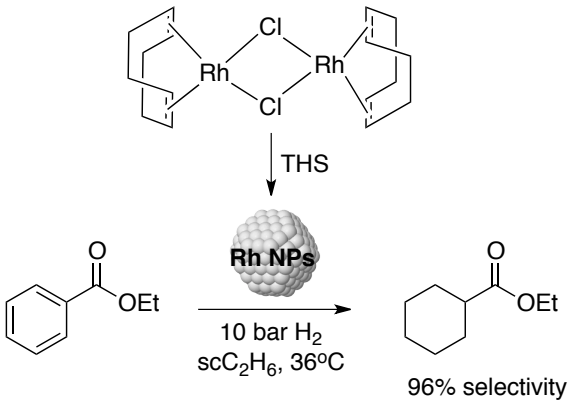

Figure 1. 19. Results reported by Jessop and co-workers for the selective hydrogenation of ethyl benzoate using Rh NPs[119]

Jessop and co-workers reported the use of colloidal Rh NPs for the selective hydrogenation of aromatic substrates containing ester groups.[119] These Rh NPs were formed *in situ* starting from $[Rh(COD)Cl]_2$ bimetallic precursor in aqueous/supercritical fluid

biphasic media using tetrabutylammonium hydrogen sulfate (THS) as stabilizing agent. When this catalytic system was applied under 10 bar of H_2 using ethyl benzoate as substrate, the aromatic ring reduction was achieved with 96% of selectivity (Figure 1. 19)

Dupont and co-workers also investigated the chemoselective hydrogenation of esters.[118] In this case, Ir NPs synthesized by simple reduction of $[Ir(COD)Cl]_2$ in the presence of 1-*n*-butyl-3-methylimidazolium hexafluorophosphate ionic liquid, revealed an efficient and recyclable catalytic system for the solventless or biphasic hydrogenation of substrates bearing carbonyl functionalities under mild reaction conditions. The hydrogenation of ethyl 2-oxopropanoate produced ethyl 2-hydroxypropanoate as the only reaction product in 98% yield after 2.5 h of reaction (Figure 1. 20).

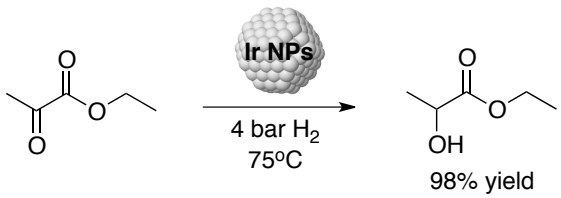

Figure 1. 20. Results reported by Dupont and co-workers for the selective hydrogenation of ethyl 2-oxopropanoate using Ir NPs

More recently, the application of Ru NPs stabilized by NHCs has also been used for the reduction of this type of compounds.[116h] In this report, a new route for the synthesis of Ru NPs using non-isolable NHC ligands was described. The catalytic activity of the resulting Ru NPs was tested in various hydrogenation reactions involving substrates having different carbonyl groups. Substrates containing

ketones were converted into the corresponding alcohols in good to excellent conversions without reducing ester functionalities (Figure 1. 22a). The reduction of substrates bearing C=C bonds was also achieved selectively, with no reduction of the corresponding ester functionality (Figure 1. 22a).

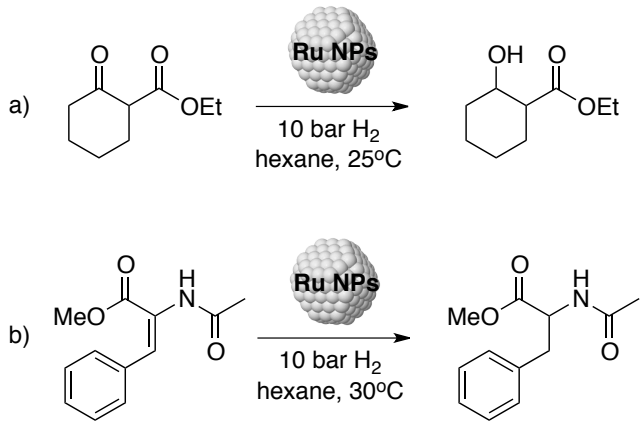

Figure 1. 21. Results reported by Chaudret and co-workers for the selective hydrogenation of esters using NHC-stabilized Ru NPs[116h]

Aromatic compounds bearing amide groups have been tested as substrate in the hydrogenation reaction using Rh NPs.[120] In this work, Leitner and co-workers reported the synthesis of Rh NPs by decomposition of [Rh(acac)$(CO)_2$] under supercritical conditions in the presence of tetrabutylammonium bromide. In contrast to conventional catalysts, this ammonium halide-stabilized Rh NPs provided good catalytic activities and significant differentiation between aromatic and olefinic moieties in the hydrogenation of (*E*)-2-(benzoylamino)-2-propenoic acids (Figure 1. 22). For these substrates, all three possible hydrogenation products were formed in a network of parallel and consecutive hydrogenation processes. In

some specific cases, the reduction of the arene took place preferentially over the C=C olefinic double bond. This trend was even more pronounced for more sterically hindered substrates, achieving in some cases up to 96% of selectivity at 60% of conversion towards selective arene reduction.

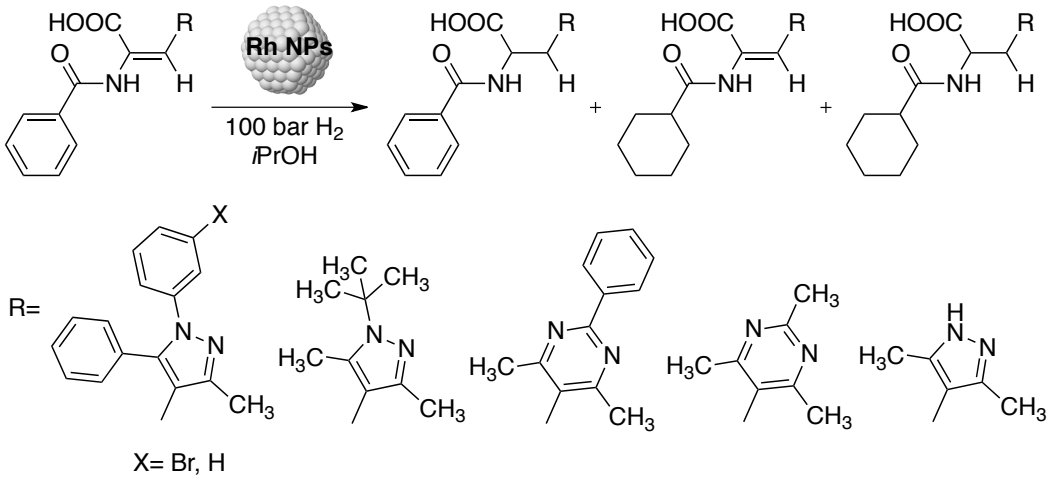

Figure 1. 22. Results reported by Leitner and co-workers for the selective hydrogenation of amides using Rh NPs[120]

As an example of aldehyde reduction, van Leeuwen and co-workers reported the synthesis of air-stable Au NPs stabilized by secondary phosphine oxides by reduction of a dinuclear Au(I)-complex using $NaBH_4$, for their application in the hydrogenation of a number of aldehydes.[121] These Au NPs revealed very active catalysts for the highly chemoselective hydrogenation of substituted aldehydes, obtaining high conversions and selectivities for a broad range of aldehydes bearing different functional groups. Essentially, full chemoselectivity was obtained towards carbonyl reduction for substrates bearing other functionalities such as arene rings, C-C

double and triple bonds and nitro, nitril, pyridine, ketone, carboxylic acid and ester moieties. Some examples of these catalytic results are shown in Figure 1. 23.

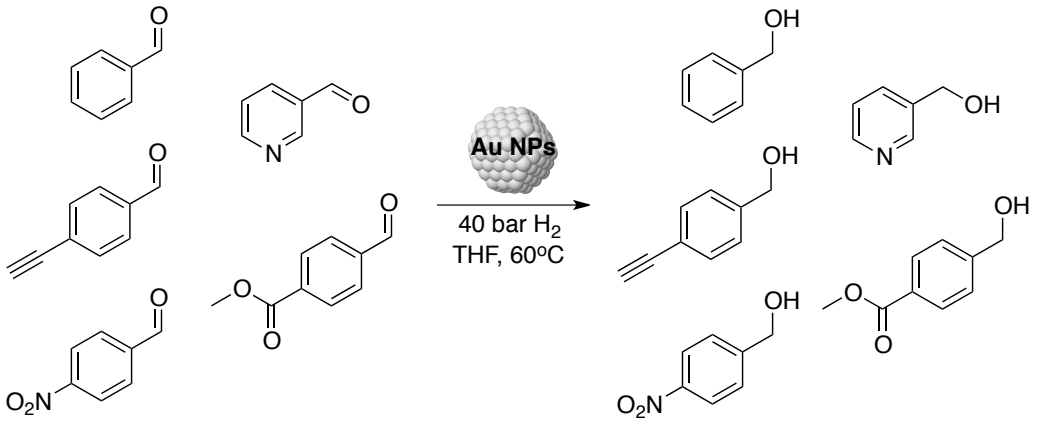

Figure 1. 23. Results reported by Leeuwen and co-workers for the selective hydrogenation of aldehydes using Au NPs[121]

The selective hydrogenation of α,β-unsaturated aldehydes to α,β-unsaturated alcohols is an important step in the preparation of various fine chemicals.[127] The selective reduction of the C=O group, when conjugated to a C=C double bond, is considered a difficult task since several metal catalysts readily reduce the C=C double bond to yield the saturated aldehyde as the main product.[128] In this field, cinnamaldehyde (Figure 1. 24) has become a model substrate.[121,122,123127,129]

In a preliminary study, Pt NPs stabilized by PVP were used for the hydrogenation of cinnamaldehyde and 12% of selectivity at 38% of conversion was obtained towards ketone reduction (formation of cinnamyl alcohol).[129a] An increase in the selectivity up to 99% at 84% of conversion was achieved for the same product using this

catalytic system after addition of $FeCl_3$ or $CoCl_2$ to the reaction mixture. In view of these results, the authors proposed that an interaction between the cation and the oxygen of the carbonyl could facilitate the adsorption of the double bond on the metallic surface and thus increasing the selective reduction of this group.

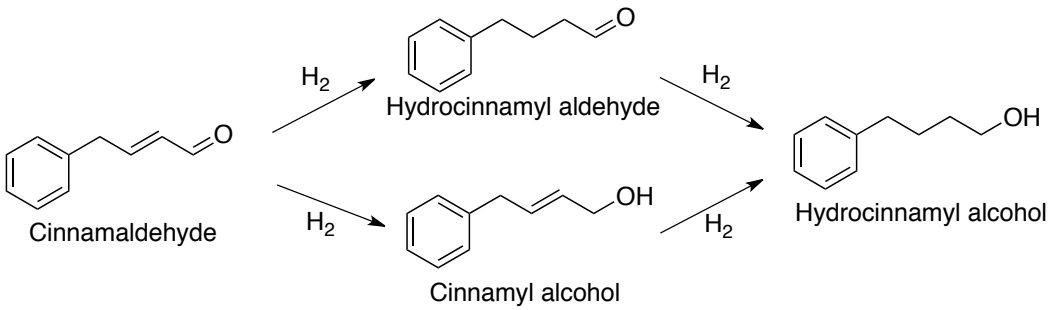

Figure 1. 24. Expected products for the selective hydrogenation of cinnamaldehyde

More recently, very interesting results have been reported where cinnamyl alcohol was formed selectively from cinnamaldehyde with no need of additives.[121,122,129d] For instance, van Leeuwen and co-workers investigated the application of air-stable Au NPs formed by decomposition of Au(I) homogeneous complexes bearing secondary phosphine oxides.[122] These NPs were completely selective to the carbonyl functionality. The hydrogenation of citral was also attempted using this catalytic system, achieving geraniol and nerol (the *cis*- and *trans*-isomers formed by the single reduction of the ketone group) as the only reaction products (Figure 1. 25).

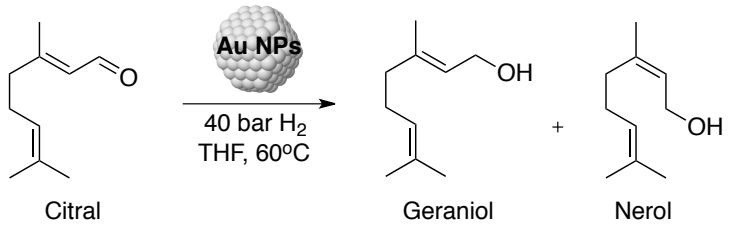

Figure 1. 25. Results reported by Leeuwen and co-workers for the selective hydrogenation of citral using Au NPs[122]

It can be therefore concluded that the use of soluble M-NPs in hydrogenation processes can provide very interesting results in terms of selectivity.

1.4.8. Colloidal M-NPs in H/D exchange reactions

Recently, the application of M-NPs in H/D exchange reactions by C-H activation has been reported.[30] Pd NPs stabilized by 4-dimethylaminopyridine (DMAP)[130] and PVP[131] were used for the selective deuteration of N-containing compounds using D_2O as deuterium source (Figure 1. 26).

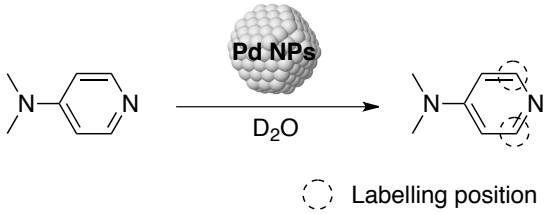

Figure 1. 26. Results reported by Sullivan for the selective deuteration of N-based compounds using Pd NPs[130]

Some years later, Chaudret and co-workers reported a method based on the application of PVP [132,133] (Figure 1. 27a) and NHC[134] stabilized Ru NPs for the selective deuteration of N-containing molecules using

D_2 under mild reaction conditions Later, the application of PVP-stabilized Ru NPs towards the selective deuteration of P-containing compounds was described by our group in collaboration with that of Chaudret (Figure 1. 27b).[135] The results obtained in the selective deuteration of these N- and P- molecules demonstrated the ability of such NPs to activate C-H bonds and provided useful information regarding the coordination mode of these species at metallic surfaces.

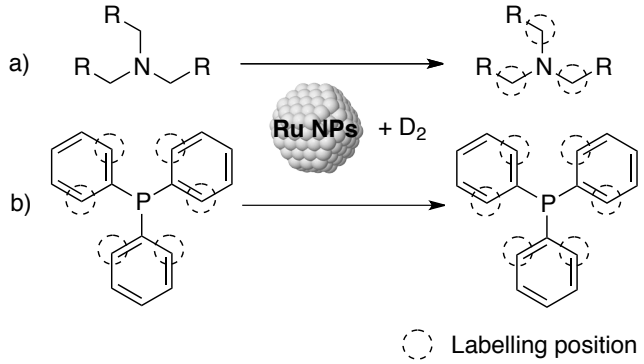

Figure 1. 27. Results reported by (a) Chaudret [132] and (b) our group [135] for the selective deuteration of N- and P-based compounds using PVP-stabilized Ru NPs

This latter aspect is particularly relevant to the work described in this thesis and a more detailed description of the reported results on the selective H/D exchange reaction of N- or P-containing substrates using the nanocatalytic systems will be presented in the introduction of Chapter 5.

In this context, the work described in this thesis deals with the synthesis and characterization of M-NPs stabilized by NHC ligands for their application in selective catalysis, including hydrogenation and H/D exchange reactions.

1.5. References

[1] G. Schmid, in *Nanoparticles: From Theory to Application*, Ed Wiley-VCH, Germany, **2004**, vol.1, ch.2 pp 4-49.

[2] J. D. Aiken III, R. G. Finke, *J. Mol. Catal. A.: Chem.* **1999**, *145*, 1-44.

[3] R. Pool, *Science*, **1990**, *248*, 1186-1188.

[4] P. Wasserscheid, W. Keim, *Angew. Chem. Int. Ed.* **2000**, *39*, 3772-3789.

[5] J. G. de Vries, When Does Catalysis with Transition Metal complexes Turn into Catalysis by Nanoparticles?, in *Selective Nanocatalysts and Nanoscience: Concepts for Heterogeneous and Homogeneous Catalysis*, Ed Wiley-VCH, Germany, **2010**, ch. 3, pp. 73-103.

[6] A. Roucoux, A. Nowicki, K. Philippot, Rhodium and Ruthenium Nanoparticles in Catalysis, in *Nanoparticles and Catalysis Volume I,* Ed Wiley-VCH, Germany, **2008**, ch. 11, pp. 329-386.

[7] L. D. Pachón, G. Rothenberg, *Appl. Organomet. Chem.* **2008**, *22*, 288-299.

[8] K. Philippot, B. Chaudret, *C. R. Chimie* **2003**, *6*, 1019-1034.

[9] A. Roucoux, *Top Organomet. Chem.* **2005**, *16*, 261-279.

[10] D. Astruc, F. Lu, J. R. Aranzaes, *Angew. Chem. Int. Ed.* **2005**, *44*, 7852-7872.

[11] M. T. Reetz, R. Breinbauer, K. Wanninger, *Tetrahedron Lett.* **1996**, *37*, 4499-4502.

[12] P. Migowski, J. Dupont, *Chem. Eur. J.* **2007**, *13*, 32-39.

[13] Z. He, P. Alexandridis, *Phys. Chem. Chem. Phys.* **2015**, 17, 18238-18261.

[14] C. Janiak, *Top. Organomet. Chem.* **2015**, *51*, 17-53.

[15] G. S. Fonseca, A. P. Umpierre, P. F. P. Fichtner, S. R. Teixeira, J. Dupont, *Chem. Eu. J.* **2003**, *9*, 3263-3269.

[16] J. Dupont, P. A. Z. Suarez, *Phys. Chem. Chem. Phys.* **2006**, *8*, 2441-2452

[17] P. Lara, K. Philippot, B. Chaudret, *ChemCatChem* **2013**, *5*, 28-45.

[18] P. J. Dyson, *Dalton Trans.* **2003**, 2964-2974.

[19] G. M. Whitesides, M. Hackett, R. L. Beainard, J. P. M. Lavalleye, A. F. Sowinski, A. N. Izumi, S. S. Moore, D. W. Brown, E. M. Staudt, *Organometallics*, **1985**, *4*, 1819-1830.

[20] F. Novio, D. Monahan, Y. Coppel, G. Antorrena, P. Lecante, K. Philippot, B. Chaudret, *Chem. Eur. J.* **2014**, *20*, 1287-1297.

[21] F. Novio, K. Philippot, B. Chaudret, *Catal. Lett.* **2010**, *140*, 1-7.

[22] M. Gómez, I. Favier, Metal Nanoparticles Dispersed in Solution: Tests to Identify the Catalyst Nature, in *Metal Nanoclusters in Catalysis and Material Science: The issue of size control.* Elsevier, Amsterdam, **2008**, ch. 31, pp. 427-436.

[23] D. J. M. Snelders, N. Yan, W. Gan, G. Laurenczy, P. J. Dyson, *ACS Catal.* **2012**, *2*, 201-207.

[24] J. Ll. Castelbou, E. Bresó-Femenia, P. Blondeau, B. Chaudret, S. Castillón, C. Claver, C. Godard, *ChemCatChem* **2014**, *6*, 3160-3168.

[25] J. Zhang, M. Ibrahim, V. Collière, H. Asakura, T. Tanaka, K. Teramura, K. Philippot, N. Yan, *J. Mol. Catal. A.: Chem.* **2016**, *422*, 188-197.

[26] M. A. Watzky, R. G. Finke, *J. Am. Chem. Soc.* **1997**, *119*, 10382-10400.

[27] K. S. Weddle, J. D. Aiken III, R. G. Finke, *J. Am. Chem. Soc.* **1998**, *120*, 5653-5666.

[28] A. Roucoux, J. Schultz, H. Patin, *Chem. Rev.* **2002**, *102*, 3757-3778.

[29] A. Gual, C. Godard, S. Castillón, D. Curulla-Ferré, C. Claver, *Catal. Today* **2012**, *183*, 154-171.

[30] D. Pla, M. Gómez, *ACS Catal.* **2016**, 3537-3552.

[31] F. Launay, H. Patin, *New J. Chem.* **1997**, *21*, 247-256.

[32] F. Launay, A. Roucoux, H. Patin, *Tetrahedron Lett.* **1998**, 39, 1353-1356.

[33] A. Denicourt-Nowicki, A. Lebedeva, C. Bellini, A. Roucoux, *ChemCatChem* **2016**, *8*, 357-362.

[34] Y. Shiraishi, N. Toshima, *J. Mol. Catal. A.: Chem.* **1999**, *141*, 187-192.

[35] H. Schulz, *Appl. Catal., A* **1999**, *186*, 3-12.

[36] A. Y. Khodakov, R. Bechara, A. Griboval-Constant, *Appl. Catal., A.* **2003**, *254*, 273-288.

[37] J. Kang, K. Cheng, L. Zhang, Q. Zhang, J. Ding, W. Hua, Y. Lou, Q. Zhai, Y. Wang, *Angew. Chem. Int. Ed.* **2011**, *50*, 5200-5203.

[38] J. Kang, S. Zhang, Q. Zhang, Y. Wang, *Angew. Chem. Int. Ed.* **2009**, *48*, 2565-2568.

[39] X.-B. Fan, Z.-Y. Tao, C.-X. Xiao, F. Liu, Y. Kou, *Green Chem.* **2010**, *12*, 795-797.

[40] H. Wang, Y. Kuo, *Chin. J. Catal.* **2013**, *34*, 1914-1925.

[41] J. A. Delgado, S. Castillón, D. Curulla-Ferré, C. Claver, C. Godard, *Catal. Commun.* **2015**, *71,* 88-92.

[42] J. A. Delgado, C. Claver, S. Castillón, D. Curulla-Ferré, C. Godard, *ACS Catal.* **2015**, *5*, 4568-4578.

[43] A. M. Caporusso, N. Panziera, P. Pertici, E. Pitzalis, P. Salvadori, G. Vitulli, G. Martra, *J. Mol. Catal. A.: Chem.* **1999**, *150*, 275-285.

[44] W. Guo, R. Pleixats, A. Shafir, T. Parella, *Adv. Synth. Catal.* **2015**, *357*, 89-99.

[45] M. Tamura, H. Fujihara, *J. Am. Chem. Soc.* **2003**, *125*, 15742-15743.

[46] M. Planellas, W. Guo, F. Alonso, M. Yus, A. Shafir, R. Pleixats, T. Parella, *Adv. Synth. Catal.* **2014**, *356*, 179-188.

[47] J. Huang, Z. Liu, X. Liu, C. He. S. Y. Chow. J. Pan, *Langmuir* **2005** ,*21*, 699-704.

[48] C. Li, D. Li, Z.-S. Zhao, X.-M. Duan, W. Hou, *Colloids Surf., A.* **2010**, *366*, 45-49.

[49] X. Peng, Q. Pan, X. Lu, *J. Appl. Polym. Sci.* **2011**, *122*, 334-341.

[50] A. Balanta, C. Godard, C. Claver, *Chem. Soc. Rev.* **2011**, *40*, 4973-4985.

[51] P. Taladriz-Blanco, P. Hervés, *Top. Catal.* **2013**, *56*, 1154-1170.

[52] E. O. Muimhneahain, G. P. McGlacken, *Organomet. Chem.* **2016**, *40*, 33-53.

[53] M. Beller, H. Fischer, K. Kühlein, C.-P. Reisinger, W. A. Herrmann, *J. Organomet. Chem.* **1996**, *520*, 257-259.

[54] A. M. Trzeiak, J. J. Ziólows, *Coord, Chem. Rev.* **2005**, *249*, 2308-2322.

[55] M. T. Reetz, J. G. de Vries, *Chem. Commun.* **2004**, 1559-1563.

[56] A. H. M. de Vries, J. M. C. A. Mulders, J. H. M. Mommers, H. J. W. Henderickx, J. G. de Vries, *Org. Lett.* **2003**, *5*, 3285-3288.

[57] M. T. Reetz, G. Lohmer, *Chem. Commun.* **1996**, 1921-1922.

[58] Y. Li, X. M. Hong, D. M. Collard, M. A. El-Sayed, *Org. Lett.* **2000**, *2*, 2385-2388.

[59] Y. Li, M. A. El-Sayed, *J. Phys. Chem. B.* **2001**, *105*, 8938-8943.

[60] F. Fernández, B. Cordero, J. Durand, G. Muller, F. Malbosc, Y. Kihn, E. Teuma, M. Gómez, *Dalton Trans.* **2007**, 5572-5581.

[61] J. Durand, E. Teuma, F. Malbosc, Y. Kihn,M. Gómez, *Catal. Commun.* **2008**, *9*, 273-275.

[62] D. Zhao, Z. Frei, T. J. Geldbach, R. Scopelliti, P. J. Dyson, *J. Am. Chem. Soc.* **2004**, *126*, 15876-15882.

[63] J.-T. Lu, J. C. Y. Lin, M.-C. Lin, N. D. Khupse, I. J. B. Lin, *Langmuir* **2014**, *30*, 10440-10448.

[64] Y. Na. S. Park, S. B. Han, H. Han, S. Ko, S. Chang, *J. Am. Chem. Soc.* **2004**, 1*26*, 250-258.

[65] A. V. Gaikward, A. Holuigue, M. B. Thathagar, J. E. ten Elshof, G. Rothenberg, *Chem. Eur. J.* **2007**, *13*, 6908-6913.

[66] Z. Fei, D. Zhao, D. Pieraccini, W. H. Ang, T. J. Geldbach, R. Scopelliti, C. Chiappe, P. J. Dyson, *Organometallics* **2007**, *26*, 1588-1598

[67] A. J. Bruss, M. A. Gelesky, G. Machado, J. Dupont, *J. Mol. Catal. A.: Chem.* **2006**, *252*, 212-218.

[68] D. Han, X. Li, H. Zhang, Z. Liu, G. Hu, C. Li, *J. Mol. Catal. A.: Chem.* **2008**, *283*, 15-22.

[69] M. R. Axet, S. Castillón, C. Claver, K. Philippot, P. Lecante, B. Chaudret, *Eur. J. Inorg. Chem.* **2008**, 3460-3466.

[70] S. E. Lyubimov, E. A. Rastorguev, K. I. Lubentsova, A. A. Korlyukov, V. A. Davankov, *Tetrahedron Lett.* **2013**, *54*, 1116-1119.

[71] M. Guerrero, N. T. T. Chau, S. Noël, A. Denicourt-Nowicki, F. Hapiot, A. Roucoux, E. Monflier, K. Philippot, *Curr. Org. Chem.* **2013**, *17*, 364-399.

[72] D. Wang, D. Astruc, *Chem. Rev.* **2015**, *115*, 6621-6686.

[73] F. Alonso, P. Riente, M. Yus, *Acc. Chem. Res.* **2011**, *44*, 379-391.

[74] F. Alonso, P. Riente, M. Yus, *Tetrahedron,* **2008**, *64*, 1847-1852.

[75] F. Alonso, P. Riente, M. Yus, *Tetrahedron Lett.* **2008**, *49*, 1939-1942.

[76] A. Dhakshinamoorthy, K. Pitchumani, *Tetrahedron Lett.* **2008**, *49*, 1818-1823.

[77] F. Alonso, P. Riente, M. Yus, *Synlett* **2008**, *9*, 1289-1292.

[78] N. M. Patil, M. A. Bhosale, B. M. Bhanage, *RSC Adv.* **2015**, *5*, 86529-86535.

[79] L. Jiang, Z. Zhang, *Int. J. Hydrogen Energy* **2016**, *41*, 22983-22990.

[80] J.-W. Zhang, G.-P. Lu, C. Cai, *Catal. Commun.* **2016**, *84*, 25-29.

[81] W. Li, Y. Wang, P. Chen, M. Zeng, J. Jiang, Z. Jin, *Catal. Sci. Technol.* **2016**, *6*, 7386.

[82] K. Vijayakrishna, K. T. P. Charan, K. Manojkumar, S. Venkatesh, N. Pothanagandhi, A. Sivaramakrishna, P. Mayuri, A. S. Kumar, B. Screedhar, *ChemCatChem*, **2016**, *8*, 1139-1145.

[83] J. F. Sonnenberg, N. Coombs, P. A. Dube, R. H. Morris, *J. Am. Chem. Soc.* **2012**, *134*, 5893-5899.

[84] L. O. Nindakova, N. M. Badyrova, V. V. Smirnov, S. S. Kolesnikov, *J. Mol. Catal. A.: Chem.* **2016**, *420*, 149-158.

[85] A. Gual, C. Godard, S. Castillón, C. Claver, *Dalton Trans.* **2010**, *39*, 11499-11512.

[86] A. Roucoux, J. Schulz, H. Patin, *Adv. Synth. Catal.* **2003**, *345*, 222-229.

[87] L. M. Rossi, G. Machado, *J. Mol. Catal. A.: Chem.* **2009**, *298*, 69-73.

[88] C. Zhao, H.-Z. Wang, N. Yan, C.-X. Xiao, X.-D. Mu, P. J. Dyson, Y. Kou, *J. Catal.* **2007**, *250*, 33-40.

[89] A. Gual, C. Godard, K. Philippot, B. Chaudret, A. Denicourt-Nowicki, A. Roucoux, S. Castillón, C. Claver, *ChemSusChem*, **2009**, *2*, 769-779.

[90] J. Ll. Castelbou, A. Gual, E. Mercadé, C. Claver, C. Godard, *Catal. Sci. Technol*. **2013**, *13*, 2828- 2833

[91] E. Bresó-Femenia, B. Chaudret, S. Castillón, *Catal. Sci. Technol.* **2015**, *5*, 2741-2751.

[92] V. Mévellec, A. Roucoux, *Inorg. Chim. Acta* **2004**, *357*, 3099-3103.

[93] M. Fang, N. Machalaba, R. A. Sánchez-Delgado, *Dalton Trans.* **2011**, *40*, 10621-10632.

[94] U. Schuchardt, D. Cardoso, R. Sercheli, R. Pereira, R. S. da Cruz, M. C. Guerreiro, D. Mandellif, E. V. Spinacé, E. L. Pires, *Appl. Catal. A.* **2001**, *211*, 1-17.

[95] *World Nylon 6 & 66 Supply/Demand Report*, PCI-Fibers & Raw Materials, Seaford, UK, **1998**.

[96] A. Nowicki, Y. Zhang, B. Léger, J-P. Rolland, H. Bricout, E. Monflier, A. Roucoux, *Chem. Commun*., **2006**, 296-298

[97] M. Guerrero, A. Roucoux, A. Denicourt- Novicki, H. Bricout, E. Monflier, V. Collière, K. Fajerwerg, K. Philippot, *Catal. Today* **2012**, *183*, 34-41

[98] P. Lara, T. Ayvali, M.-J. Casanove, P. Lecante, A. Mayoral, P.- F. Fazzini, K. Philippot, B. Chaudret, *Dalton Trans.* **2013**, *42*, 372-382

[99] M. Jahjah, Y. Kihn, E. Teuma, M. Gomez, *J. Mol. Catal. A.: Chem.* **2010**, *332*, 106-112

[100] X. Yang, N. Yan, Z. Fei, R. M. Crespo- Quesada, G. Laurency, L. Kiwi-Misker, Y. Kou, Y. Li, P. Dyson, *J. Inorg. Chem*. **2008**, *47*, 7444-7446

[101] V. Mervellec, B. Leger, M. Mauduit, A. Roucoux, *Chem. Commun*. **2005**, 2838-2839

[102] B. Leger, A. Denicourt- Nowicki, H. Olivier- Bourbigou, A. Roucoux, *Inorg. Chem*. **2008**, *47*, 9090- 9096

[103] C.-H. Yen, H.-H. Wei, H.-W. Lin, C.-S. Tan, *Appl. Organomet. Chem*. **2012**, *26*, 736-742

[104] M. R. Nabid, N. Nazari, S. Asadi, M. M. Heravi R. Sedghi, *Curr. Org. Chem.* **2016**, *20*, 696-734.

[105] S. Cai, H. Duan, H. Rong, D. Wang, L. Li, W. He, Y. Li, *ACS Catal.* **2013**, *3*, 608-612.

[106] M. A. Harrad, B. Boualy, L. E. Firdoussi, A. Mehdi, C. Santi, S. Giovagnoli, M. Nocchetti, M. A. Ali, *Catal. Coomun.* **2013**, *32*, 92-100.

[107] A. Ferry, K. Schaepe, P. Togeder, C. Richter, K. M. Chepiga, B. J. Ravoo, F. Glorius, *ACS Catal.* **2015**, *5*, 5414-5420.

[108] Y. Lee, S. Jang, C.-W. Cho, J.-S- Bae, S. Park, K. H. Park, *J. Nanosci. Nanotechnol.* **2013**, *13*, 7477-7481.

[109] H.-Y. Jiang, X.-X. Zheng, *Appl. Catal. A.* **2015**, *499*, 118-123.

[110] D. Gonzalez-Galvez, P. Lara, O. Rivada-Wheelaghan, S. Conejero, B. Chaudret, K. Philippot, P. W. N. M. van Leeuwen, *Catal. Sci. Technol.* **2013**, *3*, 99-105.

[111] Md. J. Sharif, P. Maity, S. Yamazoe, T. Tsukuda, *Chem. Lett*. **2013**, *42*, 1023-1025

[112] I. Cano, L. M. Martínez-Prieto, B. Chaudret, P. W. N. M. van Leeuwen, *Chem. Eur. J.* **2017**, *23*, 1444-1450.

[113] X. Yuan, N. Yan, C. Xiao, C. Li, Z. Fei, Z. Cai, Y. Kou, P. J. Dyson, *Green Chem.* **2010**, *12*, 228-233.

[114] P. Lara, A. Suárez, V. Collière, K. Philippot, B. Chaudret, *ChemCatChem* **2014**, *6*, 87-90.

[115] M. Liu, J. Zhang, J. Liu, W. W. Yu, *J. Catal.* **2011**, *278*, 1-7.

[116] a) Y.-Z. Xiang, Y.-A. Lv, T.-Y. Xu, X.-N. Li, J. -G. Wang, *J. Mol. Catal. A: Chem.* **2011**, *351*, 70-75. b) A. Denicourt-Nowicki, B. Léger, A. Roucoux, *Phys.*

Chem. Chem. Phys. **2011**, *13*, 13510-13517. c) E. Rafter, T. Gutmann, F. Löw, G. Buntkowsky, K. Philippot, B. Chaudret, P. W. N. M. van Leeuwen *Catal. Sci. Technol.* **2013**, *3*, 595-599. d) l. Song, X. Li, H. Wang, *Catal. Lett.* **2009**, *133*, 63-69. e) N. T. T. Chau, S. Handjani, J.-P. Guegan, M. Guerrero, E. Monflier, K. Philippot, A. Denicourt-Nowicki, A. Roucoux, *ChemCatChem* **2013**, *5*, 1497-1503. f) I. S. Park, M. S. Kwon, K. Y. Kang, J. S. Lee, J. Park *Adv. Synth. Catal.* **2007**, *349*, 2039-2047. g) J. A. Anderson, A. Athawale, F. E. Imrie, F.-M. McKenna, A. McCue, D. Molyneux, K. Power, *J. Catal.* **2010**, *270*, 9-15. h) L. M. Martinez-Prieto, A. Ferry, P. Lara, C. Richter, K. Philippot, F. Glorius, B. Chaudret, *Chem. Eur. J.* **2015**, *21*, 17495-17502.

[117]F. Jutz, J.-M. Andanson, A. Baiker, *J. Catal.* **2009**, *268*, 256-266.

[118] G. S. Fonseca, J. D. Scholten, J. Dupont, *Synlett* **2004**, *9*, 1525-1528.

[119] R. J. Bonilla, B. R. James, P . G. Jessop, *Chem. Commun.* **2000**, 941-942.

[120] V. Cimpeanu, M. Kocevar, V. I. Parvulescu, W. Leitner, *Angew. Chem. Int. Ed.* **2009**, *48*, 1085-1088.

[121] I. Cano, A. M. Chapman, A. Urakawa, P. W. N. M. Leeuwen, *J. Am. Chem. Soc.* **2014**, *136*, 2520-2528.

[122] I. Cano, M. A. Huertos, A. M. Chapman, G. Buntkowsky, T. Gutmann, P. B. Groszewicz, P. W. N. M. van Leeuwen, *J. Am. Chem. Soc.* **2015**, *137*, 7718-7727.

[123] H. Jeong, C. Kim, S. Yang, H. Lee, *J. Catal.* **2016**, *344*, 609-615.

[124] W. Yu, H. Liu, M. Liu, Z. Liu, *React. Funct. Polym.* **2000**, *44*, 21-29.

[125] W. Yu, M. Liu, X. Ma, Z. Liu, *J. Colloid Interface Sci.* **1998**, *208*, 439-444.

[126] a) F. A. Khan and G. Süss-Fink *Eur. J. Inorg. Chem.* **2012**, 727-732. b) W.W. Yu, H. Liu *J. Mol. Catal. A.: Chem.* **2006**, *243*, 120–141. c) W. Yu, H. Liu, M. Liu, Z. Liu, *React. Funct. Polym.* **2000**, *44*, 21–29. d) J. Julis, M. Holscher, W. Leitner *Green Chem.* **2010**, *12*, 1634-1639. e) A. Pournara, D. Kovala-Demertzi,, N. Kourkoumelis, S. Georgakopoulos, I. D. Kostas *Catal. Commun.*

2014, *43*, 57–60. f) Z. Ming, M. Xindong, Y. Ning, K. Yuan *Chin. J. Catal.* **2007**, *28*, 389–391.

[127] W.-Y. Yu, Y. Wang, H.-F. Liu, W. Zheng, *Polym. Adv. Technol.* **1996**, *7*, 719-722.

[128] B. Sen, M. A. Vannice, *J. Catal.* **1989**, *115*, 65-78.

[129] a) W. Yu, H. Liu, Q. Tao, *Chem. Commun.* **1996**, 1773-1774. b) W. Yu, Y. Wang, H. Liu, W. Zheng, *J. Mol. Catal. A.: Chem.* **1996**, *112*, 105-113. c) M. G. Prakash, R. Mahalakshmy, K. R. Krishnamurthy, B. Viswanathan, *Catal. Today* **2016**, *263*, 105-111. d) C. Dietrich, D. Schild, W. Wang, C. Kübel, S. Behrens, *Z. Anorg. Allg. Chem.* **2017**, *643*, 120-129.

[130] J. A. Sullivan, K. A. Flanagan, H. Hain, *Catal. Today* **2008**, *139*, 154-160.

[131] K. A. Guy, J. R. Shapley, *Organometallics* **2009**, *28*, 4020-4027.

[132] G. Pieters, . Taglang, E. Bonnefille, T. Gutmann, C. Puente, J.-C. Berthet, C. Dugave, B. Chaudret, B. Rousseau, *Angew. Chem. Int. Ed.* **2014**, *53*, 230-234.

[133] C. Taglang, L. M. Martínez-Prieto, I. del Rosal, L. Maron, R. Poteau, K. Philippot, B. Chaudret, S. Perato, A. S. Lone, C. Puente, C. Dugave, B. Rousseau, G. Pieters, *Angew. Chem. Int. Ed.* **2015**, *54*, 10474-10477.

[134] L. M Martínez-Prieto, E. A. Baquero, G. Pieters, J. C. Flores, E. de Jesús, C. Nayral, F. Delpech, P. W. N. M. van Leeuwen, G. Lippens, B. Chaudret, *Chem. Commun.*, 2017, *53*, 5850-5853.

[135] E. Bresó-Femenia, C. Godard, C. Claver, B. Chaudret, S. Castillón, *Chem. Commun.* **2015**, *51*, 16342-16345.

Chapter 2

Objectives

2.1. Objectives of the thesis

The work described in this thesis deals with the synthesis and characterization of Rh NPs stabilized by NHCs for their use in selective catalytic processes such as hydrogenation and H/D exchange reactions of different substrates.

The main objectives of this work can be thus summarized as follow:

- Chapter 3: Synthesis and characterization of Rh NPs stabilized by NHCs, followed by study of the availability of catalytic sites at the surface of these Rh NPs by CO adsorption experiments (Figure 2. 1).

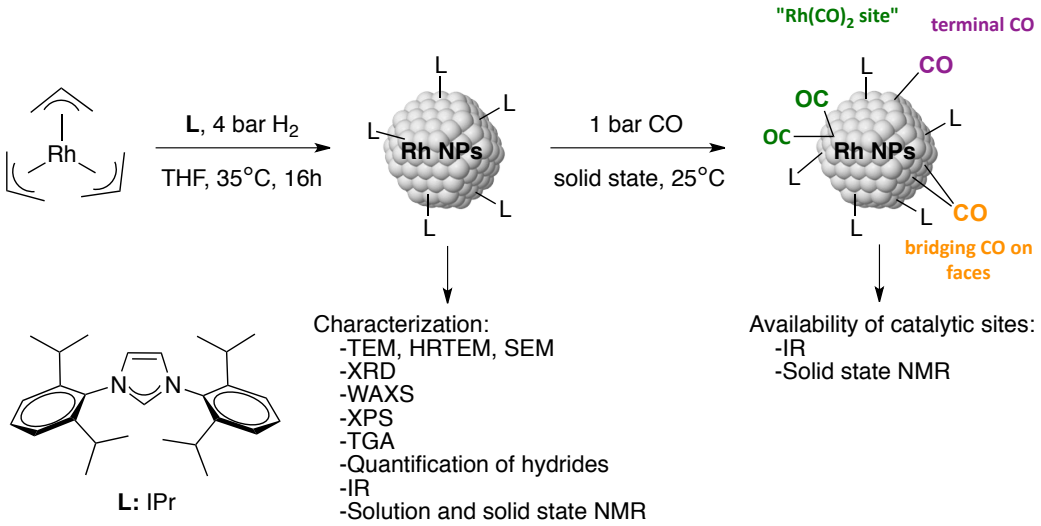

Figure 2. 1. Schematic representation of the synthesis and characterization of Rh NPs stabilized by NHCs

- Chapter 4: Study the catalytic performance (activity and selectivity) of Rh NPs in the selective hydrogenation of aromatic ketones, phenols and N-heteroaromatic compounds such as pyridines and quinoline (Figure 2. 2).

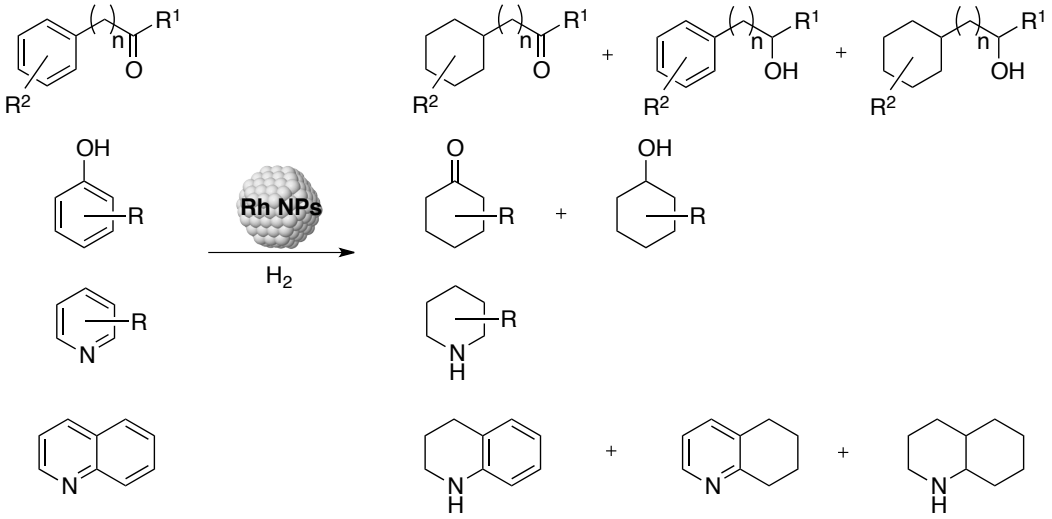

Figure 2. 2. Schematic catalytic hydrogenation of aromatic ketones, phenols, pyridines and quinoline using NHC-stabilized Rh NPs

- Chapter 5: Study the coordination mode of P-based ligands (Figure 2. 3) at the surface of Rh NPs by H/D exchange reactions using D_2 as deuterium source under mild reaction conditions. Furthermore, another objective of this chapter is to compare the catalytic performance of several M-NPs to get insights into the effects of: the nature of the M (Ru *vs*. Rh), the stabilizer (PVP *vs*. IPr) and the structure of the P-based substrates.

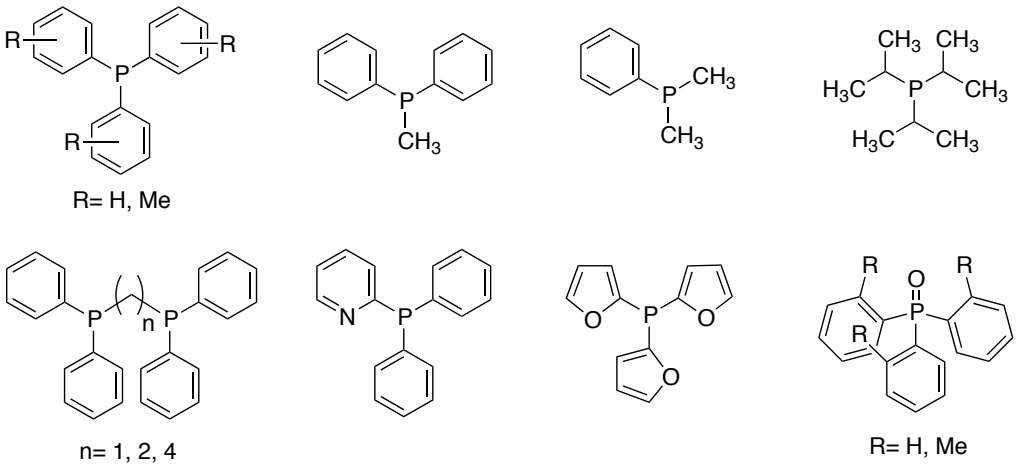

Figure 2. 3. Substrates of study in the H/D exchange reaction using Rh and Ru NPs stabilized by PVP or NHCs

Chapter 3

Synthesis and characterization of Rh NPs stabilized by IPr

3.1. Introduction

3.1.1. Stabilizing agents used for the formation of Rh NPs

Several studies on the synthesis and characterization of colloidal Rh NPs were reported using different stabilizing agents and were mainly based on the reduction of metal salts or metallic precursors using reducing agents such as H_2 or $NaBH_4$.[1] Among the different stabilizing agents used for the preparation of colloidal Rh NPs, compounds such as ionic liquids, polymers or ligands containing N or P-donor atoms were utilized.

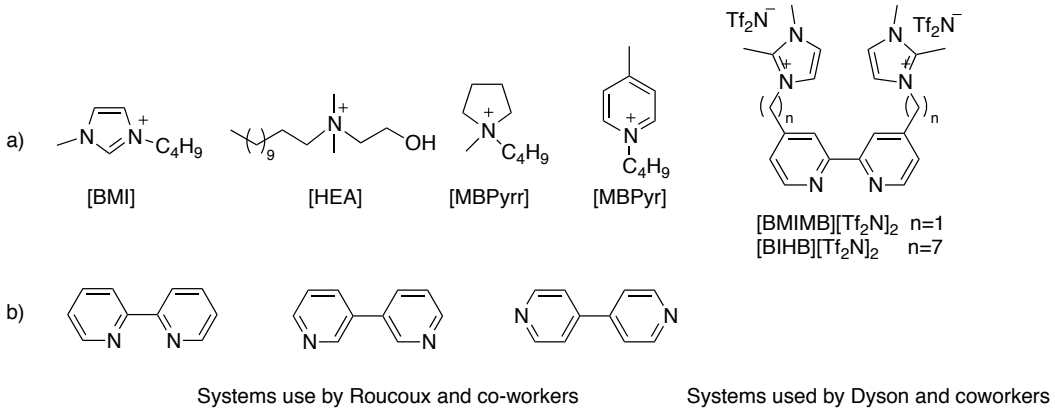

Figure 3. 1. (a) Ionic liquids[4,56] and (b) bipyridine compounds used for the stabilization of Rh NPs[4,5]

Ionic liquids

Ionic liquids (ILs) revealed interesting protecting agents for the stabilization of NPs because of the ability of these compounds to play the dual role of solvent and stabilizing agent.[2,3] As an example, Roucoux and co-workers reported the preparation of Rh NPs by reduction of $RhCl_3$ with $NaBH_4$ in the presence of bipyridine and ILs

(Figure 3. 1a).[4,5] The synthesis was performed under aerobic conditions at room temperature, obtaining small NPs of *ca*. 2-2.5 nm in diameter. The catalytic activity of these Rh NPs was evaluated in the hydrogenation of various aromatic compounds in various ILs.

A similar approach was reported by Dyson and co-workers a few years later using ILs containing imidazolium groups modified with pyridines as stabilizers (Figure 3. 1b).[6] The application in catalysis of the resulting Rh systems was described and correlated to the steric and electronic effects of the modified ligands. Functionalization showed to increase the activity of these Rh NPs in the hydrogenation of arenes and also in the retention of the NPs in the reaction medium during product extraction.

The stabilization of Rh NPs in the presence of phosphine functionalized ionic liquids (PFILs) was also reported.[7] These Rh NPs were synthesized by reduction of $Rh(\eta^3\text{-}C_3H_5)_3$ under H_2 in the presence of the corresponding PFIL (Figure 3. 2) and were found to be active in the biphasic catalytic hydrogenation of toluene, styrene and xylenes under mild conditions. More recently, Rh NPs stabilized in ILs were also reported as active catalysts for the selective reductive cleavage of C-O and hydrodeoxygenation of lignin model compounds.[8]

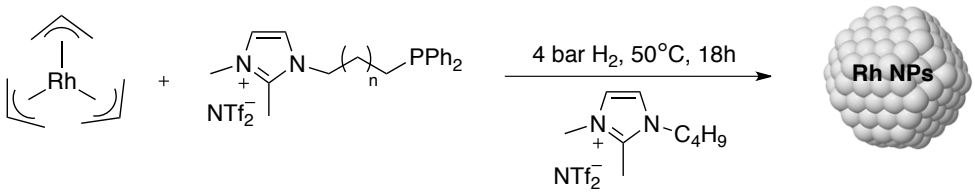

Figure 3. 2. Synthetic strategy reported by Zhang and co-workers for the formation of Rh NPs stabilized by phosphine- functionalized ionic liquids[7]

Polymers

Polymers provide stabilization for metal NPs through the steric bulk of their framework, but also by weakly binding to the NPs surface through heteroatoms. Polyvinylpyrrolidone (PVP) (Figure 3. 3a) is the most used ligand because it fulfil both steric and binding requirements.[9,10,11,12]

In 2007, Kou and co-workers investigated the modification of PVP by the introduction of an imidazolium salt group, for the formation of an ionic-liquid-like copolymer that could be used for the formation of Rh NPs (Figure 3. 3b).[13] The resulting Rh NPs exhibited a mean diameter of 3 nm and were highly active catalysts in the hydrogenation of arenes. Moreover, when the deactivation of these NPs was examined by CO adsorption/ IR experiments, a direct correlation between the activity of the catalyst and the availability of catalytic sites at the Rh surface was observed.

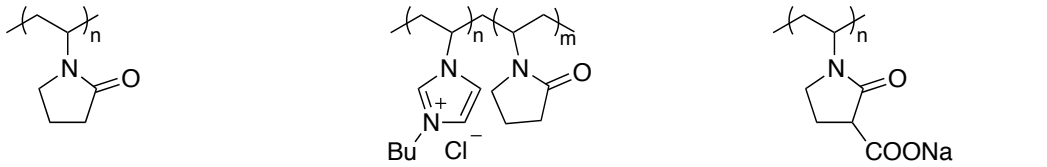

a) PVP

b) IL modified PVP poly[NVP-*co*-VBIM]Cl

c) Carboxylic acid modified PVP

Figure 3. 3. Molecular structures of polymeric compounds used for the stabilization of Rh NPs

In 2011, Dyson and co-workers reported the synthesis of Rh NPs stabilized by a PVP-derived polymer bearing a carboxylate group in its structure (Figure 3. 3c).[14] The formation of these NPs was carried out by reduction of $RhCl_3$ with $NaBH_4$ in the presence of the corresponding PVP-derived polymer. The thermal stability of the resulting Rh NPs was examined, displaying superior behaviour than those of the unfunctionalised PVP-stabilized Rh nanocatalysts.

More recently, the synthesis of Rh NPs stabilized by PVP has been reported by Philippot and co-workers for their application in the chemoselective hydrogenation of arenes.[15] The surface modification of the PVP stabilized Rh NPs via the introduction of NiO_x was reported. In contrast to PVP stabilized Rh NPs, the resulting NiO_x/Rh NPs, revealed efficient catalysts for C-O bond hydrogenolysis without hydrogenating benzene rings, which is crucial for lignin conversion under hydrogen treatment.[16]

Ligands

The application of ligands for NPs stabilization is of special interest because it focuses on the precise molecular definition of the nanocatalytic materials. This strategy potentially allows the fine

tuning of the parameters that govern the efficiency of NPs when applied in a catalytic reaction.[9] Among ligands, phosphorus containing molecules such as phosphites and phosphines have been extensively applied in homogeneous catalysis due to their strong coordinating nature to transition metals. Indeed, the possibility to fine-tune the electronic and steric properties of the metal catalyst through structural modifications of these ligands was found to have an effect on the performance of the catalyst, resulting in high activities and selectivities in several catalytic processes.[17] In the last decade these ligands have also been reported to allow stabilization of metal NPs, which are applied as catalysts in many catalytic reactions.[1,18]

In 2008, Chaudret, Claver and co-workers reported the organometallic synthesis of Rh NPs in the presence of chiral diphosphite ligands derived from carbohydrates.[19] These Rh NPs were obtained by decomposition of two different Rh precursors, $Rh(\eta^3\text{-}C_3H_5)_3$ and $[Rh(\mu\text{-}OMe)(COD)]_2$, under at H_2 atmosphere. The resulting Rh NPs were characterized by TEM, WAXS and elemental analysis, observing a clear dependence of the shape, size and dispersion of the resulting NPs on the metal precursor used. When these Rh systems were tested in the asymmetric hydroformylation of styrene, the formation of molecular species was detected by NMR techniques during the course of the catalytic reaction, suggesting that these NPs could act as a reservoir for molecular catalysts.

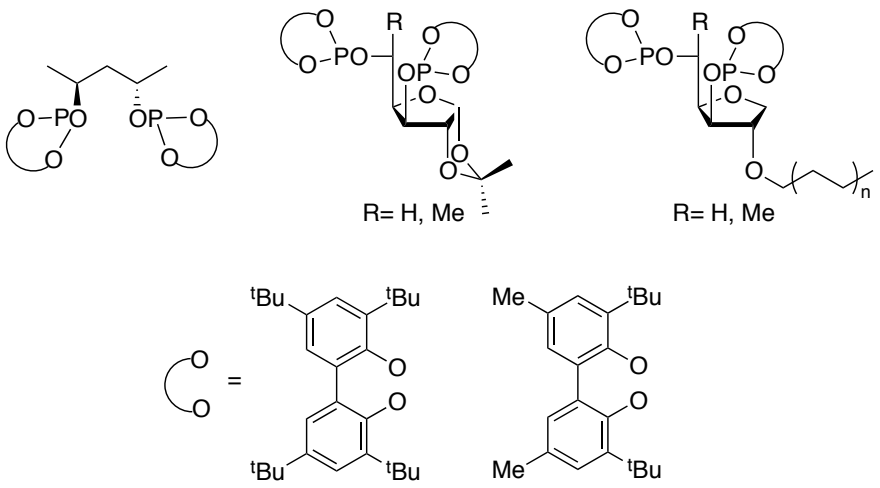

Figure 3. 4. 1,3-diphosphite ligands reported by Chaudret, Claver and co-workers for the stabilization of Rh NPs[20]

One year later, the same groups examined the use of similar 1,3-diphosphite ligands derived from carbohydrates (Figure 3. 4) as stabilizers for Rh NPs and their application in the catalytic hydrogenation of prochiral monocyclic arenes.[20] A comparative study in terms of catalytic activity and selectivity between these Rh, Ru and Ir NPs stabilized by the same ligands was performed. These NPs showed to be active in the hydrogenation of *m*- and *o*-methylanisole. The order of activity was Rh>Ru>Ir, achieving in all cases high *cis*-selectivity. The structure of the stabilizing ligand also showed to have a drastic effect on the catalytic activity of these hydrogenation reactions. However, low or no ee was obtained in all cases.

In terms of Rh NPs stabilized by phosphine ligands, Li and co-workers reported the chemical reduction of $RhCl_3$ by $NaBH_4$ employing the chiral (*R*)-BINAP ligand as stabiliser in the presence of the tetraoctylammonium bromide salt (TOAB) (Figure 3. 5).[21] These

systems were used in the asymmetric hydroformylation of styrene and vinyl acetate, obtaining enantioinduction in some cases. Although the authors assumed that a heterogeneous process was taking place, Philippot and co-workers proposed the formation of molecular species acting as the real catalysts for these systems.[22]

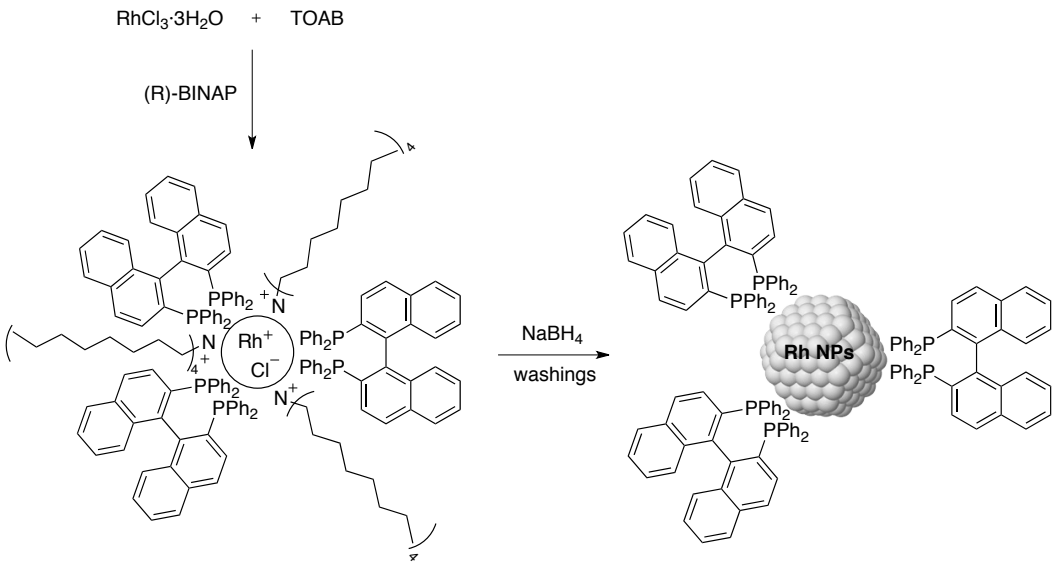

Figure 3. 5. Synthetic strategy reported by Li and co-workers for the formation of Rh NPs stabilized by (R)-BINAP[21]

Jin and co-workers investigated the formation of Rh NPs stabilized by the thermoregulated ligand $Ph_2P(CH_2CH_2O)_nCH_3$ (n=16) from $RhCl_3$ under H_2 using a mixture of 1-butanol/water as solvent.[23] These types of ligands allow the transfer of the system from aqueous phase to 1-butanol phase and vice versa by means of temperature variation, which was thought to be useful in terms of product separation and recycling of the nanocatalyst.

In 2009, Masdeu-Bultó and co-workers reported the synthesis of Rh NPs stabilized by commercially available PPh_3 and its fluorinated

derivatives with the aim of increasing the affinity of the metallic NPs to $scCO_2$.[24] The precursor $[Rh(\mu\text{-}OMe)(COD)]_2$ was decomposed under H_2 in the presence of the corresponding phosphine ligand and the resulting Rh NPs were characterized by TEM, revealing systems of *ca*. 2 nm with tendency to agglomerate. These NPs were used as catalysts for the hydrogenation of substrates containing aromatic groups using $scCO_2$ and THF as solvents, showing different activities related with solubility issues. Moreover, the selectivity obtained when employing these systems revealed the strong coordination between the phenyl moieties of the substrates and the surface of the NPs.

In 2010, an interesting study involving the application of water-soluble sulfonated phosphines used as additives for the modification of the surface state of PVP stabilized Rh NPs was reported by Dyson and co-workers (Figure 3. 6).[25] The sulfonated phosphines were added after formation of Rh NPs by alcoholic reduction in the presence of PVP. Then, the effect of the presence of these phosphine ligands at the surface of these NPs was examined by CO adsorption IR spectroscopy, and revealed site blocking at the surface of the NPs. These phosphines also showed to have an effect when the NPs were applied in the hydrogenation of phenyl acetone, preventing binding of the substrate molecules to certain sites of the NPs surface, which resulted in lower conversions but higher selectivities towards the reduction of the arene ring over the ketone.

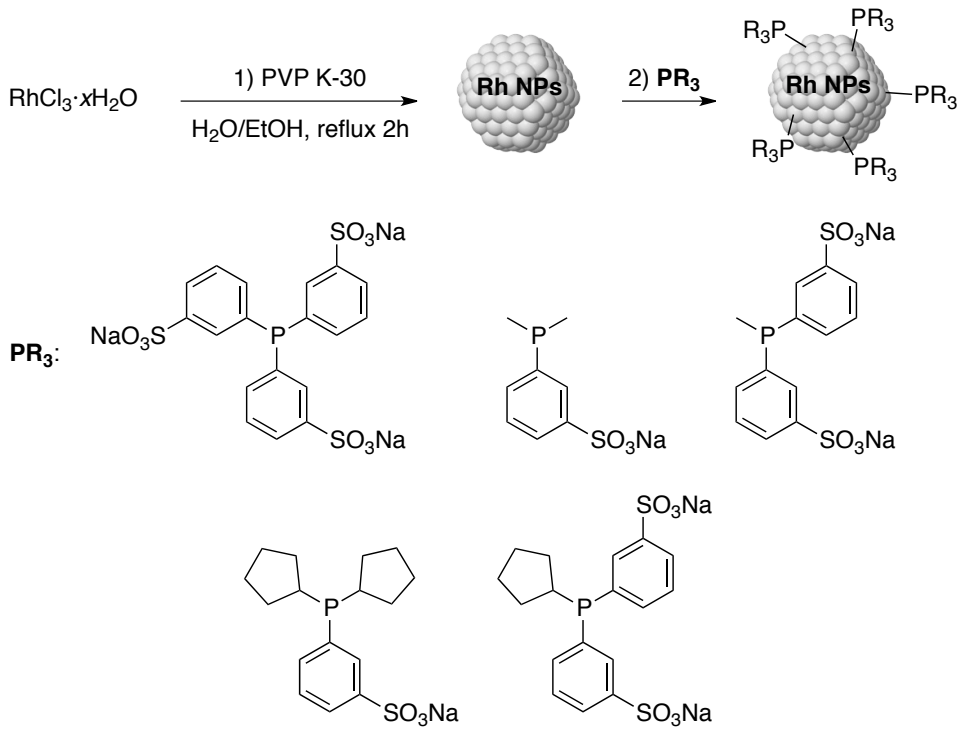

Figure 3. 6. Synthetic strategy reported by Dyson and co-workers for the formation of Rh NPs stabilized by sulfonated phosphines[25]

More recently, the synthesis of Rh NPs stabilized by P-donors such as a mono- and diphosphine and a mono- and a diphosphite has also been investigated by our group (Figure 3. 7).[26] Rh NPs of *ca*. 1.6 nm were formed by the reduction of $Rh(\eta^3\text{-}C_3H_5)_3$ under H_2 in the presence of the corresponding P-donor ligands and the activity of these nanocatalysts was examined in the hydrogenation of styrene and the partial hydrogenation of substituted arenes. The effect of the [L]/[Rh] molar ratio used for the synthesis of Rh NPs stabilized by PPh_3 and $P(OPh)_3$ on the size and distribution of the NPs was examined.[27] The analysis of the surface of these NPs by CO adsorption IR spectroscopy revealed the availability of faces, edges and apexes where catalytic reactions could take place. Moreover,

application of Rh NPs stabilized by PPh_3 and dppb in the selective hydrogenation of aromatic ketones was also reported, which showed that the coordination of the arene dominates the interaction of the substrate with the surface of the NPs, whereas the coordination of the ketone group was not evidenced.[28]

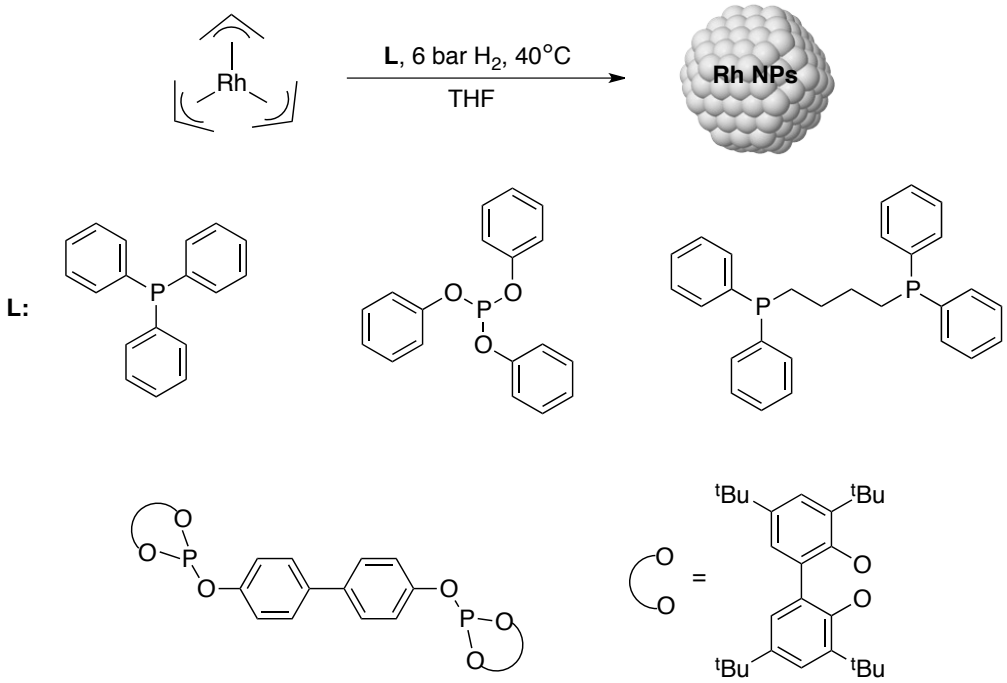

Figure 3. 7. Phosphine and phosphite ligands reported by Godard and co-workers for the stabilization of Rh NPs[26]

More recently, Philippot and co-workers also investigated the synthesis of Rh NPs stabilized by PPh_3 and dppb by reduction of $Rh(\eta^3\text{-}C_3H_5)_3$ under H_2.[29] The surface properties of these nanocatalysts were compared using a model catalysis reaction namely, hydrogenation of cyclohexene, first under colloidal conditions and then under supported conditions after their

immobilization onto an amino functionalized silica-coated magnetite support.

3.1.2. N-Heterocyclic Carbene stabilized M-NPs

Among ligands, N-Heterocyclic Carbenes (NHCs) constitute an interesting class of stabilizers owing to their high electron-donating properties, which allow them to form very strong bonds to transition metals.[30] Since NHCs only contain C, H and N atoms, they cannot be oxidized as happens with other ligands such as phosphines, which have been widely used for the stabilization of metal NPs.[24,26,27,31,32,33] Indeed, NHCs are easily tuneable ligands, which steric hindrance and electronic properties can be modified through simple modification of their substituents. For these reasons, NHCs have been considered an essential class of ligands during the last years, being used for the formation of Ru, Pt, Pd, Au, Ag and Ni NPs.

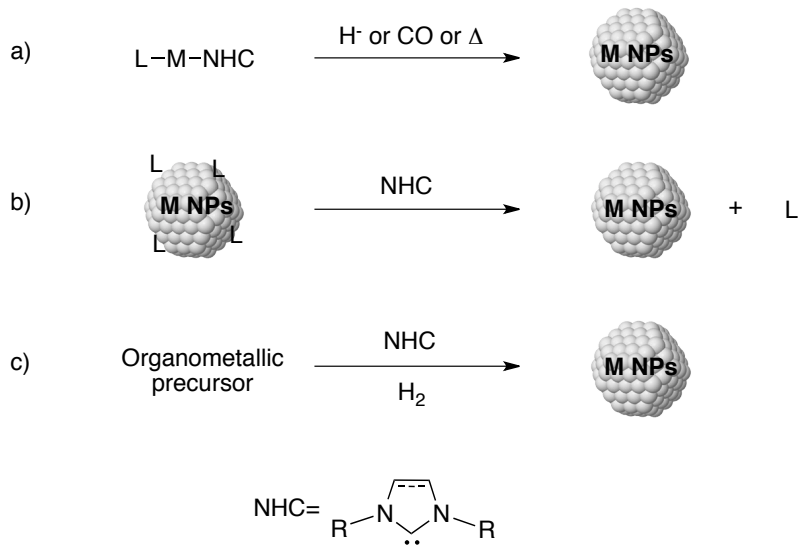

Figure 3. 8. Strategies followed for the formation of NHC-stabilized metal NPs

Several strategies have been followed for obtaining metal NPs bearing NHCs as stabilizers: by direct reduction or decomposition of organometallic complexes bearing the NHCs (Figure 3. 8a), by ligand exchange (Figure 3. 8b) and by the organometallic approach (Figure 3. 8c), based on the stabilization of metal NPs starting from an organometallic precursor[34,35]. However, other methods based on the modification of the surface from already stabilized metal NPs via the addition of imidazolium salts under basic conditions also revealed efficient for the tuning of the catalytic performance of the final catalyst. As an example, Glorius and co-workers reported the application of Pd NPs on magnetite (Fe_3O_4) modified by chiral NHCs for their application in asymmetric catalysis.[36] These Pd NPs showed to be catalytically active towards the asymmetric α-arylation of ketones with aryl halides, achieving up to 85% *ee*.

The synthesis of metal NPs by decomposition of metallic complexes bearing NHCs was reported for Pt, Pd, Au and Ag NPs. In 2014 Chaudret and co-workers reported the use of sulfonated NHC ligands for the stabilization of Pt NPs.[37] These NPs were formed by thermal decomposition of a preformed molecular Pt complex containing the desired sulfonated ligand (Figure 3. 9). These NPs of 1.3 – 2 nm, which were purified by dialysis using a regular cellulose membrane, were soluble in water and stable under air for an indefinite period of time. ^{13}C solid state NMR studies showed the coordination of the NHC ligand to the surface of the Pt NPs through the carbenic carbon and allowed the determination of the ^{13}C-^{195}Pt coupling constant ($^1J_{Pt\text{-}C}$= 940 Hz) for the first time in a nanosystem.

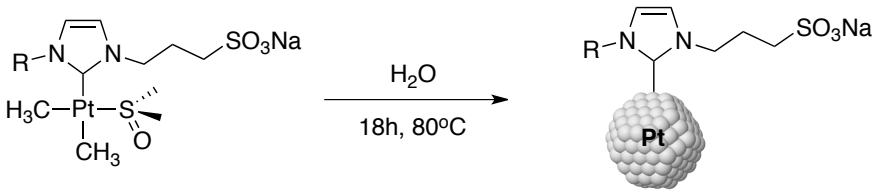

Figure 3. 9. Synthetic strategy reported by Chaudret and co-workers for the formation of Pt NPs stabilized by sulfonated NHCs[37]

More recently, a similar procedure based on the thermal decomposition of a Pd complex bearing a similar sulfonated NHC ligands was also followed for the formation of water soluble Pd NPs of 4.6 – 3 nm.[38] The formation of NPs by reduction of the metallic complex using CO was also attempted leading to the formation of smaller Pd NPs of 1.3 ± 0.3 nm. When Pd NPs of 3.7 nm were analysed by ^{13}C NMR spectroscopy, the observation of Knight Shift in the ^{13}C resonance of the carbonic carbon confirmed the coordination of NHC ligands at the NPs surface.

The synthesis of Au and Ag NPs by reduction of Au(I) complexes, bearing different NHC ligands, using $KBEt_3H$, [39] NH_3BH_3 or tBuNH$_2$BH$_3$[40] as reducing agents has also been reported. Besides, a modified procedure for the formation of Pd and Au NPs starting from the bis(hexyl)imidazolium metallate Pd and Au complex was also described.[41] The NHC-stabilization of these NPs was obtained by deprotonation of the imidazolium cation by reacting the imidazolium salt with NaH, before adding $NaBH_4$ to reduce the metals for the formation of Au and Pd NPs (Figure 3. 10a). On the other hand, the direct $NaBH_4$ reduction of the metallate bearing the imidazolium salt

was also tested, showing the formation of Pd NPs stabilized by the imidazolium cations in this case (Figure 3. 10b).

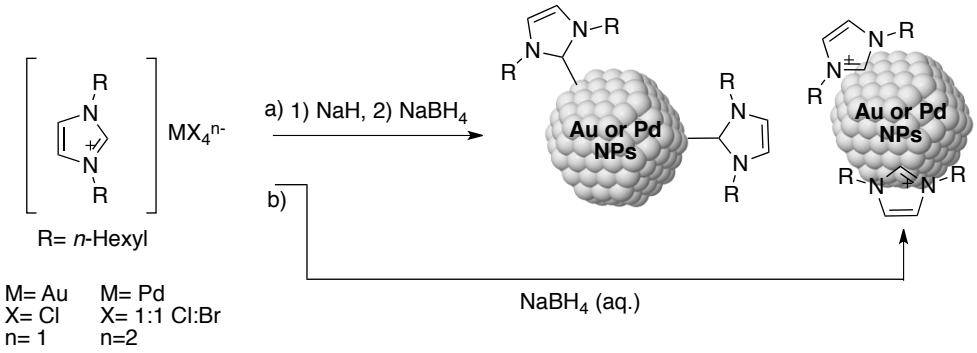

Figure 3. 10. Synthetic strategy reported by Beer and co-workers for the formation of NHC and imidazolium stabilized Au and Pd NPs[41]

The ligand exchange at the surface of already formed NPs has also been considered to be a useful technique for the synthesis of NHC-stabilized metal NPs. This technique consists in the displacement of low coordinative stabilizing ligands, mainly thioethers, located at the surface of NPs to be exchanged by stronger donor ligands such as NHCs. In 2009, the first example based on the synthesis of metal NPs by ligand exchange was reported.[42] In this study, Au NPs of 2.6 ± 0.5 nm stabilized by NHCs were prepared by reaction of freshly prepared *It*Bu with Au NPs stabilized by weakly bonded long-chain thioethers (Figure 3. 11). The complete ligand exchange was confirmed by the total disappearance of the strong sulphur peak in the XPS spectrum of the resulting Au NPs.

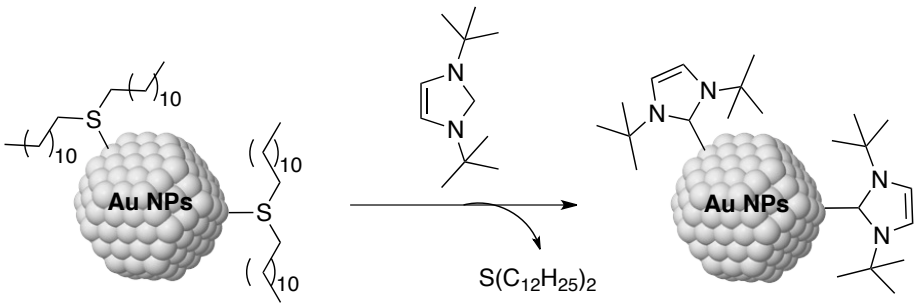

Figure 3. 11. Ligand Exchange synthesis reported by Chechik and co-workers for the formation of Au NPs stabilized by I*t*Bu[42]

Some years later, Ravoo and co-workers reported the first example based on the formation of long-term stable Pd NPs synthetized by ligand exchange.[43] Stabilization using rationally designed NHCs bearing long carbon chains at the imidazole backbone (Figure 3. 12a) gave rise to the formation of small NPs with a mean diameter of about 4.4 – 5.6 nm. Then, Glorius and co-workers used the same synthetic protocol for the formation of Au and Pd NPs stabilized by negatively charged NHC ligands bearing sulfonate and carboxylate groups in their structures (Figure 3. 12b).[44] The metal content, the size distributions and the long term stability of these NPs was investigated by TGA, TEM, DLS and UV-vis and the coordination of the NHC ligand at the NPs surface was confirmed by ^{1}H and ^{13}C NMR spectroscopy. The hydrophilic character of these NPs was key for obtaining high activities and chemoselectivities in catalytic hydrogenation reactions. More recently, the same group also used the ligand exchange strategy for the formation of bidentate hybrid NHC-thioether (Figure 3. 12c) stabilized Pd NPs. These NPs showed high chemoselectivities in the catalytic hydrogenation of olefins.[45]

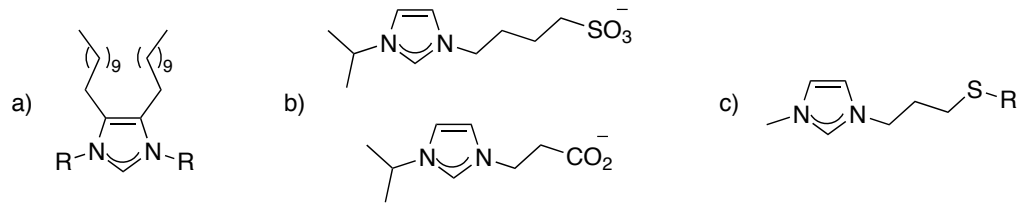

Figure 3. 12. NHC ligands used for the synthesis of metal NPs by ligand exchange[43,44,45]

As previously exposed, the synthesis of metal NPs stabilized by NHCs by decomposition of an organometallic precursor (known as the organometallic approach)[34,35] has also been explored. This procedure reported by Chaudret and co-workers allows the formation of small with narrow size distribution metal NPs with clean surfaces. The fact that clean-surface metal NPs can be formed is crucial for subsequent surface studies and in order to perform reproducible chemistry.

In 2011, Chaudret and co-workers reported the synthesis of Ru NPs by decomposition of [Ru(COD)(COT)] under 3 bar of H_2 in the presence of variable amounts of **IPr** and **I^{t}Bu** free NHCs (Figure 3. 13).[46] In order to avoid any pollution of the surface of the NPs, the carbenes and not the imidazolium precursors were used for the synthesis of the Ru NPs. TEM and HRTEM analysis revealed the presence of non-agglomerated, spherical, monodisperse and highly crystalline NPs and the presence of coordinated hydrides at the NPs surface was evidenced by titration using 2-norbornene.[32] Furthermore, thanks to the synthesis of these NPs in the presence of the analogous ^{13}C-labelled ligands on the carbene carbon, the NMR spectroscopic evidence for the direct binding between the NHC

ligands and the surface of the Ru NPs was presented. Indeed, the use of highly coordinative molecules such as CO was found to give valuable information about the availability of catalytic sites at the surface of the NPs where catalytic reactions can take place. Later reports based on the application of these NPs in the catalytic hydrogenation of arenes revealed the high activity of these nanocatalysts.[47]

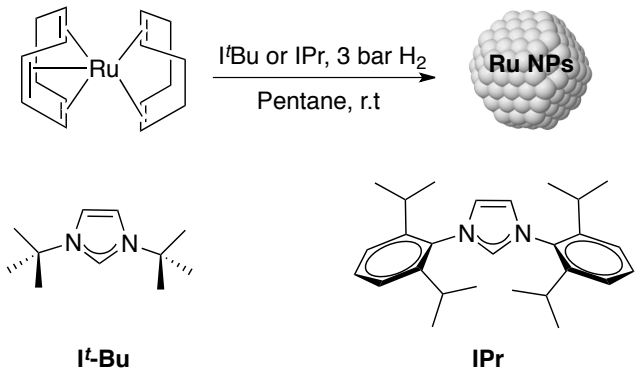

Figure 3. 13. Synthetic strategy used by Chaudret and co-workers for the preparation of NHC-stabilised Ru NPs[46]

Some years later, the same group carried out the stabilization of Ru NPs using a family of distinct NHC ligands and studied their impact on the NPs growth and reactivity.[48] The influence of the structure of these ligands, especially the groups bound to the N atoms (arylic or alkylic) and the substituents and saturation of the imidazole ring, on the size of the NPs, their dispersion and their surface state was investigated. [Ru(COD)(COT)] was also used as metal precursor, under H_2 in the presence of the different NHCs for the formation of the Ru NPs. As in the previous example, the location of the different NHC ligands at the NPs surface was explored by CO adsorption NMR

experiments, which gave information about the availability of catalytic sites for each system.

Recently, the synthesis of water-soluble Ru NPs stabilized by sulfonated NHC ligands has also been reported using this synthetic procedure. [49] The resulting Ru NPs were applied in the enantiospecific H/D exchange of the amino acid L-Lysine, exhibiting high activities when D_2O was used as solvent.

The application of this procedure for the synthesis of Pt NPs was also investigated. [50] These NPs were synthesized starting from the [Pt(dba)$_2$] organometallic precursor in the presence of similar NHCs under H_2. Even in this case, the formation of well-defined NPs was achieved, which was at that time the only example of Pt NPs stabilized by NHC ligands. These NPs were used as catalysts in the chemoselective hydrogenation of nitroarenes.

More recently, the same group reported a new methodology that provides the preparation of NHC-stabilized Ru NPs, with no need to isolate the corresponding free carbenes prior to NPs formation (Figure 3. 14).[51]

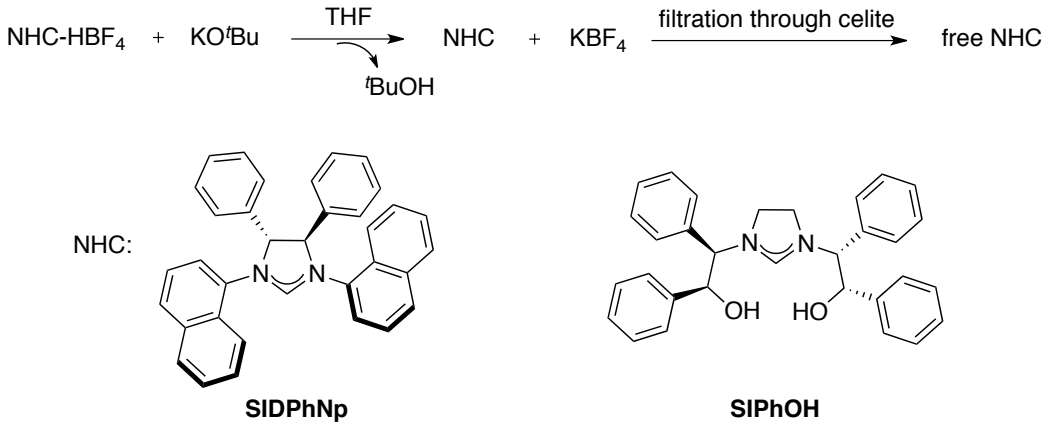

Figure 3. 14. In situ formation of free NHCs reported by Chaudret and co-workers used in the synthesis of Ru NPs[51]

This new method was of great interest since it allows the formation of Ru NPs stabilized by NHCs that are not stable when isolated, extending the range of potentially useful NHC ligands on the field of metallic NPs. The new procedure is based on the in situ formation of the free carbene by deprotonation using KO*t*Bu with consequent transfer into the reactor containing the organometallic precursor. Filtration through Celite was crucial to eliminate inorganic salts produced during the deprotonation step that could coordinate at the metal surface and thus poison it. With this aim, Ru NPs stabilized by two chiral NHCs (SIDPhNp and SIPhOH) that are not accessible as pure solids were synthesized. The surface chemistry of these NPs was also investigated by CO adsorption IR and NMR spectroscopic techniques, as well as their reactivity in asymmetric hydrogenation reactions. Then, this new method was applied for the formation of Ru NPs stabilized with long aliphatic chain NHCs, containing either small or bulky substituents at the N atoms of the imidazole ring and

the effect of the presence of different N-substituents on the size and reactivity of the resulting Ru NPs was finally evaluated.[52]

Lately, the synthesis of Ni NPs stabilized by NHCs through a new methodology involving the decarboxylation of a zwitterionic CO_2 adduct has been reported by our group.[53] These NPs were thoroughly characterised and supported onto carbon nanotubes. These latter NPs revealed efficient catalysts in the selective hydrogenation of terminal alkynes into the corresponding (Z)-alkenes under very mild reaction conditions. Furthermore, these heterogeneous catalysts could be readily recovered by simple filtration and reused 3 times without relevant decrease in activity.

Among all these examples and taking into account several precedents based on the stabilization of Rh NPs by different ligands, the fact that any examples were reported related to the stabilization of Rh NPs by NHC ligands encourage us to study the formation of Rh NPs in the presence these type of ligands. Besides, since previous studies related to the synthesis of metal NPs by the organometallic approach showed the possible formation of clean surface NPs, it was the chosen procedure for the synthesis of NHC-stabilized Rh NPs.

3.2. Results and discussion

3.2.1. Synthesis and characterization of Rh NPs stabilized by IPr

The rhodium nanoparticles described in this work were synthesized by decomposition of $Rh(\eta^3\text{-}C_3H_5)_3$ in THF at 35°C under 4 bar of H_2 in the presence of substoichiometric amounts of free IPr ligand (Figure 3. 15). This IPr ligand was synthesized by deprotonation of the imidazolium salt IPr·HBF_4 prior to NPs formation (See experimental part). This methodology allows the formation of metal NPs by olefin reduction and displacement from organometallic compounds, providing NPs with small size and narrow size distribution.[34,35]

In order to study the effect of the amount of stabilizing ligand used for the formation of these NPs, [IPr]/[Rh] molar ratios of 0.2, 0.4 and 0.6 were used, providing the corresponding **Rh$^{0.2}$**, **Rh$^{0.4}$** and **Rh$^{0.6}$** NPs, respectively.

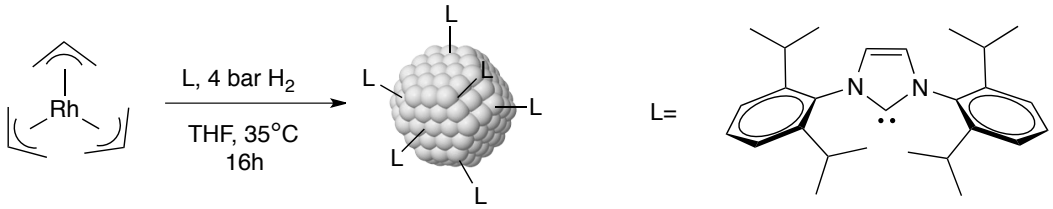

Figure 3. 15. Synthesis of Rh NPs stabilized by IPr

After 16h of reaction under 4 bar of H_2 at 35°C, the initial pale yellow solution was observed to slowly turn black, confirming the decomposition of the Rh precursor. The Rh NPs were isolated as

black powders after washing with pentane. Analysis of the black solution by Transmission Electron Microscopy (TEM) revealed the formation of small and well-dispersed Rh NPs with mean diameters of 1.68 ± 0.26 nm for **Rh$^{0.2}$**, 1.26 ± 0.25 nm for **Rh$^{0.4}$** and 1.29 ± 0.21 nm for **Rh$^{0.6}$**, exhibiting in all cases spherical shapes and narrow size distributions (Figure 3. 16). The size obtained for **Rh$^{0.2}$** was similar to a hydrodynamic radius value of 1.4 nm obtained from the Stokes-Einstein equation using an obtained diffusion coefficient of 3.4×10^{-10} m^2s^{-1} by Diffusion-Ordered NMR SpectroscopY (DOSY) for the same sample.

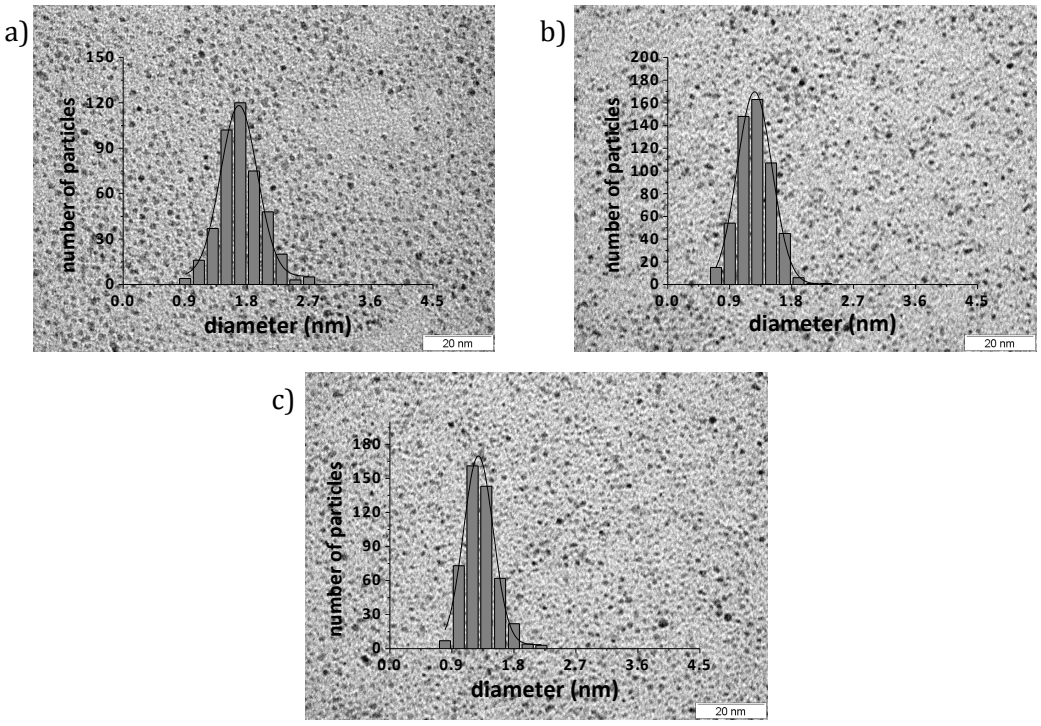

Figure 3. 16. TEM micrographs and size distributions of a) **Rh$^{0.2}$**, b) **Rh$^{0.4}$** and c) **Rh$^{0.6}$**

Similar mean sizes were reported for Ru[46,47] and Pt[50] NPs stabilized using a [IPr]/[M] molar ratio of 0.2. A slight decrease in size at higher

[IPr]/[Rh] molar ratios was observed for the formation of these NPs, which is in agreement with previously reported results based for the formation of Ru[46,48,52] and Pt[50] NPs stabilized by NHC ligands. However, the fact that similar size distributions were obtained for **Rh$^{0.4}$** and **Rh$^{0.6}$** would indicate the formation of similar NPs when [IPr]/[Rh] molar ratios greater than 0.4 are used in the NPs synthesis. These results suggest the complete coverage at the NPs surface when a [IPr]/[Rh] molar ratio of 0.4 is used.

Analysis by High Resolution Transmission Electron Microscopy (HRTEM) showed the high crystalline character of these Rh NPs exhibiting a *fcc* (face-centred cubic) packing structure (Figure 3. 17a). The Fourier (FTT) analysis performed to these high resolution acquisitions provide a bond length between the Rh atoms of 0.27 nm that is in agreement with a *fcc* structure. Analysis by Scanning Electron Microscopy (SEM) also showed the presence of highly crystalline Rh NPs (Figure 3. 17b).

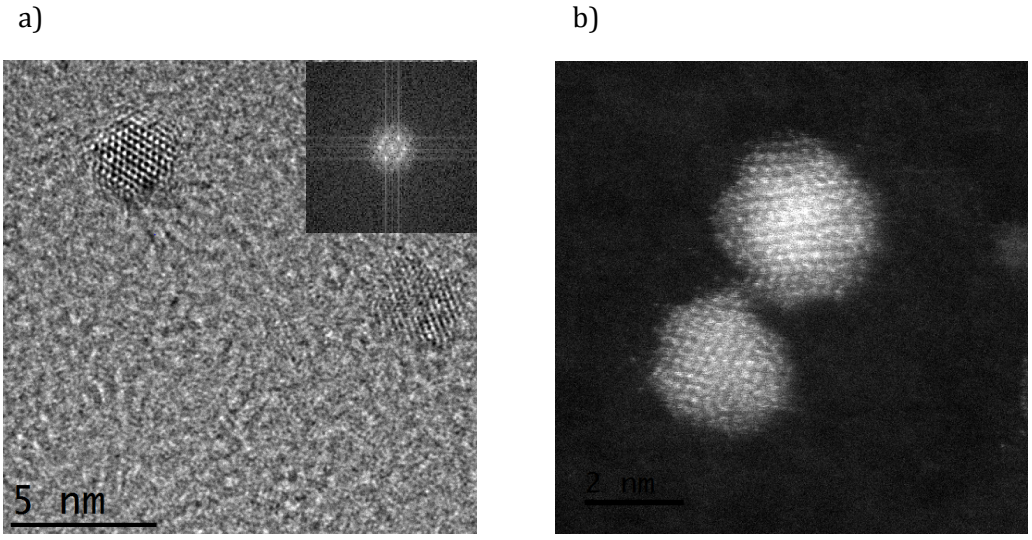

Figure 3. 17. (a) HRTEM and (b) SEM micrographs of **Rh$^{0.2}$**

The structure of **Rh$^{0.2}$**, **Rh$^{0.4}$** and **Rh$^{0.6}$** was investigated by X-Ray Diffraction (XRD) and Wide Angle X-ray Scattering (WAXS). First, the structural determination of **Rh$^{0.2}$** was performed by XRD, obtaining the diffraction pattern shown in (Figure 3. 18). The detection of strong Bragg's diffraction peaks detected at 41.07°, 47.78°, 61.88° and 89.11° from planes (111), (200), (220) and (222), respectively, which are related to the facets of the *fcc* structure confirmed this type of packing for **Rh$^{0.2}$**.[54] These results were in agreement with previously reported results by our group for Rh NPs stabilized by phosphorus containing ligands.[55] No reflections due to Rh oxide were observed in this case. A crystalline size of 1.79 ± 0.05 nm was observed during this analysis, which match the size distribution determined from TEM analysis (1.68 ± 0.26 nm). Similar results in terms of packing structure and crystallinity were obtained when **Rh$^{0.4}$** and **Rh$^{0.6}$** were analysed (Figures S8 and S9, Supporting information). Surprisingly, crystallite sizes of 1.97 ± 0.03 and 2.17± 0.06 nm, respectively, were obtained for these samples, which are higher than the values observed by TEM.

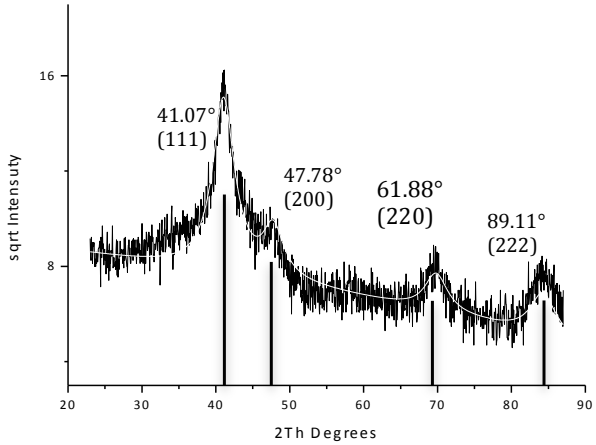

Figure 3. 18. XRD pattern recorded for **Rh$^{0.2}$**

WAXS analysis of these samples were also performed, revealing the presence of highly crystalline Rh domains displaying a *fcc* structure with a coherence length of 2.5 nm for **Rh$^{0.2}$** and 3.4-3.5 nm for **Rh$^{0.4}$** and **Rh$^{0.6}$** (Figure 3. 19). These coherence lengths were higher than those measured by TEM and XRD. The observation of higher sizes by WAXS compared to TEM has been previously reported; concluding that the mean size obtained by WAXS could be affected by NPs agglomeration.[56]

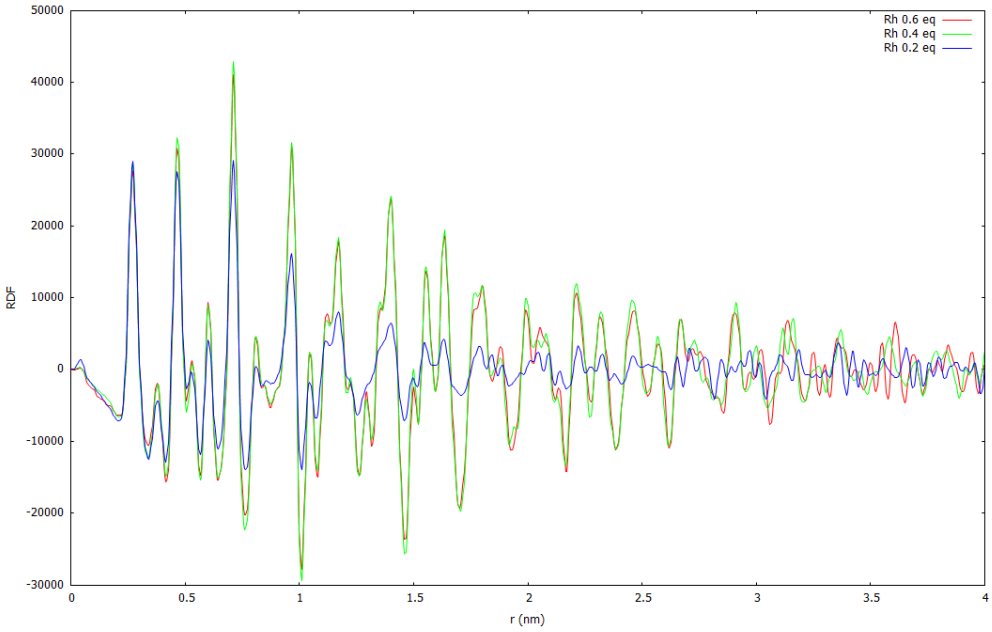

Figure 3. 19. Experimental RDF of **Rh$^{0.2}$** (blue), **Rh$^{0.4}$** (green) and **Rh$^{0.6}$** (red).

Moreover, the mean size value can differ between the different techniques and depend on the approximation used for the calculations. However, similar packing was obtained by XRD and WAXS in all cases, corresponding to *fcc* structured crystalline Rh NPs. In all cases, a bond length of 0.269 nm between Rh atoms was observed by WAXS, which value is similar to the one obtained by HRTEM. The WAXS analysis of **Rh$^{0.4}$** and **Rh$^{0.6}$** showed the formation of almost identical Rh NPs, as previously observed by TEM.

X-ray Photoelectron Spectroscopy (XPS) measurements were also performed on freshly prepared samples to obtain information on the oxidation state of the Rh atoms at the surface of these NPs. In the spectrum corresponding to **Rh$^{0.2}$**, the expected peaks for Rh(0) $3d_{5/2}$ and $3d_{3/2}$ were observed at 306.7eV for $3d_{5/2}$ and 311.40eV for $3d_{3/2}$ (Figure 3. 20), which is very similar to the theoretical values (307.2

and 311.9eV, respectively). Using calculations based on Monte-Carlo approximation and taking into account the parameters optimised for Rh surfaces,[57] the analysis revealed >99% of Rh(0) at the surface of the NPs **Rh$^{0.2}$**. Lower percentages of Rh in zero valent at the surface of the NPs of 99% for **Rh$^{0.4}$** and 97% for **Rh$^{0.4}$** were obtained based on the same analysis (Figures S13 and S14, Supporting information).

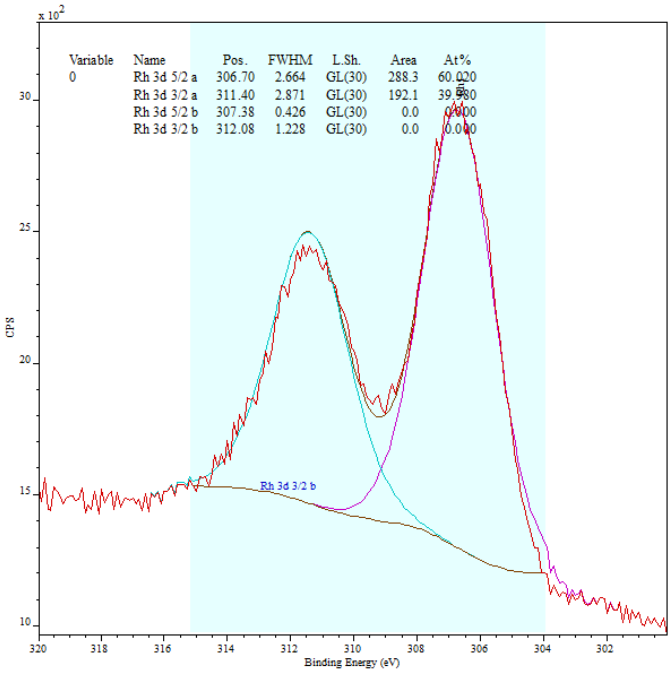

Figure 3. 20. XPS spectra of Rh 3d for **Rh$^{0.2}$**

To evaluate the content of stabilizer at the surface of these NPs, thermogravimetric analysis (TGA) was performed. As a reference, the free ligand (IPr) was first analysed, observing a unique weight loss at *ca.* 300°C (Figure 3. 21, black). When the NPs **Rh$^{0.2}$**, **Rh$^{0.4}$** and **Rh$^{0.6}$** were examined, a main weight loss (21.5%, 37% and 36.1%, respectively) was observed, which was attributed to the IPr ligand (Figure 3. 21, red, green and blue). The observed increase in the

weight loss corresponding to the IPr ligand, between **Rh$^{0.2}$** and **Rh$^{0.4}$/Rh$^{0.6}$** is in agreement with an increase in surface coverage when the [IPr]/[Rh] molar ratio is increased from 0.2 to 0.4/0.6 during the synthesis of the NPs. In contrast, the similar values obtained for **Rh$^{0.4}$** (37wt%) and **Rh$^{0.6}$** (36.1wt%) indicated a similar surface coverage for these NPs, again suggesting the saturation of the Rh surface when a [IPr]/[Rh] molar ratio higher than 0.4 was used.

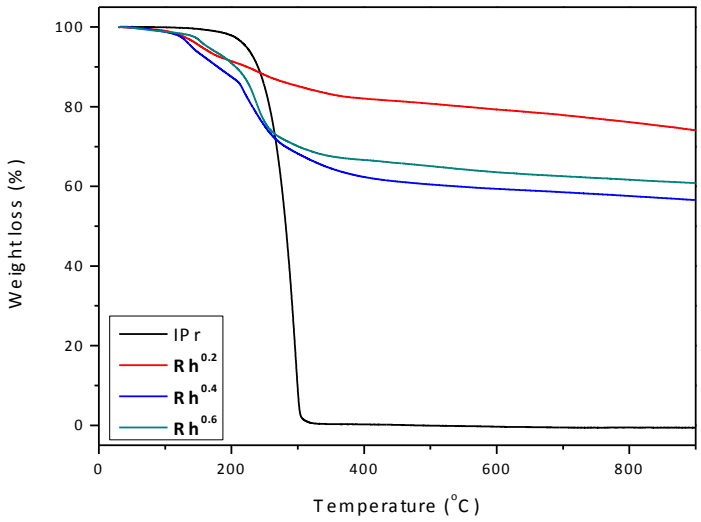

Figure 3. 21. TGA curves of the IPr free ligand (black), **Rh$^{0.2}$** (red), **Rh$^{0.4}$** (blue) and **Rh$^{0.6}$** (green)

A minor weight loss of 3.1-6.4wt% was also observed at lower temperatures (<150°C) for all samples, and was attributed to THF on the surface of the Rh NPs. The Rh content of the different samples was calculated at 900°C, obtaining values of 74% for **Rh$^{0.2}$**, 56.6% for **Rh$^{0.4}$** and 60.8% **Rh$^{0.6}$**. The fact that very similar results were obtained in terms of ligand weight loss and Rh content between

Rh$^{0.4}$ and **Rh$^{0.6}$** confirmed that both nanosystems are almost identical.

Using the mean sizes obtained by TEM for the synthesized Rh NPs and applying the VHH model,[58] the approximate total number of Rh atoms (Nt) and of Rh atoms at the surface (Ns) of **Rh$^{0.2}$**, **Rh$^{0.4}$** and **Rh$^{0.6}$** was calculated (Table 3. 1). The IPr/Rh$_s$ molar ratio was also calculated from the Ns and the data obtained by TGA, providing values between 0.12 and 0.24, which represents *ca*. 1 IPr ligand for 8-4 Rh surface atoms, respectively. These L/Rh$_s$ values are similar to the values previously obtained by our group for Rh NPs stabilized by phosphine ligands (0.17-0.33).[55,59]

Table 3. 1. Approximate structural features for systems **Rh$^{0.2}$**, **Rh$^{0.4}$** and **Rh$^{0.6}$**. Calculations based on the diameter (nm) obtained by TEM and the ligand content measured by TGA analysis.

	1.68 nm (Rh$^{0.2}$)	**1.26 nm (Rh$^{0.4}$)**	**1.29 nm (Rh$^{0.6}$)**
Nt	178	75	80
Ns	111	54	57
Ns/Nt	0.62	0.72	0.71
IPr/Rh$_s$	0.12	0.24	0.22

These results reflected that small differences in size produce significant changes in the total and surface number of Rh atoms, while the ratio of surface Rh atoms per total of Rh atoms remained very similar.

In an attempt to directly detect the presence of the IPr ligand coordinated at the surface of the Rh NPs, Infrared spectroscopy (IR)

experiments of the Rh NPs in KBr pellets were carried out. Then, the analysis of the IPr free ligand was also performed for comparison (Figure 3. 22, green). Similar IR spectra were obtained for NPs **Rh$^{0.2}$**, **Rh$^{0.4}$** and **Rh$^{0.6}$**. As an example, the spectrum obtained for **Rh$^{0.4}$** is shown in Figure 3. 22 (blue). A main set of signals, also observed for the IPr free ligand, was detected at high frequencies of 2960cm^{-1} < υ < 2850cm^{-1} and attributed to alkyl C-H stretching. The bands from alkenyl C-H stretching above 3000 cm^{-1}, which were observed in the case of the IPr free ligands, could not be detected for **Rh$^{0.4}$**. At lower frequencies, the detection of several bands between 1700 and 1500 cm^{-1} from aromatic C=C bending and the presence of sharp signals between 860 and 680 cm^{-1} attributed to aromatic C-H bending would confirm the presence of aromatic moieties from the IPr ligand.

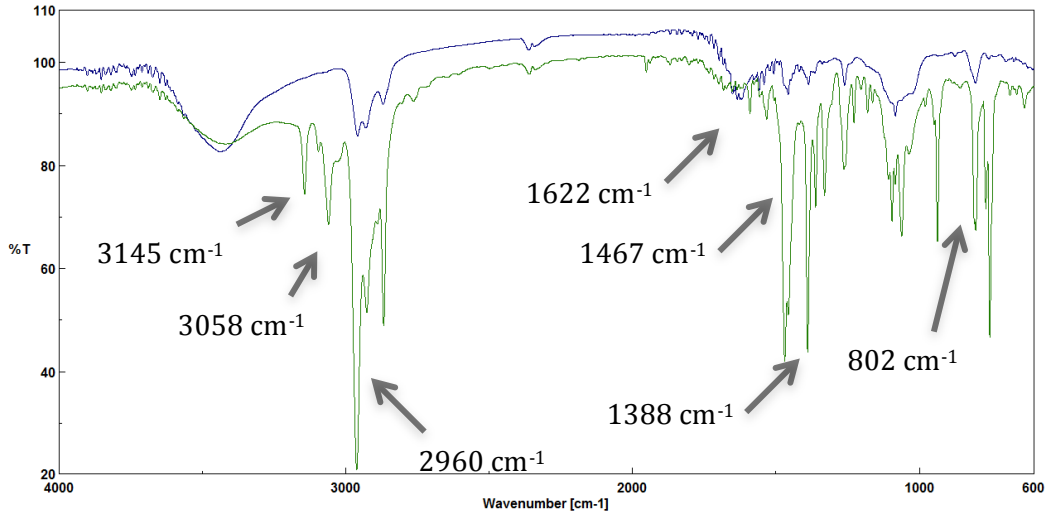

Figure 3. 22. IR spectra of IPr free ligand (green) and **Rh$^{0.4}$** (blue)

The presence of hydrides at the surface of NPs was demonstrated by Chaudret and co-workers, using NMR spectroscopy in the case of Ru NPs stabilized by hexadecylamine (HDA).[60] Some years later, a

methodology for the quantification of these hydrides by titration using 2-norbornene and 1-octene in the absence of added H_2 was reported.[32, 33, 61] Values between 1.1-2.5 were reported for Ru NPs stabilized by NHC ligands.[46]

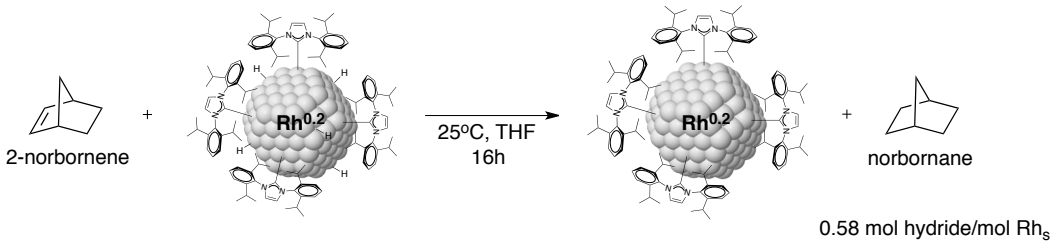

Figure 3. 23. Hydride titration of **Rh$^{0.2}$** using 2-norbornene

In order to quantify the presence of hydrides at the surface of the Rh NPs, **Rh$^{0.2}$** was first reacted with 2-norbornene following the methodology described by Chaudret and co-workers. The production of norbornane by reduction of 2-norbornene via surface hydrides was determined by GC-MS, revealing a hydride/Rh_s molar ratio 0.58 (Figure 3. 23). The fact that lower hydride/Rh_s molar ratios of 0.39 and 0.34 were obtained for **Rh$^{0.4}$** and **Rh$^{0.6}$** respectively (Table 3. 2) suggests a lower availability of sites when more stabilizing ligands are coordinated to the NPs surface, compared to **Rh$^{0.2}$**. It is noteworthy that these values were lower than the ones reported for Rh NPs stabilised by P-based ligands (0.8 hydride/Rh_s)[59] and Ru NPs stabilized by PVP, HDA and dppb (1.3, 1.3 and 1.1 hydride/Ru_s)[61,32].

Table 3. 2. Conversion of 2-norbornene to 2-norbornane and the corresponding values of mol H/ mol Rh surface and mol Rh surface/mol H

	$Rh^{0.2}$	**$Rh^{0.4}$**	**$Rh^{0.6}$**
Conversion of 2-norbornene	18%	14%	12%
mol H / mol Rh surface	0.58	0.39	0.34
mol Rh surface / mol H	1.72	2.58	2.98

Solution Nuclear Magnetic Resonance (NMR) technique was then used in order to confirm the presence of ligand at the surface of these Rh NPs. This technique is not commonly used for the characterization of colloids due to the width of the signals (if observable) from molecules close to the NPs surface as a result of slow molecular tumbling, presence of different chemical environments and magnetic effects as the Knight shift.[38,62,63] For this reason, no signals from groups close to the surface of metallic NPs were detected by solution NMR spectroscopy.[45,56,64] On the other hand, some reports described the detection of sharp or broad signals that were attributed to ligands located at the surface of Pd NPs stabilized by phosphorus[65] and imidalzolium salts[44,66] and Au NPs stabilized by imidalzolium salts[41].

In this work, a solution NMR study was first performed on **$Rh^{0.4}$** after their dissolution into THF-d^8 and the signals were compared to the ones present in the ^{1}H NMR spectrum of the free IPr ligand (Figure 3. 24a). When a ^{1}H NMR spectrum of **$Rh^{0.4}$** was recorded at room temperature (Figure 3. 24b), a broad signal between 6.75-7.75 ppm was observed, which was attributed to the $-CH_{arom}-$ of the phenyl rings of the coordinated ligand. A signal detected at 7.94 ppm was assigned to the protons of the imidazole backbone and the two pairs

of "doublets" centred at 0.82 and 1.29 ppm were attributed to the –CH_3 of the *i*Pr groups. Another signal was observed at 5.19 ppm and was assigned to methylene fragments formed via the reduction of the backbone of the IPr ligand, based on literature data.[67] When the synthesis of NPs **Rh$^{0.4}$** was performed under D_2, this signal disappeared, thus confirming this signal assignment (Figure 3. 25).

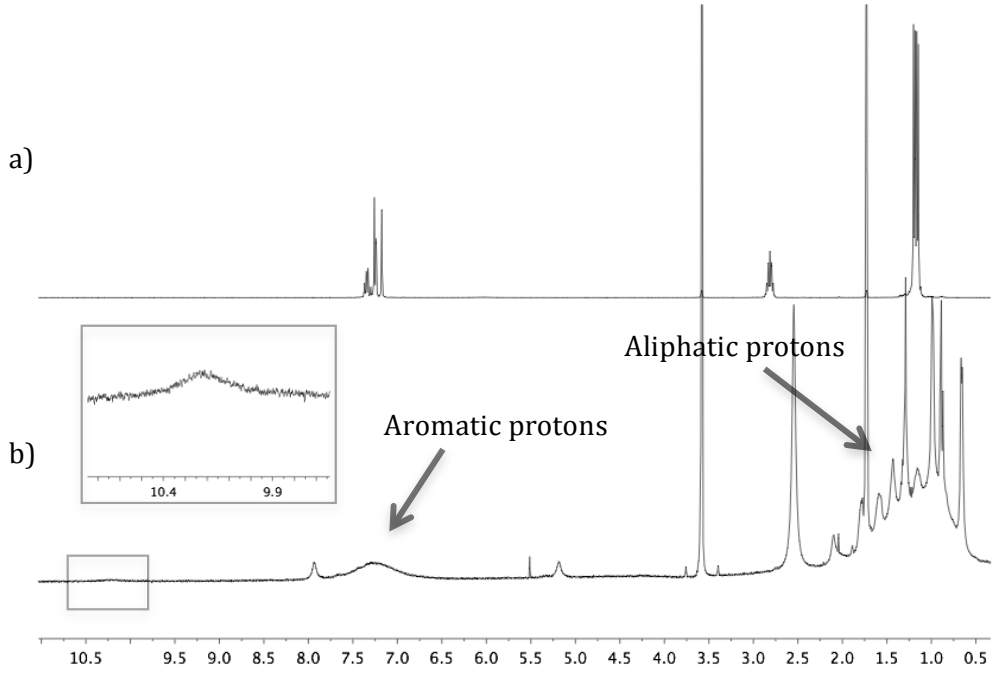

Figure 3. 24. ^{1}H NMR (THF-d^8, 400MHz) spectra of a) IPr free ligand and b) **Rh$^{0.4}$**

The detection of several broad signals at low chemical shifts (0.5-2 ppm) were also attributed to aliphatic protons due to hydrogenation of the IPr ligand, as previously reported in the case of Ru NPs stabilized by the same NHC.[46] Besides, signals corresponding to the -CH- groups of the *i*Pr moieties could not be detected.

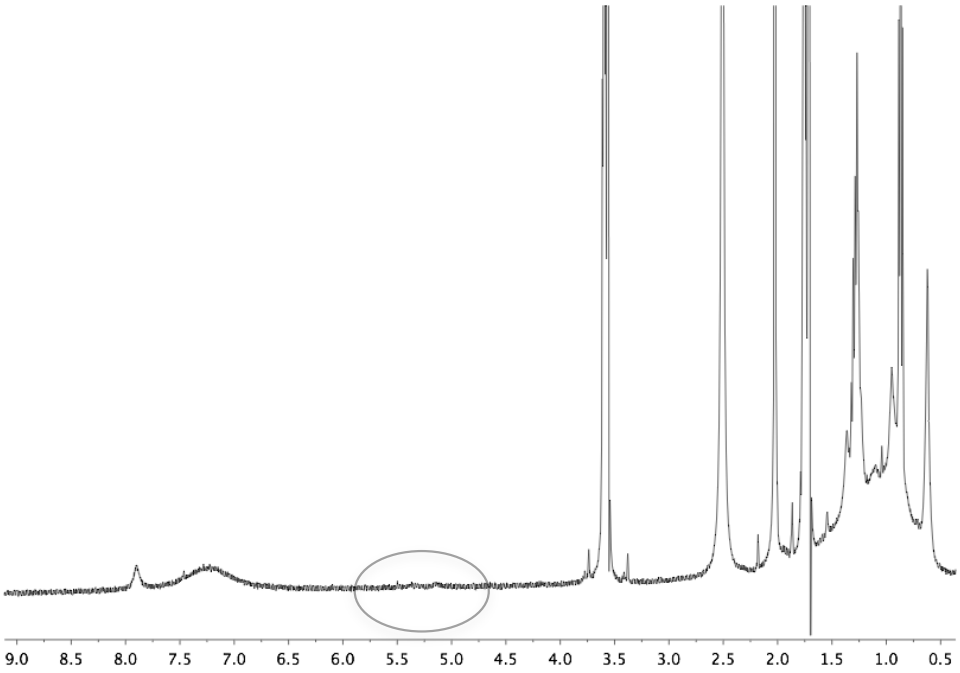

Figure 3. 25. ^{1}H NMR (THF-d^{8}, 400MHz) spectrum of **Rh$^{0.4}$** synthesized under D_2

Surprisingly, a broad signal with low intensity corresponding to an acidic proton of a protonated imidazolium species was also observed at 10.23 ppm. This observation could indicate that the nanoparticles could be not only stabilized by the carbene ligand, but also by the protonated ligand. Moreover, the difference between the chemical shifts of the acidic proton observed for the imidazolium salt IPr·HCl (8.7 ppm) and the protonated species that are thought to stabilize the Rh NPs (10.23 ppm) may be related to the interaction of the latter with the Rh NPs surface. Similar signals were observed when ^{1}H NMR spectra were recorded for **Rh$^{0.4}$** and **Rh$^{0.6}$** (Figure 3. 26b and c). Besides, an increase in the sharpness of the signal attributed to the imidazole backbone (7.94 ppm) was detected when higher amounts of the ligand were used during the NPs formation

In summary, ^{1}H signals of almost all the protons from the ligand could be observed, in contrast with the data reported for Ru NPs stabilized by the same NHC ligand.[46]

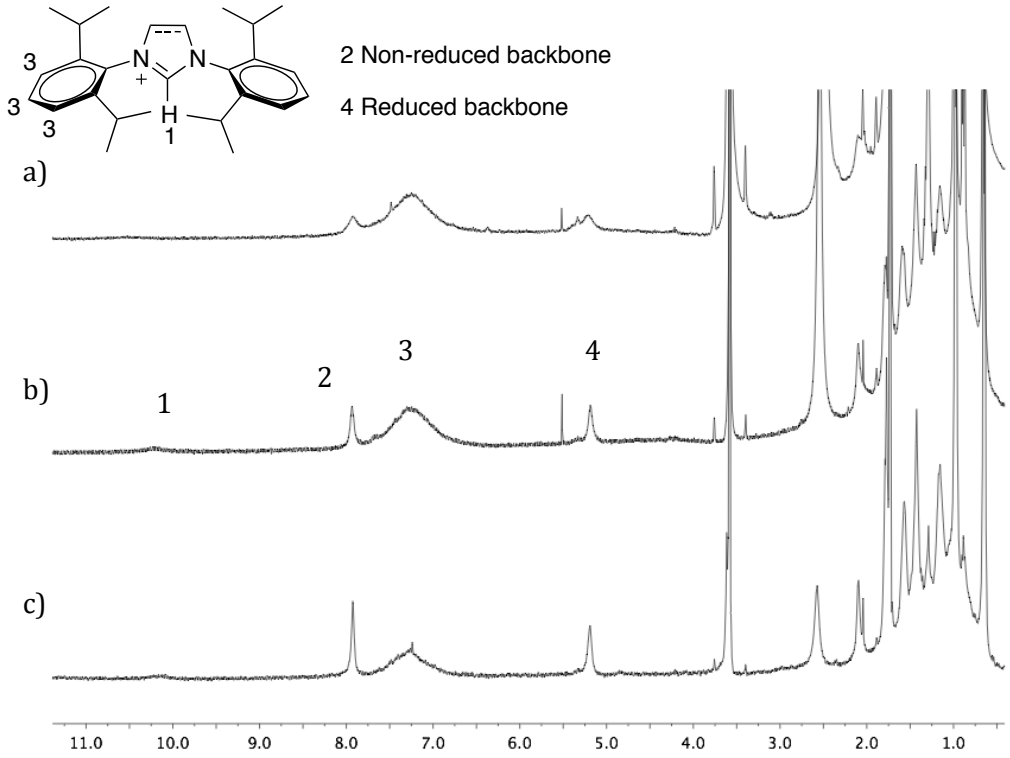

Figure 3. 26. ^{1}H NMR (THF-d^{8}, 400MHz) spectra of a) **Rh$^{0.2}$**, b) **Rh$^{0.4}$** and c) **Rh$^{0.6}$**

The stability of these Rh NPs in solution under CO pressure was also studied. In a high-pressure (HP) sapphire NMR tube containing a solution of NPs **Rh$^{0.4}$** in THF-d^{8}, 30 bar CO were added. When a ^{1}H NMR spectrum was recorded (Figure 3. 27), new signals were observed: sharp signals were detected at 7.56, 7.47 and 7.34 ppm corresponding to the protons of the imidazole backbone and of the aryl rings of an imidazole-based species, along with the septuplet centred at 2.97 ppm corresponding to the –CH- groups of the *i*Pr

moieties that was previously not detected. Moreover, two doublets at 1.35 and 1.12 ppm were also observed and attributed to the $-CH_3$ substituents of the aryl rings of the ligand. Furthermore, a sharp signal at 9.31 ppm could also be detected and attributed to an acidic proton. It is noteworthy that this chemical shift is lower than that previously observed for the coordinated imidazolium coordinated species (10.23 ppm).

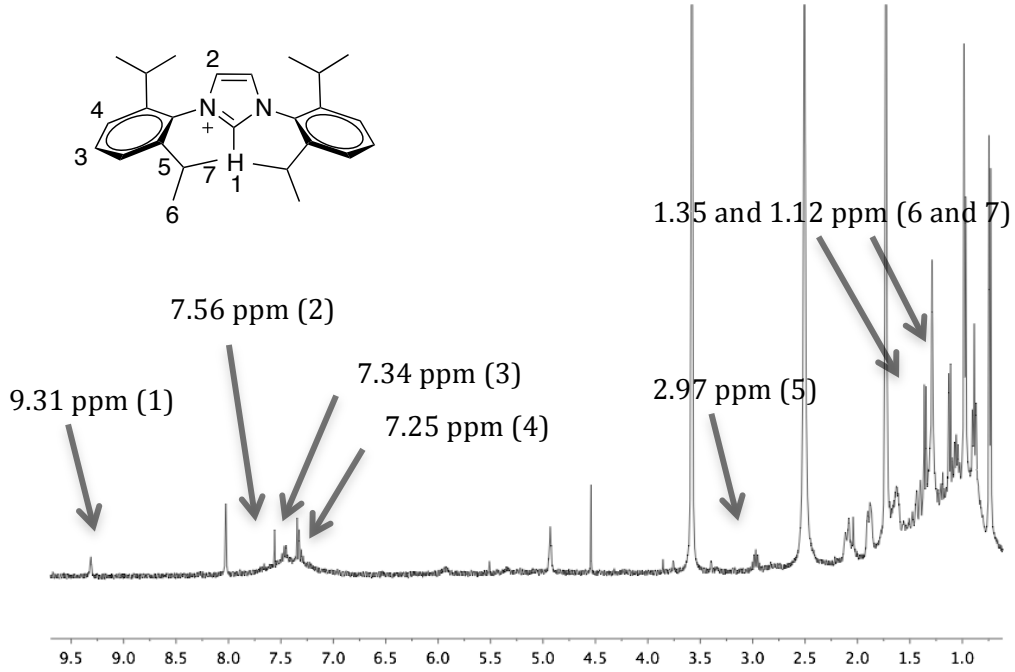

Figure 3. 27. ^{1}H NMR (THF-d^8, 400MHz) spectrum of **Rh$^{0.4}$** + 30 bar CO

This observation together with the detection of sharp signals, which match those of IPr·HCl, suggested the release of some protonated NHC ligand. This fact has been also observed for Ru NPs stabilized by similar NHC ligands.[52]

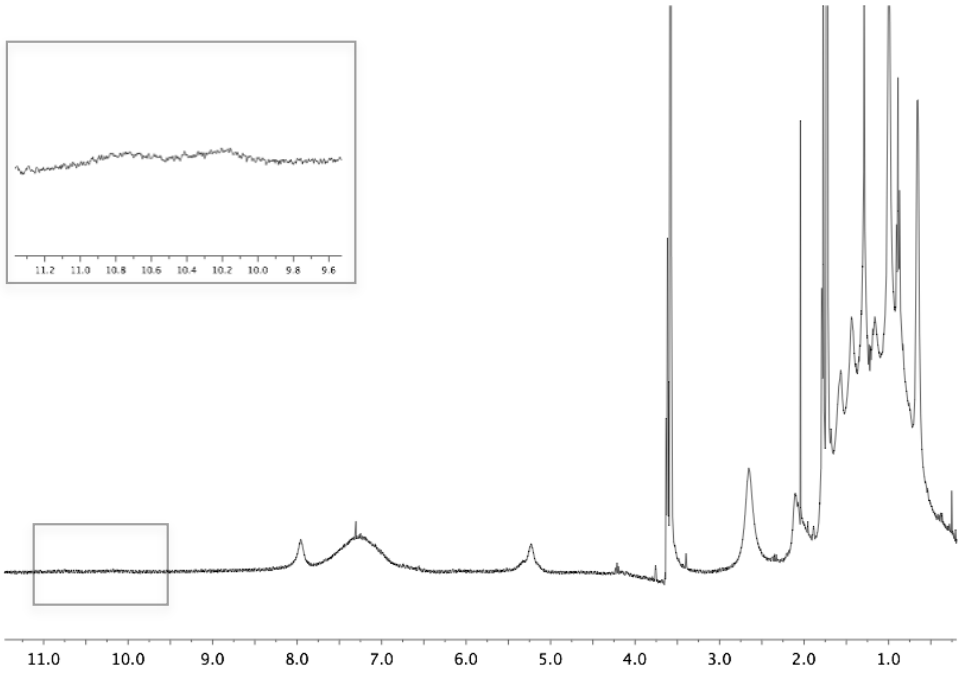

Figure 3. 28. ^{1}H NMR (THF-d^{8}, 400MHz) spectrum of **^{13}C-Rh$^{0.4}$**

In order to inspect the coordination of the NHC ligand at the surface of the NPs, a set of Rh NPs stabilized by ^{13}C-labelled IPr ligand in the C2-carbon (carbenic carbon) was synthesized using a [IPr]/[Rh] molar ratio of 0.4 (**^{13}C-Rh$^{0.4}$**). When a ^{1}H NMR spectrum of these NPs was recorded (Figure 3. 28), the only difference with the spectrum obtained for the unlabelled NPs (**Rh$^{0.4}$**) was the acidic signal at 10.49 ppm, which exhibited a large ^{13}C-^{1}H coupling (233.21Hz) (Figure 3. 28 inset), thus confirming that this signal was arising from the protonated ligand and that these NPs were stabilized by both the IPr ligand and its protonated analogue.

When a solution ^{13}C{^{1}H} NMR spectrum of **^{13}C-Rh$^{0.4}$** was recorded in THF-d^{8}, two main signals centred at 170 and 140 ppm were detected (Figure 3. 29). The latter signal is characteristic of the corresponding

imidazolium salt respectively, while that at 170 ppm was attributed to a metal-coordinated carbenic carbon atom.

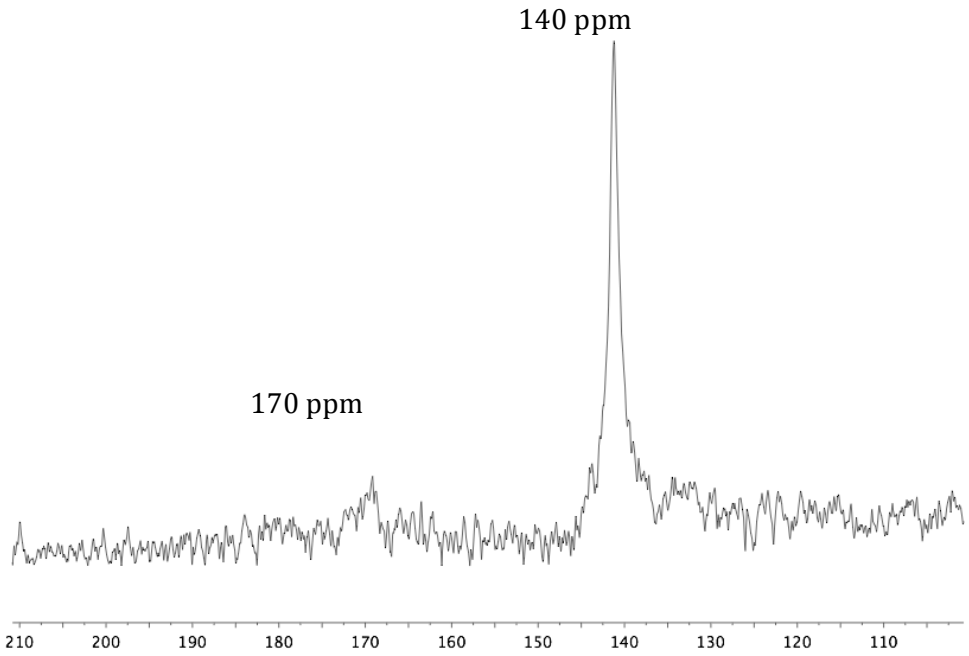

Figure 3. 29. $^{13}C\{^{1}H\}$ NMR (THF-d^8, 100.6MHz) spectrum of **^{13}C-Rh$^{0.4}$**

In an attempt to remove the protonated species from the surface of the NPs, a sample of **Rh$^{0.4}$** was washed with H_2O. However, no decrease in the intensity of the signal centred at 140 ppm was observed by $^{13}C\{^{1}H\}$ NMR, suggesting that this species is relatively strongly adsorbed, presumably in the second coordination sphere of these Rh NPs. This fact is in agreement with some reports regarding the use of imidazolium salts for the formation of M-NPs.[41,44,66] Moreover, the bond strength of these two stabilizers to the Rh surface was tested by reaction with PPh_3 and $P(OPh)_3$. However, as previously observed for Ru NPs stabilized by the same NHC ligand[46], no difference in the ^{1}H NMR spectrum was observed, confirming the

strong binding of both stabilising agents at the NPs environment.

Next, the same sample containing **^{13}C-Rh$^{0.4}$** in THF-d^8 was exposed to 30 bar of CO following the previously described procedure for **Rh$^{0.4}$**, and ^{1}H and ^{13}C{^{1}H} NMR spectra were recorded. In the ^{1}H NMR spectrum, a series of new sharp signals were detected (Figure 3. 30). The only difference compared to **Rh$^{0.4}$** was the observation of a doublet centred at 9.27 ppm due to the ^{13}C-^{1}H coupling for a free protonated species, which chemical shift is also lower than the previous one observed for the coordinated labelled imidazolium species (detected at 10.49 ppm). Thus, decoordination of some species containing the NHC ligand from the NPs surface was also observed in this case. Besides, a new doublet resonance centred at 180.8 ppm (J_{Rh-C}=46 Hz) was detected in the ^{13}C{^{1}H} NMR spectrum under these conditions (Figure 3. 30, inset). This latter signal was assigned to a Rh(I)-L complex formed by leaching from the surface of the Rh NPs under high CO pressure.[68] This experiment therefore demonstrated the decoordination of the protonated species from the Rh surface of the NPs and the formation of Rh-NHC species under these reaction conditions. Furthermore, this last result therefore indicated the strong binding of the NHC ligand IPr to the surface Rh atoms, since no free ligand was detected during this experiment. A signal at 126.09 ppm was also detected and was tentatively attributed to CO_2.[69] No changes were observed when the CO was evacuated from the HP-NMR tube and a ^{1}H and ^{13}C NMR spectra were recorded after repressuring the HP-NMR tube with 5 bar of H_2.

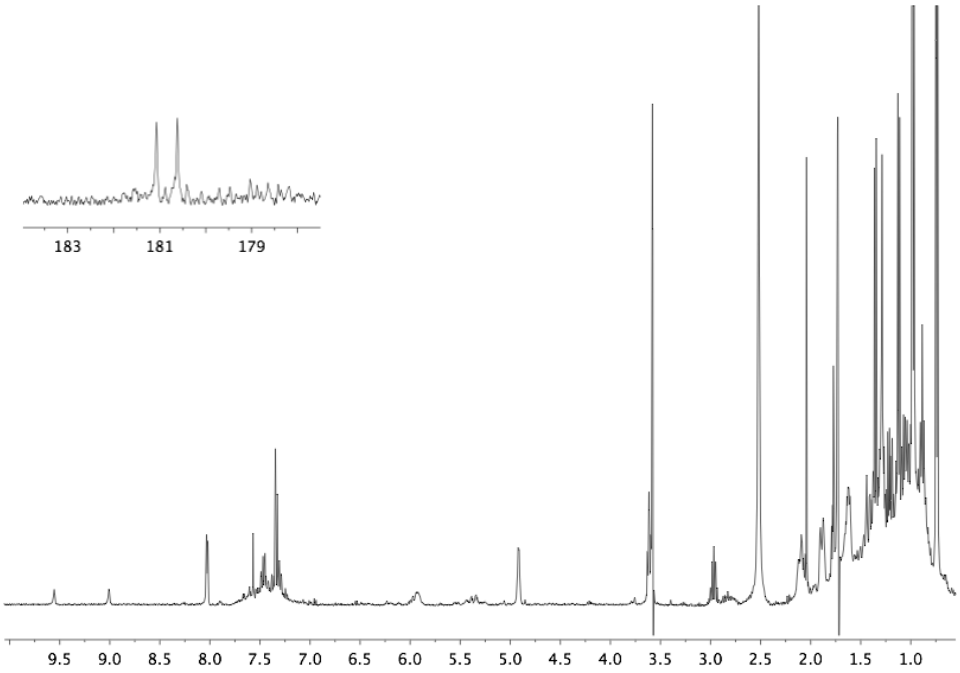

Figure 3. 30. ^{1}H NMR (THF-d^{8}, 400MHz) spectrum **^{13}C-Rh$^{0.4}$** + 30 bars of CO. Inset: ^{13}C{^{1}H} NMR (THF-d^{8}, 100.6MHz) spectrum of **^{13}C-Rh$^{0.4}$** + 30 bars CO

Other NMR techniques such as ^{13}C Magic Angle Spinning (MAS) have been reported to provide valuable information for the detection and location of ligands coordinated to the surface of metallic NPs.[70,71] Furthermore, regarding the stabilization of Ru[46], Pd[62c,44] and Pt[37] NPs by NHC ligands, the direct bonding between the ^{13}C labelled carbenic carbon and the surface of the NPs have been successfully detected using ^{13}C MAS NMR technique, which have never been proved by solution NMR spectroscopic techniques.

The coordination of the NHC ligand on the surface of the Rh NPs was studied by ^{1}H-^{13}C Cross Polarization Magic Angle Spinning NMR spectroscopy (CP-MAS NMR) with the aim of determining their location and possible dynamics. The CP-MAS spectrum of the NPs

stabilized using a high [IPr]/[Rh] molar ratio of 0.4 (**Rh$^{0.4}$**) (Figure 3. 31b), displayed 3 signals at 25.6, 29.8 and 32.6 ppm that were attributed to two $-CH_3$ groups and the –CH- of the *i*Pr moieties respectively. Regarding the aromatic region, an intense signal centred at 127.28 ppm and two more signals with very low intensity were detected at 142.23 and 149.53 ppm, arising from aromatic carbons and those from the imidazole backbone of the NHC ligand. These chemical shifts were in agreement with the ones obtained from the ^{13}C CP-MAS spectrum of the free ^{13}C-IPr ligand (Figure 3. 31a). Besides, signals corresponding to hydrogenated NHC species were observed, in agreement with the results obtained by solution NMR and previously reported results based on NHC-stabilized Ru NPs.[51] These signals, detected at 51.5 and 65.9 ppm, were attributed to $-CH_2-$ carbons by ^{13}C CP-MAS Attached Proton Test NMR (CP-MAS APT) (Figure 3. 48, Experimental part). The detection of similar signals was observed when samples of **Rh$^{0.2}$** and **Rh$^{0.6}$** were analysed by ^{13}C CP-MAS NMR spectroscopy.

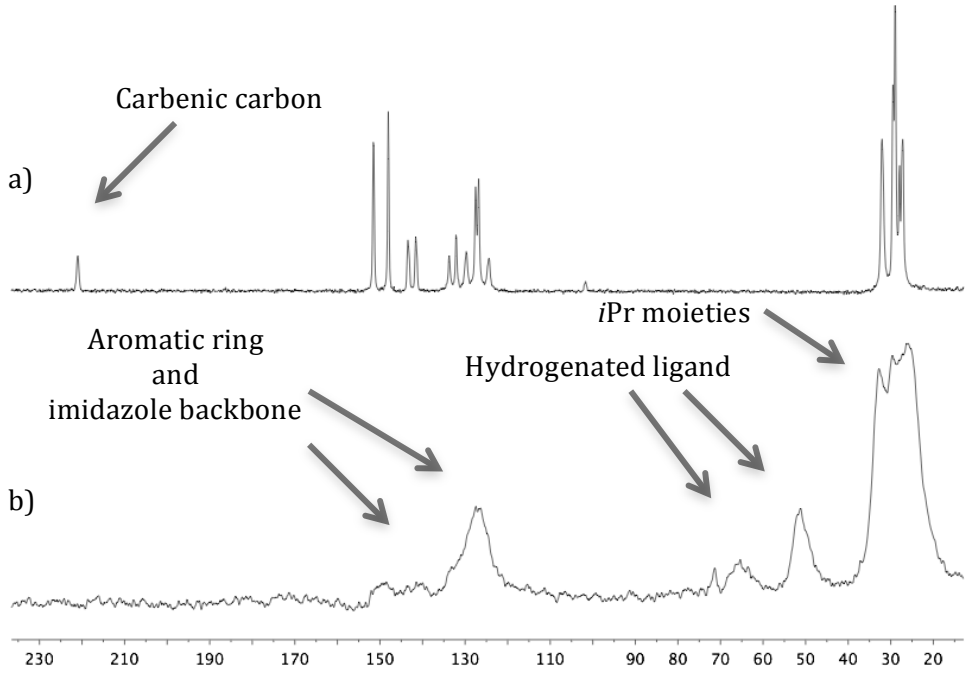

Figure 3. 31. $^{13}C\{^{1}H\}$ CP-MAS spectra of a) ^{13}C-IPr free ligand and b) **Rh$^{0.4}$**

To obtain evidence of the carbenic carbon of the NHC coordinated at the NPs surface, the analysis of the Rh NPs stabilized by the ^{13}C labelled IPr ligand (**^{13}C-Rh$^{0.4}$**) was carried out. The fact that two new main signals at *ca*. 140 and 170 ppm were detected in this case (Figure 3. 32b), compared to the spectrum obtained for **Rh$^{0.4}$** (Figure 3. 32a), suggested the presence of two different ^{13}C-labelled species at the NPs surface. These chemical shifts are in agreement with the ones observed by the analysis of the same sample using solution NMR techniques. Thus, the ^{13}C signals detected at *ca*. 140 ppm were attributed to imidazolium protonated species and the ^{13}C signal detected at *ca*. 170 ppm was attributed to a directly bonded carbenic carbon to the surface of the Rh NPs. This chemical shift was in agreement with signals for carbenic carbon atoms coordinated to Pd[44] and Pt[37] NPs detected at 166-172 ppm using similar NMR

techniques. In addition, the fact that spinning side bands were detected for the ^{13}C signal at *ca.* 170 ppm corroborates the strong coordination between this species and the surface of the Rh NPs. Besides, the detection of signals at 138.4 ppm and 144.1 ppm were assigned to protonated species could explain the presence of more than one protonated imidazolium species. Similar results were obtained for **^{13}C-Rh$^{0.2}$** and **^{13}C-Rh$^{0.6}$**.

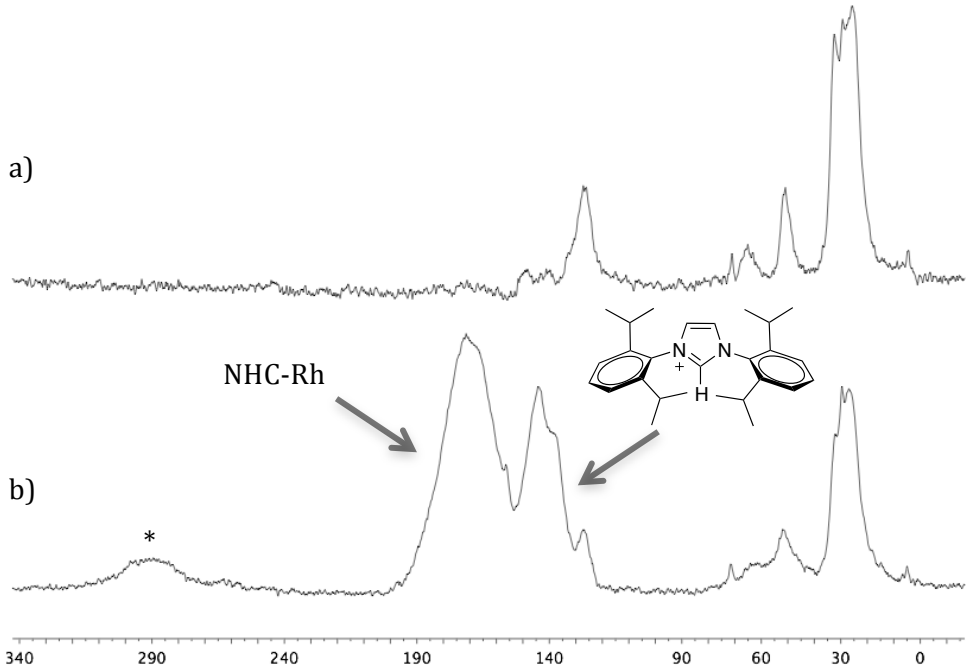

Figure 3. 32. $^{13}C\{^1H\}$ CP-MAS spectra of a) **^{13}C-Rh$^{0.4}$** and b) **Rh$^{0.4}$** (*spinning sidebands at 12 KHz)

Experiments increasing the time of contact during the acquisition of the ^{13}C CP-MAS NMR spectrum of **^{13}C-Rh$^{0.4}$** from 35 to 10000 μs were also performed to further demonstrate that the signals at *ca.* 140 ppm corresponded to protonated imidazolium species.

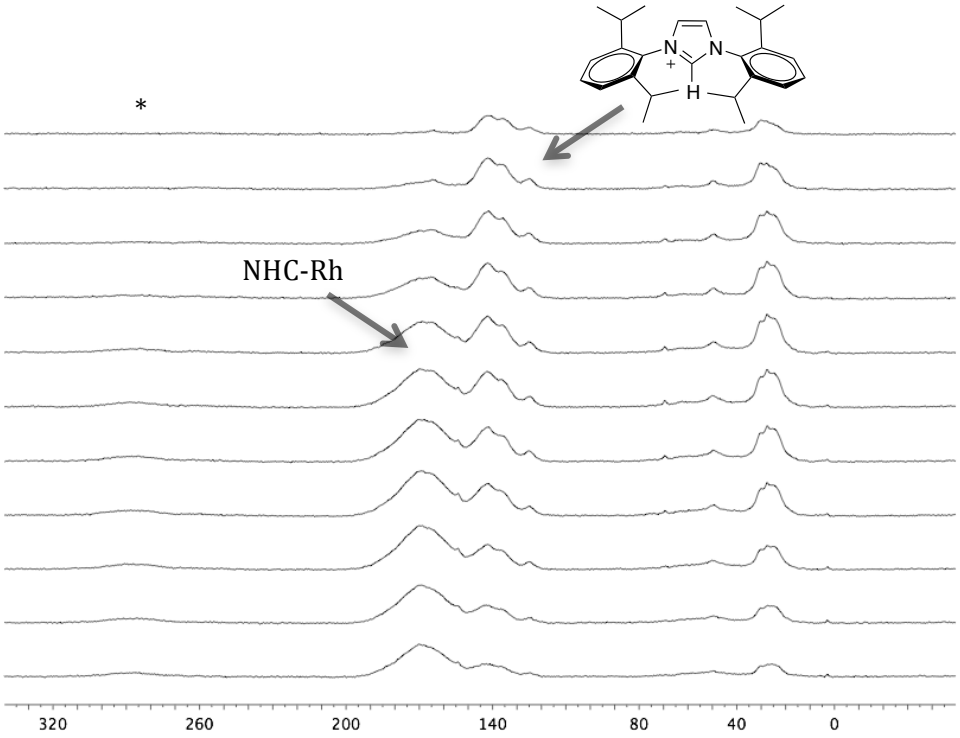

Figure 3. 33. $^{13}C\{^{1}H\}$ CP-MAS spectra of **^{13}C-Rh$^{0.4}$** increasing the time of contact from 35 to 10000 μs during the acquisition (from top to bottom) (*spinning sidebands at 12 KHz)

As the CP MAS technique is based in obtaining ^{13}C signals from cross polarization of the signals obtained from the ^{1}H, the ^{13}C signals from carbon atoms close to hydrogen atoms appear at low contact time. In these experiments (Figure 3. 33), the signals centred at *ca.* 140 ppm grew much more faster compared to the one at *ca*. 170 ppm and was thus attributed to carbon atoms directly bonded to a hydrogen atom, confirming that the signal at *ca*. 170 ppm was a quaternary carbon and thus corresponded to the C_2-carbon of the ligand coordinated to the Rh surface. This study therefore demonstrated for the first time the direct coordination of the IPr ligand by the carbenic carbon at the metallic surface of Rh NPs.

Next, the analysis of solid samples after washing with H_2O as performed in an attempt to eliminate the presence of imidazolium protonated species at the surface of the NPs. However, no change was observed after these washings, and confirmed that this species is relatively strongly coordinated to the NPs surface (Figure 3. 34). This is in agreement with results reported on Au[41] and Pd[66] NPs stabilized by imidazolium salts.

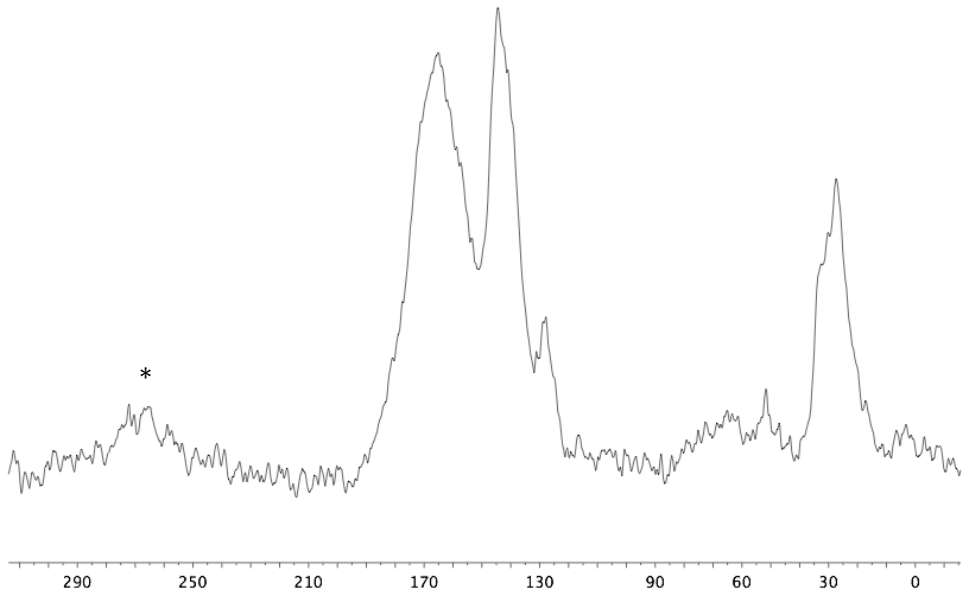

Figure 3. 34. $^{13}C\{^1H\}$ CP-MAS spectrum of **^{13}C-Rh$^{0.4}$** after washings with H_2O (*spinning sidebands at 10 KHz)

3.2.2. Surface characterization using CO adsorption/ Infra-red spectroscopy

Infrared spectroscopy (IR) analysis on NPs exposed was shown to provide interesting information on the availability of sites at the surface of these species. In these experiments, two main types of carbonyl groups have been reported.[72,73] Signals from bridging CO

are detected at frequencies between 1750 and 1900 cm^{-1} and attributed to COs coordinated at the faces of the NPs (Figure 3. 35), while terminal CO groups, detected at higher frequency values (1950-2050 cm^{-1}), are mainly located on low coordination sites such as edges and apexes. In the latter case, one or two COs can be coordinated to these sites, giving rise to one or two stretching bands.

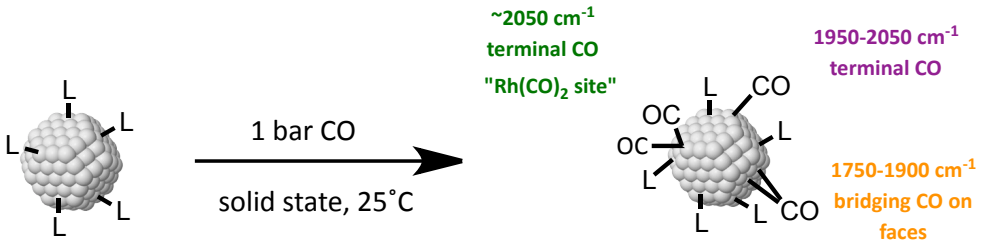

Figure 3. 35. Representation of CO adsorption onto metallic NPs

Recently, the groups of Chaudret and co-workers demonstrated that IR spectroscopic studies could be useful for the precise location of stabilizing ligands at the surface of Ru[32,74,75,51], Pt[76] and RuPt[33] bimetallic NPs. Dyson and co-workers also used CO adsoption-IR spectroscopy to study the location of different aromatic phosphines at the surface of Rh NPs stabilized by PVP.[25] The selective coordination of these phosphine ligands showed to modify the steric hindrance at specific sites of these Rh NPs, generating selectivity in catalysis. More recently, our group reported the synthesis of Rh NPs stabilized by phosphine and phosphite ligands and a study based on CO adsorption-IR spectroscopy was also used to locate coordinated phosphorus compounds at the surface of the Rh NPs.[59] The nature of the ligands, the ligand content and the steric hindrance induced by

the ligands of the NPs was observed to influence the formation of geminal "$Rh(CO)_2$" sites.

In order to study the availability of sites at the surface of our NPs, samples from NPs **$Rh^{0.2}$**, **$Rh^{0.4}$** and **$Rh^{0.6}$** were analysed after 16h exposure to 1 bar of CO by IR spectroscopy using KBr pellets. When the **$Rh^{0.2}$** NPs were analysed, three different CO stretching frequencies between 2200 and 1700 cm^{-1} were detected and attributed to geminal-terminal (or multicarbonyl) "$Rh(CO)_2$" units (2067 cm^{-1}), terminal CO (2009 cm^{-1}) and bridging CO (broad band centred at around 1864 cm^{-1}) based on previously reported results (Figure 3. 36, green).

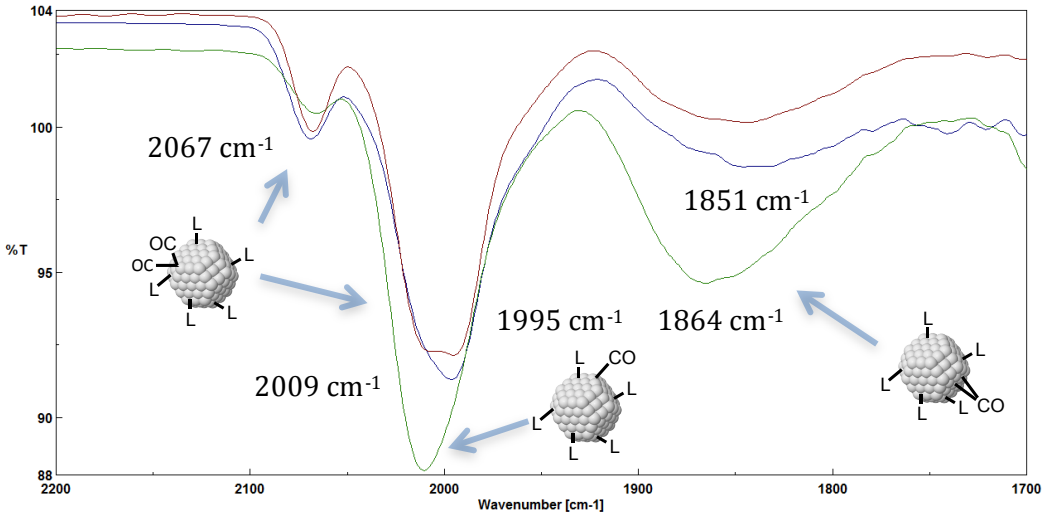

Figure 3. 36. IR spectra of **$Rh^{0.2}$** (green), **$Rh^{0.4}$** (blue) and **$Rh^{0.6}$** (red) after CO exposure

The detection of bridging COs indicated the availability of the faces, while the detection of terminal CO bands also indicated availability of edges and apexes for **$Rh^{0.2}$**. The detection of geminal, terminal and

bridging COs when samples of **Rh$^{0.4}$** and **Rh$^{0.6}$** were examined (Figure 3. 36, blue and red), also suggested the availability of edges, apexes and faces for these NPs. In addition, more intense geminal "$Rh(CO)_2$" bands at 2009 cm^{-1} for a [L]/[Rh] molar ratio of 0.6 (**Rh$^{0.6}$**) were observed compared to **Rh$^{0.4}$**, which evidence has been previously reported for Rh systems stabilized by PPh_3.[59] The evidence that less intense CO bands for bridging COs were observed for **Rh$^{0.4}$** and **Rh$^{0.6}$** compared to **Rh$^{0.2}$** suggested higher occupation of faces due to the presence of excess of ligand at higher [IPr]/[Rh] molar ratios.[46] Interestingly, both, terminal and bridging CO bands were shifted to lower frequencies when the ligand coverage increased (**Rh$^{0.4}$** and **Rh$^{0.6}$** vs. **Rh$^{0.2}$**), as expected for an increase in electronic density of the Rh surface and the low amount of CO molecules coordinated at the metallic surface.

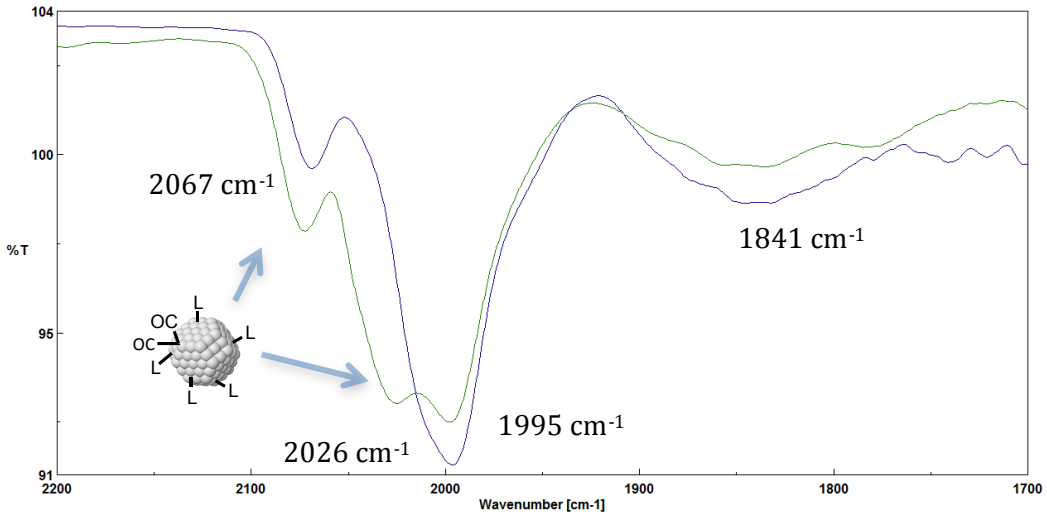

Figure 3. 37. IR spectra of **Rh$^{0.4}$** after exposure to 1 (blue) and 30 (green) bar of CO.

To explore the effect of the CO pressure on the adsorption of CO molecules onto the surface, a sample of **$Rh^{0.4}$** was analysed after exposure to 30 bars of CO and the IR spectrum was compared to that obtained after exposure to 1 bar of CO. (Figure 3. 37). An increase in intensity of the bands corresponding to germinal "$Rh(CO)_2$" units located at *ca.* 2070 and 2020 cm^{-1} was observed while no relevant changes were detected in the rest of the spectra (terminal COs at *ca.*1996 cm^{-1} and bridging COs at *ca.* 1841 cm^{-1}) (Figure 3. 37, green). This increase in "$Rh(CO)_2$" groups on the NPs surface indicated that the coordination of a second CO on coordinatively unsaturated Rh centres depend on the CO pressure.

The application of ^{13}C MAS NMR spectroscopy for samples exposed to CO have also been reported as a useful technique for obtaining information related to the availability of free sites and the location of ligands at the NPs surface. The coordination of CO on metal NPs was first monitored by ^{13}C MAS NMR, with and without ^{1}H-^{13}C Cross Polarization (CP), for Ru NPs stabilized using PVP and dppb.[32] Studies based on ^{13}C MAS NMR analysis of these samples after exposure to ^{13}CO revealed that CO groups are mobile at the surface of polymer stabilized Ru NPs (Ru/PVP) but notably less mobile on ligand stabilized Ru NPs (Ru/dppb), probably because of the steric hindrance induced by the presence of these ligands at the NPs surface. Furthermore, the analysis of Ru/dppb by ^{13}C CP-MAS NMR evidenced the presence of dppb on the edges or the apexes of the NPs. These results were then used to study how the presence of anchillary ligands can influence catalytic reactions such as CO oxidation, CO_2 reduction and styrene hydrogenation.[77] Similar

results in terms of CO adsorption were obtained on Ru NPs stabilized by heptanol and heptanol-dppb[78] and on Pt NPs stabilized by PVP and dppb[76]. In addition, the effect of the presence of other phosphine ligands such as PPh_3 on the CO coordination at the NPs surface was found to be similar to the one observed for dppb.[70] In contrast, the availability of only the apexes and edges on bimetallic RuPt NPs was observed by the same procedure.[33]

More recently, this technique has also been used for surface characterization of Ru NPs stabilized by NHC ligands.[46] Detection of diffusing bridging COs at the faces of the NPs and static terminal COs, from CO groups coordinated at the edges and apexes of the NPs, was observed when Ru NPs stabilized by I*t*Bu and IPr were analysed after exposure to ^{13}CO. On the other hand, the fact that no signals for bridging COs were detected when Ru NPs formed by an excess of the IPr ligand were examined following the same procedure, evidenced that coordination of this excess of ligand had taken place on the faces of these NPs. This result was correlated with a decrease in catalytic activity of this nanocatalyst in the hydrogenation of substrates bearing aromatic rings.[47]

In this work, the surface of the NPs **$Rh^{0.2}$-$Rh^{0.6}$** was analysed by ^{13}C CP-MAS NMR using similar procedures: the solid samples were exposed to 0.5 atm of ^{13}CO of at room temperature for 16h prior to NMR analysis. The detection of two new signals centred at *ca.* 170 and 190 ppm in the ^{13}C CP-MAS NMR spectrum (Figure 3. 38b), compared to the spectrum obtained for the same sample before exposure to ^{13}CO (Figure 3. 38a), evidenced the coordination of ^{13}CO

to the surface of the NPs. These signals were assigned to bridging and terminal CO molecules, respectively, and therefore corresponded to the COs coordinated to the faces and the apexes/edges of the Rh NPs, respectively.

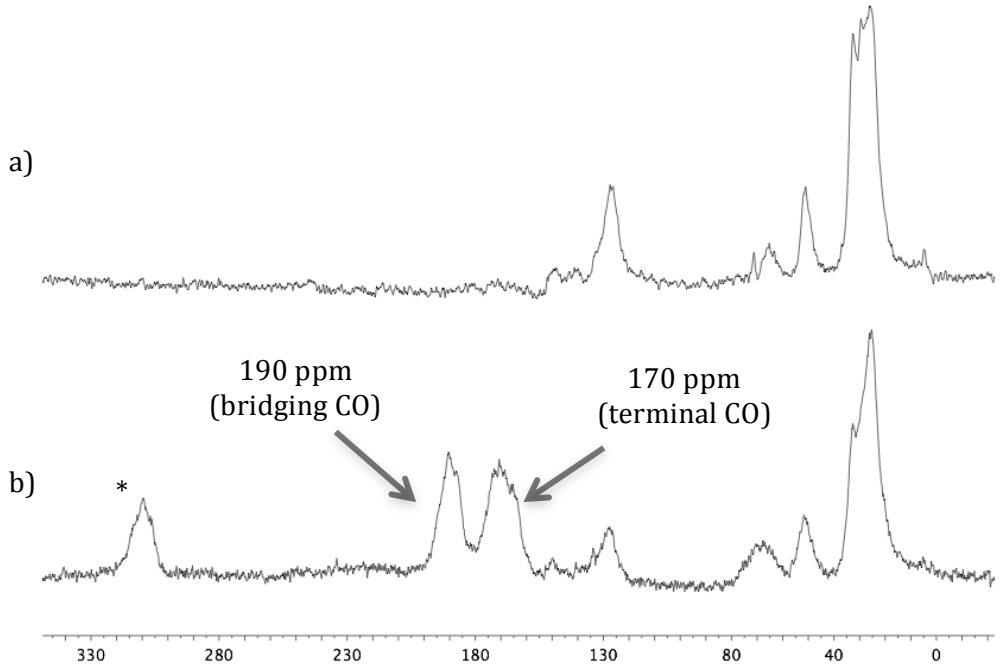

Figure 3. 38. $^{13}C\{^{1}H\}$ CP-MAS spectrum of a) **Rh$^{0.2}$** and ^{13}C CP-MAS spectrum of **Rh$^{0.2}$** after exposition to 0.5 bar ^{13}CO for 16h (*spinning sidebands at 12 KHz)

It is noteworthy that previous results on Rh/silica surfaces described higher chemical shifts (222 ppm for the adsorption of bridging COs and 177 ppm for terminal ones).[79] The chemical shifts of the signals described here were also slightly lower than those previously reported for systems based on Ru[46,48,32,51,70,78], Pt[76] and RuPt[33] bimetallic NPs (~250 for bridging and ~200 ppm for terminal CO).

The fact that similar intensities were observed for both signals at *ca*. 190 and 170 ppm using ^{13}C CP-MAS NMR, suggested the presence of

similar amounts hydrogen carriers, mainly stabilizing ligand, at the apexes/edges and the faces of NPs **Rh$^{0.2}$**.

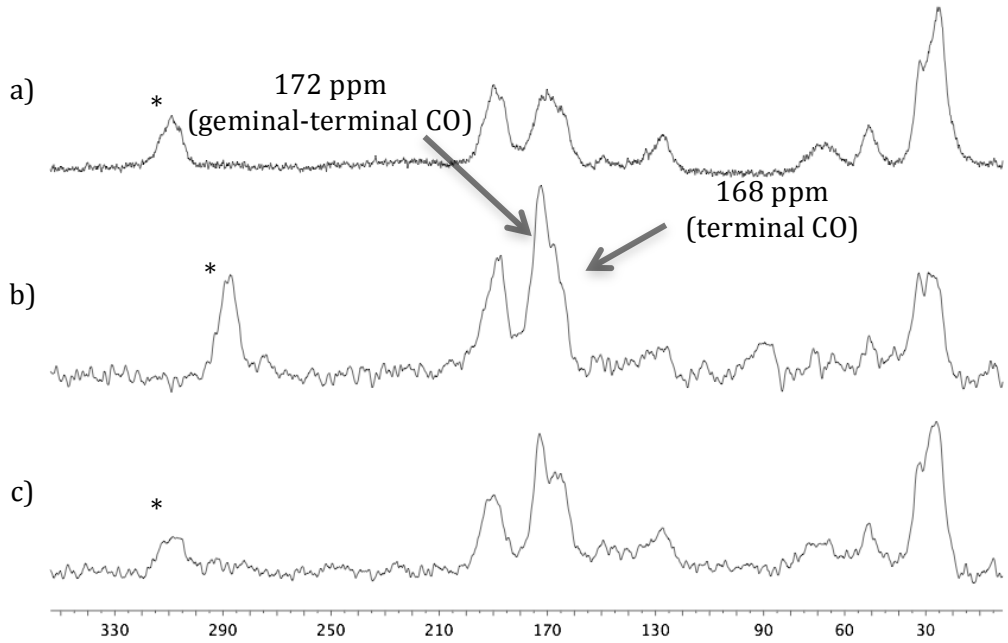

Figure 3. 39. $^{13}C\{^{1}H\}$ CP-MAS spectra of a) **Rh$^{0.2}$**, b) **Rh$^{0.4}$** and c) **Rh$^{0.6}$** after exposition to 0.5 bar ^{13}CO for 16h (*spinning sidebands at 12 KHz for **Rh$^{0.2}$** and **Rh$^{0.6}$**; and at 10 KHz for **Rh$^{0.4}$**)

When **Rh$^{0.4}$** and **Rh$^{0.6}$** were analysed following the same methodology, signals were detected at similar chemical shifts (Figure 3. 39b and c). In these cases, the observation of two signals arising from terminal COs at 168 and 172 ppm confirmed the possible formation terminal and geminal (or multicarbonyl) COs, as previously observed by IR spectroscopy. By comparison with IR results, the increase in intensity of the resonance at 172 ppm suggested that this signal arose from geminal-terminal (or multicarbonyl) "$Rh(CO)_2$". On the other hand, the fact that higher intensities were observed for terminal COs in the case of **Rh$^{0.4}$** and

Rh$^{0.6}$ compared to **Rh$^{0.2}$** (in reference to the signals from the ligand) would evidence the greater presence of stabilizing ligands on the faces of NPs **Rh$^{0.4}$** and **Rh$^{0.6}$**.

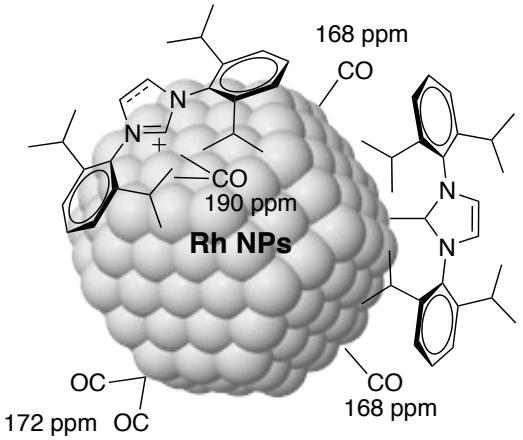

Figure 3. 40. Representation of CO adsorption and stabilizing ligands onto metallic Rh NPs

Surprisingly, spinning side bands from static bridging COs were detected in all cases, in contrast with previously reported results for Ru/IPr NPs.[46] This observation evidenced the static nature of the COs coordinated on the faces of these Rh NPs, possibly due to the presence of the stabilizing agents (NHC and imidazoliums).

3.3. Conclusions

- Well dispersed spherical Rh NPs with fcc packing structure and mean diameters between 1.26 - 1.68 nm were successfully synthesised in the presence of IPr ligands using the organometallic approach. The surface Rh atoms of these NPs were shown to be in the 0 oxidation state.

- A decrease in the mean diameter was observed at higher [IPr]/[Rh] molar ratios.

- An increase in the [IPr]/[Rh] molar ratio from 0.2 to 0.4 showed an increase in the ligand content at the surface of the NPs from 21.5 to 37 wt%; and a decrease in the hydride/Rh_s molar ratio from 0.58 to 0.39.

- The presence of stabilizing ligand at the Rh NPs surface was evidenced by IR and solution/solid-state NMR spectroscopy.

-The presence of an imidazolium species at the surface of the Rh NPs was detected by solution-state NMR spectroscopy.

- The availability of faces, edges and apexes for **$Rh^{0.2}$**, **$Rh^{0.4}$** and **$Rh^{0.6}$** was investigated using CO adsorption-IR/solid state NMR spectroscopy. COs adsorbed on the faces, edges and apexes were detected. Edges and apexes revealed less available at high [IPr]/[Rh] molar ratios (0.4 and 0.6).

- The presence of static COs on the faces of these NPs was evidenced by NMR spectroscopy.

- High-pressure solution NMR experiments under CO showed:

  1) The decoordination of imidazolium species from the Rh surface of the NPs.

  2) The strong binding of the NHC ligand IPr at the surface of the NPs via the formation of Rh-NHC species (no free NHC detected).

3.4. Experimental part

General procedures

All operations were carried out using standard Schlenk tubes, Fischer-Porter bottle techniques or in a glove-box under argon atmosphere. The chemicals were purchased from Sigma-Aldrich and used without further purification. THF and pentane were dried over sodium/benzophenone, distilled and then thoroughly degassed before use by three freeze- pump cycles. IPr carbene and $Rh(\eta^3\text{-}C_3H_5)_3$ were synthesized from previously published methodologies. Rh nanoparticles were synthesized following a reported methodology starting from the appropriate metal precursor and stored in a glove box under argon atmosphere. The synthesis of the nanoparticles and the catalysis was carried out in a Fischer-Porter glassware under argon.

Synthesis of the ligand

Synthesis of N,Nμ-Bis(2,6-diisopropylphenyl)-1,4-diazabutadiene[80]:

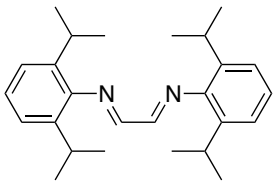

2,6-diisopropylaniline (11 g, 0.056 mol) was dissolved in methanol (112 ml), treated with aqueous glyoxal solution (3.23 ml, 0.028 mol) and three drops of formic acid. The reaction mixture was stirred for 16 h at room temperature. The yellow solid was filtered off, washed with cold methanol and dried in vacuum. The volume of the mother liquor was halved and the remaining

solution kept at 4°C over night for a second batch of product. (Yield=7.9 g, 68%).

Spectroscopic data are in agreement with the reported in the literature.

Synthesis of IPr·HCl[67]:

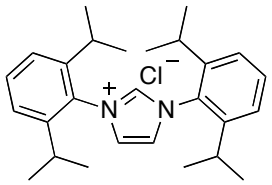

Diazabutadiene (10 g, 0.027 mol) was dissolved in anhydrous THF (250 ml) under an atmosphere of Ar. A solution of paraformaldehyde (1 g, 0.033 mol) in HCl in dioxane (10 ml, 0.04 mol) was prepared and added to the diimine solution at 0°C via syringe. The reaction mixture was stirred at room temperature for 16 h to observe the formation of a white precipitate. The precipitate was filtered off and washed with THF (3 x 50 ml). (Yield: 6.69 g, 60%). A similar procedure was followed for the synthesis of the ^{13}C-labelled IPr·HCl in similar yields. **^{1}H-NMR** ($CDCl_3$, 400MHz, δ in ppm): δ = 8.7 (s, 1H, H_{acidic}), 7.83 (d, 2H, -CH=CH-), 7.60 (t, 2H, -$CH_{arom,para}$-), 7.37 (d, 3H, -$CH_{arom,meta}$-), 2.43 (sept, 4H, -CH-$(CH_3)_2$), 1.29 (d, 12H, -CH_3), 1.21 (d, 12H, -CH_3). **^{13}C{^{1}H}-NMR** ($CDCl_3$, 100.6MHz, δ in ppm): δ = 145.05 (-CH_{ortho}-), 138.26 (-N-C-N-), 132.09 (-C_{ipso}-N-), 129.95 (-CH_{para}-), 126.9(-CH_{meta}-), 124.65 (=CH), 29 (-CH-$(CH_3)_2$), 24.98 (-CH_3), 23.9 (-CH_3).

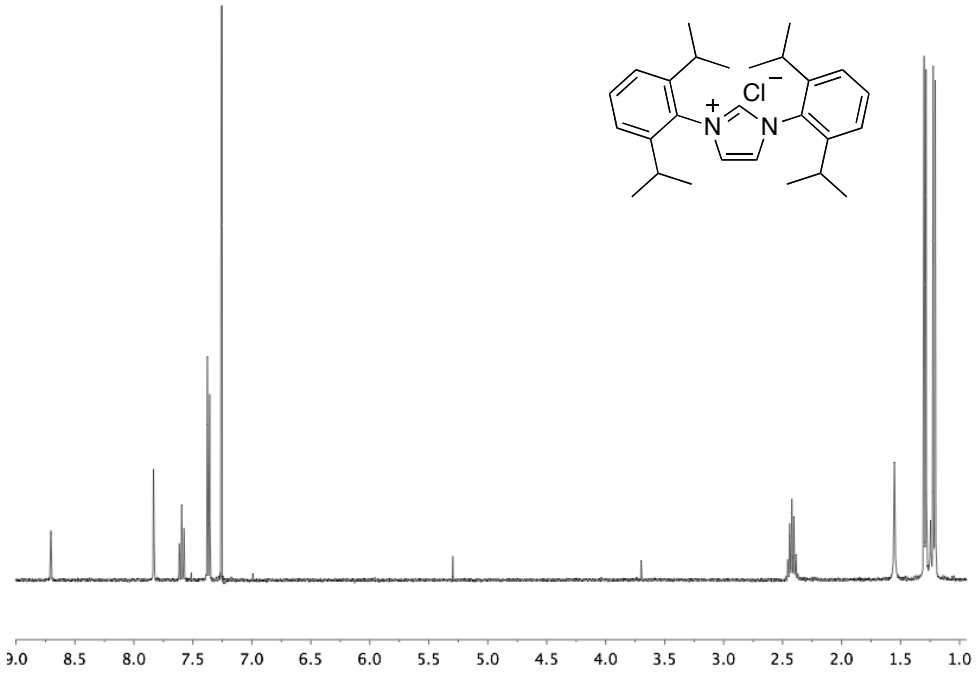

Figure 3. 41. ^{1}H NMR ($CDCl_3$, 400MHz) spectrum of IPr·HCl

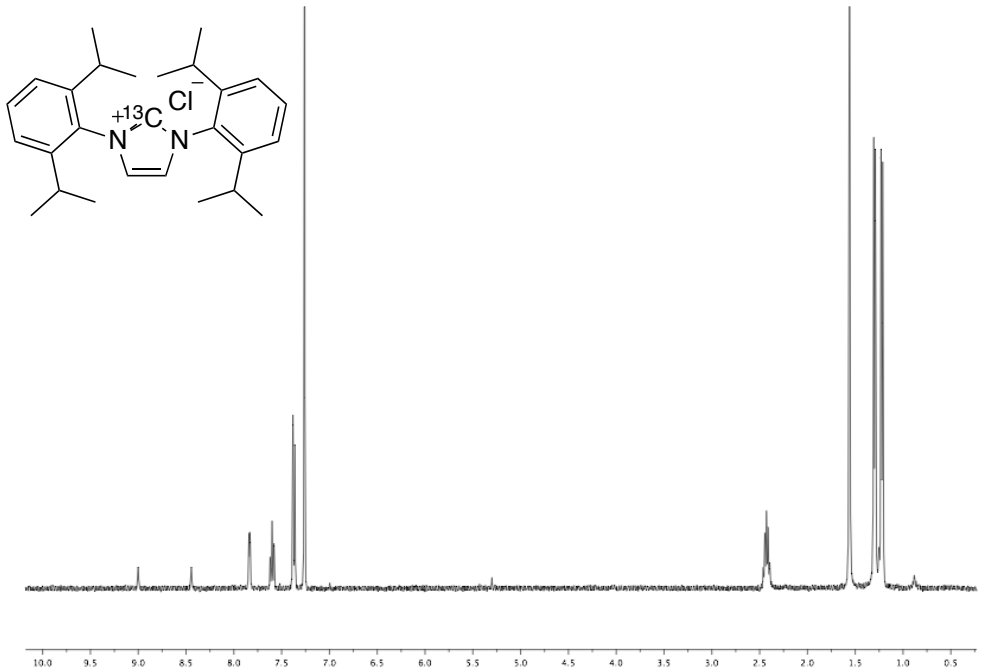

Figure 3. 42. ^{1}H NMR ($CDCl_3$, 400MHz) spectrum of ^{13}C-IPr·HCl

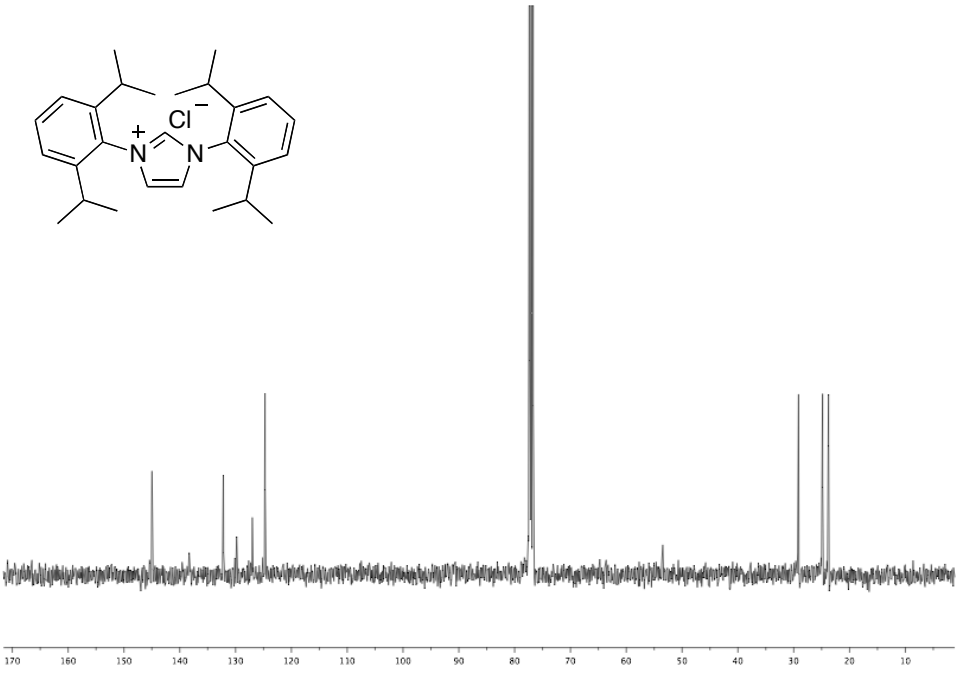

Figure 3. 43. $^{13}C\{H\}$ NMR (THF-d^8, 100.6MHz) spectrum of IPr·HCl

Synthesis of IPr·HBF_4[81]:

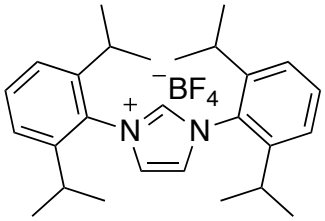

IPr·HCl (3.89 g, 9.16 mmol) was dissolved in the minimum amount of water (150 ml). HBF_4 (1.89 ml, 13.7 mmol) was added to the solution and a white precipitate was formed instantaneously. The aqueous phase was extracted with CH_2Cl_2 (3 x 30 ml) and the combined organic phases were dried with $MgSO_4$ and concentrate under vacuum to obtain a white powder. (Yield: 2.84 g, 65%).

Spectroscopic data are in agreement with the reported in the literature.

Synthesis of IPr[67]:

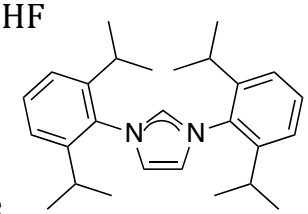

A solution of KO^{t}Bu (94.51 mg, 0.84 mmol) in THF (10ml) was added drop wise to a stirred suspension of IPr·HBF_4 (267.5 mg, 0.56 mmol) in THF (15ml) at room temperature. After the mixture was stirred for 30 min, the solution was evaporated and the crude white powder was extracted with hexane (3 x 10 ml) to remove the excess of base and evaporated to dryness to give the isolated product as a white powder. (Yield: 160 mg, 73%). A similar procedure was followed for the synthesis of the ^{13}C-labelled IPr in similar yields. **^{1}H-NMR** (THF-d^8, 400MHz, δ in ppm): δ = 7.35 (t, 2H, -$CH_{arom,para}$-) 7.25 (d, 4H, -$CH_{arom,meta}$-), 7.17 (s, 2H, -N-CH=), 2.81 (m, 4H, -CH-$(CH_3)_2$, 1.19 (d, 12H, -CH_3), 1.15 (d, 12H, -CH_3). **^{13}C{^{1}H}-NMR** (THF-d^8, 100.6MHz, δ in ppm): δ = 221.3 (-N-C-N-), 146.71 (-CH_{ortho}-), 139.61 (-C_{ipso}-N-), 129.17 (-CH_{para}-), 123.88 (-CH_{meta}-), 122.47 (=CH), 29.20 (-CH-$(CH_3)_2$), 24.87 (-CH_3), 23.70 (-CH_3).

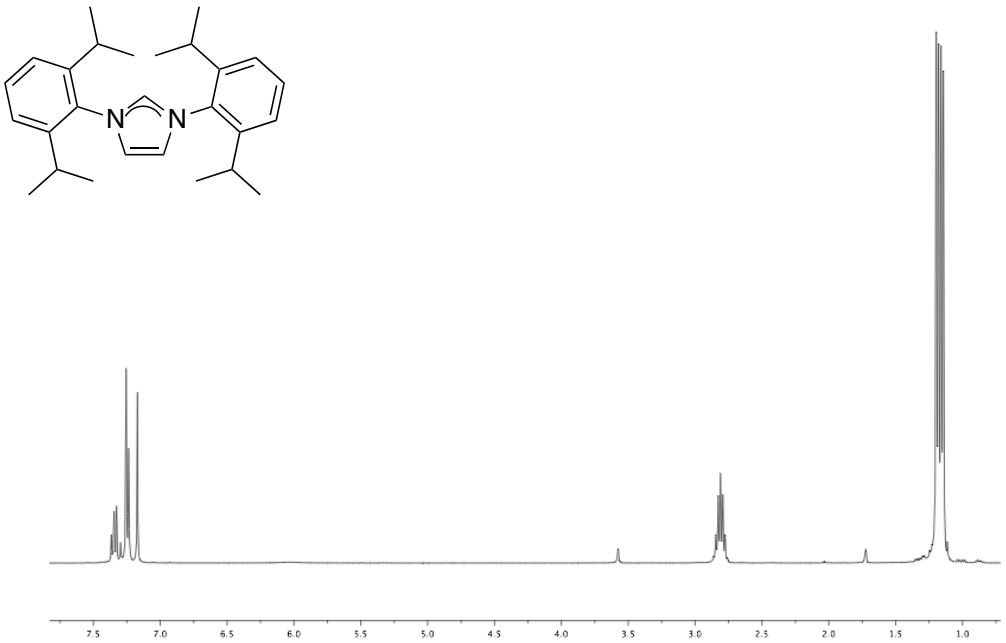

Figure 3. 44. ^{1}H NMR (THF-d^{8}, 400MHz) spectrum of IPr

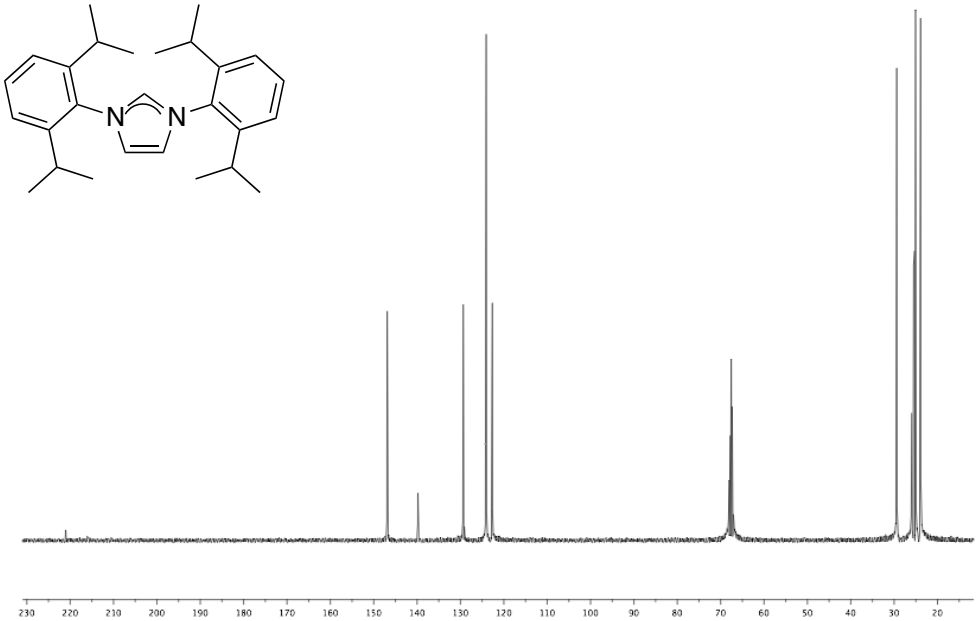

Figure 3. 45. $^{13}C\{^{1}H\}$ NMR (THF-d^{8}, 100.6MHz) spectrum of IPr

Synthesis of the Rh precursor

Synthesis of $[Rh(\eta^3\text{-}C_3H_5)_3]$[82,83]:

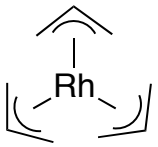

An allylmagnesium bromide solution (35mmol) was added to a cold suspension (-10°C) of $RhCl_3 \cdot 3H_2O$ (1.1g, 5.3mmol) in THF (93ml). The solution slowly lost its red-brown colour to become yellow. The solution was then allowed to warm to room temperature and stirred for an additional 16h. The solvent was removed under reduced pressure and the residue extracted with pentane (previously distilled and deoxygenated) (3x20ml). The sublimation was carried out in a water bath at 40°C and the formation of yellow crystals was observed onto the cold finger. (Yield: 520mg, 55%).

The purity of this complex was checked by ^1H and ^{13}C NMR spectroscopy.[84]

Synthesis of Rh NPs stabilized by IPr

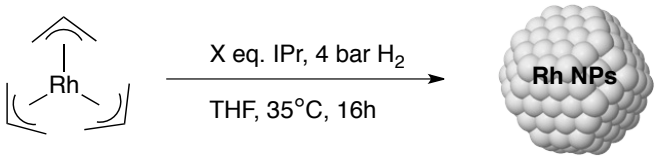

In a typical procedure, the [Rh(ŋ^3-(C_3H_5)$_3$] (250mg, 0.22mmol) was placed into a Fischer-Porter reactor and dissolved in 230 ml of dry and deoxygenated THF by three freeze-pump cycles. The resulting yellow solution was cooled at -110°C (acetone/N_2 bath) and a solution of 20 ml of THF containing the appropriate amount of equivalents of the IPr carbene was added into the reactor. The Fischer-Porter reactor was then pressurized under 4 bar H_2 and stirred for 30 minutes at room temperature. The solution was then heated to 35°C and stirred at this temperature during 16 h. The initial yellow solution became black after 1 h. A small amount (2 drops approx.) of the solution was deposited under an Argon atmosphere on a carbon-covered copper grid for transmission electron microscopy analysis. The rest of the solution was evaporated to dryness. Precipitation and washings with pentane (3 x 15 ml) was then carried out, obtaining a black powder. (Yield: ca. 150 mg, 98%). A similar procedure was followed for the synthesis of the ^{13}C-Rh NPs in similar yields.

Rh NPs stabilized by 0.2 eq. of IPr (**$Rh^{0.2}$**):

TEM: 1.68 ± 0.26 nm

XRD: *fcc* structure, coherence length 1.79 ± 0.05 nm

WAXS: *fcc* structure, coherence length 2.5 nm

XPS: Rh(0) $3d_{5/2}$ (306.7eV) $3d_{3/2}$ (311.40eV), >99% Rh(0)

TGA: 74% Rh, 21.5% organic part, 4.5% THF

Rh NPs stabilized by 0.4 eq. of IPr (**$Rh^{0.4}$**):

TEM: 1.26 ± 0.25 nm

XRD: *fcc* structure, coherence length 1.97 ± 0.03 nm

WAXS: *fcc* structure, coherence length 3.4-3.5 nm

XPS: Rh(0) $3d_{5/2}$ (308.98eV) $3d_{3/2}$ (313.68eV), 99% Rh(0)

TGA: 56.6% Rh, 37% organic part, 6.4% THF

Rh NPs stabilized by 0.6 eq. of IPr (**$Rh^{0.6}$**):

TEM: 1.29 ± 0.21 nm

XRD: *fcc* structure, coherence length 2.17 ± 0.06 nm

WAXS: *fcc* structure, coherence length 3.4-3.5 nm

XPS: Rh(0) $3d_{5/2}$ (308.45eV) $3d_{3/2}$ (313.35eV), 97% Rh(0)

TGA: 60.8% Rh, 36.1% organic part, 3.1% THF

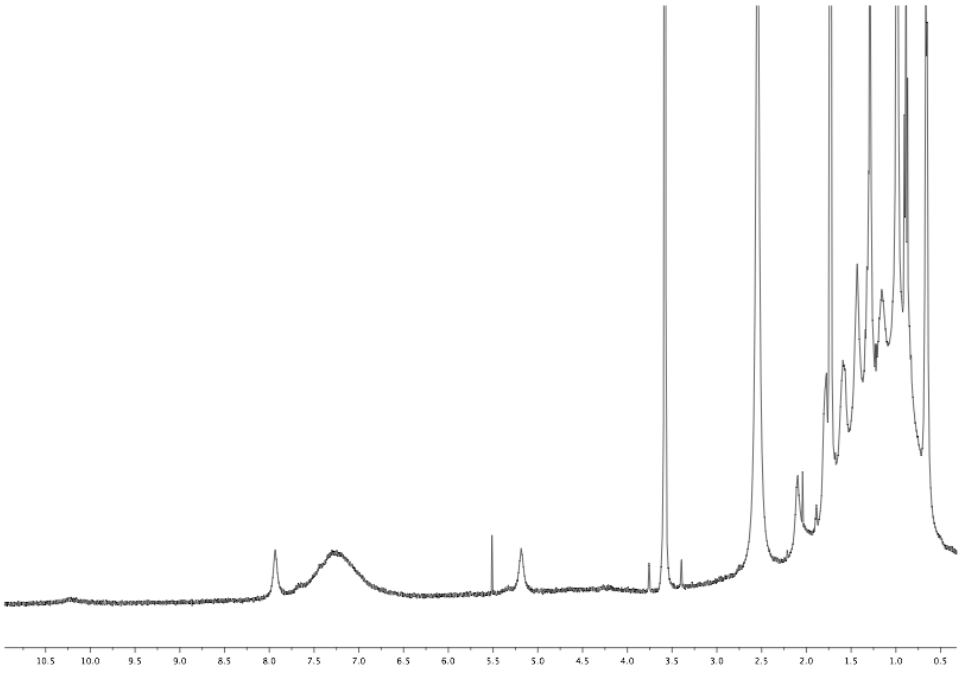

Figure 3. 46. ^{1}H NMR (THF-d^{8}, 400MHz) spectrum of **$Rh^{0.4}$**

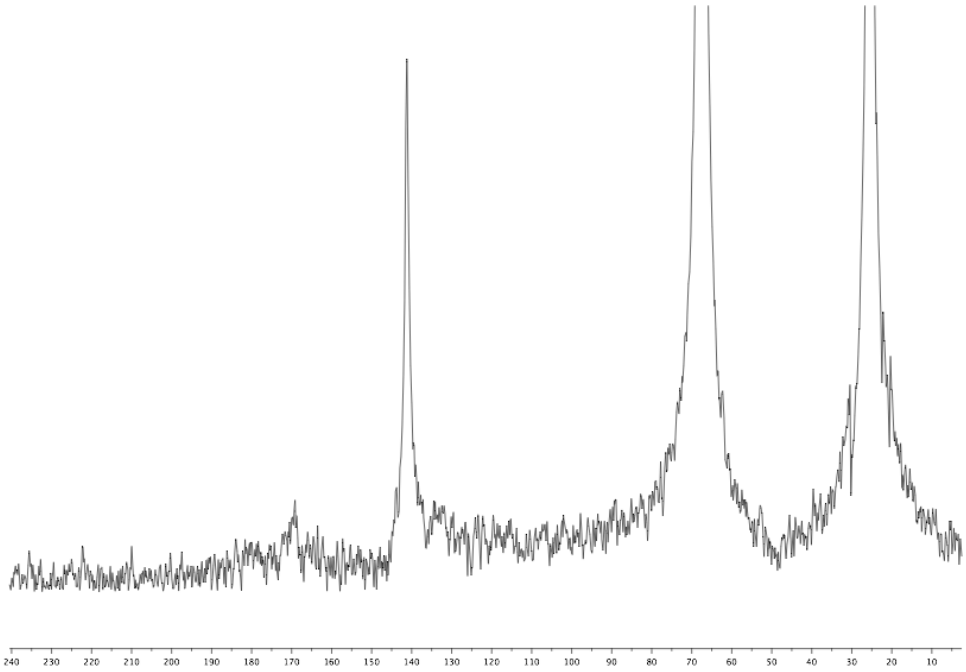

Figure 3. 47. $^{13}C\{^{1}H\}$ NMR (THF-d^{8}, 100.6MHz) spectrum of **^{13}C-$Rh^{0.4}$**

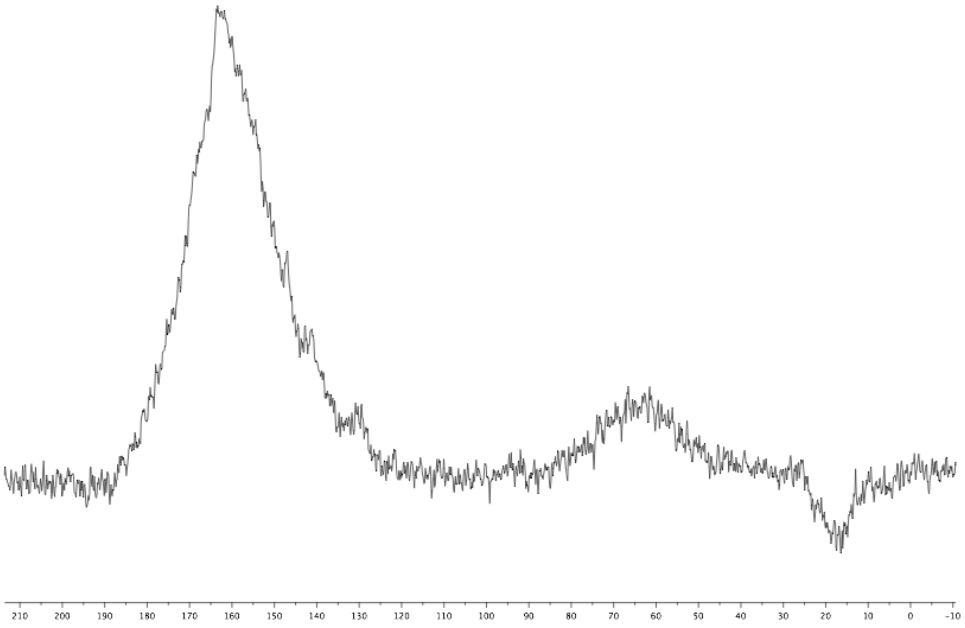

Figure 3. 48. $^{13}C\{^{1}H\}$ APT CP-MAS spectrum of **^{13}C-Rh$^{0.4}$**

General characterization techniques

Transmission Electron Microscopy (TEM), For High Resolution Transmission Electron Microscopy (HRTEM) and Scanning Electron Microscopy (SEM):

TEM analysis were performed at the "Unitat de Microscopia dels Serveis Cientificotècnics de la Universitat Rovira i Virgili" (TEM-SCAN) in Tarragona with a Zeiss 10 CA electron microscope operating at 100 kV with resolution of 3 Å. The particles size distributions were determined by a manual analysis of enlarged images. At least 300 particles on a given grid were measured in order to obtain a statistical size distribution and a mean diameter. For HRTEM and SEM a probe-corrected, cold-FEG JEOL ARM microscope equipped with a centurio EDX detector operated at 200keV was used.

X-Ray Diffraction (XRD):

XRD measurements were made using a Siemens D5000 difractometer (Bragg Brentano parafocusing geometry and vertical θ-θ goniometer) fitted with a curved graphite diffracted beam monochromator, incident and diffracted beam Soller slits, a 0.06° receiving slit and scintillation counter as a detector. The angular 2θ diffraction range was between 26 and 95°. The data were collected with an angular step of 0.05° at 16s per step and sample rotation. A low background Si(510) wafer was used as Sample holder. $Cu_{k\alpha}$ radiation was obtained from a copper X-Ray tube operated at 40kV and 30mA.

Wide Angle X-ray Scattering (WAXS):

WAXS was performed at CEMES-CNRS. Samples were sealed in 1 mm diameter Lindemann glass capillaries. The samples were irradiated with graphite-monochromatized molybdenum Kα (0.071069) radiation and the X-ray intensity scattered measurements were performed using a dedicated two-axis diffractometer. Radial distribution functions (RDF) were obtained after Fourier Transformation of the reduced intensity functions.

X-ray Photoelectron Spectroscopy (XPS):

XPS analysis were performed at the "Centres Científics i Tecnològics de la Universitat de Barcelona" (CCiT UB) in a PHI 5500 Multitechnique System (from Physical Electronics) with a monochromatic X-Raysource (Aluminium Kalfa line of 1486.6 eV

energy and 350W), placed perpendicular to the Analyser axis and calibrated using the 3d5/2 line of Ag with a full width at half maximum (FWHM) of 0.8 eV. The analysed area was a circle of 0.8 mm diameter, and the selected resolution for the spectra was 187.5 eV of Pass Energy and 0.8!eV/ step fort the general spectra and 23.5 eV of Pass Energy and 0.1 eV/step for the spectra of the different elements in the depth profile spectra. A low energy electron gun (<10 eV) was used in order to discharge the surface when necessary. All measurements were performed in an ultra high vacuum (UHV) chamber pressure between 5x1039 and 2x1038 torr. For this analysis, the data processing was carried out with the program CasaXPS. Initially, the general spectrum of the different binding energies observed for this sample was analysed and was used to calibrate the following calculations. This calibration was performed using the values for the rhodium that is the element of interest for these analyses.

ThermoGravimetric Analysis(TGA):

TGA analysis was carried out in the furnace of a Mettler Toledo TGA/SDTA851 instrument. As a typical TGA experiment, 132 mg of NPs were placed in the simple holder in the furnace and the material was heated up at a rate of 10°C min in N_2, while the weight was recorded continuously from 30°C to 900°C. The weight loss of the organic part and the metal were used to calculate an approximate number of ligands coordinated to the metal surface. The ligand loss was attributed to the weight loss observed between 150 and 900°C. For the calculation, the molecular weight of the corresponding

ligands and the metal, and the number of metal atoms at the surface from TEM data were taken into account.

Infrared spectroscopy (IR):

IR analysis was performed by the preparation of samples as KBr pellets. The nanoparticles were used without any preparation step, mixed and crushed with dry KBr in the glove box before the preparation of the pellet. For CO coordination studies, Rh nanoparticles were introduced in a Fischer Porter bottle and were pressurised with 3 bars of H_2 in solid state for 5h. After this period of time, the H_2 gas was evacuated under vacuum for 10 min. The Fischer Porter bottle was then pressurised with 1 atm of CO for 16h. HEL 24 Cat reactor was used for high CO pressure exposures. Then, the gas was evacuated under vacuum for 15 min and IR spectroscopy samples were prepared as KBr pellets in the glove box.

General procedure to perform hydrides titration:

A previously reported procedure was used for the quantification of hydrides coordinated on the surface of the Rh nanoparticles.[61,32]
The colloidal solution has been prepared in THF as previously described and on each fresh colloidal solution, five cycles of 1 minute vacuum/1 minute bubbling of argon were performed in order to eliminate the H_2 solved into the solvent. After that, 1 equivalent of 2-norbornene was added and samples were regularly taken from the solution every 24h. All samples were filtrate throught an Al_2O_3 pad. and analysed by GC and estimation of the olefin conversion into

alkenes were obtained. The method used for the quantification of hydrides consists of 15 min at 40°C and a ramp of 8°C/min. until 250°C.

The number of hydrogen atoms was calculated from the respective conversion obtained for the hydrogenation of 2-norbornene to norbornane and taking into account the number of atoms of Rh in the surface of the NPs calculated by the Van Hardeveld-Hartog model, the mol H / mol Rh surface ratio was calculated. The systems used for these measurements were: **$Rh^{0.2}$**, **$Rh^{0.4}$** and **$Rh^{0.6}$**; and their mean sizes and surface rhodium atom contents were: **$Rh^{0.2}$** (mean size: 1.68/ 62% surface atoms), **$Rh^{0.4}$** (mean size: 1.26/ 72% surface atoms), **$Rh^{0.6}$** (mean size: 1.29/ 71% surface atoms).

Nuclear Magnetic Resonance (NMR):

^{1}H, ^{2}D, ^{13}C, ^{31}P spectra were recorded on a Varian® Mercury VX 400 (400 MHz, 61.49 MHz, 100.6 MHz, 162 MHz respectively). Chemical shift values for ^{1}H and ^{13}C were referred to internal $SiMe_4$ (0.0ppm) and for ^{31}P was referred to H_3PO_4 (85% solution in THF, 0 ppm). Chemical shifts are reported in parts per million (ppm) and coupling constants are reported in Hertz (Hz).

Cross Polarization - Magic Angle Spinning (CPMAS):

CPMAS experiments were performed on a BRUKER Avance III spectrometer operating at a magnetic field of 9.4 T and equipped with a double channel 4.0 mm MAS probe. The powder materials were packed into 4 mm ZrO_2 rotors and were sealed with tight fitting

Kel-F caps. Sample spinning was set to 10 and 12 KHz, depending on the experiment. Chemical shifts are reported in parts per million (ppm) externally referenced to adamantane (CH_2 peak set to 38.5 ppm). Cross polarization time was set to 2500 ms and performed with a radio-field strength of 83 KHz and a ^1H ramp pulse was used (ramp70100 in Bruker nomenclature). ^1H-decoupling was performed using SPINAL-64 pulse scheme. The recovery delay was set to 1 s and overall experimental time was set from 12 to 24h by varying the number of scans depending on the sample sensitivity. Spectra were acquired at 20°C controlled by a BRUKER BCU unit.

For CO coordination studies, Rh nanoparticles were introduced in a Fischer-Porter reactor and were pressurized with 3 bar of H_2 for 5h to avoid the presence of oxygen on the surface. After this period of time, the H_2 was evacuated under vacuum for 15min. The Fischer-Porter reactor was further pressurized with 0.5 bar of ^{13}CO for 16 h. Then, the gas was evacuated under vacuum for 15 min. ^{13}C CP-MAS NMR experiments were recorded after transfering the sample into a NMR rotor after its dilution using KBr.

3.5. References

[1] A. Roucoux, J. Schulz, H. Patin, *Chem. Rev.* **2002**, *102*, 3757-3778.

[2] G. S. Fonseca, A. P. Umpierre, P. F. P. Fichtner, S. R. Teixeira, J. Dupont, *Chem. Eu. J.* **2003**, *9*, 3263-3269.

[3] P. Migowski, J. Dupont, *Chem. Eur. J.* **2007**, *13*, 32-39.

[4] B. Léger, A. Denicourt-Nowicki, A. Roucoux, H. Olivier-Bourbigou, *Adv. Synth. Catal.* **2008**, *350*, 153-159.

[5] B. Léger, A. Denicourt-Nowicki, H. Olivier-Bourbigou, A. Roucoux, *Inorg. Chem.* **2008**, *47*, 9090-9096.

[6] R. R. Dykeman, N. Yan, R. Scopelliti, P. J. Dyson, *Inorg. Chem.* **2011**, *50*, 717-719.

[7] S. A. Stratton, K. L. Luska, A. Moores, *Catal. Today.* **2012**, *183*, 96-100.

[8] L. Chen, J. Xin, L. Ni, H. Dong, D. Yan, X. Lu, S. Zhang, *Green. Chem.* **2016**, *18*, 2341-2352.

[9] D. Astruc, F. Lu, J. R. Aranzaes, *Angew. Chem. Int. Ed.* **2005**, *44*, 7852-7872.

[10] J. D. Hoefelmeyer, K. Niesz, G. A. Somorjai, T. D. Tilley, *Nano Lett.* **2005**, *5*, 435-438.

[11] Y. Borodko, H. S. Lee, S. H. Joo, Y. Zhang, G. Somorjai, *J. Phys. Chem. C.* **2010**, *114*, 1117-1126.

[12] X. Yang, N. Yan, Z. Fei, R. M. Crespo-Quesada, G. Laurenczy, L. Kiwi-Minsker, Y. Kou, Y. Li, P. J. Dyson, *Inorg. chem.* **2008**, *47*, 7444-7446.

[13] C. Zhao, H.-Z. Wang, N. Yan, C.-X. Xiao, X.-D. Mu, P. J. Dyson, Y. Kou, *J. Catal.* **2007**, *250*, 33-40.

[14] N. Yan, Y. Yuan, P. J. Dyson, *Chem. Commun.* **2011**, *47*, 2529-2531.

[15] M. Ibrahim, R. Poreddy, K. Philippot, A. Riisager, E. J. Garcia-Suarez, *Dalton Trans.* **2016**, *45*, 19368-19373.

[16] J. Zhang, M. Ibrahim, V. Collière, H. Asakura, T. Tanaka, K. Teramura, K. Philippot, N. Yan, *J. Mol. Catal. A: Chem.* **2016**, *422*, 188-197.

[17] Fine Chemical Synthesis – Homogeneous, J. G. de Vries, *Wiley*, **2002**.

[18] P. Lara, K. Philippot, B. Chaudret, *ChemCatChem* **2013**, *5*, 28-45.

[19] M. R. Axet, S. Castillón, C. Claver, K. Philippot, P. Lecante, B. Chaudret, *Eur. J. Inorg. Chem.* **2008**, *22*, 3460-3466.

[20] A. Gual, C. Godard, K. Philippot, B. Chaudret, A. Denicourt-Nowicki, A. Roucoux, S. Castillón, C. Claver, *ChemSusChem* **2009**, *2*, 769-779.

[21] D. Han, X. Li, H. Zhang, Z. Liu, G. Hu, C. Li, *J. Mol. Catal. a.: Chem.* **2008**, *283*, 15-22.

[22] M. Guerrero, N. T. T. Chau, S. Nöel, A. Denicourt-Nowicki, F. Hapiot, A. Roucoux, E. Monflier, K. Philippot, *Curr. Org. Chem.* **2013**, *17*, 364-399.

[23] K. Li, Y. Wang, J. Jiang, Z. Jin, *Catal. Commun.* **2010**, *11*, 542-546.

[24] M. V. Escárcega-Bobadilla, C. Tortosa, E. Teuma, C. Pradel, A. Orejón, M. Gómez, A. M. Masdeu-Bultó, *Catal. Today* **2009**, *148*, 398-404.

[25] D. J. M. Snelders, N. Yan, W. Gan, G. Laurenczy, P. J. Dyson, *ACS Catal.* **2012**, *2*, 201-207.

[26] J. Llop, A. Gual, E. Mercadé, C. Claver, C. Godard, *Catal. Sci. Technol.* **2013**, *3*, 2828-2833.

[27] J. Llop Castelbou, P. Blondeau, C. Claver, C. Godard, *RSC Adv.* **2015**, *5*, 97036-97043.

[28] J. Llop Castelbou, E. Bresó-Femenia, P. Blondeau, B. Chaudret, S. Castillón, C. Claver, C. Godard, *ChemCatChem* **2014**, *6*, 3160-3168.

[29] M. Ibrahim, M. A. S. Garcia, L. L. R. Vono, M. Guerrero, P. Lecante, L. M. Rossi, K. Philippot, *Dalton Trans.* **2016**, *45*, 17782-17791.

[30] M. N. Hopkinson, C. Richter, M. Schedler, F. Glorius, *Nature* **2014**, *510*, 485-496.

[31] E. Bresó-Femenia, B. Chaudret, S. Castillón, *Catal. Sci. Technol.* **2015**, *5*, 2741-2751.

[32] F. Novio, K. Philippot, B. Chaudret, *Catal. Lett.* **2010**, *140*, 1-7.

[33] P. Lara, T. Ayvali, M.-J. Casanove, P. Lecante, A. Mayoral, P.-F. Fazzini, K. Philippot, B. Chaudret, *Dalton Trans.* **2013**, *42*, 372-382.

[34] K. Philippot, B. Chaudret, *C. R. Chemie* **2003**, *6*, 1019-1034.

[35] C. Amiens, B. Chaudret, D. Ciuculescu-Pradines, V. Collière, K. Fajerwerg, P. Fau, M. Kahn, A. Maisonnat, K. Soulantica, K. Philippot, *New, J. Chem.* **2013**, *37*, 3374-3401.

[36] K. V. S. Ranganath, J. Kloesges, A. H. Schäfer, F. Glorius, *Angew. Chem. Int. Ed.* **2010**, *49*, 7786-7789.

[37] E. A. Baquero, S. Tricard, J. C. Flores, E. de Jesús, B. Chaudret, *Angew. Chem. Int. Ed.* **2014**, *53*, 13220-13224.

[38] J. M. Asensio, S. Tricard, Y. Coppel, R. Andrés, B. Chaudret, E. de Jesús, *Angew. Chem. Int. Ed.* **2017**, *56*, 865-869.

[39] J. Vignolle, T. D. Tilley, *Chem. Commun.* **2009**, 7230-7232.

[40] X. Ling, N. Schaeffer, S. Roland, M.-P. Pileni, *Langmuir* **2013**, *29*, 12647-12656.

[41] C. J. Serpell, J. Cookson, A. L. Thompson, C. M. Brown, P. D. Beer, *Dalton Trans.* **2013**, *42*, 1385-1393.

[42] E. C. Hurst, K. Wilson, I. J. S. Fairlamb, V. Chechik, *New. J. Chem.* **2009**, *33*, 1837-1840.

[43] C. Richter, K. schaepe, F. Glorius, B. J. Ravoo, *Chem. Commun.* **2014**, *50*, 3204-3207.

[44] A. Ferry, K. Schaepe, P. Tegeder, C. Richter, K. M. Chepiga, B. J. Ravoo, F. Glorius, *ACS Catal.* **2015**, *5*, 5414-5420.

[45] A. Rühling, K. Schaepe, L. Rakers, B. Vonhören, P. Tegeder, B. J. Ravoo, F. Glorius, *Angew. Chem. Int. Ed.* **2016**, *55*, 5856-5860.

[46] P. Lara, O. Rivada-Wheelaghan, S. Conejero, R. Poteau, K. Philippot, B. Chaudret, *Angew. Chem. Int. Ed.* **2011**, *50*, 12080-12084.

[47] D. Gonzalez-Galvez, P. Lara, O. Rivada-Wheelaghan, S. Conejero, B. Chaudret, K. Philippot, P. W. N. M. van Leeuwen, *Catal. Sci. Technol.* **2013**, *3*, 99-105.

[48] P. Lara, L. M. Martínez-Prieto, M. Roselló-Merino, C. Richter, F. Glorius, S. Conejero, K. Philippot, B. Chaudret, *Nano-Structures & Nano-Objects* **2016**, *6*, 39-45.

[49] L. M Martínez-Prieto, E. A. Baquero, G. Pieters, J. C. Flores, E. de Jesús, C. Nayral, F. Delpech, P. W. N. M. van Leeuwen, G. Lippens, B. Chaudret, *Chem. Commun.*, 2017, *53*, 5850-5853.

[50] P. Lara, A. Suárez, V. Collière, K. Philippot, B. Chaudret, *ChemCatChem*, **2014**, *6*, 87-90.

[51] L. M. Martínez-Prieto, A. Ferry, P. Lara, C. Richter, K. Philippot, F. Glorius, B. Chaudret, *Chem. Eur. J.* **2015**, *21*, 17495-17502.

[52] L. M. Martínez-Prieto, A. Ferry, L. Rakers, C. Richter, P. Lecante, K. Philippot, B. Chaudret, F. Glorius, *Chem. Commun.* 2016, *52*, 4768-4771.

[53] DOI: 10.1039/C7CC01779K

[54] Library of the International Centre of Diffraction Data

[55] J. Ll. Castelbou, E. Bresó-Femenia, P. Blondeau, B. Chaudret, S. Castillón, C. Claver, C. Godard, *ChemCatChem*, **2014**, *6*, 3160-3168.

[56] K. Pelzer, B. Laleu, F. Lefebvre, K. Philippot, B. Chaudret, J. P. Candy, J. M Basset, *Chem. Mater.* **2004**, *16*, 4937-4941.

[57] B. M. Austin, D. Y. Zubarev, W. A. J. Lester, *Chem. Rev.* **2012**, *112*, 263-288.

[58] V. Hardevel, V. Hartog, *Surf. Sci.* **1969**, *15*, 189-230.

[59] J. Ll. Castelbou, P. Blondeau, C. Claver, C. Godard, *RSC Adv.* **2015**, *5*, 97036-97043.

[60] T. Pery, K. Pelzer, G. Buntkowsky, K. Philippot, H.-H. Limbach, B. Chaudret, *ChemPhysChem*, **2005**, *6*, 605-607.

[61] J. García-Antón, M. Rosa Axet, S. Jansat, K. Philippot, B. Chaudret, T. Pery, G. Buntkowsky,H-H. Limbach, *Angew. Chem.* **2008**, *120*, 2104-2108.

[62] a) W. D. Knight, *Phys. Rev.* **1949**, *76*, 1259-1260. b) J. J. van der Klink, H. B. Brom, *Prog. Nucl. Magn. Reson. Spectrosc.* **2000**, *36*, 89-201.

[63] E. Ramirez, L. Eradès, K. Philippot, P. Lecante, B. Chaudret *Adv. Funct. Mater.* **2007**, *17*, 2219-2228

[64] a) C. Pan, K. Pelzer, K. Philippot, B. Chaudret, F. Dassenoy, P. Lecante, M.-J. Casanove, *J. Am. Chem. Soc.* **2001**, *123*, 7584 – 7593. b) R. H. Terril, T. A. Postlethwaite, C.-H. Chen, C.-D. Poon, A. Terzis, A. Chen, J. E. Hutchison, M. R. Clark, G. Wignall, *J. Am. Chem. Soc.* **1995**, *117*, 12537-12548. c) A. Badia, W. GAo, S. Singh, L. Demers, L. Cuccia, L. Reven, *Langmuir* **1996**, *12*, 1262-1269. d) I. Favier, S. Massou, E. Teuma, K. Philippot, B. Chaudret, M. Gómez, *Chem. Commun.* **2008**, 3296 – 3298

[65] S. U. Son, Y. Jang, K. Y. Yoon, E. Kang, T. Hyeon *Nano Lett.* **2004**, *4*, 1147-1151

[66] J.-T. Lu, J. C. Y. Lin, M.-C.Lin, N. D. Khupse, I. J. B. Lin, *Langmuir* **2014**, *30*, 10440−10448

[67] A. J. Arduengo, R. Krafczyk, R. Schmutzler, *Tetrahedron* **1999**, *55*, 14523-14534.

[68] X.-Y. Yu, B. O. Patrick, B. R. James *Organometallics*, **2006**, *25*, 2359-2363.

[69] G. R. Fulmer, A. J. M. Miller, N. H. Sherden, H. E. Gottlieb, A. Nudelman, B. M. Stoltz, J. E. Bercaw, K. I. Goldberg, *Organometallics,* **2010**, *29*, 2176-2179.

[70] T. Gutmann, E. Bonnefille, H. Breitzke, P.-J. Debouttière, K. Philippot, R. Poteau, G. Buntkowsky, B. Chaudret, *Phys. Chem. Chem. Phys.* **2013**, *15*, 17383-17394.

[71] E. Rafter, T. Gutmann, F. Löw, G. Buntkowsky, K. Philippot, B. Chaudret, P. W. N. M. van Leeuwen, *Catal. Sci. Technol.* **2013**, *3*, 595-599.

[72] B. L. Mojet, S. D. Ebbesen, L. Lefferts, *Chem. Soc. Rev.* **2010**, *39*, 4643-4655.

[73] A. C. Yang, C. W. Garland, *J. Phys. Chem.* **1957**, *61*, 1504-1512.

[74] R. Bronger, T. D. Le. S. Bastin, J. García-Antón, C. Citadelle, B. Chaudret, P. Lecante, A. Igau, K. Philippot, *New J. chem.* **2011**, *35*, 2653-2660.

[75] C. Pan, K. Pelzer, K. Philippot, B. Chaudret, F. Dassenoy, P. Lecante, M.-J. Casanove, *J. Am. Chem. Soc.* **2001**, *123*, 7584- 7593.

[76] S. Kinayyigit, P. Lara, P. Lecante, K. Philippot, B. Chaudret, *Nanoscale*, **2014**, 539-546.

[77] F. Novio, D. Monahan, Y. Coppel, G. Antorrena, P. Lecante, K. Philippot, B. Chaudret, *Chem. Eur. J.* **2014**, 2*0*, 1287-1297

[78] L. M. Martinez-Prieto, S. Carenco, C. H. Wu, E. Bonnefille, S. Axnanda, Z. Liu, P. F. Fazzini, K. Philippot, M. Salmeron, B. Chaudret, *ACS Catal,* **2014**, *4*, 3160-3168

[79] T. M. Duncan, K. W. Zilm, D. M. Hamilton, T. W. Root, *J. Phys. Chem.* **1989**, *93*, 2583-2590

[80] S. Leuthäuβer, V. Schmidts, C. M. Thiele, H. Plenio, *Chem. Eur. J.* **2008**, *14*, 5465-5481.

[81] X. Bantreil, S. P. Nolan, *Nat. Protoc.* **2011**, *6*, 69-77.

[82] M. D. Fryzuk, W. E. Piers in Organometallic Syntheses Eds. R. B. King, J. J. Eisch, Elsevier, Amsterdam, 1986, vol. 3, p. 128.

[83] W. A. Herrmann in Synthetic Methods of Organometallic and Inorganic Chemistry, Ed.: W. A. Herrmann, Thieme, Stuttgart, 1996, p. 38.

[84] K. D. John, K. V. Salazar, B. L. Scott, R. T. Baker, A. P. Sattelberger, *Organometallics,* **2001**, *20*, 296-304.

Chapter 4

Selective hydrogenation of aromatic compounds using RhNPs

4.1. Introduction

As exposed in Chapter 1, metallic NPs (M-NPs) have been applied in a number of catalytic reactions. Among the studied reactions, systems based on M-NPs have been applied in the hydrogenation of substrates bearing aromatic rings. In this chapter, the use of these catalysts for the selective reduction of aromatic ketones, phenol derivatives and N-heteroaromatic compounds such as pyridine or quinoline derivatives will be exposed.[1,2,3]

4.1.1. Selective hydrogenation of aromatic ketones

The hydrogenation of aromatic ketones using M-NPs has gained much interest since these catalysts offer the possibility of selectively reduce the aromatic ring or the keto group (Figure 4. 1). In this area, the use of Ru and Rh NPs was mainly reported, although some examples of application of Pd, Ir and to a less extent Fe and Pt have also been described.[4]

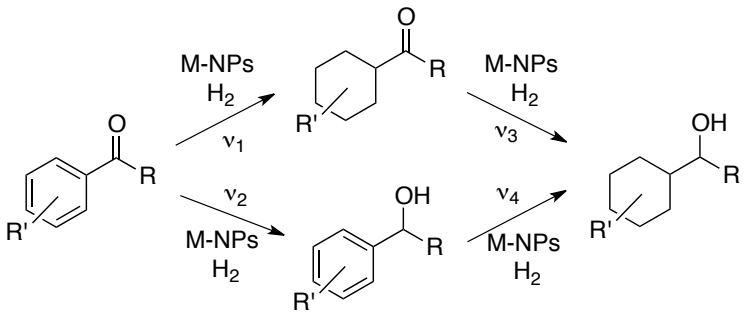

Figure 4. 1. Hydrogenation of aromatic ketones using M-NPs

The chemoselective hydrogenation of aromatic ketones bearing different R and R' groups (Figure 4. 1) is extremely challenging and in many cases, acetophenone was employed as model substrate.[5]

In 2010, Gómez and co-workers reported one of the first examples of the application of Ru NPs in the hydrogenation of aromatic ketones.[6] Recycling studies via their immobilization onto MWCNTs were also performed. These Ru NPs were prepared following the organometallic approach [7, 8], through the decomposition of [Ru(COD)(COT)] under H_2 in the presence of 4-(3-phenylpropyl)pyridine as stabilising agent, as previously reported by the same group.[9] Small and homogeneous NPs with a mean diameter of 1.3 ± 0.3 nm and narrow size distribution were obtained.

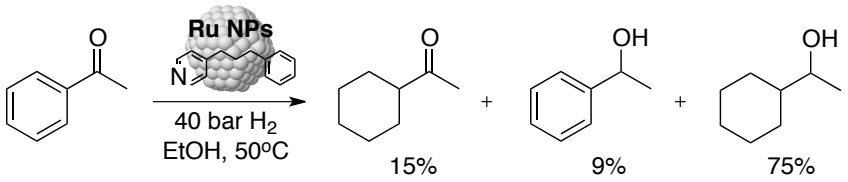

Figure 4. 2. Results reported by Gómez and co-workers for the selective hydrogenation of acetophenone catalysed by Ru NPs[6]

These Ru NPs were applied in the hydrogenation of acetophenone (among other aromatic substrates such as methylbenzene, 4-methyl anisole and styrene) providing 99% conversion after 16h of reaction with 75% of selectively towards the totally hydrogenated product (Figure 4. 2). The catalysts supported onto MWCNT provided similar results although they revealed slightly more activity than the unsupported NPs.

Some years later, Philippot and co-workers reported the use of water-soluble Ru NPs synthesised using various alkyl sulfonated diphosphines (**L**) as stabilizers. [10] These nanocatalysts were

synthesised by decomposition of [Ru(COD)(COT)] under H_2 in the presence of various [**L**]/[metal] molar ratios (0.1, 0.2 and 0.5) to achieve the formation of small and well dispersed Ru NPs with a mean diameter of 1.2 – 1.5 nm, depending on the [**L**]/[metal] molar ratio and the sulfonated diphosphine used in each case.

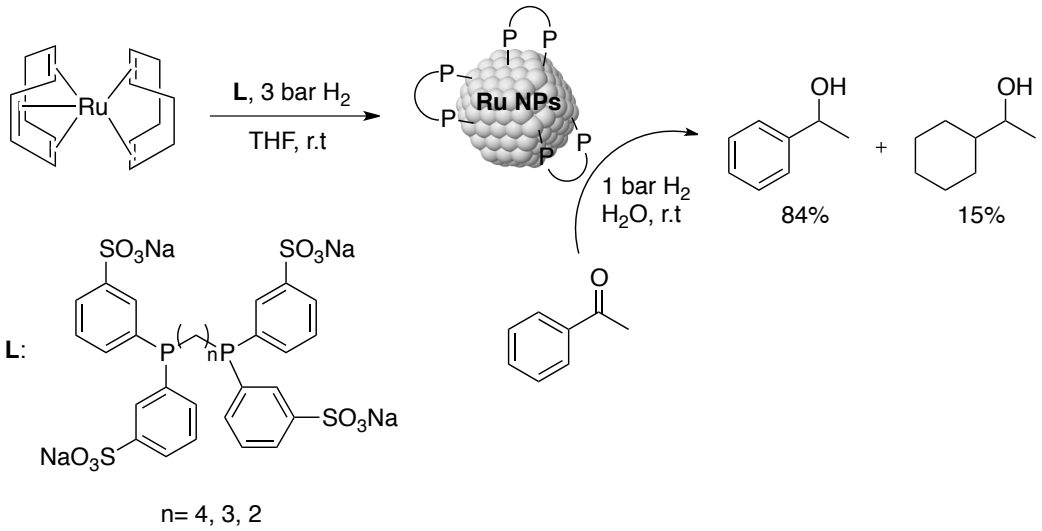

Figure 4. 3. Catalytic system reported by Philippot and co-workers for the selective hydrogenation of acetophenone[10]

When these systems were applied in the hydrogenation of acetophenone under 1 bar of H_2 (Figure 4. 3), 100% conversion was achieved after 20 h of reaction with the formation of phenylethan-1-ol in 84% of selectivity. In contrast, when the H_2 pressure was increased to 10 bar of H_2, full conversion towards the totally hydrogenated product was obtained after 2 h of reaction.

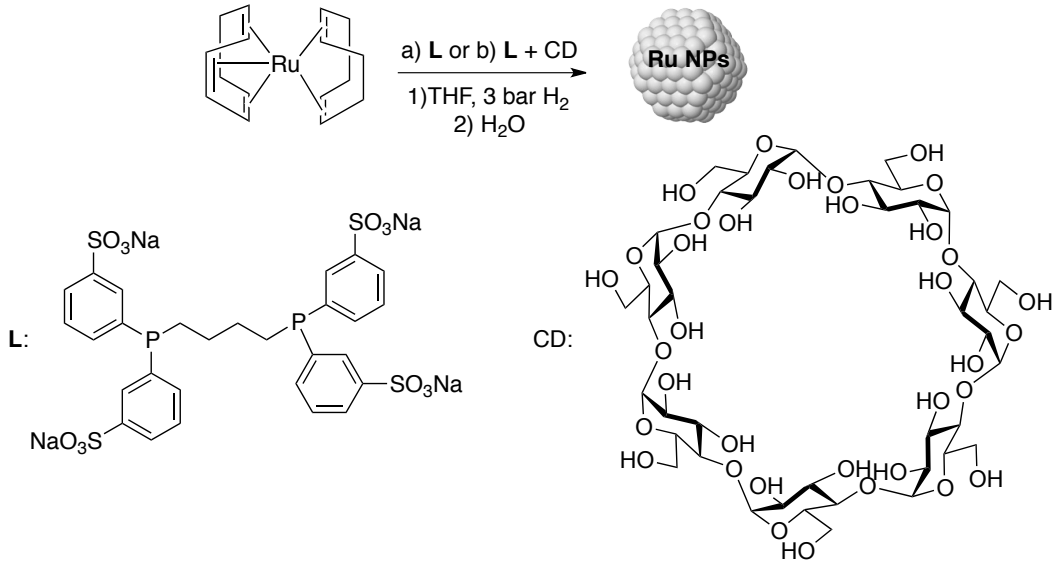

Figure 4. 4. Synthetic strategy reported by Philippot and co-workers for the preparation of water soluble Ru NPs[11]

Later, the same group studied the combination of sulfonated diphosphine ligands and cyclodextrin (CD) as stabilizers for Ru NPs surface.[11] For the synthesis of these Ru NPs, a mixture of 1,4-bis[(di-*m*-sulfonatophenyl)]phosphine]butane (L) and RAME-β-CD (0.2, 1.0 and 5.0 equiv.) was used (Figure 4. 4). The ability of CDs to form supramolecular inclusion entities with the sulfonated diphosphine ligands was studied by DLS and NOESY experiments, observing a clear increase in the mean size of the NPs when higher CD concentrations were used during the synthesis of the NPs and the interaction between **L** and the CD by NMR, respectively. The activity and selectivity of the sulfonated diphosphine-stabilized Ru NPs and the sulfonated diphosphine-cyclodextrin-stabilized Ru NPs were studied in the hydrogenation of acetophenone. When the reaction was performed under 1 bar o H_2, higher TONs were obtained for those systems bearing CD. In terms of selectivity, up to 91%

selectivity towards the formation of phenylethanol was obtained when the Ru NPs stabilised using a [L]/[CD] molar ratio of 5.0 after 20 h of reaction. An increase in the pressure of H_2 in the catalytic reaction from 1 to 10 bar of H_2 provided strong acceleration of the reaction for all catalytic systems, increasing the TON and TOF values with an increase in the amount of CD present in the reaction mixture during the synthesis of the Ru NPs. In terms of selectivity, the totally hydrogenated product, cyclohexylethan-1-ol, was obtained with 100% of selectivity when Ru/L and Ru/L/0.2CD were used as catalysts after 2 h of reaction, while richer systems in CD such as Ru/L/1.0CD and Ru/L/5.0CD presented only 34 and 26% of selectivity towards the same product, respectively. These results highlighted the tuning of the catalytic performances in the hydrogenation of acetophenone of these nanocatalysts in the presence of CD.

In 2013, Chaudret, van Leeuwen and co-workers demonstrated the influence of the ligands coordinated to the NPs surface on their catalytic activity, studying the application of Ru NPs stabilized by N-heterocyclic carbene ligands (NHCs) in the catalytic hydrogenation of acetophenone and other substrates bearing aromatic and ketone groups.[12] The nanoparticles were prepared by decomposition of [Ru(COD)(COT)] using H_2 in the presence of the carbenes I^{t}Bu and IPr used as stabilizers, following the reported procedure[13] (Figure 4. 5). Under these reaction conditions, monodisperse nanoparticles with a mean size of 1.7 ± 0.2 nm for the Ru NPs prepared using 0.5 equiv. of I^{t}Bu (RuI^{t}Bu$^{0.5}$) and 1.7 ± 0.2 nm and 1.5 ± 0.2 nm for the

NPs prepared using 0.2 (RuIPr$^{0.2}$) and 0.5 equiv. of IPr (RuIPr$^{0.5}$) per Ru were obtained, respectively.

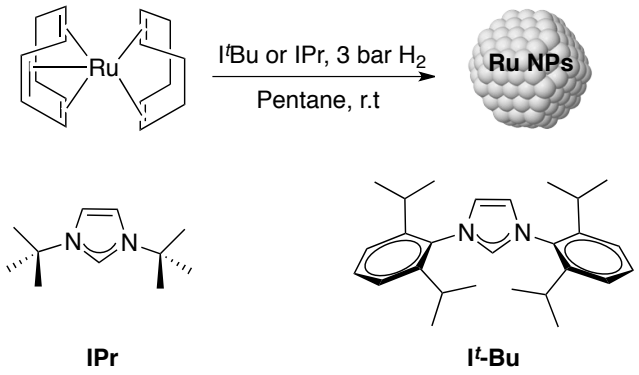

Figure 4. 5. Synthetic strategy used by Chaudret and co-workers for the preparation of NHC-stabilized Ru NPs[13]

When RuIPr$^{0.2}$ were applied in the hydrogenation of acetophenone under 40 bar of H_2 in THF, up to 80% selectivity towards the hydrogenation of the aromatic ring was observed with conversions under 50% using only 0.03% of total Ru. On the other hand, at higher Ru loading (0.1–0.3%), over 60% was obtained at almost full conversion of acetophenone. The hydrogenation of other aromatic compounds containing ketones was also tested using the same nanocatalysts. An increase in the chain length between both functionalities led to an increase in the selectivity towards the hydrogenation of the aromatic ring, achieving selectivities of 98% and 99% for 4-phenyl-2-butanone and 5-phenyl-2-pentanone at full conversion (Figure 4. 6).

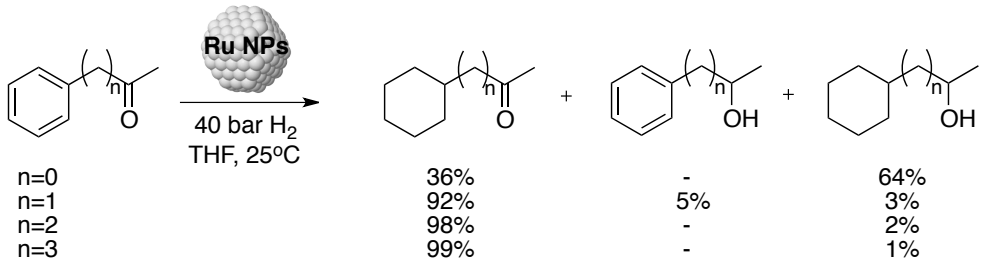

Figure 4. 6. Results reported by Chaudret and co-workers for the hydrogenation of aromatic ketones using Ru NPs stabilized by NHC ligands[12]

More recently, ruthenium NPs stabilized by phosphine-functionalized ionic liquids (PFILs) were synthesized using an imidazolium-based ionic liquid as solvent and starting from Ru precursors such as [Ru(COD)(2-methylallyl)$_2$] or $RuO_2{\cdot}xH_2O$ under H_2 atmosphere (Figure 4. 7).[14] Characterization of these NPs showed well-dispersed NPs of *ca.* 2.2 nm in size.

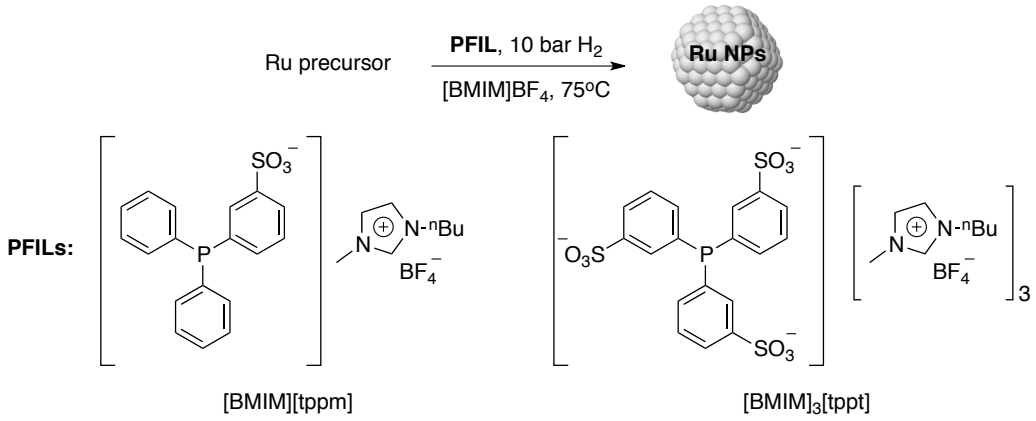

Figure 4. 7. Synthetic methodology reported for the synthesis of Ru NPs stabilized by PFILs[14]

Initially, when the [BMIM][tppm]-Ru NPs were tested in the chemoselective reduction of acetophenone using [BMIM]BF_4 as

solvent, no activity was observed at room temperature in the absence of a basic additive, as previously reported using homogeneous[15] and heterogeneous Pt/C modified[16] catalysts. The addition of [BMIM]OH (1-butyl-2,3-dimethylimidazolium hydroxide) to the solution improved the catalytic performance, achieving 99% selectivity to 1-phenylethanol at 77% of conversion (Figure 4. 8). Lower selectivities were obtained using Ru NPs synthesized in the absence of PFIL (76.6% of selectivity towards 1-phenylethanol at 94% of conversion). On the other hand, when H_2O was used as solvent using [BMIM][tppm]-Ru NPs, the reaction progressed very fast with a chemoselectivity of 99.6% to cyclohexylethan-1-ol, which was attributed to an increase in the substrate solubility in this solvent.[17]

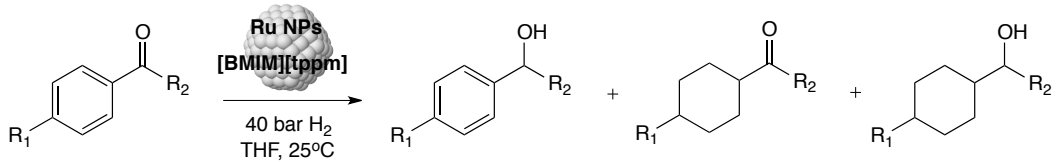

	Conversion			
R_1= -H, R_2= $-CH_3$	77%	99%	0.4%	0.6%
R_1= -H, R_2= $-CH_2CH_3$	21%	86%	14%	0%
R_1= -H, R_2= -*iPr*	10.4%	80%	20%	0%
R_1= -OMe, R_2= $-CH_3$	2%	100%	0%	0%
R_1= $-CF_3$, R_2= $-CH_3$	100%	100%	0%	0%

Figure 4. 8. Results reported for the selective hydrogenation of aromatic compounds bearing ketone moieties using Ru NPs stabilised by PILFs[14]

Other aromatic ketones were also tested using the same nanocatalyst, generally obtaining lower activities and chemoselectivities for the corresponding phenylethan-1-ol derivatives when the steric hindrance of the alkyl group close to the ketone function was increased. In the case of substrates bearing electron-donating groups

in the *para* position of the phenyl ring, poor activity with excellent chemoselectivity to the C=O hydrogenated product was observed in [BMIM]BF_4, while substrates bearing electron-withdrawing groups in the same position showed an excellent reaction activity with full chemoselectivity towards C=O hydrogenated products.

In 2004, Dupont and co-workers reported the application of Ir NPs stabilized by ionic liquids in the reduction of acetophenone and benzylmethylketone.[18] The Ir NPs were prepared by decomposition of $[Ir(COD)(\mu\text{-}Cl)]_2$ under H_2 in 1-*n*-butyl-3-methylimidazolium hexafluorophosphate [BMIM]PF_6. The resulting NPs revealed an efficient and recyclable catalytic system for the solventless or biphasic hydrogenation of ketones under mild reaction conditions. In the hydrogenation of cyclohexanone, the dispersion of Ir NPs in [BMIM]PF_6 required longer reaction times than when the reaction was carried out under solventless conditions. These results were attributed to the characteristic biphasic nature of the reaction in the ionic liquid. However, the recovered nanocatalyst, could be recycled for reuse at least 15 times without significant loss in activity, in contrast to the solventless system, which started to lose activity after the third recycle. When the hydrogenation of acetophenone was tested using these Ir NPs at 75°C under 4 atm of H_2, a moderate selectivity of 35% for the hydrogenation of the aromatic ring over the carbonyl group was obtained at 50% of acetophenone conversion. It was concluded that for this substrate, there is no preferential coordination mode of the arene ring or the carbonyl group to the NPs surface during the catalysis. The same system was also applied in the hydrogenation of benzylmethylketone under

same reaction conditions, achieving a selectivity of 92% for the hydrogenation of the aromatic ring at 97% of substrate conversion (Figure 4. 9).

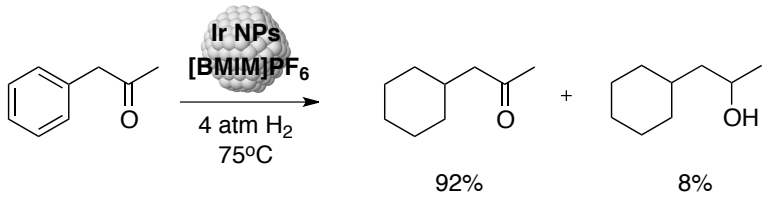

Figure 4. 9. Results reported by Dupont and co-workers in the hydrogenation of phenylacetone using Ir NPs stabilized by ILs[18]

More recently, van Leeuwen and co-workers reported the application of chiral Ir NPs stabilized by a secondary phosphine oxide towards the enantioselective hydrogenation of prochiral ketones bearing aryl rings.[19] Well dispersed Ir NPs with a size of *ca*. 1.4 nm were formed by reduction of $[Ir(\mu\text{-}OMe)(COD)]_2$ under H_2 at room temperature in the presence of a [L]/[Ir] molar ratio of 0.5 (Figure 4. 10). First the hydrogenation of acetophenone was attempted using this catalytic system, detecting the selective reduction of the ketone group in 88% conversion and 55% *ee* at room temperature using THF as solvent. When the asymmetric hydrogenation of substituted aromatic ketones was examined, almost full selectivity for the reduction of the ketone group over the arene ring could be achieved with promising enantioselectivities and moderate to high conversions.

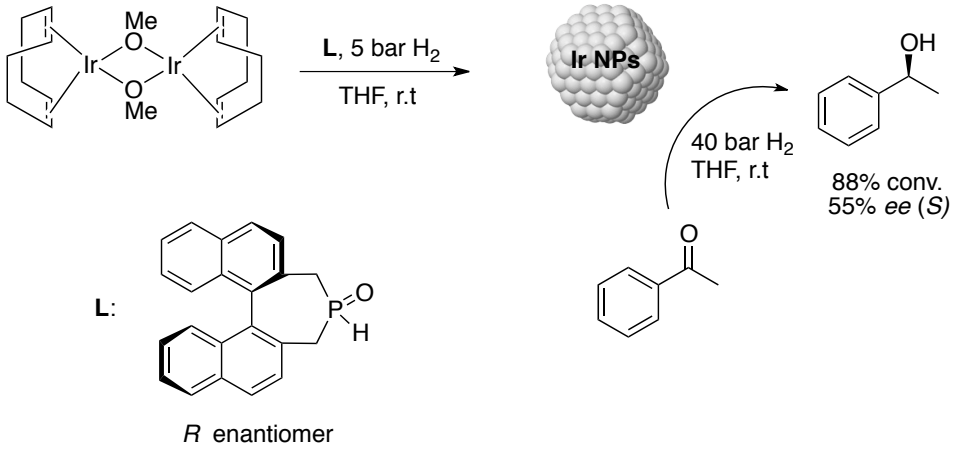

Figure 4. 10. Catalytic system reported by van Leeuwen and co-workers for the enantioselective hydrogenation of acetophenone[19]

Concerning the application of Rh NPs in the selective hydrogenation reactions of aromatic ketones, Dyson and co-workers reported in 2012 the application of phosphine modified PVP stabilized Rh NPs.[20] These NPs were synthesised by alcoholic reduction of $RhCl_3{\cdot}xH_2O$ in the presence of PVP and subsequently, sulfonated water-soluble phosphine ligands were added in a [phosphine]/[Rh] molar ratio of 0.5 to investigate the possible effect of the presence of these phosphines at the surface of the NPs in catalysis (Figure 4. 11).

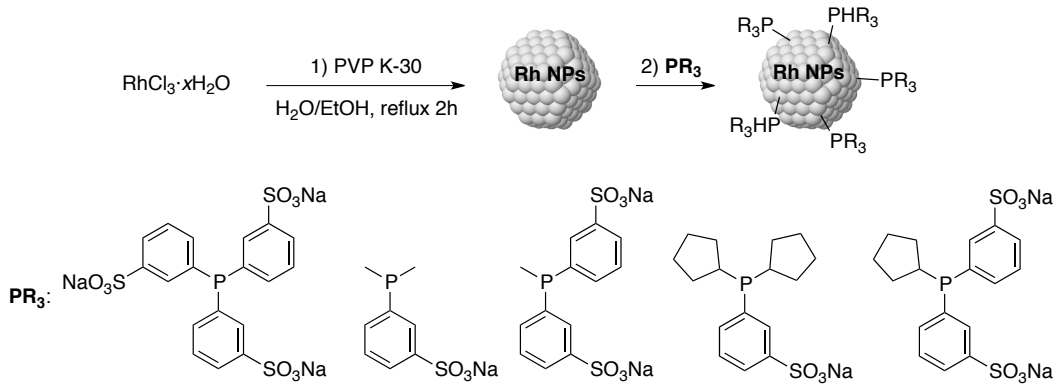

Figure 4. 11. Synthetic methodology reported by Dyson and co-workers for the synthesis of PVP-PR_3-Rh[20]

A series of phosphine ligands with distinct steric and electronic properties and polarities were investigated and several trends were observed, showing the capacity of these phosphine ligands as modifiers in nanocatalysis. No differences were observed from the point of view of nanoparticle size distributions, but differences in activity and selectivity were observed when the Rh NPs were applied in the hydrogenation of phenylacetone, which were attributed to the modification of the NPs surface (site blocking) and to a modification of the polarity of the surface of the NPs because of the presence of hydrophobic phosphine ligands.

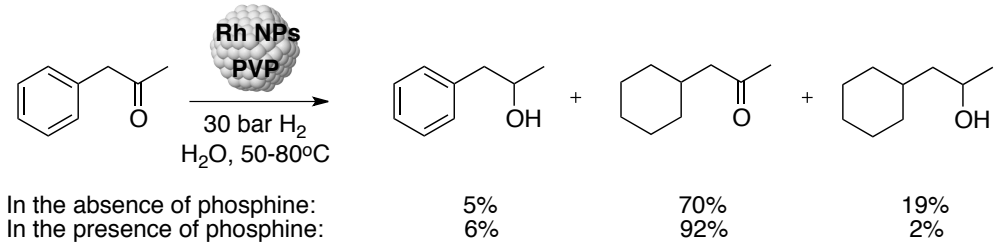

Figure 4. 12. Results reported by Dyson and co-workers in the selective hydrogenation of phenylacetone using PVP-Rh and PVP-PR_3-Rh NPs[20]

The PVP stabilized Rh NPs afforded 1-cyclohexylpropan-2-one in 70% selectivity in the absence of phosphine ligand and this value was increased up to 92% upon addition of one of the sulfonated phosphine ligands after optimization of the catalytic reaction conditions (Figure 4. 12).

Previously, this transformation had been studied using Rh NPs in biphasic aqueous/supercritical ethane reaction media and was the first successful example of an unsupported colloid-catalysed hydrogenation of a substrate in a supercritical fluid.[21] The selective hydrogenation of 4-phenylbutanone was essentially complete with the selective hydrogenation of the arene ring (97%).

Jutz and co-workers studied the employment of *in situ* synthetized Pd and Rh NPs stabilized by various ionic liquids ([BMIM]PF_6, [BMIM][OTf] and $N(C_6H_{13})_4Br$) in the solventless selective hydrogenation of acetophenone.[22] Supercritical CO_2 extraction was performed for the removal of the metal precursor used for the synthesis of the NPs as well as for the separation of the hydrogenation products from the reaction media. In terms of catalyst performance, high selectivities for the formation of phenylethan-1-ol (up to 90%) were obtained using [BMIM][PF_6]-Pd NPs under 50 bar of H_2 at 80°C, while in the case of [BMIM][PF_6]-Rh NPs lower selectivities towards the hydrogenation of the carbonyl group were achieved. Recycle experiments were carried out with no noticeable deactivation after at least 6 recycles.

Roucoux and co-workers reported the synthesis of Rh nanocatalysts protected by self-assembled supramolecular complexes based on

cyclodextrins and surfactants (Figure 4. 13) for application in the biphasic hydrogenation of acetophenone, among other reductible compounds.[23] The inclusion complexation of randomly methylated CDs (RaMeCD) with an ammonium surfactant[24] or a sulfonated phosphine[11] as guests molecules was previously used for the synthesis of Ru NPs, and although some studies proved the stabilization of Ru NPs using CDs alone,[25,26] no studies were reported related to the stabilization of Rh NPs using CDs alone. Rh NPs stabilized by RaMeCD or the ammonium surfactants were synthesized following the previously reported methodology for Ru NPs[24] by chemical reduction of $RhCl_3 \cdot 3H_2O$ using $NaBH_4$ (Figure 4. 13).

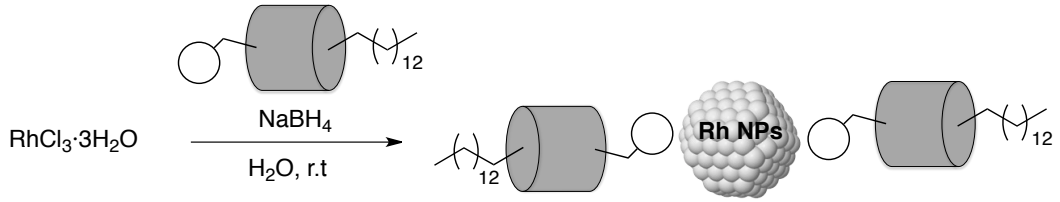

Figure 4. 13. Synthetic methodology reported by Roucoux and co-workers for the synthesis of Rh NPs stabilized by methylated-CD/ammonium surfactant inclusion complexes[23]

Then, the chemoselective hydrogenation of acetophenone using these nanocatalysts was studied. In general, high values of selectivity for the hydrogenation of the ketone group were obtained, however, the significant quantity of cyclohexylethanone formed during the catalysis proved that these nanocatalysts could not surround the aromatic ring and avoid its hydrogenation.

In 2016, Philippot and co-workers reported the application of PVP-stabilized Rh NPs for the chemoselective hydrogenation of arenes. Among other substrates, the chemoselective hydrogenation of acetophenone was tested using these Rh NPs, achieving 20% of selectivity towards arene ring reduction over the ketone, in 20% yield.[27]

Recently, our research group reported the stabilization of Rh NPs using P-donor ligands, such as phosphines and phosphites, for the selective hydrogenation of aromatic substrates.[28] In this context, a comparative study using Rh and Ru NPs stabilized by triphenylphosphine (PPh_3) and diphenylphosphinobutane (dppb) was performed (Figure 4. 14), and their application in the selective hydrogenation of aromatic ketones was examined.[29] These NPs were synthesized in THF by decomposition under H_2 pressure of [Rh(η^3-C_3H_5)$_3$] and [Ru(COD)(COT)], respectively.

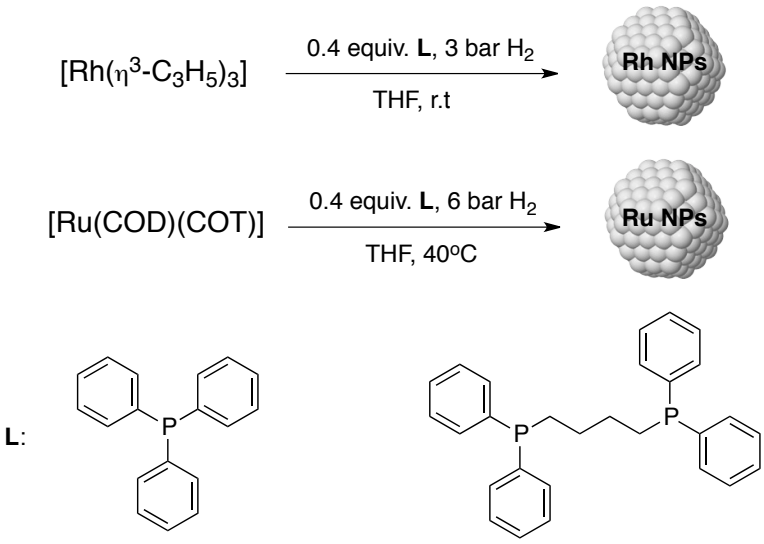

Figure 4. 14. Synthetic methodology reported by our group for the synthesis of Rh and Ru NPs stabilized by P-donor ligands[29]

In all cases, spherical shape NPs with a narrow size distribution of 1.3 – 1.5 nm were obtained. When PPh_3-Ru NPs were used for the hydrogenation of acetophenone, 13% of selectivity for cyclohexylethanone and 87% for the totally hydrogenated product were achieved, while in the case of PPh_3-Rh NPs the same products were obtained in 15% and 33% of selectivities respectively, under the same catalytic conditions. Hydrogenolysis products (ethylbenzene and ethylcyclohexane) were also detected in this last case.

An increase in the alkyl chain between the arene ring and the ketone group was studied by using these nanocatalysts in the selective hydrogenation of 1-phenylpropan-2-one and 4-phenyl-butan-2-one. For these substrates, the nature of the metal showed to affect the catalytic results significantly. Using Rh NPs, the selectivity for arene reduction increased when the separation between the arene and the carbonyl group was larger, achieving up to 94% of selectivity for 4-cyclohexylbutan-2-one, suggesting coordination through the aromatic ring (Figure 4. 15a). A possible competition between coordination through arene ring and carbonyl group could explain lower selectivities obtained using Ru nanocatalysts stabilized using the same ligands (Figure 4. 15b).

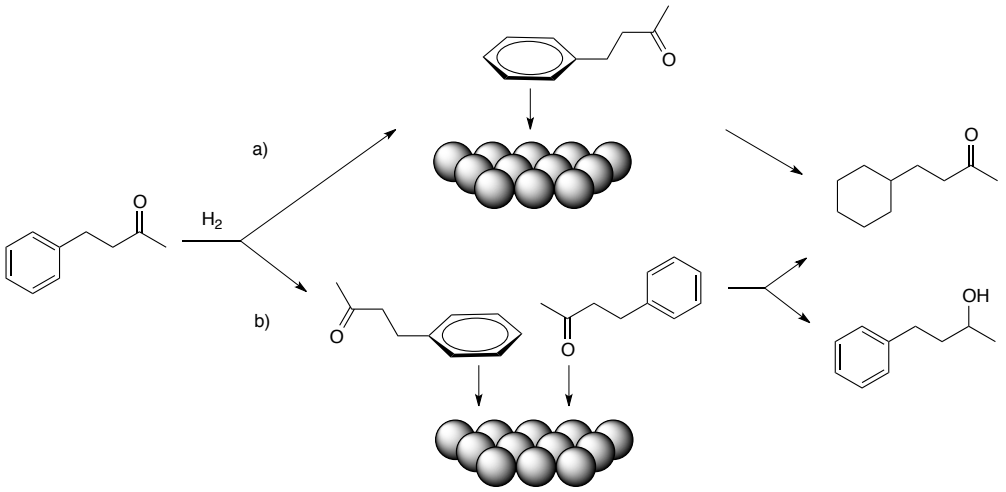

Figure 4. 15. Schematic representation of the selectivity trends reported by our group in the selective hydrogenation of aryl ketones using (a) Rh and (b) Ru NPs stabilized by P-containing ligands[29]

The effect of the presence of different substituents in the alkyl and phenyl moieties was also investigated and in the case of Rh NPs, the activity of the nanocatalysts decreased significantly by the presence of bulky alkyl substituents close to the carbonyl group. Besides, the presence of different substituents on the aromatic ring showed to have an influence in selectivity since in all cases, products obtained for the selective hydrogenation of the ketone group were obtained in >70% selectivity.

In summary, it was considered that for Rh NPs, coordination through the arene ring dominates the interaction between the substrate and the NPs surface, while in the case of Ru NPs the results showed that both the arene ring and the ketone group can coordinate to the metallic surface competively.

The high affinity for the selective coordination of the arene ring when the reduction of aromatic ketones was performed using Rh

NPs, together with the reported evidence that high activities and selectivities towards the selective reduction of this moiety were achieved using Ru NPs stabilized by NHC ligands,[13] encourage us to investigate the application of NHC-stabilized Rh NPs in the hydrogenation of this kind of substrates.

4.1.2. Selective hydrogenation of phenols

The hydrogenation of phenol and derivatives is one of the most important processes in industrial organic chemistry and plays an important role in the processing of various types of renewable raw materials. The catalytic hydrogenation of phenol is of commercial and environmental significance for the formation of cyclohexanone and cyclohexanol, which is the primary stage for the production of adipic acid and ε-caprolactam (Figure 4. 16)[30] used for the production of Nylon 6 and Nylon 66.[31]

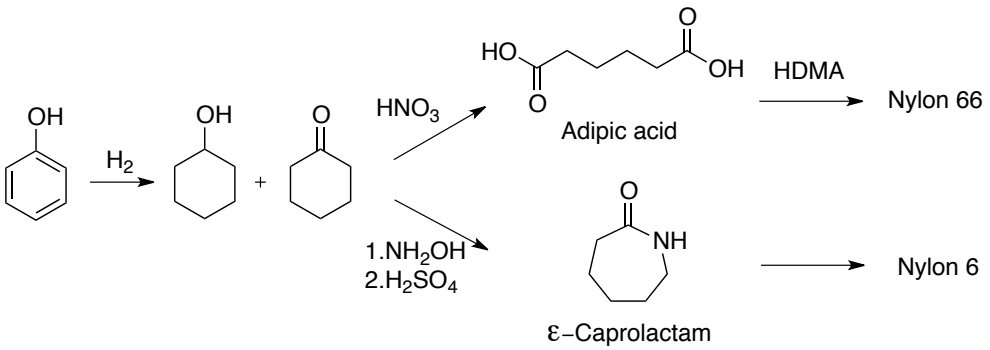

Figure 4. 16. Schematic synthesis of Nylon 6 and Nylon 66 using cyclohexanone produced by phenol reduction

Hydrogenation products of phenol derivatives are also used as feedstock for the manufacture of synthetic lubricants, oil and fuel additives, special solvents, surfactants and synthetic fragrances. Indeed, the reduction of various types of substituted phenols is also important for the production of hydrocarbon or alcohols. In this case, works focused on processing phenol compounds that can be used as models of lignin fragments have attracted much attention.[32,33,34,35]

In this context, the application of either supported or immobilized Pd, Ir, Ru and Rh NPs has gained interest due to the high activity of these nanocatalyts towards the hydrogenation of phenols, where Pd is the most efficient metal, achieving almost full selectivity towards the cyclohexanone products.[36]

As an example, the application of Pd NPs supported on mesoporous MMT-1 silica (Pd@sMMT-1), formed by reduction of the palladium precursor $PdCl_2(MeCN)_2$ under H_2, in the aqueous-phase hydrogenation of phenol showed high selectivities for the formation of cyclohexanone over cyclohexanol.[37] A high selectivity (98%) for the formation of cyclohexanone over cyclohexanol (2%) was detected when the reaction was carried out at 25°C under atmospheric H_2 pressure (1 bar H_2) at 99% of phenol conversion (Figure 4. 17a). A lower selectivity of 85% towards cyclohexanone in 43% of conversion was obtained when Pd/C was used as catalyst compared to Pd@sMMT-1. The reduction of substituted phenols into the ketone product using this catalytic system was also studied achieving moderate to high conversions of 42-99% at 25-45°C in high selectivities (Figure 4. 17b, c, d).

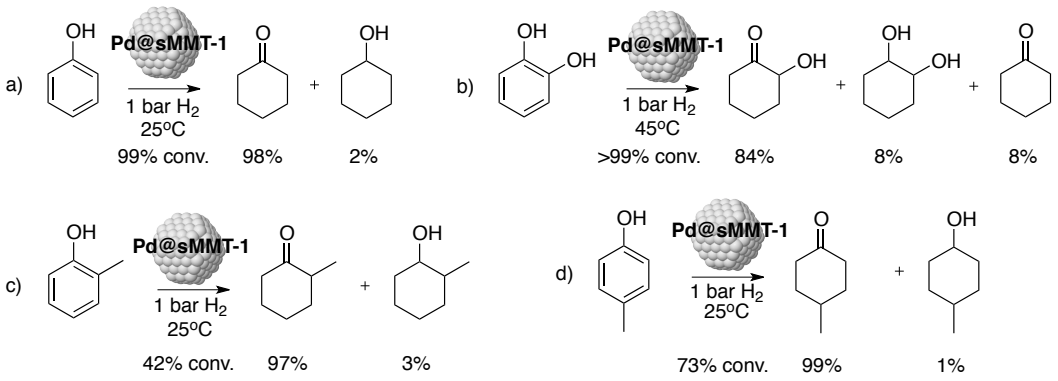

Figure 4. 17. Results reported for the aqueous-phase hydrogenation of phenol and its derivatives using Pd@sMMT-1[37]

These results were attributed to the relatively strong interaction between these phenols and the Pd surface (through hydrogen bonding to silanol groups), resulting in a non-planar adsorption. The arene ring of phenol may then be partially hydrogenated to the enol (Figure 4. 18, Step 1), which can rapidly isomerize to give the ketone product. The fact that the ketone group interacts weakly to the Pd surface could explain its desorption, hence avoiding further hydrogenation.

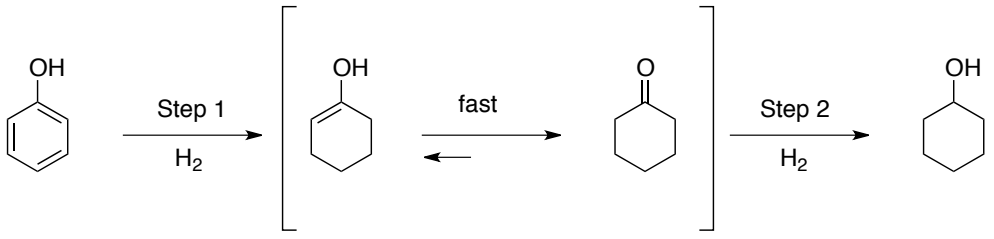

Figure 4. 18. Phenol hydrogenation over Pd catalyst[37]

To a much lesser extent, the application of Ir NPs in the hydrogenation of phenols was also investigated. Ir NPs prepared by $NaBH_4$ reduction of $IrCl_3$ in the presence of N,N-dimethyl-N-cetyl-N-

(2-hydroxyethyl)ammonium chloride salt displayed quantitative activity for phenol reduction at 20°C under 40 bar of H_2.[38] However, full selectivity for the formation of cyclohexanol was obtained in this case. The hydrogenation of methyl-substituted phenols in the *ortho*, *meta* and *para* position of the arene ring was also performed, also resulting in full selectivity for the formation of the corresponding methylcyclohexanol products, with high stereoselectivities towards the *cis* diastereomer.

The application of Ru NPs in the hydrogenation of phenol was also reported. Catalytic systems based on Ru NPs stabilized by PVP[39] and Ru NPs supported on a nitrogen-doped carbon material have been used for the reduction of phenol.[40] However, as in the case of Ir NPs, full selectivity for the formation of cyclohexanol was also obtained in these cases.

Several studies have been reported in the literature regarding the catalytic hydrogenation of phenols using Rh NPs. Among these studies, a few examples were reported to produce cyclohexanol as the exclusive hydrogenation reaction product. Rh NPs were prepared in water in the presence of polyvinylpyrollidin-2-one-3-carboxylate.[41] These NPs were tested under high H_2 pressure (40 bar H_2), forming cyclohexanol in 99.8% of selectivity. Other systems based on the application of PVP stabilized Rh NPs were also reported.[20,42] Indeed, the application of Rh NPs stabilized by *N*,*N*-dimethyl-*N*-alkyl-*N*-(2-hydroxyethyl)ammonium bromide salts ($HEAC_{16}Br$) in the reduction of phenol and *m*-cresol also showed full selectivity for cyclohexanol products when the reaction was performed under 1 bar of H_2.[43]

On the other hand, catalytic systems based on Rh NPs have also been developed to achieve the formation of the ketone product. For instance, Rh NPs prepared by reduction of $RhCl_3$ under H_2 and stabilized with an IL-like copolymer Poly(NVP-*co*-VBIMCl)] provided a selectivity of 29% towards cyclohexanone at 37% conversion (TOF=247) when the reaction was performed under 40 bar of H_2 using [BMIM][BF_4] as solvent (Figure 4. 19a).[44] The reduction of substituted phenols was also tested, reaching higher selectivity for the ketone (49%) in the case of *p*-propylphenol, but at lower conversion (11%, TOF=25) (Figure 4. 19b). A slightly higher conversion was achieved when *p*-methoxyphenol was used as substrate (TOF=70); however, the formation of 4-methoxycyclohexanone was not detected (Figure 4. 19c).

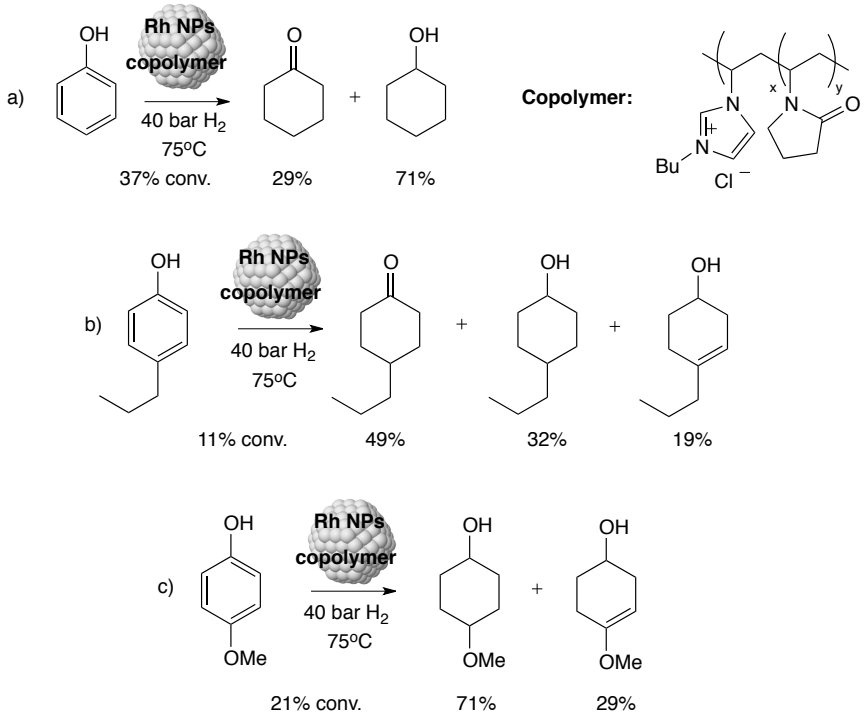

Figure 4. 19. Results reported for the hydrogenation of phenol and its derivatives using IL-like copolymer stabilized Rh NPs[44]

More recently, the hydrogenation of phenols in ILs using Rh NPs stabilized by hexyltriethyl-ammonium bromide was reported.[45] Although only 36% of selectivity for cyclohexanone was achieved when phenol was used as substrate under 40 bar of H_2, an increase to 66% selectivity for the same product was obtained when the pressure was lowered to 10 bar of H_2, and 84% selectivity when the reaction was carried out under 5 bar of H_2 (Figure 4. 20). These results evidenced the direct effect of the H_2 pressure on the selectivity to the ketone product using this catalytic system, in agreement with other reported studies.[46]

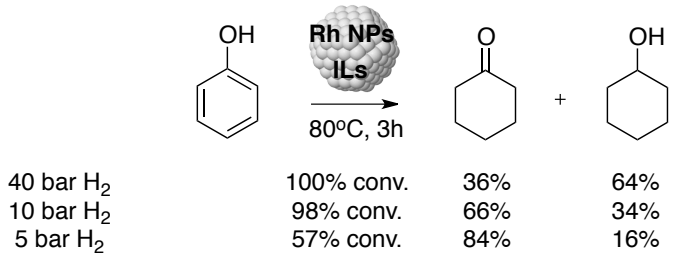

Figure 4. 20. Effect of the H_2 pressure for the hydrogenation of phenol using ILs stabilized Rh NPs[45]

The hydrogenation of methyl-substituted phenols in different positions of the aromatic ring was also investigated, detecting only the formation of the corresponding cyclohexanol products, although in lower conversions than for phenol under the same reaction conditions. The application of Rh NPs stabilized by the partially hydrogenated ligand 1-(phenyl)iminoethyl pyridine has also been reported and provided full selectivity to cyclohexanone.[47]

More recently, the effect of cyclodextrins on the activity and selectivity of a catalytic system based on Rh NPs stabilized by

polyacrylic acid (PAA) in the hydrogenation of phenol in aqueous solution and ILs has also been reported.[48] In this case, the ability of cyclodextrins to form host-guest inclusion complexes with the cyclohexenol intermediate was the key factor for obtaining 100% selectivity towards cyclohexanone (Figure 4. 21).

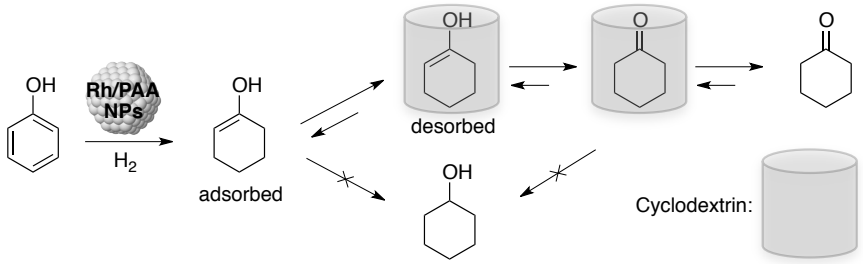

Figure 4. 21. Effect of cyclodextrin in the selectivity towards formation of cyclohexanone from phenol reduction[48]

In view of these reports and since no studies based on ligand-stabilized Rh NPs have been reported in this field, it was decided to investigate the use of our Rh NPs stabilized by NHC ligands as catalysts in the hydrogenation of phenol and derivatives.

4.1.3. Selective hydrogenation of N-heteroaromatics

The piperidine scaffold is commonly present in a wide range of natural products from both marine and terrestrial sources, and many of them are used in pharmacy (Figure 4. 22).

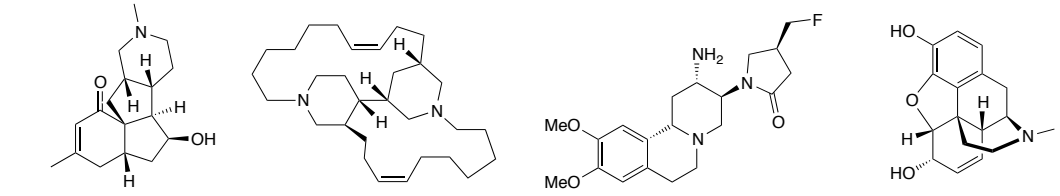

Figure 4. 22. Piperidine containing natural products and pharmaceutical agents

From a chemical point of view, piperidine is after pyridine the second most common ring structure that is present in thousand of compounds in clinical and preclinical research.[49] For this reason, the synthesis of piperidine has been subject of intense study for the last years.[50,51,52] While there are various methods for the synthesis of piperidine derivatives, the reduction of pyridine analogues is one of the most straightforward. In this field, metallic NPs mainly based on Rh and Ru have been applied.

The catalytic hydrogenation of pyridine,[53,54,55,56,57,47] 2-picoline[53,58,56] 4-picoline[56] and pyridine-3-ol[59] under H_2 pressure between 1-10 bar has been reported using systems based on Rh NPs.

Recently, the diastereoselective reduction of pyridine analogues bearing an amine group such as substituted-4-aminopyridines, have

also been reported using Rh/C as catalyst.[60] This study demonstrated the need to protect the amine with an electron-withdrawing group in order to decrease the Lewis basicity of the nitrogen, so the nucleophilic pyridine nitrogen does not coordinate and deactivate the metal catalyst (this effect is enhanced due to the presence of an amino group in C4). When 2-methyl-4-boc-aminopyridine was used as substrate at 80°C under 8 bar of H_2 (Figure 4. 23), the desired product was obtained in quantitative yield with an unexpected 2:1 (*cis:trans*) mixture of diastereoisomers. Such a result could be explained by the desorption of a partially hydrogenated intermediate prior to complete hydrogenation. Surprisingly, in the case of slightly larger substituents at C2 (ethyl substituent), only the *cis* diastereomer was obtained in 75% isolated yield.

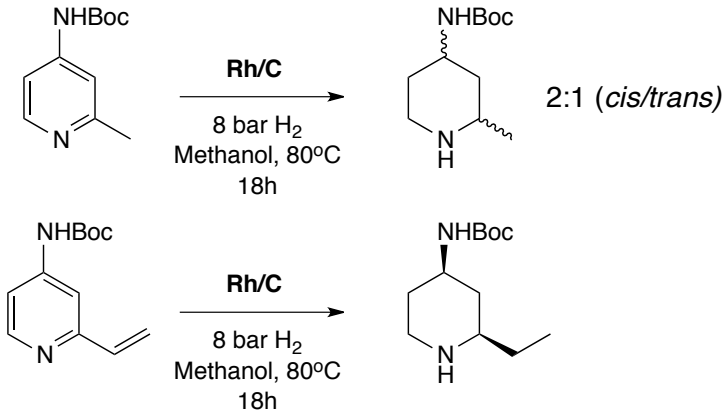

Figure 4. 23. Results reported by Murphy and co-workers in the diastereoselective hydrogenation of substituted-4-aminopirydines using Rh/C[60]

The competitive reduction of aromatic *vs*. heteroaromatic was evaluated using 2-phenyl-4-Boc-aminopyridine as substrate,

nevertheless very low conversions into the full reduction product were obtained after 16h of reaction.

The reduction of pyridine was reported using Ru NPs supported on magnesium oxide.[61] The reduction of compounds bearing N-heterocyclic rings and a ketone group were also studied using Ru NPs stabilized by NHC ligands[12] and PFILs.[14] In these cases, high selectivity for the ketone moiety reduction (at 26% conversion) (Figure 4. 24a) and almost full selectivity of the ketone reduction were observed when [BMIM]BF_4 was used as solvent under 50 bar of H_2 (Figure 4. 24b).

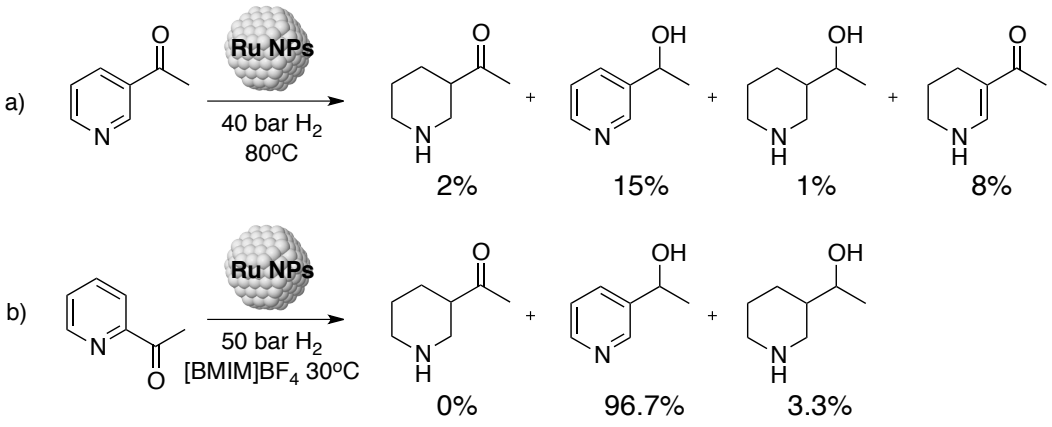

Figure 4. 24. Results reported for the hydrogenation of acetyl substituted pyridine derivatives using Ru NPs stabilized by (a) NHC ligands[12] and (b) PFILs[14]

Despite these reports, most of the studies in this area focused on the reduction of quinoline (Q) and derivatives since the hydrogenation of Q and analogues are of considerable industrial interest for the production of petrochemicals, [62] fine chemicals and pharmaceuticals.[63] The manufacture of decahydroquinoline (DHQ) is particularly challenging and although it has been extensively studied,

the production of DHQ via catalytic hydrogenation rather than stoichiometric reduction remains unusual. The complete hydrogenation of Q to DHQ occurs in two different reaction steps: Q is first hydrogenated to 1,2,3,4-tetrahydroquinoline (^{1}THQ) and 5,6,7,8-tetrahydroquinoline (^{5}THQ), and both compounds are then hydrogenated to DHQ (Figure 4. 25).

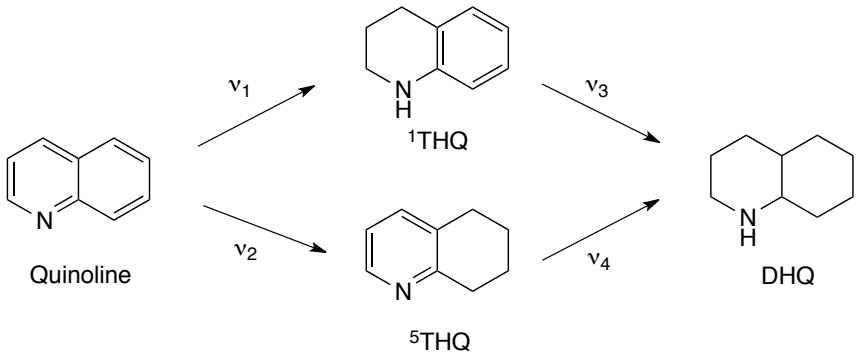

Figure 4. 25. Reaction pathways for the hydrogenation of quinolone

Several reports describe the application of Rh[64,55,56,58], Ru[61,65,14,66,40], Pd[67] and Pt[68] catalysts for the reduction of Q into DHQ; however, relatively high temperatures (50-200°C) and hydrogen pressures (20-40 bar H_2) were needed for obtaining full conversion of Q. Indeed, the selective reduction of the N-heterocyclic ring of Q was observed in most of these examples. The selective formation of ^{1}THQ was attributed to both the low activity of these catalytic systems for the hydrogenation of ^{1}THQ to DHQ under this reaction conditions and/or deactivation of the catalyst due to strong adsorption of ^{1}THQ on the active sites.[64c]

In contrast, the recent application of Rh/AlO(OH) in this reaction provided excellent results for the complete hydrogenation of Q into

DHQ under relatively mild conditions.[69] These Rh NPs were prepared by sol-gel method starting from $RhCl_3 \cdot xH_2O$ in the presence of 2-butanol and $Al(O\text{-}Sec\text{-}Bu)_3$ and were characterized by ICP, TEM, XPS and FT-IR. When the Rh/AlO(OH) catalyst was tested in the hydrogenation of Q and its analogues, high to full conversion to DHQ and its derivatives was achieved under 8 bar H_2 at 100°C (Figure 4. 26).

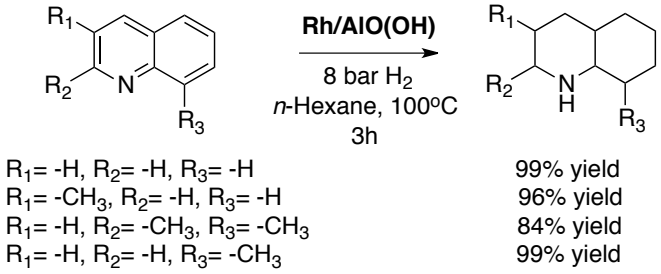

Figure 4. 26. Results reported for the hydrogenation of Q to DHQ using Rh/AlO(OH) catalyst[69]

The effect of the hydroxyl groups of the support on the formation of DHQ was investigated by varying the calcination temperature of the catalyst. An increase in the activity and selectivity to DHQ was observed when the catalyst was calcined at lower temperatures, evidencing the importance of the presence of structural water and surface hydroxyl groups on the catalyst surface. These results suggested that the formation of hydrogen bonds between the surface hydroxyl groups of Rh/AlO(OH) and the nitrogen atom of Q could promote the first hydrogenation of the N-heterocycle of Q into ^{1}THQ. Similarly, the aromatic cycle of ^{1}THQ could be easily adsorbed onto the surface of the catalyst via the same hydrogen bond thus facilitating its reduction into DHQ.

Ru catalysts supported on hydroxyapatite (HAP) also provided excellent results for the hydrogenation of Q into DHQ.[70] The Ru/HAP catalyst was prepared through the impregnation of the previously synthesized HAP with an aqueous solution of $RuCl_3$, followed by reduction under 30bar H_2 at 180°C. In the hydrogenation of Q over Ru/HAP, 56.3% selectivity to DHQ was achieved when the reaction was performed at 150°C under 50 bar H_2 (Figure 4. 27). The reduction of substituted quinolines over Ru/HAP was also tested, yielding high to full selectivity to the corresponding DHQ under the same reaction conditions.

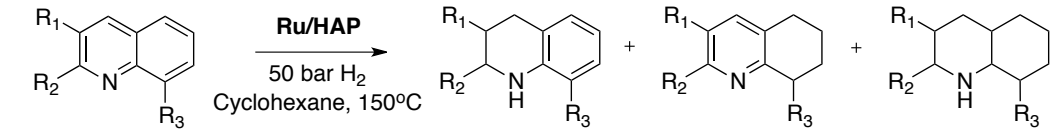

R_1= -H, R_2= -H, R_3= -H	41.7%	2.0%	56.3%
R_1= -CH_3, R_2= -H, R_3= -H	0%	22.8%	77.8%
R_1= -H, R_2= -CH_3, R_3= -H	0%	0%	100%
R_1= -H, R_2= -H, R_3= -CH_3	0%	0%	100%

Figure 4. 27. Results reported by Sun and co-workers for the hydrogenation of Q and derivatives using the Ru/HAP catalyst[70]

In view of these results, a mechanism similar to that reported for Rh/AlO(OH)[69] and based on the formation of hydrogen bonds between the hydroxyl groups of the HAP and the nitrogen atom of the substrate, was proposed (Figure 4. 28).

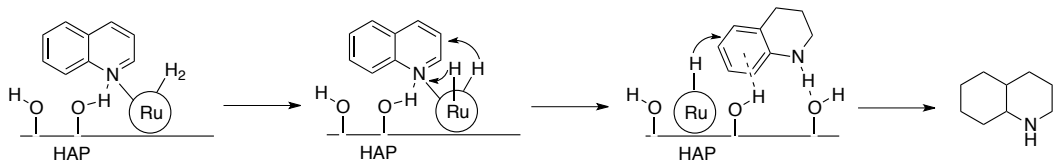

Figure 4. 28. Proposed mechanism for the reduction of Q into DHQ using Ru/HAP catalyst[70]

The group of Sánchez-Delgado reported the application of Ru NPs stabilized by poly(4-vinylpyridine) (PVPy) in the hydrogenation of Q.[71] This functional polymer (PVPy) showed to be particularly attractive for the stabilization of Ru NPs due to the strong affinity of the pyridyl group for metallic surfaces. Moreover, PVPy was employed as stabilizing agent as it provides a unique opportunity to immobilize Ru NPs in close proximity to quaternizable nitrogen atoms, thereby creating a nanostructure capable of promoting the heterolytic activation of hydrogen.

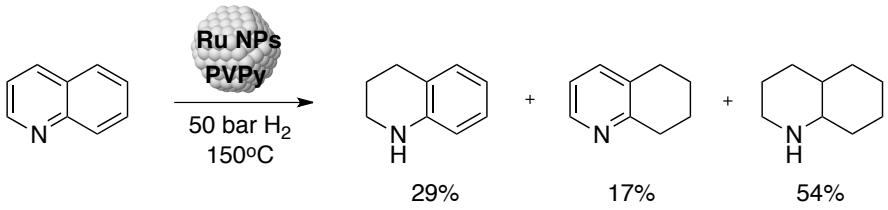

Figure 4. 29. Results reported by Sánchez-Delgado and co-workers for the hydrogenation of Q using Ru NPs stabilized by PVPy[53]

Although Q was selectively reduced (99%) into ^{1}THQ at 120°C under 10 bar H_2, an increase in selectivity towards ^{5}THQ was observed when the temperature was increased up to 150°C under higher

pressures of 50 bar H_2, detecting up to 54% of the totally reduced product DHQ (Figure 4. 29).[53]

4.2. Results and discussion

In the following sections, the results obtained in the hydrogenation of aromatic ketones, phenol and derivatives and N-heteroaromatic compounds using the NHC-stabilized Rh NPs introduced in Chapter 2 will be described.

4.2.1. Selective hydrogenation of aromatic ketones

Acetophenone (**1**) was first used as model substrate to evaluate the selectivity (reduction of arene ring *vs.* carbonyl group) of the Rh NPs stabilized by 0.2 (**Rh$^{0.2}$**), 0.4 (**Rh$^{0.4}$**) and 0.6 (**Rh$^{0.6}$**) [IPr]/[Rh] molar ratios in the hydrogenation of aromatic ketones. Three main products are expected for this process: cyclohexyl methyl ketone (**1a**) formed from the selective reduction of the arene ring, 1-phenylethan-1-ol (**1b**) formed from the selective reduction of the carbonyl group and 1-cyclohexylethan-1-ol (**1c**) formed from complete reduction of the substrate (Figure 4. 30).

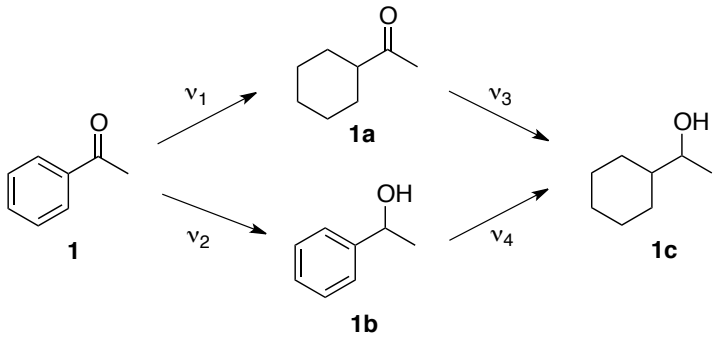

Figure 4. 30. Expected products for the selective hydrogenation of acetophenone (**1**)

The hydrogenation of **1** was initially attempted using **Rh$^{0.2}$** as catalyst under reaction conditions previously optimized by our group in the same reaction using similar Rh and Ru NPs stabilized by P-donor ligands (30°C, 20 bar of H_2, THF),[29] and the reaction was monitored by GC (Figure 4. 31). Complete conversion of **1** was observed after 50 min of reaction, with a selectivity of 45% towards **1a**, which remained unaltered after longer reaction times. The selectivity towards **1b** after 5 min was 58%, and progressively decreased due to its hydrogenation into **1c**. After 120 min, **1c** was formed in 55%. The stability of **1a** under the reaction conditions was not surprising since a similar behaviour was previously observed for Rh NPs stabilized by PPh_3.[29] The lack of reactivity of alkyl ketones suggests coordination of **1** to the NPs surface through the arene ring during the reaction. In contrast with the results previously reported using Rh NPs stabilized by PPh_3 as catalysts, no hydrogenolysis products were detected in this study.

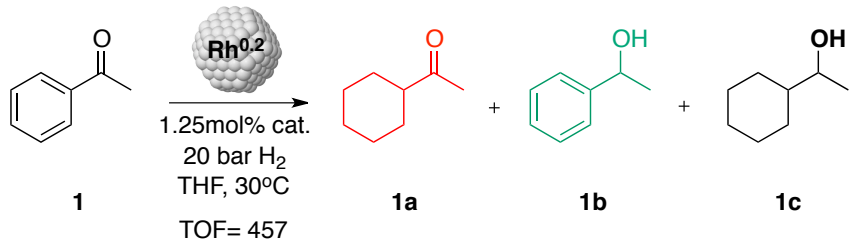

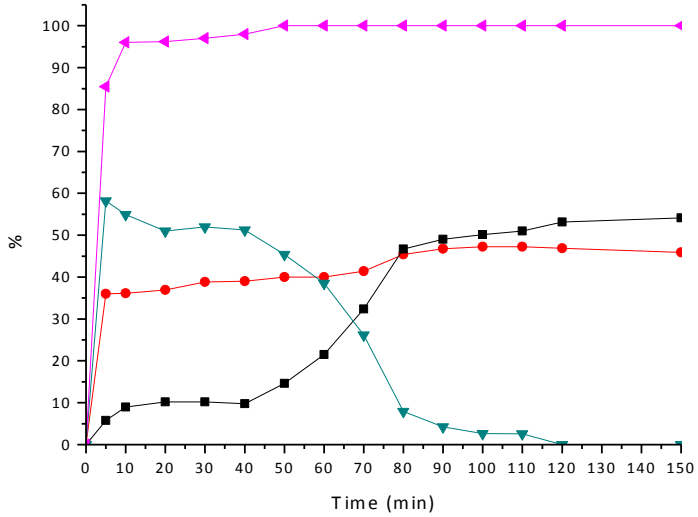

Figure 4. 31. Monitoring of the catalytic hydrogenation of acetophenone (**1**) using **Rh$^{0.2}$** as catalyst. Conversion in pink.

A higher selectivity (60%) to **1a** was previously reported using Ru NPs stabilized by the same ligand and [IPr]/[metal] molar ratio.[12] However, Ru/IPr were able to reduce **1a** into **1c**. This fact informs that the coordination mode of **1** to Rh/IPr is distinct than that to Ru/IPr. In the case of Ru/IPr, the coordination can probably take place through both the aryl and the carbonyl groups.

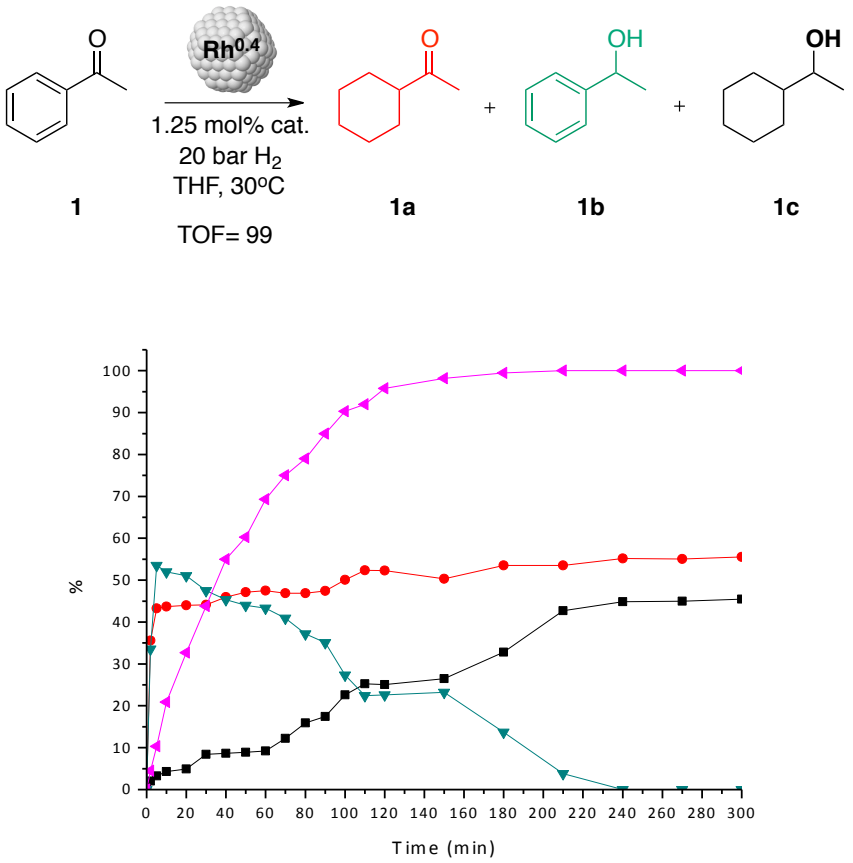

Figure 4. 32. Monitoring of the catalytic hydrogenation of acetophenone (**1**) using **Rh$^{0.4}$** as catalyst. Conversion in pink.

To study the effect of the amount of ligand present at the surface of these nanocatalysts, **Rh$^{0.4}$** was tested in the hydrogenation of **1** under the same reaction conditions and the reaction was again monitored by GC. As displayed in Figure 4. 32, complete conversion of **1** was achieved after 180 min of reaction, with a slight increase of selectivity up to 55% for the formation of **1a** (45% using **Rh$^{0.2)}$**. Also in this case, the compound **1a** was not converted into **1c** at longer reaction times. The fully hydrogenated product **1c** was thus formed by hydrogenation of **1b**, achieving a selectivity of 45% after 240 min.

Using **Rh$^{0.6}$** as catalyst, comparable results were obtained. The fact that conversion and selectivity for the formation of **1a** and **1c** using **Rh$^{0.6}$** and **Rh$^{0.4}$** were similar, confirmed our previous assumption that both catalytic systems were very similar. Based on these results, the evidence that reaction rates in the hydrogenation of **1** with catalysts **Rh$^{0.4}$** and **Rh$^{0.6}$** were lower than with catalyst **Rh$^{0.2}$** is in agreement with a higher surface coverage for those NPs, as previously indicated by the study of CO adsorption / IR on **Rh$^{0.4}$** and **Rh$^{0.6}$** NPs. A similar behaviour concerning CO adsorption and catalytic activity[12] was also described for Ru/IPr.[72]

Table 4. 1. Rh NPs (**Rh$^{0.2}$, Rh$^{0.4}$**) catalysed hydrogenation of aromatic ketones (**1**, **2**, **3**)[a]

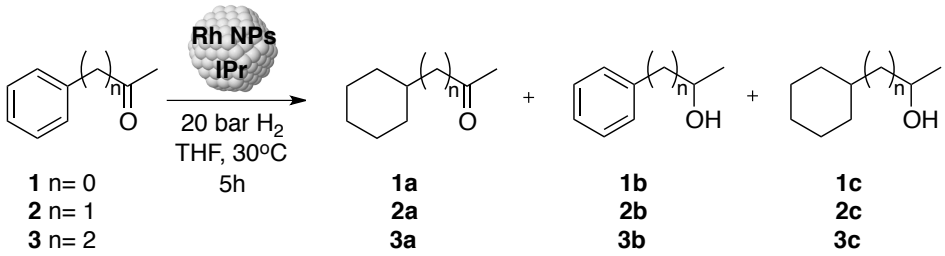

Entry	Substrate	Cat.	Conv.[b] (%)	TOF	a (%)[b]	b (%)[b]	c (%)[b]
1	**1**	**Rh$^{0.2}$**	100	457	45	-	55
2	**1**	**Rh$^{0.4}$**	100	99	55	3	42
3	**2**	**Rh$^{0.2}$**	100	-[d]	50	50	-
4	**2**	**Rh$^{0.4}$**	100	-[d]	53	47	-
5	**3**	**Rh$^{0.2}$**	100	147	91	7	2
6	**3**	**Rh$^{0.4}$**	100	-[d]	91	7	2

[a]Catalytic conditions: 1.24 mmol substrate, 1.25 mol% cat. [b]Calculated by GC using undecane as internal standard [d] Not calculated.

Next, the influence of an increase in the chain length between the aromatic ring and the carbonyl group on the selectivity was studied by the hydrogenation of ketones 1-phenylpropan-2-one (**2**) and 4-phenylbutan-2-one (**3**) using **Rh$^{0.2}$** and **Rh$^{0.4}$** as catalysts. Results of the reduction of **2** and **3** are collected in Table 4. 1 (results obtained using **1** under the same reaction conditions are also included for comparison).

Hydrogenation of **2** with both **Rh$^{0.2}$** and **Rh$^{0.4}$** catalysts afforded full conversions and similar selectivities (*ca*. 50:50) to compounds 1-cyclohexylpropan-2-one (**2a**) and 1-phenylpropan-2-ol (**2b**) (Table 4. 1, Entries 1 and 2 *vs.* 3 and 4).

The hydrogenation of **3** using both **Rh$^{0.2}$** and **Rh$^{0.4}$** nanocatalysts also provided full conversion but selectivity to 4-cyclohexylbutan-2-one (**3a**) improved up to 91% for both catalysts (Table 4. 1, Entries 5 and 6). Monitoring the hydrogenation of **3** in the presence of **Rh$^{0.2}$** (Figure 4. 33) also revealed lower reaction rates for this substrate than for **1**, with full conversion reached after 110 min of reaction (calculated TOF = 147).

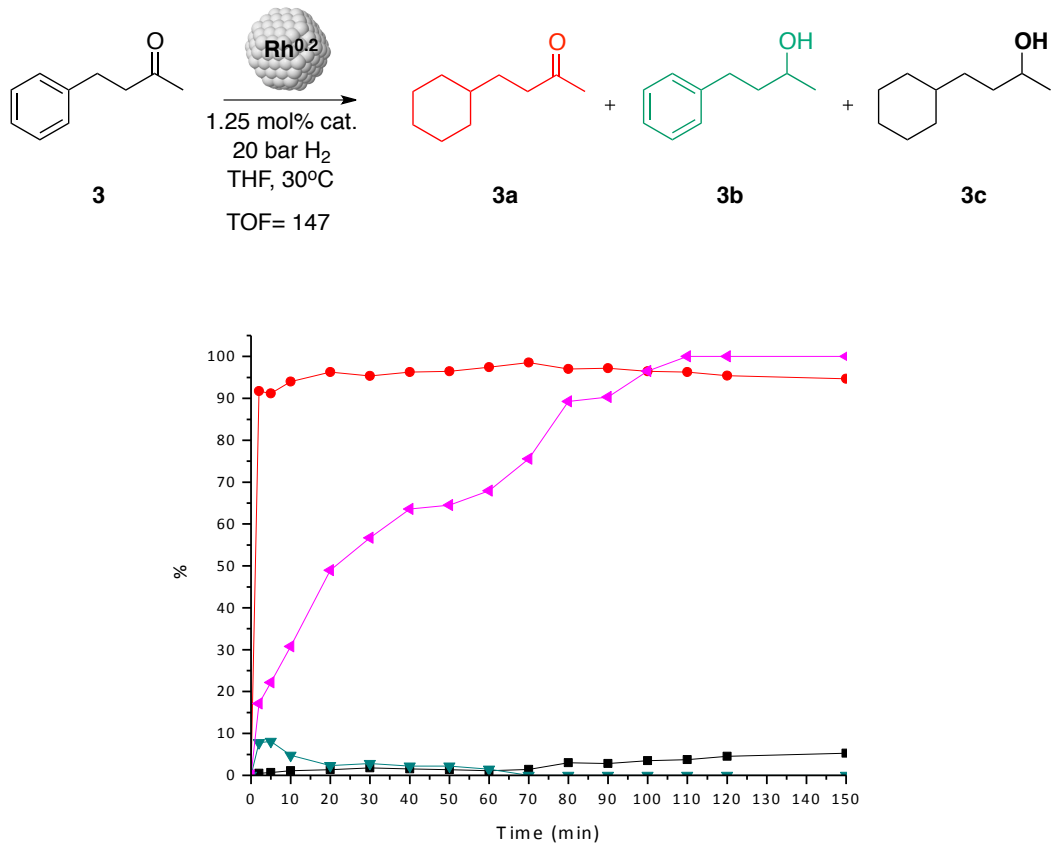

Figure 4. 33. Monitoring of the catalytic hydrogenation of 4-phenylbutan-2-one (**3**) using **Rh$^{0.2}$** as catalyst. Conversion in pink.

The lack of reduction of the alkyl ketone **3a** over the reaction time corroborates that ketone group is only reduced when an aromatic ring is present in the substrate structure. Moreover, when the carbonyl group is distant from the arene (n>2), only reduction of the arene ring takes place. This fact was also observed using Ir[18], Ru[12] and Rh[20,29] NPs.

The effect of the presence of bulky alkyl groups close to the ketone moiety in the activity and selectivity of the reaction was then studied via the use of 2-methyl-1-phenylpropan-1-one (**4**) and 2,2-dimethyl-

1-phenylpropan-1-one (**5**) as substrates. The results of the reduction of **4** and **5** are summarized in Table 4. 2 (results obtained using **1** under the same reaction conditions are also included for comparison).

Table 4. 2. Rh NPs (**$Rh^{0.2}$, $Rh^{0.4}$**) catalysed hydrogenation of aromatic ketones (**1**, **4**, **5**)[a]

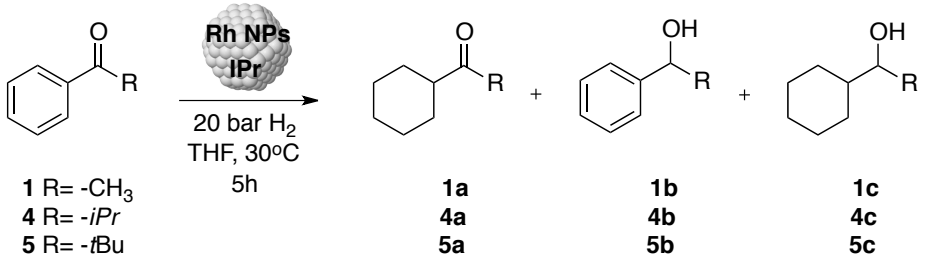

Entry	Substrate	Cat.	Conv.[b] (%)	a (%)[b]	b (%)[b]	c (%)[b]
1	**1**	**$Rh^{0.2}$**	100	45	-	55
2	**1**	**$Rh^{0.4}$**	100	55	3	42
3	**4**	**$Rh^{0.2}$**	100	19	74	7
4	**4**	**$Rh^{0.4}$**	100	25	58	17
5	**5**	**$Rh^{0.2}$**	100	23	7	70
6	**5**	**$Rh^{0.4}$**	100	22	63	15

[a] Catalytic conditions: 1.24 mmol substrate, 1.25 mol% cat. [b] Calculated from GC using undecane as internal standard.

When the hydrogenation of **4** was carried out, full conversion was achieved using both **$Rh^{0.2}$** and **$Rh^{0.4}$** after 5 h of reaction, and the reduction of the ketone group to give **4b** was the main process. The selectivities towards the reduction of the aromatic ring (formation of **4a**) were 19% using **$Rh^{0.2}$** and 25% using **$Rh^{0.4}$**, which was clearly lower to those obtained in the hydrogenation of **1** (45% and 55% respectively, Table 4. 2, Entries 1 and 2 *vs.* 3 and 4). The fully

hydrogenated product **4c** was formed in 7% and 17% using **Rh$^{0.2}$** and **Rh$^{0.4}$**, respectively. In the case of **5**, selectivities were similar to those obtained for **4** (Table 4. 2, Entries 3 and 4 *vs.* 5 and 6), which indicated that an increase in the bulkiness of the substituent from -*i*Pr to –*t*Bu does not have a strong effect on the selectivity of the reaction.

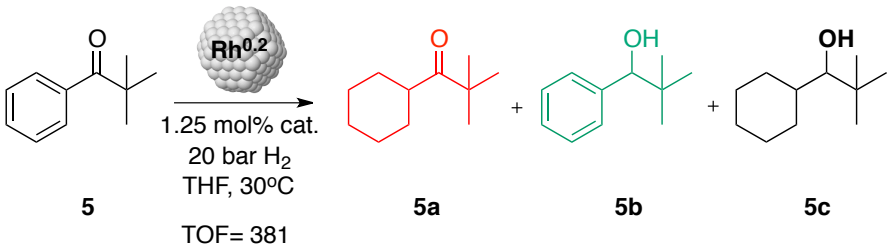

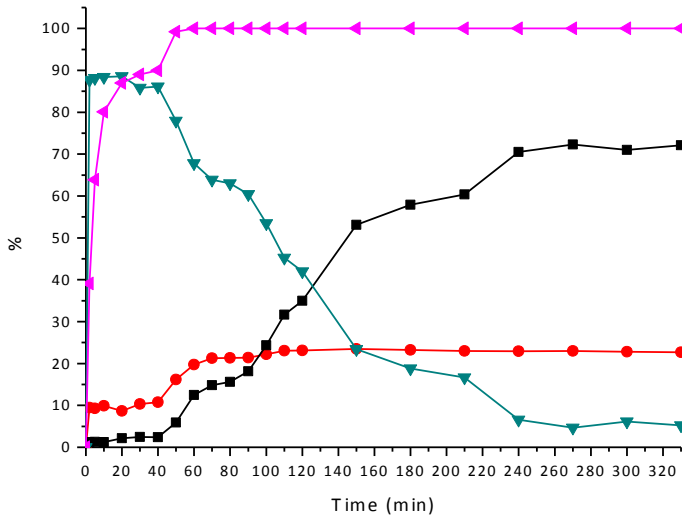

Figure 4. 34. Monitoring of the catalytic hydrogenation of 1-phenylpropan-1-one (**5**) using **Rh$^{0.2}$** as catalyst. Conversion in pink.

In order to get more information on the selective hydrogenation of **5**, monitoring of the reaction by GC using **Rh$^{0.2}$** was performed (Figure 4. 34). At the beginning of the reaction, the product **5b** resulting from the reduction of the keto group was formed with very high selectivity

(88%), but progressively decreased as a result of its conversion into the fully hydrogenated product **1c**. Reduction of arene to give **5a** reached 22% after 1h and remained constant along the time, similarly to that observed for **1**. The decrease in selectivity to **4a** and **5a** observed may be explained by the hindered coordination of the arene ring at the Rh surface. Thus, a change in selectivity for the hydrogenation of **4** and **5** was observed compared to **1** using $\mathbf{Rh^{0.2}}$ and $\mathbf{Rh^{0.4}}$, in contrast to what was previously reported using Rh-PPh_3 NPs.[29] Moreover, the TOF of 381 calculated for **5** using $\mathbf{Rh^{0.2}}$ was lower that that obtained for the hydrogenation of **1** using the same catalyst (457), which indicated that the presence of bulky groups as in **4** and **5** decrease the overall reaction rate. It is noteworthy that distinct trends were previously reported using Ru NPs stabilized by PFILs as catalysts and an imidazolium-based ionic liquid as solvent.[14]

Table 4. 3. Rh NPs (**$Rh^{0.2}$, $Rh^{0.4}$**) catalysed hydrogenation of aromatic ketones (**1**, **6**, **7**)[a]

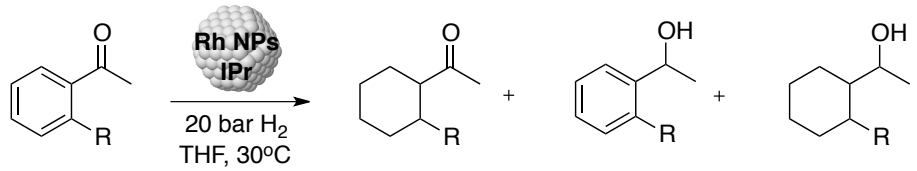

1 R= -H
6 R= -CH_3
7 R= -OCH_3

1a **6a** **7a** **1b** **6b** **7b** **1c** **6c** **7c**

Entry	Substrate	Cat.	Conv. (%)[b]	a (%)[b]	b (%)[b]	c (%)[b]
1	**1**	**$Rh^{0.2}$**	100	45	-	55
2	**1**	**$Rh^{0.4}$**	100	55	3	42
3	**6**	**$Rh^{0.2}$**	74	29	66	5
4	**6**	**$Rh^{0.4}$**	67	25	60	15
5	**7**	**$Rh^{0.2}$**	95	38	62	-
6	**7**	**$Rh^{0.4}$**	91	42	58	-

[a] Catalytic conditions: 1.24 mmol substrate, 1.25 mol% cat. [b] Calculated from GC using undecane as internal standard.

Next, acetophenone derivatives bearing substituents in *ortho* and *para* position of the aromatic ring such as compounds **6-9** were used as substrates. The results obtained for *ortho*-substituted derivatives are collected in Table 4. 3 (results obtained using **1** under the same reaction conditions are also included for comparison). The reaction rates for both substrates were lower, especially for substrate **6** (Table 4. 3, Entry 1 and 2 *vs.* 3-6). In these cases, the ketone reduction to give compounds **6b** and **7b** was the main process. A difference between reduction of ketones **6** and **7** is the absence of fully reduced product **7c** during the reduction of **7**, with both catalysts **$Rh^{0.2}$** and **$Rh^{0.4}$** (Table 4. 3, Entries 5 and 6). This is probably due to the distinct steric hindrance induced by the substituent -OMe

versus -Me, but also to the higher electron donating properties of the -OMe group.

Table 4. 4. Rh NPs (**$Rh^{0.2}$, $Rh^{0.4}$**) catalysed hydrogenation of aromatic ketones (**1**, **8**, **9**)[a]

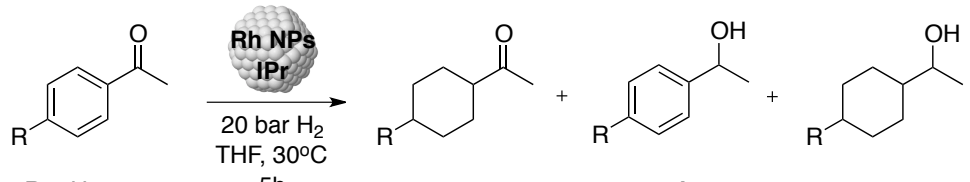

1 R= -H
8 R= -OCH_3
9 R= -CF_3

1a **8a** **9a** **1b** **8b** **9b** **1c** **6c** **9c**

Entry	Substrate	Cat.	Conv. (%)[b]	a (%)[b]	b (%)[b]	c (%)[b]
1	**1**	**$Rh^{0.2}$**	100	45	-	55
2	**1**	**$Rh^{0.4}$**	100	55	3	42
3	**8**	**$Rh^{0.2}$**	99	2	71	27
4	**8**	**$Rh^{0.4}$**	74	5	48	47
5	**9**	**$Rh^{0.2}$**	99	13	87	-
6	**9**	**$Rh^{0.4}$**	81	35	65	-

[a] Catalytic conditions: 1.24 mmol substrate, 1.25 mol% cat. [b] Calculated from GC using undecane as internal standard

Next, the hydrogenation of the *para* substituted acetophenone derivatives **8** and **9** bearing the electron donating and electron withdrawing groups -OCH_3 and -CF_3 was studied. The results are collected in Table 4. 4 (results obtained using **1** under the same reaction conditions are also included for comparison).

A lower conversion was obtained for **$Rh^{0.4}$** than for **$Rh^{0.2}$** with substrates, in agreement with the surface availability for these catalysts.

A striking difference was observed between the -OMe derivatives *ortho* (**7**) and *para* (**8**). In the case of **7**, the fully reduced product **7c** was not observed while for **8**, significant amounts of **8c** were formed (Table 4. 3, Entries 5 and 6 *vs.* Table 4. 4, Entries 3 and 4). Comparing the data of both substrates, the selectivities to **7b-8b** were similar, and the main difference is that **7a** was not reduced under these conditions, in contrast with **8a**.

A difference in selectivity was observed using $\mathbf{Rh^{0.2}}$ or $\mathbf{Rh^{0.4}}$ as catalyst in the case of **9**, with $\mathbf{Rh^{0.2}}$ being more selective towards the reduction of the ketone group (Table 4. 4, Entries 5 *vs.* 6). This was surprising since the lower availability of the faces in the case of $\mathbf{Rh^{0.4}}$ would be expected to disfavour the reduction of the aromatic ring over that of the ketone group.

Table 4. 5. Rh NPs ($\mathbf{Rh^{0.2}}$, $\mathbf{Rh^{0.4}}$) catalysed hydrogenation of **10**[a]

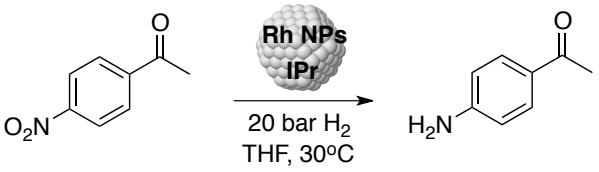

10 **10a**

Entry	Substrate	Catalyst	Conversion (%)[b]
1	**10**	$\mathbf{Rh^{0.2}}$	14
2	**10**	$\mathbf{Rh^{0.4}}$	18

[a] Catalytic conditions: 1.24 mmol substrate, 1.25 mol% cat. [b] Calculated from GC using undecane as internal standard.

Finally, the reduction of the aromatic ketone **10** bearing a reducible nitro group was looked at using $\mathbf{Rh^{0.2}}$ and $\mathbf{Rh^{0.4}}$. Standard reaction

conditions used previously were exclusively tested. Under these conditions, conversions were very low with both catalysts and only the reduction of the nitro group to afford the aniline **10a** was observed (Table 4. 5, Entries 1 and 2). These results were in agreement with those previously reported using Rh[64b,73, 74], Ru[12] and Pt[75] NPs. The lack of reduction of the arene ring and the ketone function once the nitro group is reduced indicated the preferred initial coordination of this substrate through the nitro group.

4.2.2. Selective hydrogenation of phenols

The hydrogenation of aromatic compounds bearing alcohol groups using Rh NPs stabilized by the IPr ligand was examined using phenol (**11**) as model substrate. Two main products are expected for this process: cyclohexanone (**11a**) formed after the fast keto-enol tautomerism of cyclohex-1-en-1-ol and cyclohexanol (**11b**) (complete reduced product) formed by reduction of the ketone group of **11a** (Figure 4. 35). As commented in the introduction of this chapter, **11a** is an intermediate for the production of caprolactam and adipic acid that can be used for the production of Nylon 6, Nylon 66 and polyamide resins.

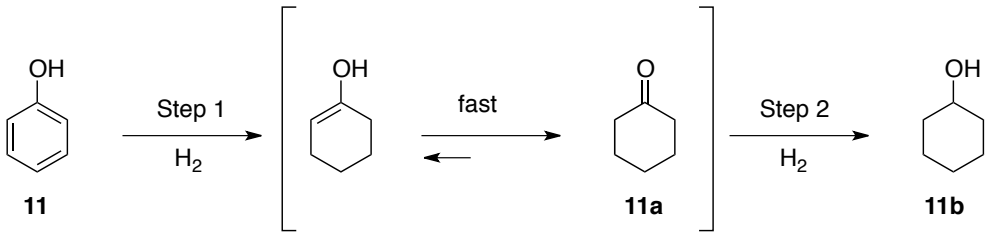

Figure 4. 35. Expected products for the hydrogenation of phenol (**11**)

The hydrogenation of phenol **11** was first carried out using 1.25mol% of $\mathbf{Rh^{0.2}}$ at 30°C under 20 bar of H_2 in THF and the reaction was monitored by GC-MS. Under these reaction conditions, 95% conversion was reached after 210 min of reaction with selectivities to cyclohexanone (**11a**) and cyclohexanol (**11b**) of 32% and 68%, respectively (Table 4. 6, Entry 1).

Table 4. 6. Rh NPs (**Rh$^{0.2}$**) catalysed hydrogenation of **11**[a]

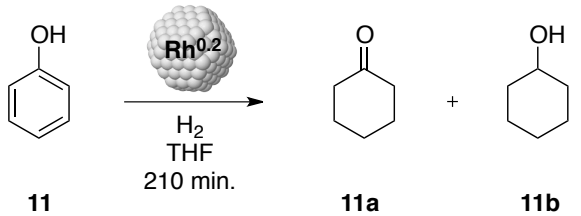

11 **11a** **11b**

Entry	Pressure (bar)	Temper. (°C)	Conv. (%)[b]	TOF[c]	11a (%)[b]	11b (%)[b]
1	20	30	95	81	32	68
2	5	30	93	86	48	52
3	1.7	30	30	23	75	25
4	1.7	60	100	43	79	21
5[d]	1.7	60	62	34	43	57

[a] Catalytic conditions: 2.48 mmol substrate, 1.25 mol% **Rh$^{0.2}$**. [b] Calculated from GC using undecane as internal standard. [c] TOF=(mmol product/mmol Rh surface)*h^{-1}, calculated at conv. <20%. [d] 1.25mol% **Rh$^{0.4}$**

When the H_2 pressure was decreased to 5 and 1.7 bar, an increase in selectivity to cyclohexanone (up to 75%) was observed while conversion diminished to 30% at similar reaction time (Table 4. 6, Entries 2 and 3).[45,46] However, an increase in temperature up to 60°C provided full conversion with no variation in selectivity (Table 4. 6, Entry 4). The use of **Rh$^{0.4}$** as catalyst afforded a lower conversion and lower selectivity towards cyclohexanone (**11a**) (Table 4. 6, Entry 5).

The results of the monitoring of the catalytic hydrogenation of **11** using **Rh$^{0.2}$** at 60°C under 20 and 1.7 bar of H_2 pressure are displayed in Figure 4. 36. When the reduction of **1** was performed under 20 bar of H_2 (Figure 4. 36), full conversion was reached after 270 min. At short reaction times, a practically equimolar mixture of **11a** and **11b** was observed, and later evolved towards the fully hydrogenated compound **11b**.

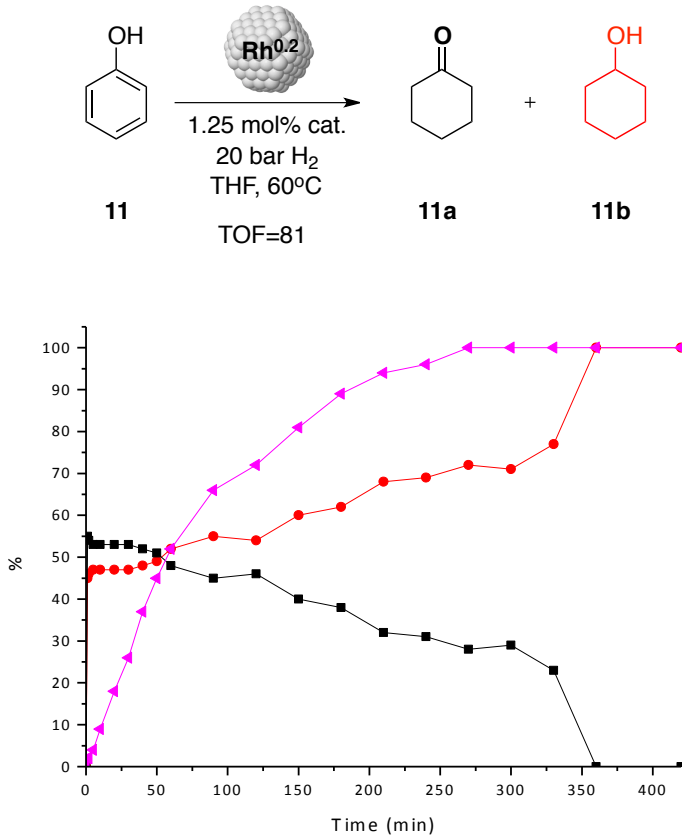

Figure 4. 36. Monitoring of the catalytic hydrogenation of phenol (**11**) using **Rh$^{0.2}$** as catalyst. Conversion in pink.

When the reaction was conducted under 1.7 bar of H_2, full conversion was achieved at similar reaction times, but in this case, the initial **11a/11b** ratio (75/25) did not vary over time (Figure 4. 37), suggesting that cyclohexanone was not reduced under these conditions.

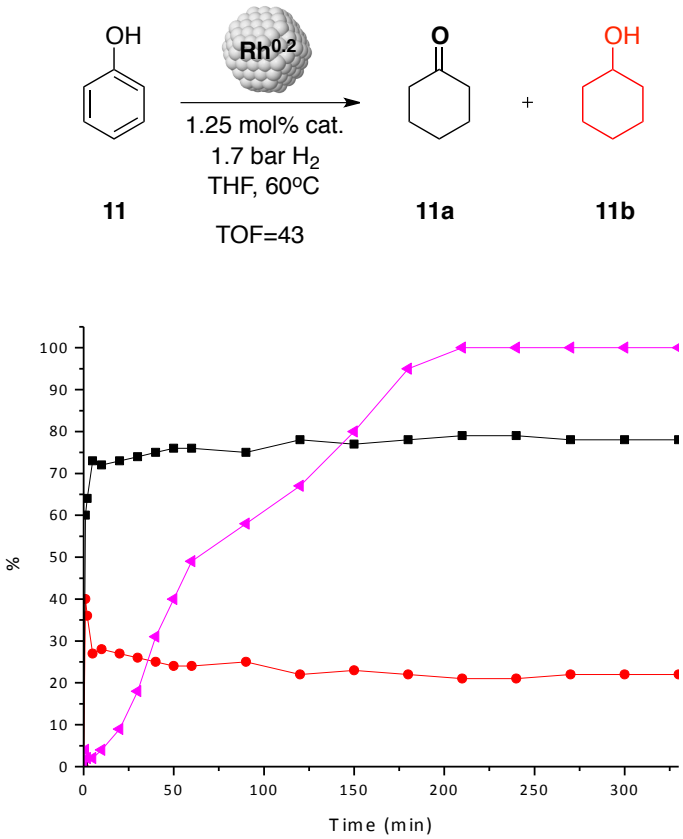

Figure 4. 37. Monitoring of the catalytic hydrogenation of phenol (**11**) using **Rh$^{0.2}$** as catalyst. Conversion in pink.

To corroborate this hypothesis, the hydrogenation of cyclohexanone **11a** was carried out using **Rh$^{0.2}$** and **Rh$^{0.4}$** as catalysts. The results showed that **11a** is reduced under 20 bar H_2 but not under 1.7 bar H_2 (Table 4. 7, Entries 1-3). It was therefore concluded that under low H_2 pressure, the selectivity is determined by the difference in rates (k2 *versus* k2') between isomerisation and hydrogenation of the enol intermediate **11'** (Figure 4. 38).

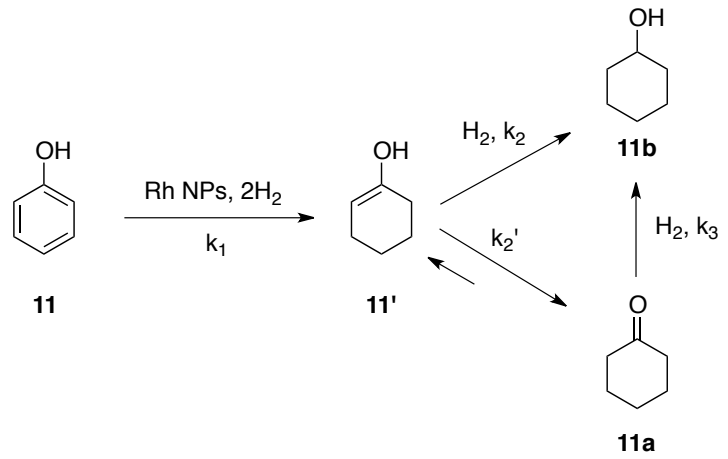

Figure 4. 38. Competitive reactions in the hydrogenation of phenol (**11**) using **Rh$^{0.2}$** as catalyst

The results of the reduction of **11** using **Rh$^{0.4}$** are presented in Figure 4. 39. Reaction rates at 60°C and 1.7bar of H_2 were lower for **Rh$^{0.4}$** than for **Rh$^{0.2}$**, achieving with **Rh$^{0.4}$** a conversion of 62% after 210 min (TOF= 34). This result is agreement with the behaviour observed in the reduction of ketones. Selectivity towards **11a** (44%) was also lower than the obtained using **Rh$^{0.2}$** (79%). This fact suggests that an increase in steric hindrance at the surface of the catalyst could disfavour desorption of the enol intermediate, promoting the reduction of **11a** and thus enhancing the selectivity towards the formation of **11b**.

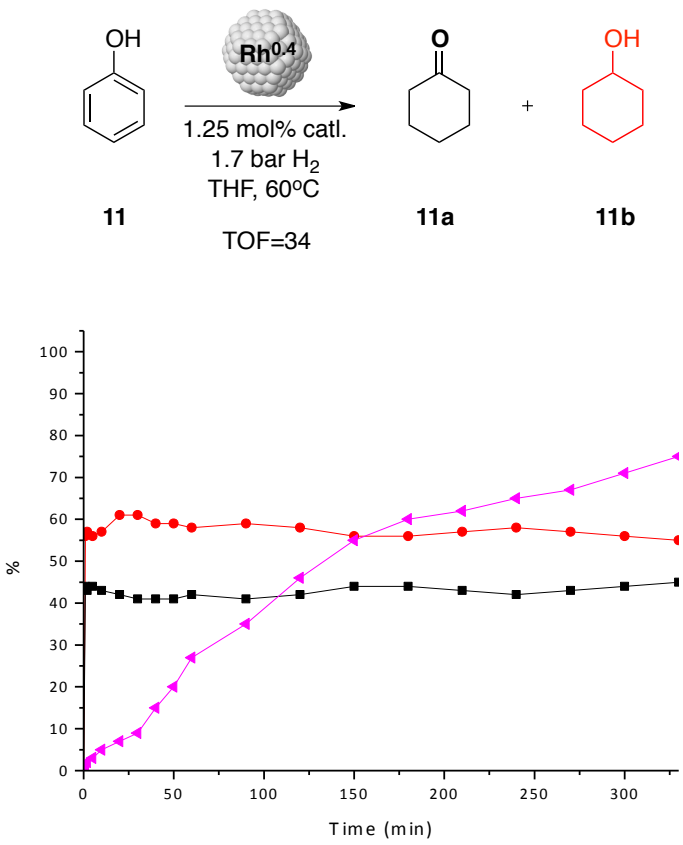

Figure 4. 39. Monitoring of the catalytic hydrogenation of phenol (**11**) using **Rh$^{0.4}$** as catalyst. Conversion in pink.

In order to examine the effect of the metal on the reaction, the application of previously reported Ru NPs stabilized using the same amount of the IPr ligand[12] were tested. Results are shown in Figure 4. 40. The reaction was conducted using **Ru$^{0.2}$** under the previously optimized reaction conditions (1.7 bar H_2, and 60°C) to afford a conversion of 64% after 210 min (TOF= 24). The ratio **11a/11b of** *ca*. 55/45 was also in this case practically constant over the reaction, but it is lower than for **Rh$^{0.2}$** (75/25). These results indicated a higher efficiency of **Ru$^{0.2}$** for the catalytic reduction of ketones,

compared to **Rh$^{0.2}$**, which is in agreement with the reported results obtained in the hydrogenation of aromatic ketones.[29]

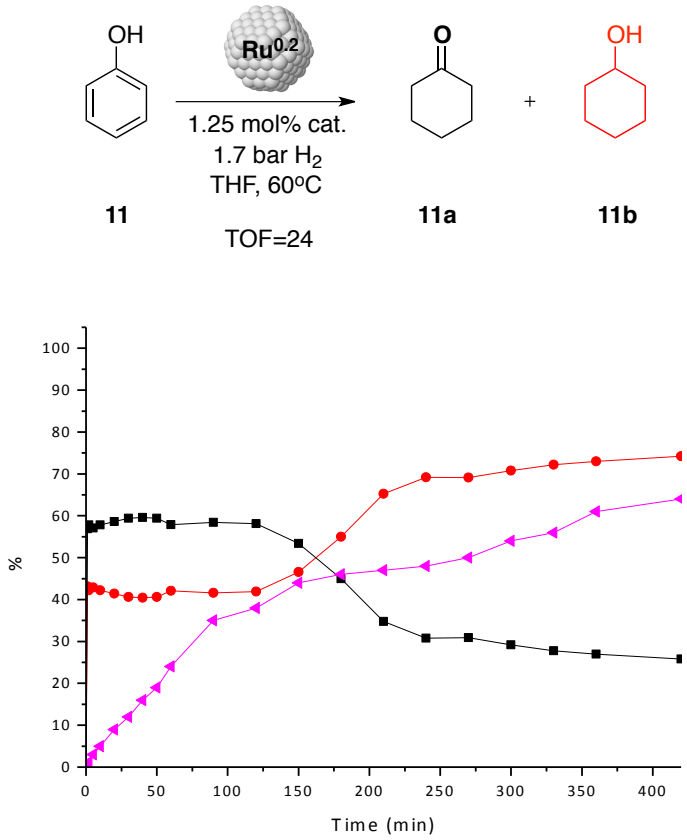

Figure 4. 40. Monitoring of the catalytic hydrogenation of phenol (**11**) using **Ru$^{0.2}$** as catalyst. Conversion in pink.

Finally, to confirm that the reduction of **11a** was depending on the H_2 pressure, catalytic tests using **11a** as substrate in the presence of **Rh$^{0.2}$**, **Rh$^{0.4}$** or **Ru$^{0.2}$** at different H_2 pressures were carried out. When the reaction was conducted under 1.7 bar of H_2 with **Rh$^{0.2}$** and **Rh$^{0.4}$** as catalysts, **11a** was not reduced (Table 4. 7, Entries 1 and 2). However, when the reaction was performed under 20 bar of H_2 using **Rh$^{0.2}$** as catalyst, **11a** was smoothly reduced to give **11b** (Table 4. 7, Entry 3). However, **Ru$^{0.2}$** reduced **11a** even under 1.7 bar of H_2,

(Table 4. 7, Entry 4), achieving a conversion of 79% (Table 4. 7, Entry 3 *vs*. 4). These results are in agreement with the selectivity observed in the phenol reduction and also with the reactivity showed by Ru NPs in ketone reduction.[29]

Table 4. 7. Rh and Ru NPs (**Rh$^{0.2}$** and **Ru$^{0.2}$**) catalysed hydrogenation of **11a**[a]

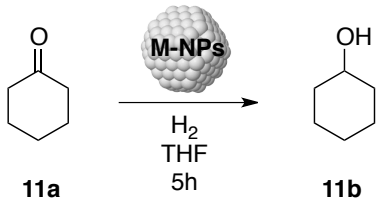

Entry	Catalyst	Pressure (bar)	Conv. (%)[b]
1	**Rh$^{0.2}$**	1.7	0
2	**Rh$^{0.4}$**	1.7	0
3	**Rh$^{0.2}$**	20	38
4	**Ru$^{0.2}$**	1.7	79

[a] Catalytic conditions: 2.48 mmol substrate, 1.25 mol% **Rh$^{0.2}$**, **Rh$^{0.4}$** or **Ru$^{0.2}$**.
[b] Calculated from GC using undecane as internal standard

Next, the hydrogenation of substituted phenols was explored. When the reaction was performed in the presence of **Rh$^{0.2}$** at 60°C under 1.7 bar of H_2 pressure, very low conversions were obtained in the hydrogenation of the phenol derivatives **12-16**. The reactions were then performed at 60°C and under 20 bar H_2 (Table 4. 8). In all cases, the conversions were lower than when **11** was used as substrate. In agreement with the results obtained in the hydrogenation of **11**, the cyclohexanols **12b-16b** were always preferably obtained, although the selectivity to the cyclohexanone **14a** reached 42% (Table 4. 8,

Entry 4). The lower selectivities to cyclohexanones obtained with these more sterically hindered substrates are in agreement with the results obtained during the hydrogenation of phenol using **Rh$^{0.4}$** as catalysts (Table 4. 6, Entry 5). Indeed, an increase in steric hindrance either at the surface of the catalyst or at the substrate favours the formation of cyclohexanols, which could indicate that desorption of the enol intermediates is disfavoured, thus enhancing the selectivity to cyclohexanols.

Table 4. 8. Rh NPs (**Rh$^{0.2}$**) catalysed hydrogenation of **11**, **12**, **13**, **14**, **15**, **16**[a]

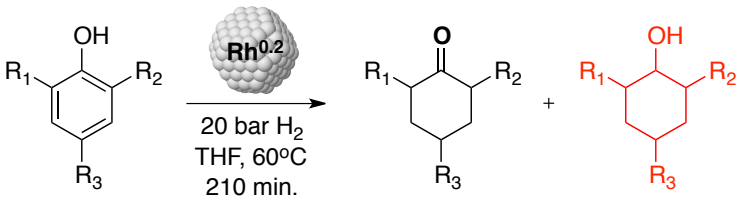

11-16 **11a-16a** **11b-16b**

Entry	Subst.	R_1	R_2	R_3	Conv. (%)[b]	TOF[c]	a (%)[b]	b (%)[b]
1	**11**	-H	-H	-H	96	43	33	67
2	**12**	-CH_3	-H	-H	12	3	27	73 *(74:26)*[d]
3	**13**	-H	-H	-CH_3	12	3	18	82[e]
4	**14**	-CH_3	-CH_3	-H	8	2	42	58[e]
5	**15**	-OH	-H	-H	38	9	7	93[e]
6	**16**	-OMe	-H	-H	14	3	0	100 *(83:17)*[d]

[a]Catalytic conditions: 2.48 mmol substrate, 1.25 mol% **Rh$^{0.2}$**. [b]Calculated by GC using undecane as internal standard. [c]TOF=(mmol product/mmol Rh surface)*h^{-1}, calculated at conv. <20% [d]*cis:tran* stereoselectivity. [e]overlapped signals in GC, not quantified.

In the case of the hydroxyl **15** or alkoxy **16** substituted derivatives, practically no cyclohexanones were detected (Table 4. 8, Entries 5 and 6). The cyclohexanol derivatives were obtained as *cis/trans* mixtures with selectivities up to 83:17 (Table 4. 8, Entry 6). These results are in agreement with those previously reported for the hydrogenation of *p*-methylanisole (*71:29*), *o*-xylene (*75:25*) and *m*-xylene (*75:25*) using Rh NPs stabilized by P-donor ligand,[28] and indicated that the desorption of partially reduced species before reaching complete reduction is not fully avoided. It can consequently be concluded that in terms of conversion, substitution of the phenol ring has a detrimental effect, which can be explained by the high steric hindrance provided by the NHC ligand at the catalyst surface.

Next, the hydrogenation of nitrobenzene (**17**) was examined under same reaction conditions and the reaction was monitored by GC (Figure 4. 41).

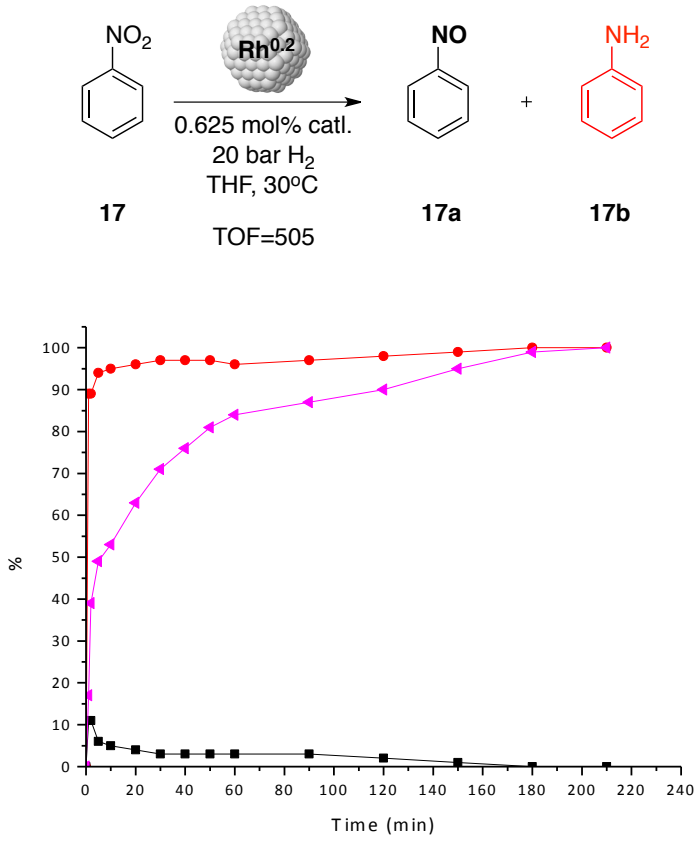

Figure 4. 41. Monitoring of the catalytic hydrogenation of nitrobenzene (**17**) using **Rh$^{0.2}$** as catalyst. Conversion in pink.

The reaction was completed after 150 min of reaction with a TOF of 505. The partially reduced product nitrosobenzene (**17a**) was detected in up to 10% selectivity at the beginning of the reaction, but was progressively reduced to aniline **17b**, which was not further reduced, similarly to the observed for the nitroderivative **10**.

4.2.3. Hydrogenation of N-heteroaromatics

The hydrogenation of N-heterocyclic compounds using **Rh$^{0.2}$** was evaluated using first pyridine (**17**) as model substrate. In Figure 4. 42, the evolution of the reaction over time at various temperatures and H_2 pressures is displayed. As expected, the decrease of both parameters has a negative influence on the conversion, although full conversion could be achieved in 180 min at 30°C under 10 bar of H_2 pressure.

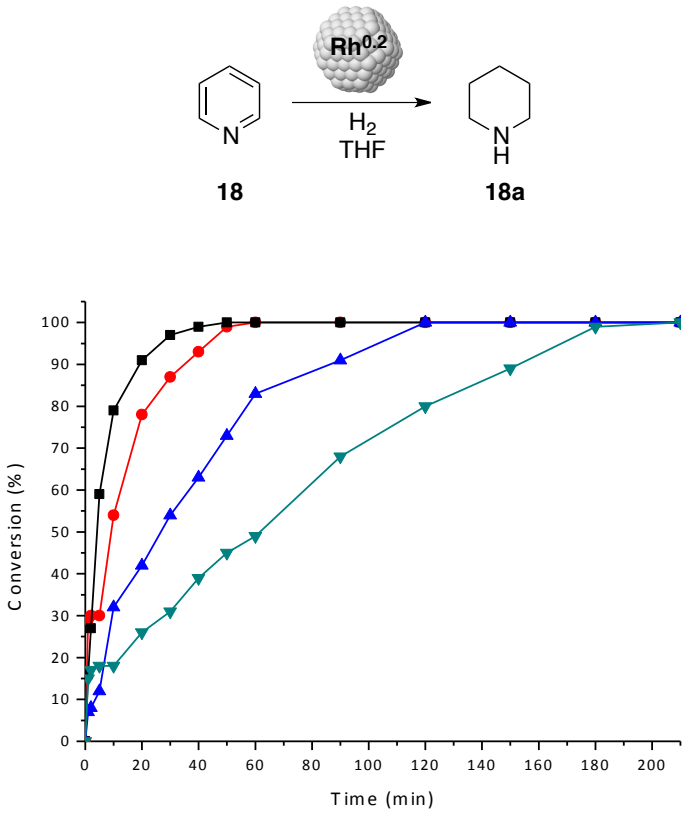

Figure 4. 42. Monitoring of the catalytic hydrogenation of pyridine (**18**) using **Rh$^{0.2}$** as catalyst. (Catalytic conditions: 2.48 mmol substrate; (black) 0.625 mol% **Rh$^{0.2}$**, 60°C, 20 bar H_2; (red) 1.25 mol% **Rh$^{0.2}$**, 60°C, 20 bar H_2; (blue) 0.625 mol% **Rh$^{0.2}$**, 30°C, 20 bar H_2; (green) 0.625 mol% **Rh$^{0.2}$**, 30°C, 10 bar H_2).

The **Rh$^{0.4}$** NPs were also applied as catalysts in the hydrogenation of **18** (0.625 mol% cat., 20 bar H_2 at 30°C) (Figure 4. 43) and a TOF of 229 was calculated at conversion<20%. This value was lower than that calculated for **Rh$^{0.2}$** (305), in agreement with the results obtained for previous substrates.

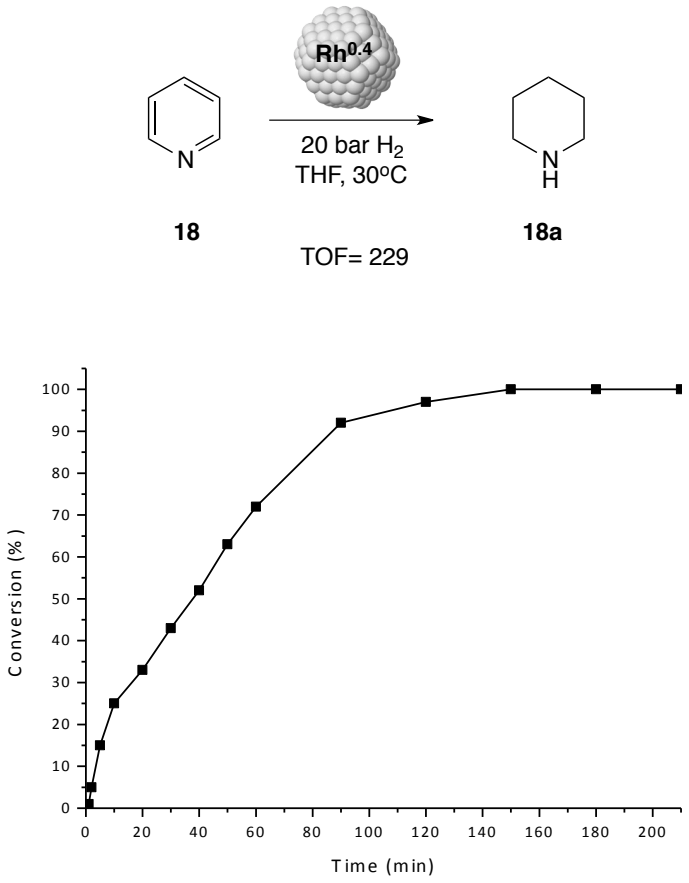

Figure 4. 43. Monitoring of the catalytic hydrogenation of pyridine (**18**) using **Rh$^{0.4}$** as catalyst. (Catalytic conditions: 2.48 mmol substrate, 0.625 mol% **Rh$^{0.4}$**).

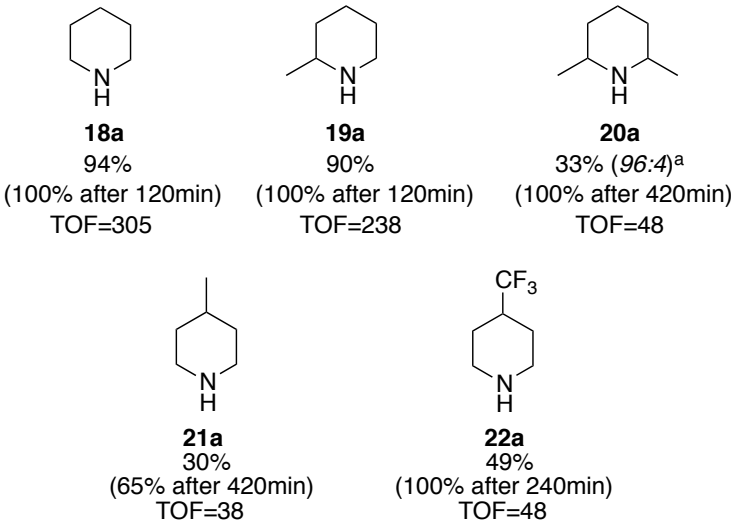

Figure 4. 44. Results obtained for the hydrogenation of **18**, **19**, **20**, **21** and **22** using $\mathbf{Rh^{0.2}}$ as catalyst. (Catalytic conditions: 2.48 mmol substrate, 0.625 mol% $\mathbf{Rh^{0.2}}$, 30°C, 20bar H_2, 90 min.) [a]*cis/trans* selectivity

With these results in hand, the effect of substituents in *ortho*- and *para*- positions of the pyridine ring was then evaluated. A negative influence of substitution on the conversion was previously reported for 2-methylpyridine[56] and substituted-quinoline derivatives using Rh/Al_2O_3 as catalysts.[68] However, using $\mathbf{Rh^{0.2}}$ as catalyst, the hydrogenation of 2-methylpyridine (**19**) to compound **19a** took place at a similar rate than the parent compound **18** (Figure 4. 44), whereas the rate of hydrogenation of the 2,6-dimethyl derivative (**20**) to afford **20a** was significantly lower under the same reaction conditions (full conversion was reached extending the reaction time). In this case, the *cis* diastereomer was almost exclusively formed, which suggested a strong interaction between the pyridine ring and the NPs surface, and hence that the decoordination necessary for the formation of the *trans* isomer after partial hydrogenation of the

aromatic ring was disfavoured. These results indicated that an increase in the ring substitution negatively influences the hydrogenation rate of these compounds; however, the stereochemistry of the product suggested that the flat coordination of the pyridine ring required for its reduction is strong enough in spite of the presence of two methyl substituents.

In view of these results, the effect of *para*-substituents was explored using 4-methylpyridine (**21**) and 4-trifluoromethylpyridine (**22**) as substrates. Surprisingly, the hydrogenation of 4-methylpyridine (**21**) to afford **10a** was the slowest of the series (TOF =38) (Figure 4. 44). Hydrogenation of 4-trifluoromethylpyridine (**22**) afforded **22a** at a slightly faster reaction rate (TOF=48) than **21**, which indicated that electronically-poorer rings are more easily reduced, in spite of the higher bulkiness of the $-CF_3$ group *vs.* $-CH_3$. These results therefore showed that under these conditions, the hydrogenation rates of *para*-substituted substrates is more similar to that of 2,6-dimethylderivative **20** than those of **18** and **19**, suggesting that the η^6-coordination of the aromatic ring to the surface of the NPs is more hindered by the presence of substituents in 4-position. This effect was not previously observed when the hydrogenation of 4-methylpyridine was performed using Lewis acid-ILs stabilized Rh NPs.[56] In order to confirm this hypothesis, the catalytic hydrogenation of **19** and **21** was carried out using $\mathbf{Rh^{0.4}}$ as catalyst under the same reaction conditions (Figure 4. 45). Lower reaction rates were observed in the reduction of both **19** and **21**, with TOFs of 143 and 19 respectively, a bit higher percentage decreases for **21**, which is in agreement with our previous supposition.

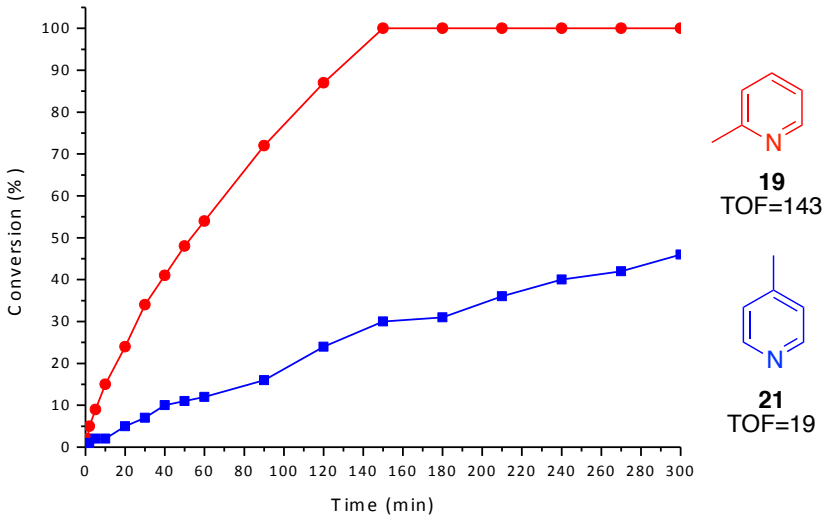

Figure 4. 45. Monitoring of the catalytic hydrogenation of 2-methylpyridine (**19**) and 4-methylpyridine (**21**) using **Rh$^{0.4}$** as catalyst. (Catalytic conditions: 2.48 mmol substrate, 0.625 mol% **Rh$^{0.4}$**, 30°C, 20 bar H_2).

In previous studies with Ru and Rh NPs, a different selectivity in ketoarenes reduction (arene *vs.* ketone) was observed depending on the distance between the keto and the arene groups.[12,29] To investigate whether this trend could be extended to pyridine derivatives, the hydrogenation of 2-acetylpyridine (**23**) and 1-pyridin-2-yl-propan-2-one (**24**) was studied.

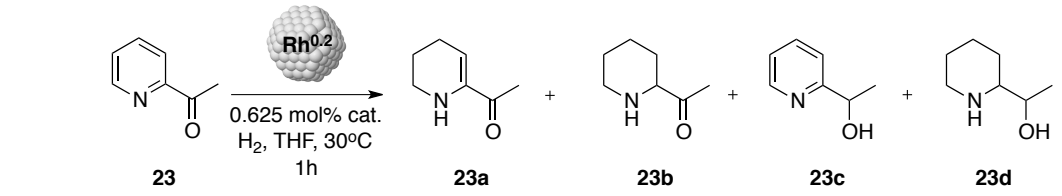

a) 20 bar H_2	100% conv. TOF= 196	0%	0%	0%	100%
b) 5 bar H_2	84% conv. TOF= 174	2%	8%	14%	76%

Figure 4. 46. Results obtained for the hydrogenation of 2-acetylpyridine (**23**) using **Rh$^{0.2}$** as catalyst.

Hydrogenation of **23** carried out at 30°C under 20 bar of H_2 afforded full conversion after 60 min of reaction with full selectivity towards the totally reduced product **23d** (Figure 4. 46a) (TOF =196). Full reduction of **23** was previously reported using Ru NPs stabilized by PFILs in water (30°C, 50 bar H_2, 15h of reaction).[12] When the H_2 pressure was decreased to 5 bar, partially reduced products **23a**, **23b** and **23c** were observed in low selectivities (2, 8 and 14%, respectively) (Figure 4. 46b), although compound **23d** was again the major product (TOF = 174). The high activities obtained for the electron-deficient pyridine ring (**23**), compared to **18**, confirmed our assumption that electronically-deficient pyridine rings are more easily reduced.

Table 4. 9. Rh NPs (**Rh$^{0.2}$**) catalysed hydrogenation of **24**[a]

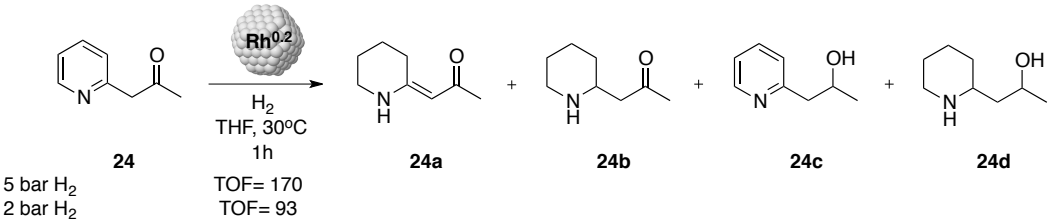

Entry	Time (min.)	Pressure (bar)	Conv. (%)[b]	24a (%)[b]	24b (%)[b]	24c (%)[b]	24d (%)[b]
1	60	5	79(100)[c]	64	8	16	12
2	240	5	100	64	0	0	36
3	60	2	39	78	12	10	0
4	240	2	89	76	12	9	3

[a]Catalytic conditions: 2.48 mmol substrate, 0.625 mol% **Rh$^{0.2}$**. [b]Calculated by GC using undecane as internal standard. [c]After 2h.

The reduction of **24** was initially studied at 30°C and under 5 bar of H_2 (Table 4. 9, Entry 1) in order to explore the possibility to obtain partially reduced compounds. Under these conditions, 79% conversion was obtained after 60 min, which was slightly lower than that obtained for **23** (84%). Interestingly, in this case, the β-enaminone **24a** was the major product of the reaction with 64% selectivity. The identity of this product was confirmed by mass spectrometry (M^+=139) (Figure S108, Supporting information) and ^{13}C and ^{1}H NMR spectroscopy (Figures S112 and S113, Supporting information), and comparison with reported values.[76] Products from the selective reduction of the pyridine ring (**24b**), ketone (**24c**) and the totally reduced product (**24d**) were also detected in 8, 16 and 12%, respectively. At longer reaction time, the reduction of **24b** and **24c** into **24d** was observed whereas the selectivity to **24a** remained

unchanged even after 4h of reaction under these conditions (Table 4. 9, Entry 2). When the reaction was repeated under 2 bar of H_2 pressure, an increase in the selectivity to **24a** up to 78% was observed (Table 4. 9, Entry 3). This selectivity was maintained when the reaction was run for 240 minutes (conv.= 89%) (Table 4. 9, Entry 4).

Comparison of the results obtained in the hydrogenation of the pyridine derivative **24** and the related arylketone **2** indicated a clearly distinct output. The product **24a** is probably formed through isomerization of a partially reduced intermediate, which takes place faster on this case than for **2** (Figure 4. 47).

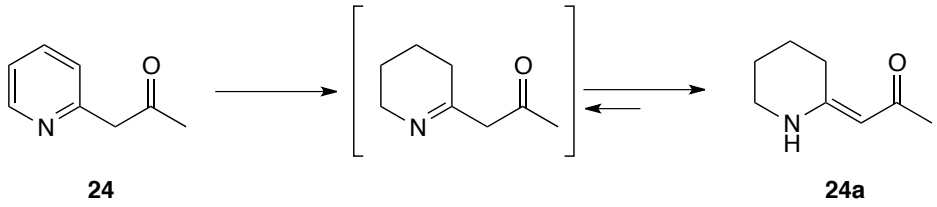

Figure 4. 47. Isomerization mechanism for the formation of 1-(2-piperidinylidene)-2-propanone (**24a**)

Next, the competitive reduction of pyridine *vs*. phenyl rings was looked at. With this purpose we studied first the hydrogenation of benzene (**25**) under the same reaction conditions than those used for pyridine (**18**) (Figure 4. 48). After 60 min, 84% conversion was obtained, similarly to the results obtained for **18**. However, when the hydrogenation of a 1:1 mixture of **18**:**25** was carried out and monitored by GC over time, complete conversion of **18** was reached when hydrogenation of **25** was only 9% of conversion (Figure 4. 49).

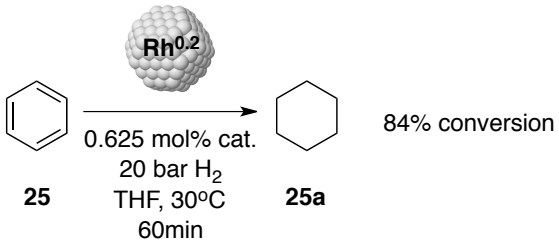

Figure 4. 48. Results obtained for the hydrogenation of benzene (**25**) using **Rh$^{0.2}$**

These results can be explained considering that piperidine (**18a**), which is produced by the reduction of **18**, can coordinate to the NPs surface and as such can act as a poison that prevent the reduction of **25**. This poisoning effect has been previously evidenced in the reduction of quinoline and imines using nanocatalysts.[63c] The fact that pyridine **18** was reduced in the presence of piperidine **18a** suggests a displacement of the reduction product **18a** by the substrate **18**, which confirms the involvement of the nitrogen coordination with the catalyst surface prior to hydrogenation.

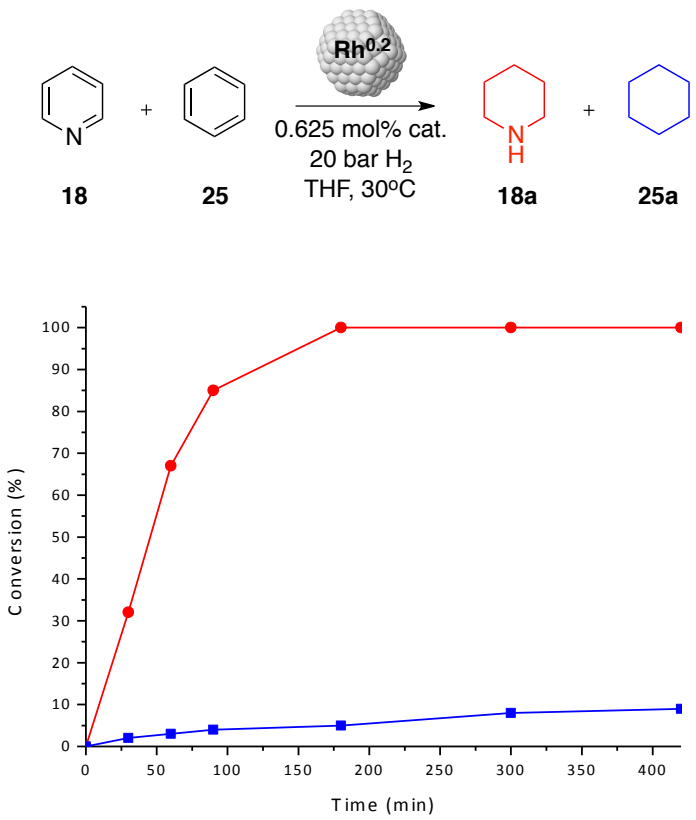

Figure 4. 49. Monitoring of the catalytic hydrogenation of **18 + 25** using **Rh$^{0.2}$** as catalyst.

Next, the hydrogenation of 2-phenylpyiridine (**26**) was looked at 30°C under 20 bar of H_2 and the reaction was monitored over time (Figure 4. 50). Under these conditions, this reaction was very slow (19% conv. after 7h). The low reactivity of 2-phenylpyridines had been already observed.[60] Three products **26a-c** can be formed and initially only **26a,b** were produced in a ratio 65:35. Compound **26b** was slowly reduced to **26c**, but **26a** was not reduced under these conditions, and a constant ratio **26a/(26b+26c)** was observed over time, corresponding to the selectivity for the pyridine *vs.* arene reduction.

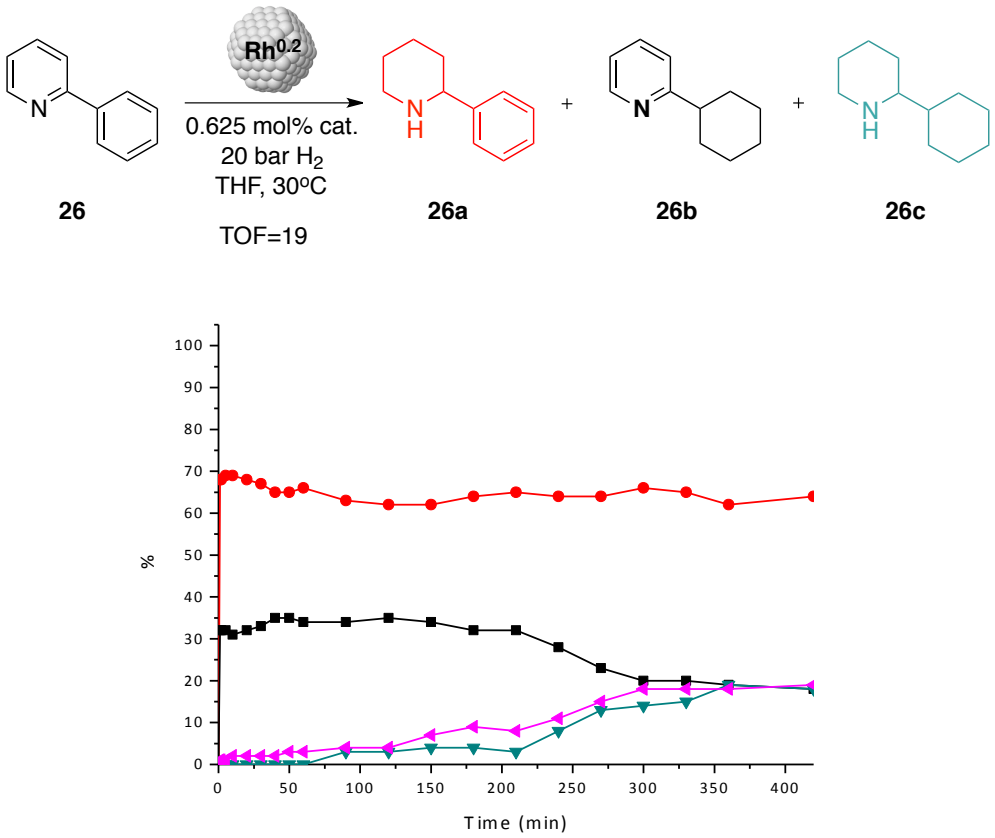

Figure 4. 50. Monitoring of the catalytic hydrogenation of 2-phenylpyiridine (**26**) using **Rh$^{0.2}$** as catalyst. Conversion in pink.

When the temperature was increased to 60°C, an increase in activity was observed (Figure 4. 51) and compound **26c** was rapidly generated. Under these conditions, the compound **26a** was also reduced and, after 48h, only the fully reduced product (**26c**) was present in the reaction mixture.

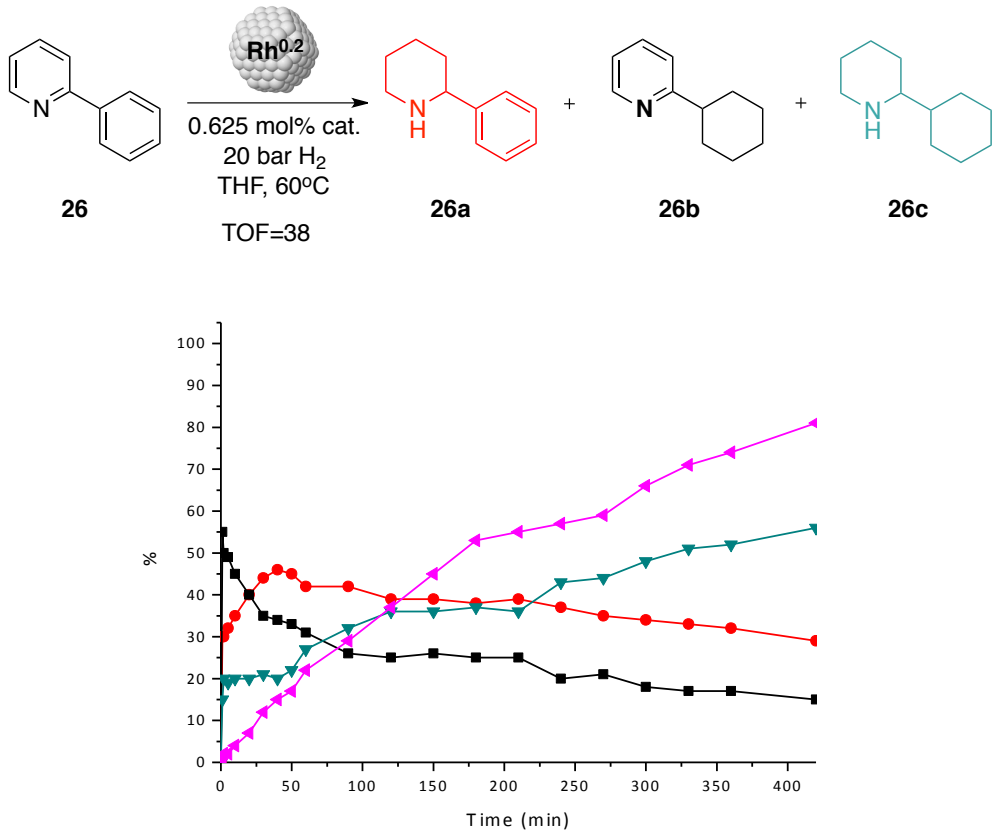

Figure 4. 51. Monitoring of the catalytic hydrogenation of 2-phenylpyiridine (**26**) using **Rh$^{0.2}$** as catalyst. Conversion in pink.

To summarize, both the pyridine moiety and the phenyl ring were reduced using **Rh$^{0.2}$** as catalyst at 20 bar of H_2 and 60°C to afford the fully reduced product **26c** in 100% selectivity.

In view of the results obtained in the hydrogenation of pyridine analogues bearing arene rings, the reduction of quinoline (**27**), was also investigated. As previously mentioned in the introduction of this chapter, three main products are expected: 1,2,3,4-tetrahydroquinoline (^{1}THQ) (**27a**) formed from the selective reduction of the pyridine ring, 5,6,7,8-tetrahydroquinoline (^{5}THQ) (**27b**) formed from the selective reduction of the arene ring and

decahydroquinoline (DHQ) (**27c**) formed from complete reduction of the substrate (Figure 4. 52).

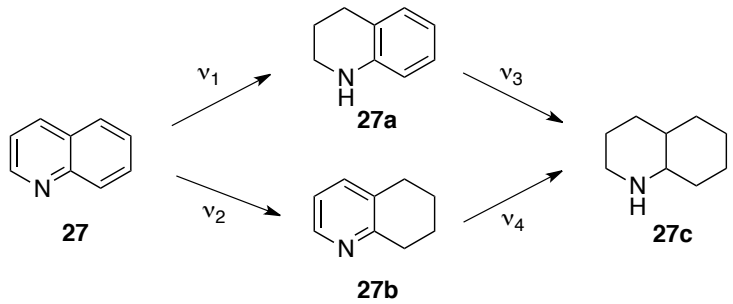

Figure 4. 52. Expected products for the hydrogenation of quinoline (**27**)

The hydrogenation of quinoline (**27**) was initially performed at 30°C under 20 bar of H_2 using **Rh$^{0.2}$** as catalysts, and the reaction was monitored by GC (Figure 4. 53). Under these conditions, full conversion was achieved after 140 min of reaction. Initially, the fully reduced product **27c** was not detected and the ratio **27a/27b** was 89:11 (conversion 33%, Figure 4. 53). This selectivity progressively decreased to 75:20 at full conversion. At this point, 5% of **27c** was formed although the reduction of both **27a** and **27b** was very slow under these conditions.

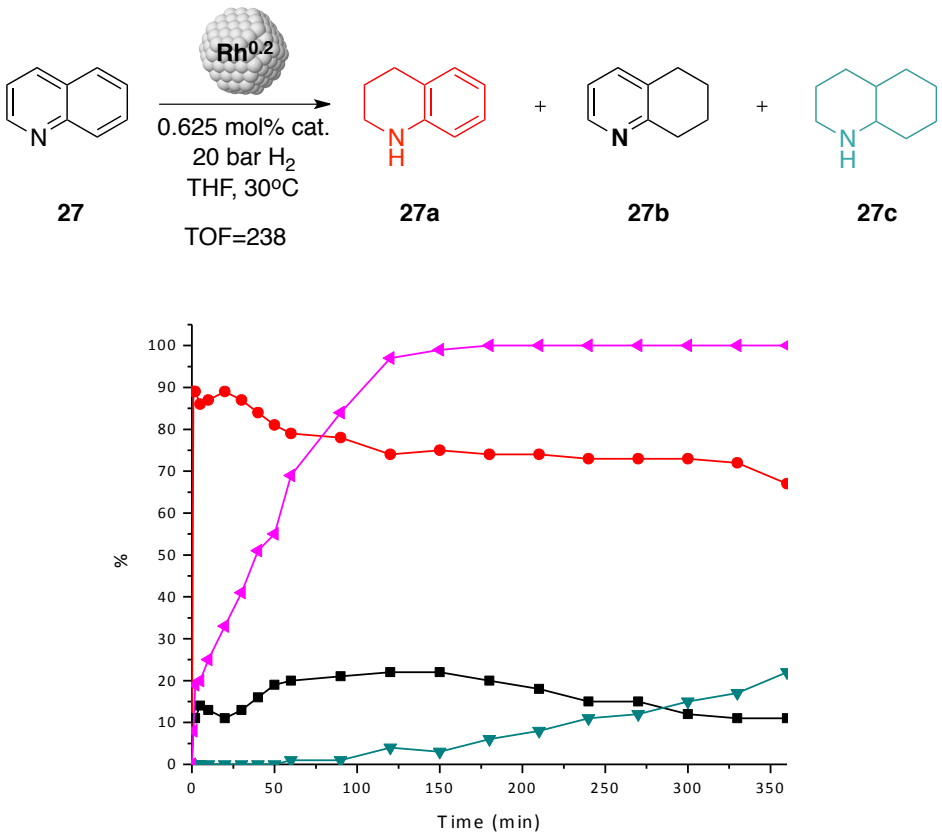

Figure 4. 53. Monitoring of the catalytic hydrogenation of quinoline (**27**) using **Rh$^{0.2}$** as catalyst. Conversion in pink.

When the reaction was conducted at 60°C, full conversion was achieved after only 30 min of reaction and at this point ratio **27a/27b** was 75:25 (TOF= 496) (Figure 4. 54), with practically no traces of the fully reduced product **27c**. After 24h of reaction, full conversion towards **27c** was achieved as a consequence of the complete reduction of **27a,b**. In summary, in the presence of **Rh$^{0.2}$** as catalyst, **27c** can be obtained as the only product after 24h in the absence of additives[53,69,70] The TOF measured for this last process (496) is the highest reported to date.

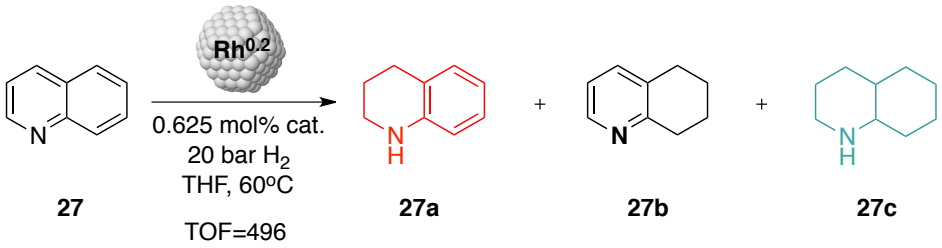

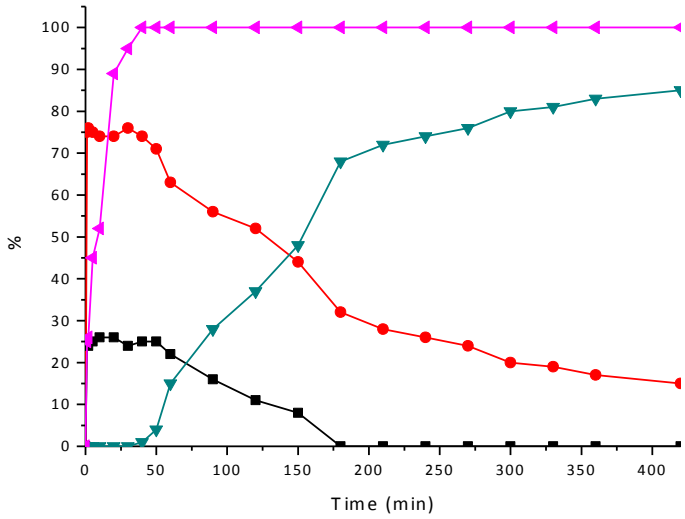

Figure 4. 54. Monitoring of the catalytic hydrogenation of quinoline (**27**) using **Rh$^{0.2}$** as catalyst. Conversion in pink.

When **Rh$^{0.4}$** was used as catalyst for the hydrogenation of **27** under the same conditions (Figure 4. 55), selectivities were similar to those obtained with **Rh$^{0.2}$**, although a slight decrease in the reaction rate was observed (TOF= 447). These results confirmed the lower activity of the catalyst with a higher coverage of stabilizing ligand at its surface.

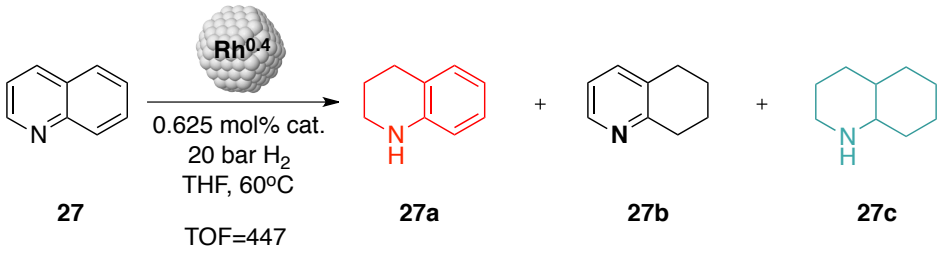

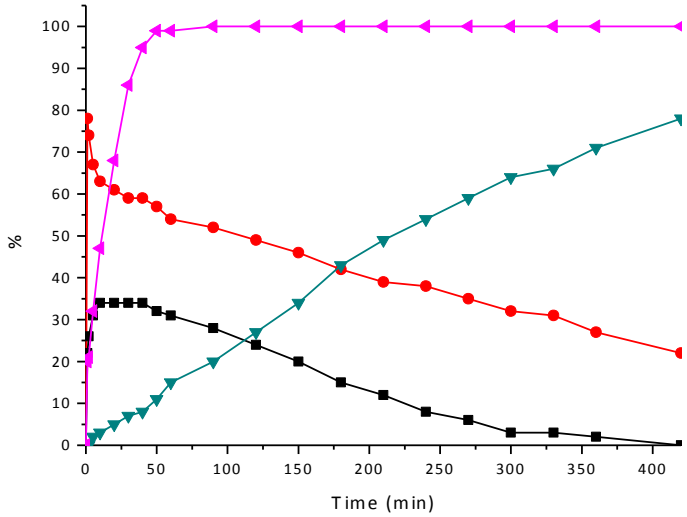

Figure 4. 55. Monitoring of the catalytic hydrogenation of quinoline (**27**) using **Rh$^{0.4}$** as catalyst. Conversion in pink.

4.3. Conclusions

Selective hydrogenation of aromatic ketones:

-Lower activities were in general obtained for the reduction of aromatic ketones using **Rh$^{0.4}$** and **Rh$^{0.6}$** compared to **Rh$^{0.2}$** due to the presence of higher amounts of ligand in the surface of the Rh NPs.

-The lack of reduction of alkyl ketones such as **1a**, **2a** and **3a** indicated interaction between the corresponding aromatic ketones and the Rh NPs surface through the arene ring. This fact was confirmed by an increase in selectivity up to 91% to **3a** when **3** was used as substrate.

-The presence of bulky groups close to the ketone group (substrates **4** and **5**) decreased the selectivity towards the arene ring reduction (products **4a** and **5a**) due to the hindered coordination of the aromatic ring to the surface of the NPs.

-In general, the presence of substituents in the *ortho* position of the aromatic ring (**6** and **7**) produced a decrease in the activity of the reaction, achieving moderate lower selectivities towards the reduction of the aromatic ring. These decreases in activity and selectivity can be due to the electron-donating properties of the groups present and/or to the higher substitution of the ring.

-The presence of both, electron-donating or electron-withdrawing substituents in the *para* position of the aromatic ring (**8** and **9**) produced a strong decrease in the selectivity towards the reduction of the aromatic ring.

Hydrogenation of phenol derivatives:

- Selectivities up to 79% to cyclohexanone (**11a**) or 100% towards cyclohexanol (**11b**) could be achieved using **Rh$^{0.2}$** depending on the reaction conditions.

-The effect of the presence of high amounts of ligand at the NPs surface showed to have a detrimental effect on the activity and selectivity towards the formation of **11a**.

-The application of **Ru$^{0.2}$** for the reduction of **11** gave rise to lower activities and selectivities towards the formation of **11a**.

-The presence of $-CH_3$ groups in the *ortho* (**12** and **14**) and *para* (**13**) position of the aromatic ring decreased the reduction reaction rate due to the hindered flat coordination of the aromatic ring to the surface of the NPs.

-The possible coordination of **15** and **16** in a chelating mode to the NPs surface produced an increase on the selectivity of the reaction towards the formation of cyclohexane-1,2-diol (**15b**) and 2-methoxycyclohexanol (**16b**).

-An increase in the electronic density of the aromatic ring for the reduction of nitrobenzene (**17**) along with the strong coordination of the aniline product (**17b**) gave rise to full selectivity towards the reduction of the nitro group.

Hydrogenation of N-heterocyclic compounds:

-**Rh$^{0.2}$** and **Rh$^{0.4}$** were able to reduce pyridine rings (**18**) with high efficiency at 30°C under 20 bar of H_2.

- The effect of the presence of high amounts of ligand at the NPs surface showed to have a detrimental effect on the activity and selectivity towards the reduction of pyridine rings (**19** and **21**).

-The presence of $-CH_3$ groups in *ortho* position of the pyridine ring (**19** and **20**) decreased the reaction rate due to an increase in the steric hindrance close to the N atom, which coordinates to the NPs surface before reduction of the aromatic ring.

-The presence of $-CH_3$ and $-CF_3$ groups in *para* position of the pyridine ring (**21** and **22**) also decreased the hydrogenation rate, which suggests an effect of these groups on the coordination of the aromatic ring to the surface of the NPs in a flat way, necessary for its reduction.

-Pyridine derivatives bearing a ketone group in *ortho* position of the aromatic ring (**23** and **24**) were hydrogenated much faster than pyridine (**18**). The totally reduced compound **23d** was the only reaction product in the case of **23**, and the β-enaminone **24a** was the major reaction product in the case of **24**, and was obtained in 78% selectivity under 5 bar of H_2.

-The formation of piperidine (**18a**) was observed to poison the NPs surface by hydrogenation experiments using 1:1 pyridine (**18**):benzene (**25**) mixtures.

-The presence of a phenyl ring in the *ortho* position of the aromatic ring have an effect on the hydrogenation reaction rate due to an increase in the steric hindrance close to the N atom.

-Reduction of **26** and **27** provided moderate to high selectivities to compounds **26a** and **27a**, up to 65 and 89% respectively, resulting from the reduction of the pyridine ring when performing the reaction at 30°C under 20 bar of H_2.

-Reduction of **26** and **27** afforded the totally reduced products **26c** and **27c** when the reactions were carried out at 60°C under 20 bar of H_2, after 48 and 24h of reaction, respectively.

4.4. Experimental part

General procedure for the hydrogenation reactions

Autoclave Par 477 equipped with PID control temperature and reservoir for kinetic measurements and HEL 24 Cat reactor for substrate scope were used as reactors for the hydrogenation reactions. In a typical experiment, the autoclave was charged in the glove-box with the desired Rh NPs (1.25 or 0.625 mol%; the catalyst concentration was calculated based on the total number of metallic Rh atoms in the surface of the NPs) and the substrate (0.124 M) in THF. Molecular hydrogen was then introduced until the desired pressure was reached and the reaction was stirred for the desired reaction time at the chosen temperature. After the reaction finished, the autoclave was depressurised and the solution was filtered over silica for subsequent analysis by GC. Samples were taken after the desired reaction time in the case of kinetic studies, at constant H_2 pressure. The conversion and the selectivities for each reaction product were determined by GC-FID on an Agilent Technologies 7890A spectrometer, with an achiral HP-5 column (30m x 0.25mm x 0.25μm). TOF was defined as: (moles of product/mol Rh_s or Ru_s)*h^{-1}.

GC methods and retention times in the selective hydrogenation of ketones.

The method used for **1**, **2**, **3**, **4**, **6**, **7**, **9** and **10** consists in an initial isotherm period at 40°C for 3 min followed by a 3°C/min ramp to 120°C and a hold time of 12 min, with a flow of 1.3ml/min. Undecane

was used as internal standard (tr:18.61 min). The method used for **8** consists in an initial isotherm period at 130°C for 10 min followed by a 10°C /min ramp to 180°C and a hold time of 20 min. Undecane was used as internal standard (tr: 1.45 min).

GC methods and retention times in the hydrogenation of phenol derivatives.

The method used for these compounds consists in an initial isotherm period at 40°C for 3 min followed by a 3°C/min ramp to 100°C and a hold time of 25 min, with a flow of 1.3ml/min. Undecane was used as internal standard (tr: 18.18 min).

GC methods and retention times in the hydrogenation of pyridine derivatives.

The method used for **17, 18**, **19**, **20** and **21** consists in an initial isotherm period at 40°C for 3 min followed by a 3°C/min ramp to 100°C, with a flow of 1.3ml/min. Undecane was used as internal standard (tr: 23.74 min). The method used for **24** consists in an initial isotherm period at 28°C for 5 min followed by a 25°C/min ramp to 200°C and a hold time of 5 min, with a flow of 1.3ml/min. Undecane was used as internal standard (tr: 9.62 min). The method used for **22**, **23**, **25** and **26** consists in an initial isotherm period at 40°C for 3 min followed by a 3°C/min ramp to 120°C and a hold time of 25 min, with a flow of 1.3ml/min. Undecane was used as internal standard (tr: 18.10 min).

4.5. References

[1] J. A. Widegren, R. G. Finke, *J. Mol. Catal. A: Chem.* **2003**, 191, 187-207.

[2] A. Roucoux, *Top. Organomet. Chem.* **2005**, *16*, 261-279.

[3] A. Gual, C. Godard, S. Castillón, C. Claver, *Dalton Trans.* **2010**, *39*, 11499-11512.

[4] a) F. Jutz, J.-M. Andanson, A. Baiker, *J. Catal.* **2009**, *268*, 356-366. b) G. S. Fonseca, A. P. Umpierre, P. F. P. Fichtner, S. R. Teixeira, J. Dupont, *Chem. Eur. J.* **2003**, *9*, 3263-3269. c) M. Bhardwaj, S. Paul, Arabian J. Chem. **2016**, http://dx.doi.org/10.1016/j.arabjc.2016.05.008. d) L. Parimala, J. Santhanalakshmi, *Journal of Nanoparticles*, **2014**, Article ID 156868, 10 pages. e) A. Chaiyanurakkul, L. Gao, T. Nishikata, K. Kojima, H. Nagashima, *Chem. Lett.* **2014**, *43*, 1233-1235, f) P. Lara, L. M. Martinez-Prieto, M. Roselló-Merino, C. Richter, F. Glorius, S. Conejero, K. Philippot, B. Chaudret, *Nano-Structures & Nano-Objects* **2016**, *6*, 39-45.

[5] a) Y.-Z. Xiang, Y.-A. Lv, T.-Y. Xu, X.-N. Li, J. -G. Wang, *J. Mol. Catal. A: Chem.* **2011**, *351*, 70-75. b) A. Denicourt-Nowicki, B. Léger, A. Roucoux, *Phys. Chem. Chem. Phys.* **2011**, *13*, 13510-13517. c) E. Rafter, T. Gutmann, F. Löw, G. Buntkowsky, K. Philippot, B. Chaudret, P. W. N. M. van Leeuwen *Catal. Sci. Technol.* **2013**, *3*, 595-599. d) l. Song, X. Li, H. Wang, *Catal. Lett.* **2009**, *133*, 63-69. e) N. T. T. Chau, S. Handjani, J.-P. Guegan, M. Guerrero, E. Monflier, K. Philippot, A. Denicourt-Nowicki, A. Roucoux, *ChemCatChem* **2013**, *5*, 1497-1503. f) I. S. Park, M. S. Kwon, K. Y. Kang, J. S. Lee, J. Park *Adv. Synth. Catal.* **2007**, *349*, 2039-2047. g) J. A. Anderson, A. Athawale, F. E. Imrie, F.-M. McKenna, A. McCue, D. Molyneux, K. Power, *J. Catal.* **2010**, *270*, 9-15. h) L. M. Martinez-Prieto, A. Ferry, P. Lara, C. Richter, K. Philippot, F. Glorius, B. Chaudret, *Chem. Eur. J.* **2015**, *21*, 17495-17502.

[6] M. Jahjah, Y. Kihn, E. Teuma, M. Gómez, *J. Mol. Catal. A: Chem.* **2010**, *332*, 106-112.

[7] K. Philippot, B. Chaudret, *C. R. Chimie* **2003**, *6*, 1019-1034.

[8] C. Amiens, B. Chaudret, D. Ciuculescu-Pradines, V. Collière, K. Fajerwerg, P. Fau, M. Kahn, A. Maisonnat, K. Soulantica, . Philippot, *New, J. Chem.* **2013**, *37*, 3374- 3401.

[9] I. Faviere, S. Massou, E. Teuma, K. Philippot, B. Chaudret, M. Gómez *Chem. commun.* **2008**, 3296-3298.

[10] M. Guerrero, A. Roucoux, A. Denicourt-Nowicki, H. Bricout, E. Monflier, V. Collière, K. Fajerwerg, K. Philippot, *Catal. Today* **2012**, *183*, 34-41.

[11] M. Guerrero, Y. Coppel, N. T. T. Chau, A. Roucoux, A. Denicourt-Nowicki, E. Monflier, H. Bricout, P. Lecante, K. Philippot, *ChemCatChem* **2013**, *5*, 3802-3811.

[12] D. Gonzalez-Galvez, P. Lara, O. Rivada-Wheelaghan, S. Conejero, B. Chaudret, K. Philippot, P. W. N. M. van Leeuwen, *Catal. Sci. Technol.* **2013**, *3*, 99-105.

[13] P. Lara, O. Rivada-Wheelaghan, S. Conejero, R. Poteau, K. Philippot, B. Chaudret, *Angew. Chem. Int. Ed.* **2011**, *50*, 12080-12084.

[14] H.-Y. Jiang, X.-X. Zheng, *Catal. Sci. Technol.* **2015**, *5*, 3728-3734.

[15] T. Ohkuma, H. Ooka, T. Ikariya, R. Noyori, *J. Am. Chem. Soc.* **1995**, *117*, 2675-2676.

[16] A. Perosa, P. Tundo, M. Selva, *J. Mol. Catal. A: Chem.* **2002**, *180*, 169-175.

[17] L. Foppa, J. Dupont, *Chem. Soc. Rev.* **2015**, *44*, 1886-1897.

[18] G. S. Fonseca, J. D. Scholten, J. Dupont, *Synlett* **2004**, 9, 1525-1528.

[19] I. Cano, M. J.-L. Tschan, L. M. Martínez-Prieto, K. Philippot, B. Chaudret, P. W. N. M. van Leeuwen, *Catal. Sci. Technol.* 2016, *6*, 3758-3766.

[20] D. J. M. Snelders, N. Yan, W. Gan, G. Laurenczy, P. J. Dupont, *ACS Catal.* **2012**, *2*, 201-207.

[21] R. J. Bonilla, B. R. James, P. G. Jessop, *Chem. Commun* **2000**, 941-942

[22] F. Jutz, J.-M. Andanson, A. Baiker, *J. Catal.* **2009**, *268*, 356-366.

[23] N. T. T. Chau, S. Menuel, S. Colombel-Rouen, M. Guerrero, E. Monflier, K. Philippot, A. Denicourt-Nowicki, A. Roucoux, *RSC Adv.* **2016**, *6*, 108125-108131.

[24] C. Hubert, A. Denicourt-Nowicki, A. Roucoux, D. Landy, B. Léger, G. Crowyn, E. Monflier, *Chem. Commun.* **2009**, *350*, 1228-1230.

[25] A. Denicourt-Nowicki, A. Ponchel, E. Monflier, A. Roucoux, *Dalton. Trans.* **2007**, *48*, 5714-5719.

[26] N. T. T. Chau, S. Handjani, J. P. Guegan, M. Guerrero, E. Monflier, K. Philippot, A. Denicourt-Nowicki, A. Roucoux, *ChemCatChem*. **2013**, *5*, 1497-1503.

[27] M. Ibrahim, R. Poreddy, K. Philippot, A. Riisager, E. J. Garcia-Suarez, *Dalton Trans.* **2016**, *45*, 19368-19373.

[28] J. Llop, A. Gual, E. Mercadé, C. Claver, C. Godard, *Catal. Sci. Technol.* **2013**, *3*, 2828-2833.

[29] J. L. Castelbou, E. Bresó-Femenia, P. Blondeau, B. Chaudret, S. Castillón, C. Claver, C. Godard, *ChemCatChem* **2014**, *6*, 3160-3168.

[30] U. Schuchardt, D. Cardoso, R. Sercheli, R. Pereira, R. S. da Cruz, M. C. Guerreiro, D. Mandellif, E. V. Spinacé, E. L. Pires, *Appl. Catal. A.* **2001**, *211*, 1-17.

[31] *World Nylon 6 & 66 Supply/Demand Report*, PCI-Fibers & Raw Materials, Seaford, UK, **1998**.

[32] C. Zhao, J. He, A. A. Lemonidou, X. Li, J. A. Lechter, *J. Catal.* **2011**, *280*, 8-16.

[33] N. Yan, Y. Yuan, R. Dykeman, Y. Kou, P. J. Dyson, *Angew. Chem. Int. Ed.* **2010**, *49*, 5549-5553.

[34] K. L. Luska, P. Migowski, S. El Sayed, W. Leitner, *Angew. Chem. Int. Ed.* **2015**, *54*, 15750-15755.

[35] L. Chen, J. Xin, L. Ni, H. Dong, D. Yan, X. Lu, S. Zhang, *Green Chem.* **2016**, *18*, 2341-2352.

[36] a) Y. Wang, J. Yao, H. Li, D. Su, M. Antonietti, *J. Am. Chem. Soc.* **2011**, *133*, 2362-2365. b) G. Feng, P. chen, H. Lou, *Catal. Sci. Technol.* **2015**, 5, 2300-2304. c) F. Zhang, S. Chen, H. Li, X.-M. Zhang, H. Yang, *RSC Adv.* **2015**, *5*, 102811-102817. d) A. Chen, G. Zhao, J. Chen, L. Chen, Y. Yu, *RSC Adv.* **2013**, *3*, 4171-4175. e) J.-F. Zhu, G.-H. Tao, H.-Y. Liu, L. He, Q.-H. Sun, H.-C. Liu, *Green Chem.* **2014**, *16*, 2664-2669. f) Z. Li, J. Liu, C. Xia, F. Li, *ACS Catal.* **2013**, *3*, 2440-2448.

[37] C.-J. Lin, S.-H. Huang, N.-C. Lai, C.-M. Yang, *ACS Catal.* **2015**, *5*, 4121-4129.

[38] V. Mévellec, A. Roucoux, E. Ramirez, K. Philippot, B. Chaudret, *Adv. Synth. Catal.* **2004**, *346*, 72-76.

[39] F. Lu, J. Liu, J. Xu, *Mater. Chem. Phys.* **2008**, *108*, 369-374.

[40] X. Cui, A.-E. Surkus, K. Junge, C. Topf, J. Radnik, C. Kreyenschulte, M. Beller. *Nat. Commun.* **2016**, *7*, 11326.

[41] N. YAn, Y. Yuan, P. J. Dyson, *Chem. Commun.* **2011**, *47*, 2529-2531.

[42] J. Zhang, M. Ibrahim, V. Collière, H. Asakura, T. Tanaka, K. Teramura, K. Philippot, N. Yan, *J. Mol. Catal. A.: Chem.* **2016**, *422*, 188-197.

[43] A. Roucoux, J. Schulz, H. Patin, *Adv. Synth. Catal.* **2003**, *345*, 222-229

[44] C. Zhao, H.-Z. Wang, N. Yan, C.-X. Xiao, X.-D. Mu, P. J. Dyson, Y. Kou, *J. Catal.* **2007**, *250*, 33-40.

[45] A. L. Maksimov, S. N. Kuklin, Y. S. Kardasheva, E. A. Karakhanov, *Petroleum Journal* **2013**, *53*, 177-184.

[46] I. E. Ertas, M. Gulcan, A. Bulut, M. Yurderi, *J. Mol. Catal. A.: Chem.* **2015**, *410*, 209-220.

[47] M. L. Buil, M. A. Esteruelas, S. Niembro, M. Olivá, L. Orzechowski, C. Pelayo, A. Vallribera, *Organometallics* **2010**, *29*, 4375-4383.

[48] S. Kuklin, A. Maximov, A. Zolotukhina, E. Karakhanov, *Catal. Commun.* **2016**, *73*, 63-68.

[49] R. d. Taylor, M. MacCoss, A. D. G. Lawson, *J. Med. Chem* **2014**, *57*, 5845-5859.

[50] M. G. P. Buffat *Tetrahedron* **2004**, *60*, 1701-1729.

[51] P. M. Weintraub, J. S. Sabol, J. M. Kane, D. R. Borcherding *Tetrahedron*, **2003**, *59*, 2953-2989.

[52] S. Laschat, T. Dickner *Synthesis* **2000**, 1781-1813.

[53] M. Fang, N. Machalaba, R. Sánchez-Delgado, *Dalton Trans.* **2011**, *40*, 10621-10632.

[54] Y. Motoyama, M. Takasaki, S.-H. Yoon, I. Mochida, H. Nagashima, *Org. Lett.* **2009**, *21*, 5042-5045.

[55] A. Sánchez, M. Fang, A. Ahmed, R. A. Sánchez-Delgado, *Appl. Catal. A* **2014**, *477*, 117-124.

[56] A. Karakulina, A. Gopakumar, I. Akçok, B. L. Roulier, T. LaGrange, S. A. Katsyuba, S. Das, P. J. Dyson, *Angew. Chem. Int. Ed.* **2016**, *55*, 292-296.

[57] Y. Zhang, G.-Y. Fan, L. Wang, R.-X. Li, H. Chen, X.-J. Li, *Acta. Phys. – Chim. Sin.* **2009**, *25*, 2270-2274.

[58] V. Mévellec, A. Roucoux, *Inorg. Chim. Acta* **2004**, 357, 3099-3103.

[59] T. Harada, S. Ikeda, Y. H. Ng, T. Sakata, H. Mori, T. Torimoto, M. Matsumura, *Adv. Funct. Mater.* **2008**, *18*, 2190-2196.

[60] R. A. Murphy, A. Y. Chen, S. K. Nair, G. M. Gallego, N. W. Sach, G. Smith, *Tetrahedron Lett.* **2016**, 5588-5591.

[61] M. Fang, R. A. Sánchez-Delgado, *J. Catal* **2014**, 311, 357-368.

[62] G. Perot, *Catal. Today* **1991**, *10*, 447-471.

[63] a) R. T. Shuman, P. L. Ornstein, J. W. Paschal, P. D. Gesellchem, *J. Org. Chem.* **1990**, *55*, 738-748. b) J. M. Schaus, D. L. Huser, R. D. Titus, *Synth. Commun.* **1990**, *20*, 3553-3562. c) P. Bouyssou, C. Le Goff, J. Chenault, *J. Heterocycl. Chem.* **1992**, *29*, 895-898.

[64] a) M. Niu, Y. Wang, P. Chen, D. Du, J. Jiang, Z. Jin, *Catal. Sci. Technol.* **2015**, *5*, 4746-4749. b) H.-Y. Jiang, X.-X. Zheng, *Appl. Catal. A.* **2015**, *499*, 118-123. c) M. Campanati, A. Vaccari, O. Piccolo, *J. Mol. Catal. A: Chem* **2002**, *179*, 287-292. d) H. Mao, X. Liao, B. Shi, *Catal. Commun.* **2011**, *16*, 210-214. e) N.

A. Beckers, S. Huynh, X. Zhang, E. J. Luber, J. M. Buriak, *ACS Catal.* **2012**, *2*, 1524-1534. f) M. Campanati, M. Casagrande, I. Fagiolino, M. Lenarda, L. Storaro, M. Battagliarin, A. Vaccari, *J. Mol. Catal. A: Chem.* **2002**, *184*, 267-272.

[65] a) C. Bianchini, V. D. Santo, A. Meli, S. Moneti, M. Moreno, W. Oberhauser, R. Psaro, L. Sordelli, F. Vizza, *J. Catal.* **2003**, *213*, 47-62. b) R.-M. Zhang, G.-Y. Fan, C. Li, Y.-Y. Wang, R.-X. Li, H. Chen, X.-J. Li, *Acta. Phys. –Chim. Sin.* **2008**, *24*, 965-970.

[66] B. Sun, D. Carnevale, G. Süss-Fink, *J. Org. Chem.* **2016**, *821*, 197-205.

[67] H. Mao, C. Chen, X. Liao, B. Shi, *J. Mol. Catal. A: Chem.* **2011**, 51-56.

[68] F. Fache, *Synlett* **2004**, *15*, 2827-2829.

[69] G.-Y. Fan, J. Wu, *Catal. Commun.* **2013**, *31*, 81-85.

[70] Y.-P. Sun, H.-Y. Fu, D.-L. Zhang, R.-X. Li, H. Chen, X.-J. Li, *Catal. Commun.* **2010**, *12*, 188-192.

[71] R. A. Sánchez-Delgado, N. Machalaba, N. Ng-A-Qui, *Catal. Commun.* **2007**, *8*, 2115-2118.

[72] P. Lara, O. Rivada-Wheelaghan, S. Conejero, R. Poteau, K. Philippot, B. Chaudret, *Angew. Chem. Int. Ed.* **2011**, *50*, 12080-12084.

[73] C.-H. Pélisson, A. Denicourt-Nowicki. a. Roucoux, *ACS Sustainable Chem. Eng.* **2016**, *4*, 1834-1839.

[74] S. M. Baghbaniana, M. Farhang, S. M. Vahdat, M. Tajbakhshc, *J. Mol. Catal. A: Chem.* **2015**, *407*, 128-136.

[75] P. Lara, A. Suárez, V. Collière, K. Philippot, B. Chaudret, *ChemCatChem* **2014**, *6*, 87-90.

[76] P. Delbecq, J.-P. Celerier, G. Lhommet, *Tetrahedron. Lett.* **1990**, 31, 4873-4874.

Chapter 5

Selective deuteration of P-ligands using Ru and Rh NPs

This work has been carried out in collaboration with Dr. Emma Bresó Femenia. The work developed using Ru NPs stabilized by PVP has been entirely carried out in the context of her PhD work.

5.1. Introduction

5.1.1. H/D exchange reactions using M-NPs

Over the last years, C-H activation has become a very powerful technique for the synthesis or functionalization of complex organic compounds by the formation of a large variety of C-C, C-N, C-O, C-B and C-D bonds.[1] Regarding this latter case, C-H activation allows the rapid access to deuterium labelled compounds, which are of interest in basic research on C-H bond activation [2] or in mechanistic investigations on catalysts and reaction pathways.[3] Application of isotopically labelled compounds as internal standards is of particular interest in the investigation of environmental, animal and human samples, in which matrix effects can interfere with quantification of toxins. For this reason, labelled compounds, which generally display the same retention and ionization behaviour in LC/MS, have been found to be useful for quantitative LC/MS analysis of new drug candidates and of metabolites in biological fluids.[4]

Basically, two synthetic strategies for the formation of these labelled compounds can be followed: a synthetic pathway starting from a commercially available isotopically labelled precursor or reagent, or through the direct exchange of a hydrogen atom (bonded to a carbon atom) by a deuterium atom, which is commonly known as H/D exchange. The fact that the H/D exchange can often be performed directly on the target molecule or at late synthetic intermediates makes this strategy preferred over the synthetic pathway involving labelled building blocks. For this reason, the development of efficient and selective methodologies for the formation of D labelled

compounds through catalytic H/D exchange reaction at carbon atoms has gained interest.[5]

In this context, many methodologies based on H/D exchange using homogeneous and heterogeneous metal catalysts were reported.[5] Among the examined substrates, the selective deuteration of N-containing molecules was widely investigated due to the presence of this heteroatom in many biologically active compounds. However, most of the labelling procedures reported in the literature using Ru complexes[6,7] or activated Rh, Pt or Pd catalysts,[8] suffered from major drawbacks such as harsh reaction conditions, poor selectivity or low deuteration incorporation in the target molecules.

The deuteration of N-containing compounds by H/D exchange using metal NPs was also described.[9] Indeed, analysis of the results obtained by the selective deuteration of N and P-containing compounds have been found to be useful for studying the coordination mode of these species at the surface of metallic NPs.

In 2008, Sullivan and co-workers reported the application of Pd NPs stabilized by 4-dimethylaminopyridine (DMAP) for the selective H/D exchange of pyridine-based compounds.[10] These NPs were synthesized by reduction of $Na_2[PdCl_4]$ using $NaBH_4$ in the presence of DMAP. During the course of the characterization, the formed Pd NPs of *ca* 3.4 nm were found to be active in promoting selective H/D exchange in α position to the endocyclic N atom of the DMAP molecule through reaction with D_2O (Figure 5. 1).[11]

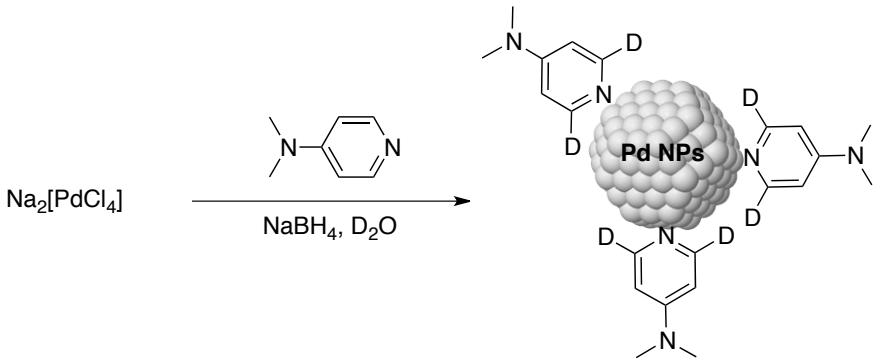

Figure 5. 1. Synthetic strategy used for the preparation of DMAP-stabilized Pd NPs[11]

This fact was confirmed by ^{1}H NMR, FTIR and high-resolution mass spectrometry. The effect of factors such as temperature, the age of the NPs dispersion and the presence of H_2 were also examined.

This catalyst was immobilized onto thiolated multi-walled carbon nanotubes (MWCNTs), which revealed beneficial for the deuteration of pyridine-based molecules not initially used in the stabilization of Pd NPs. A dramatic increase in reactivity was observed for the deuteration of DMAP in this case, but selectivity decreased, since the protons in β position of the aromatic rings were also exchanged (Figure 5. 2a). The supported catalytic system was also applied in the deuteration of 4-aminopyridine, and similar results were obtained (Figure 5. 2b). Deuteration of 4-hydroxypyridine was less selective and deuteration at β positions were in this case preferred (34%), in front of only a 6% for α positions (Figure 5. 2c).

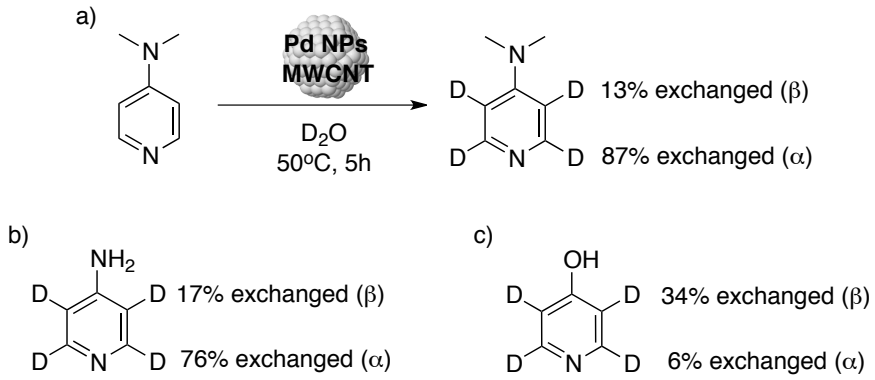

Figure 5. 2. H/D exchange of pyridine derivatives using MWCNTs supported DMAP-stabilised Pd NPs[10]

When other N-containing molecules were tested as substrates, lower activity and selectivity were observed, which was attributed to different coordination modes of these substrates at the Pd NPs surface.

Following this study, the application of Pd NPs stabilised by PVP (Pd@PVP) as catalysts in the deuteration of similar pyridine-based molecules in D_2O was investigated.[12] These NPs were formed by the reduction of $Pd(OAc)_2$ by 2-ethoxyethanol in the presence of PVP. Using this catalyst, the selective deuteration of pyridine and 4-substituted pyridines in α position to the endocyclic nitrogen was achieved at room temperature. These results, as previously observed using Pd NPs stabilized by DMAP,[10] suggested coordination of these substrates to the surface of these Pd NPs through the lone pair of the N atom (Figure 5. 3a).

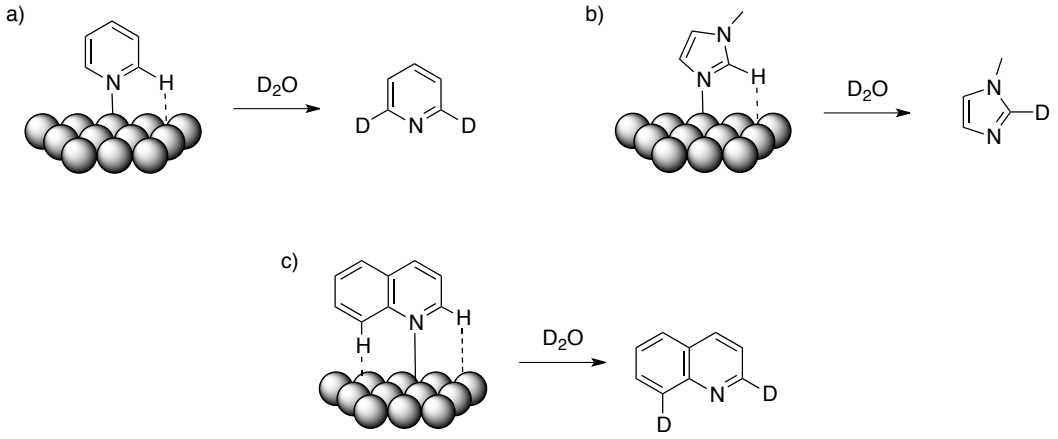

Figure 5. 3. Proposed coordination modes for the deuteration of N-containing compounds at the surface of Pd@PVP[12]

The case of 4-methylpyridine showed to be slightly different; achieving also deuteration of methyl group. The only pyridine derivative that showed deuteration at all aromatic positions was 3-methylpyridine, which suggested coordination by π electrons of the aromatic ring at the Pd surface. Interaction between the NPs surface and the N atom of N-methylimidazole (Figure 5. 3b), quinoline (Figure 5. 3c), 3-cyanopyridine and nicotinic acid was also proposed. The presence of a cyano or a carboxylic acid group affected the activity/selectivity of the reaction, probably due to an electronic/steric effect or the competitive coordination of these groups at the NPs surface.

The deuteration of compounds used as stabilizers has also been observed in the case of Ru NPs synthesised according to the organometallic approach procedure.[13] The presence of mobile and reactive hydride species at the surface of metallic NPs was reported for Ru NPs stabilized by hexadecylamine (HDA).[14] These surface

species were also found to perform H/D exchange reactions with the alkyl chain of HDA when exposed to a D_2 atmosphere (Figure 5. 4).

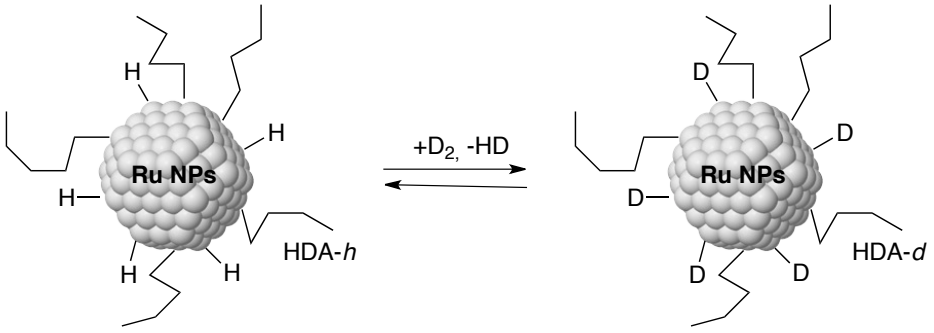

Figure 5. 4. H/D exchange between surface deuterides and HAD used for the stabilisation of Ru NPs[14]

Some years later, the quantification of hydride species at the surface for Ru NPs stabilised by HDA, PVP and dppb by titration with olefins such as 1-octene and 2-norbornene was reported.[15,16] The presence of ligands showed to directly affect the amount of surface hydrides, and values were higher when the ligand produces lower steric hindrance at the surface of the particles.

H/D exchange at molecules such as4-(3-phenylpropyl)pyridine[17] and secondary phosphine oxides[18,19] while used for the stabilization of Ru NPs has also been observed by ^{2}D MAS NMR spectroscopy after exposure to D_2.

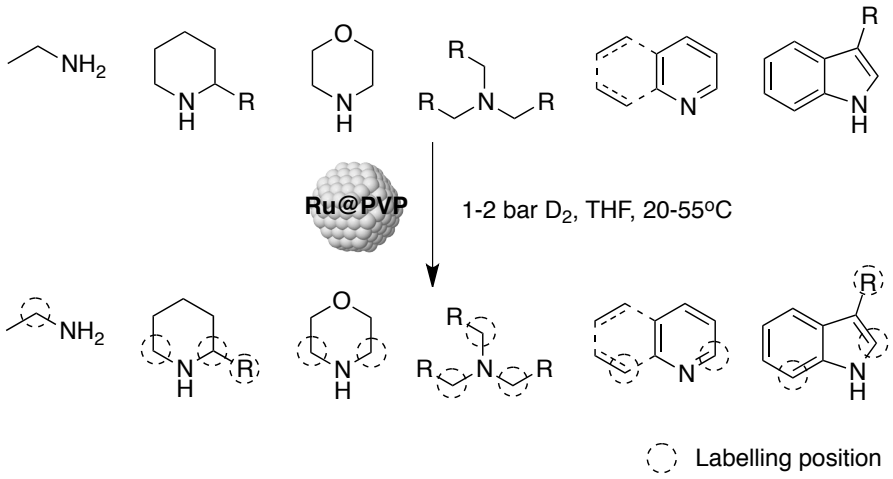

Figure 5. 5. H/D exchange methodology reported by Chaudret and co-workers for the deuteration of N-containing compounds using Ru@PVP[20]

Based on these results, Chaudret and co-workers reported the application of Ru NPs for the regioselective and stereospecific deuteration of N-containing substrates.[20] In order to facilitate the interactions between the substrate and the metallic surface, Ru NPs stabilized by PVP (Ru@PVP), which are considered as "naked particles", were used as catalyst.[21]

Deuteration experiments carried out using 3mol% of Ru@PVP in THF under 1 or 2 bar of D_2 allowed the regioselective deuteration of pyridines, quinolines, indoles and alkyl amines, with high isotopic enrichment in positions close to the N atom (Figure 5. 5). For substrates bearing an O atom in their structure no deuteration close to the oxygen was observed, suggesting the direct and selective coordination of N to the surface of these Ru NPs. Moreover, the deuteration of indoles at 2- and 3-positions indicated the possible formation of a transition carbene, which could compete with N coordination.

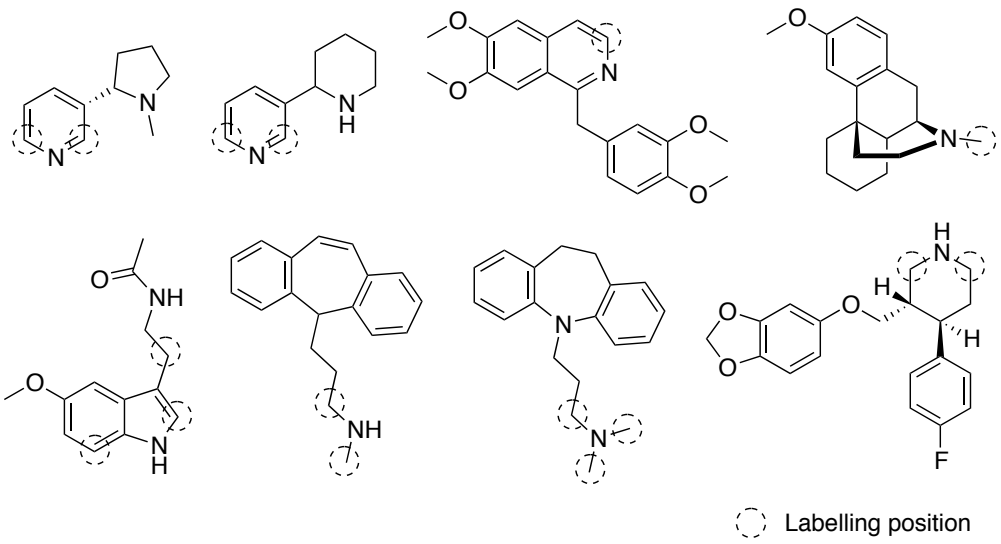

Figure 5. 6. Products obtained in the deuteration of biologically active compounds using Ru@PVP[20]

Then, the viability of this procedure for the deuteration of aza compounds was demonstrated by the labelling of eight biologically active compounds, achieving the corresponding deuterated products in high levels of isotopic enrichment (Figure 5. 6). In addition, conservation of the enantiomeric purity was observed for chiral compounds, even when the deuteration took place in the vicinity of the asymmetric centre.

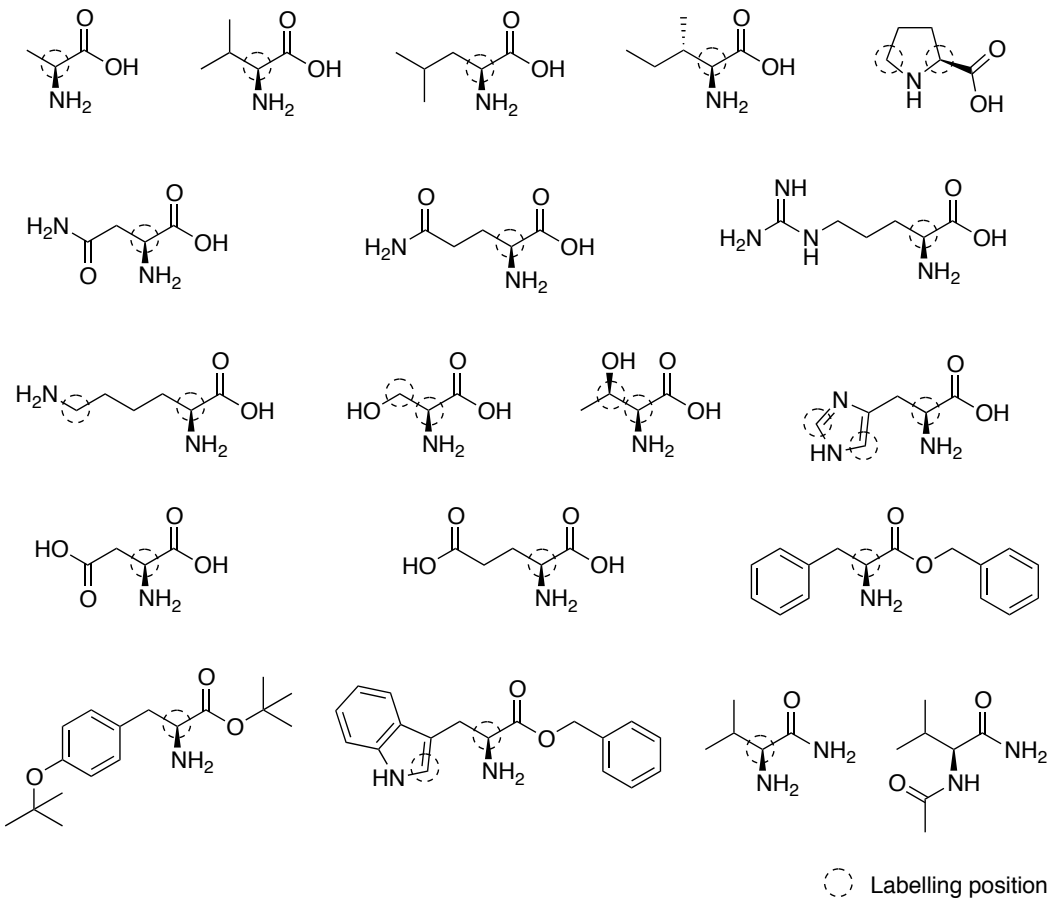

Figure 5. 7. Products obtained in the enantiospecific deuteration of amino acids using Ru@PVP[22]

More recently, the same group reported the application of this deuteration procedure for the enantiospecific deuterium incorporation at stereogenic centers of amino acids (Figure 5. 7).[22]

Efficient enantiospecific deuteration was achieved for amino acids with aliphatic, amide and N-containing side chains in α-position of the coordinating N atom, detecting also deuteration at the β-position or other additional sites for substrates bearing alcohol or imidazole functionalities. In the case of substrates bearing more than three

coordination units such as amines, carboxylic acids and aromatic rings, lower deuterium incorporation was measured. Additionally, this procedure was applied for the deuteration of more complex, biologically relevant structures (Figure 5. 8).

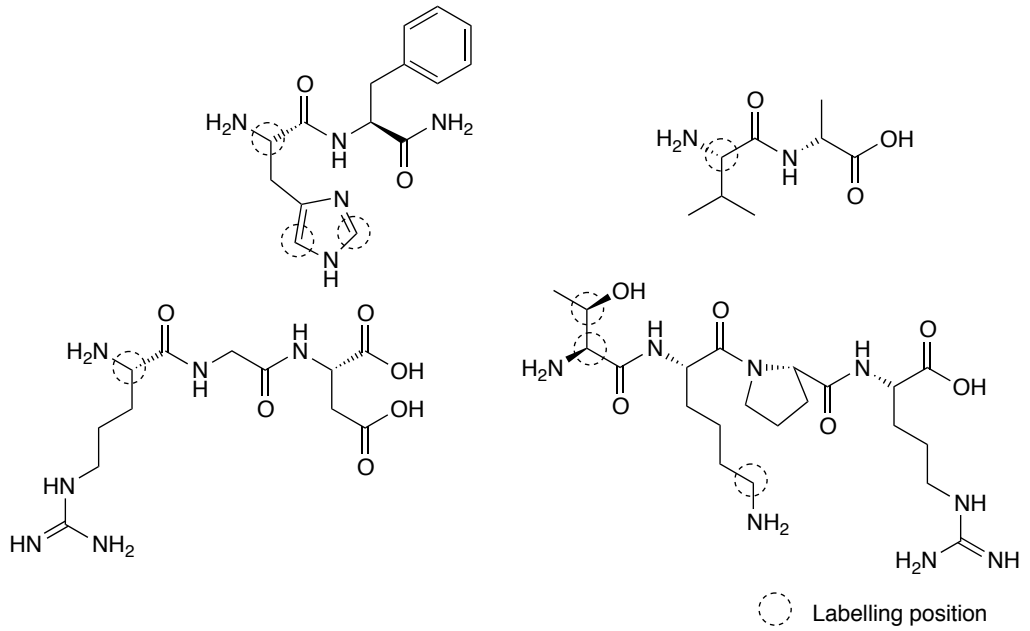

Figure 5. 8. Products obtained in the enantiospecific deuteration of biologically relevant amino acids using Ru@PVP[22]

In all cases, the expected C-H activation occurred at the α carbon atom of the N-terminal amino acid with moderate to high deuterium incorporation.

In order to obtain more insights into the mechanism, DFT calculations were then performed on a 13 atom scale model (Ru_{13}) with 1.6 deuterium atoms per Ru surface atoms, being the most relevant pathways validated with a fully deuterated Ru_{55} nanocluster with 1.6 deuterium atoms per Ru surface atoms. Considering a Langmuir-Hinshelwood mechanism ($amine_{ads}$ + D_{ads} → deuterated

$amine_{ads}$ + H_{ads}), two competitive pathways based on oxidative addition and a less favoured mechanism involving σ–bond metathesis were found. Both pathways proceeded through the formation of a four-membered dimetallacycle, with the C-H bond breaking as the rate-limiting step (Figure 5. 9). Indeed, the high rigidity of this dimetallacycle was hold responsible of the joint grafting of the N and the C atoms onto two vicinal Ru atoms at the surface of the NPs with retention of configuration. Besides, a decrease of the presence of deuterides close to the coordinated amine showed to affect the reaction rate, reducing the energy for the activation of the C-H bond and thus favouring the reaction.

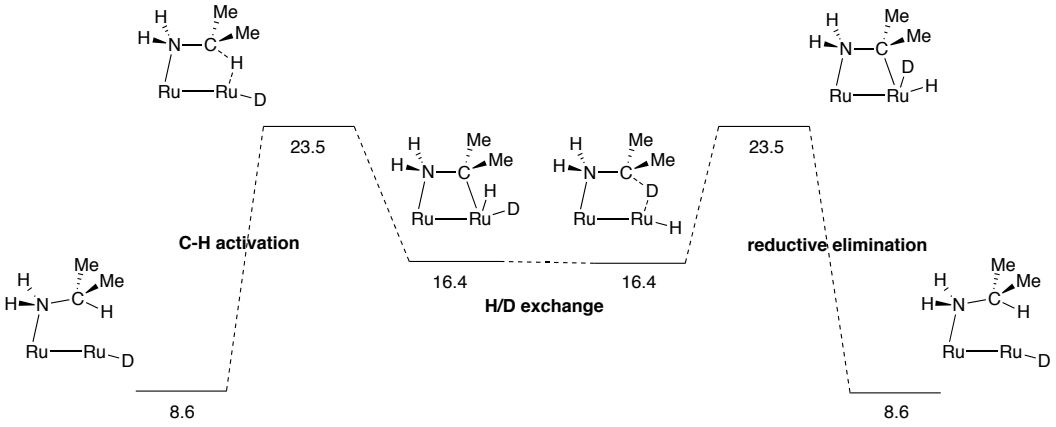

Figure 5. 9. Energy diagram for the Langmuir-Hinshelwood-type H/D exchange mechanism for $Ru_{55}D_n$ clusters (energies given in kcal·mol^{-1})[22]

This work clearly demonstrated the great potential of NPs for C-H activation.

More recently, the same group reported the application of water-soluble Ru NPs stabilized by sulfonated NHC ligands for the H/D

exchange of L-Lysine in D_2O, under reaction conditions similar to those previously reported for Ru@PVP.[23] The water-soluble nature of this novel Ru NPs gave access to a direct measurement of the substrate-metallic surface interaction by NMR. A study based on chemical shift perturbations (CSPs) gave valuable information on the proximity of different H and C atoms from the substrate at the surface of the NPs.

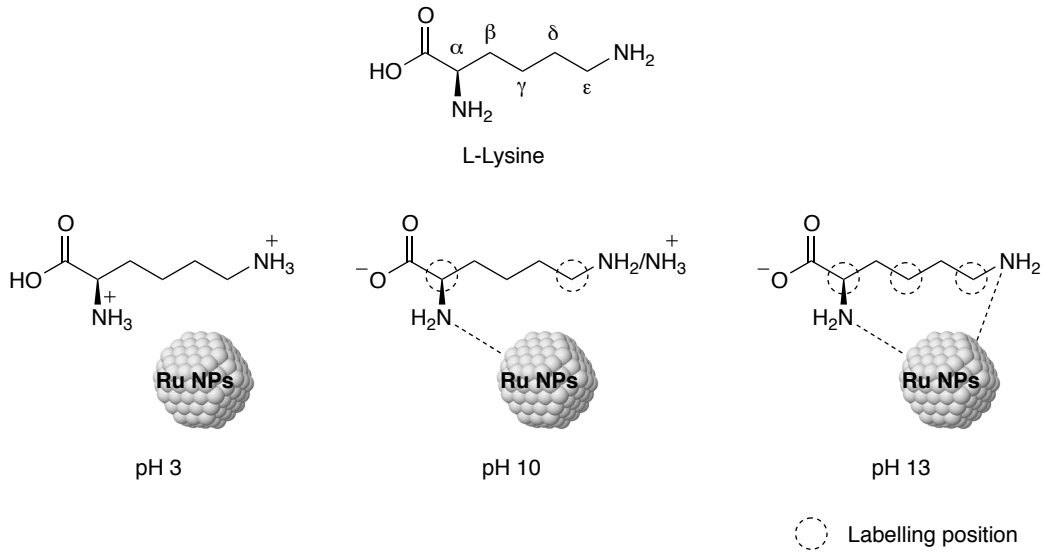

Figure 5. 10. Products obtained in the enantiospecific deuteration of L-Lysine depending on the pH using sulfonated NHC-stabilised Ru NPs[23]

L-Lysine exists in different forms as a function of the pH: Lys^{++} (the two amino and carboxylate groups protonated), Lys^{+} (the two amino groups protonated), Lys (the ε amino group protonated) and Lys^{-} (no groups protonated). An increase on the pH value (from 1.6 to 13.8) showed to have a clear influence on the activity and the selectivity of the H/D exchange reaction by enhancing the catalytic activity (Figure 5. 10). These results suggested that NH_2 groups are required for

coordination of this compound to the Ru NPs surface. This real time monitoring of the interaction between L-Lysine and the NPs surface at different pH values demonstrated that the orientation of the substrate with the Ru surface is a crucial aspect in this deuteration reaction.

At the same time, Chaudret and our group reported that phosphorus containing ligands such as phosphines or phosphites, which had been previously used for the stabilization of metal NPs,[24,25,26,27,28] could be labelled following a similar procedure.[29] Ru@PVP NPs was described as an efficient catalytic system for the selective deuteration of aryl phosphines (Figure 5. 11) such as PPh_3 (and derivatives), PPh_2Me and dppb in *ortho* position. However, and in contrast to what was previously observed for N-containing compounds,[20] the methyl and methylene groups remained unaltered.

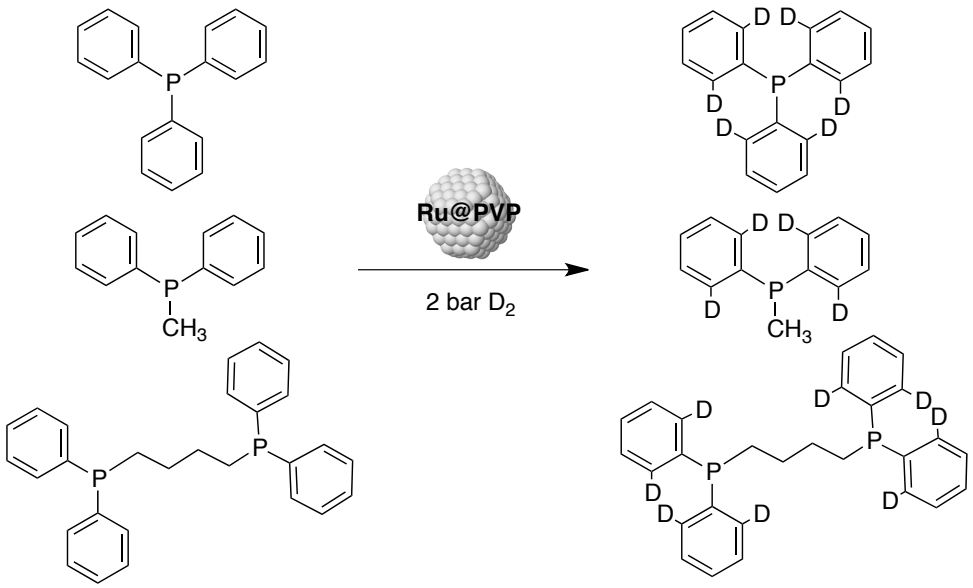

Figure 5. 11. H/D exchange of P-containing compounds using Ru@PVP as catalyst[29]

Phosphines bearing electron donating and electron withdrawing groups in *para* position of the aromatic ring were selectively deuterated at the *ortho* position. However, the reaction rate in these cases was lower than for PPh_3.

These results suggested that phosphines coordinate to the nanoparticles surface through their P atom, thus placing the *ortho* protons very close to the surface and as such favouring the H/D exchange (Figure 5. 12a). As in the case of N-containing substrates,[22] a reaction mechanism based on the formation of five membered-ring intermediates Ru-P-C-C-Ru' via oxidative addition was expected.

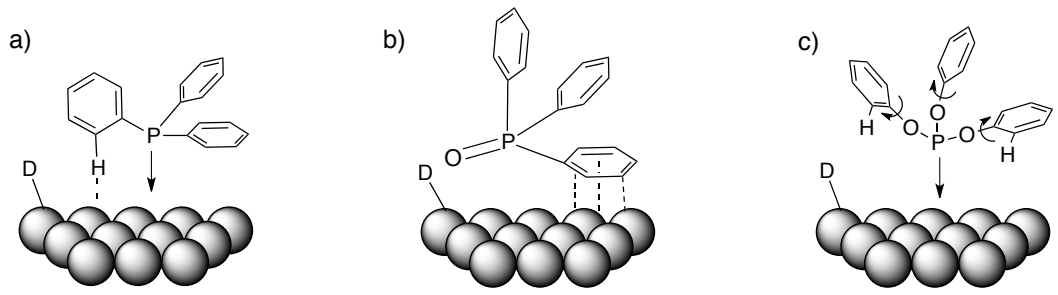

Figure 5. 12. Proposed coordination modes for the deuteration of P-containing compounds at the surface of Ru@PVP[29]

Interestingly, when triphenylphosphine oxide ($O=PPh_3$) was tested as substrate, a distinct behaviour was observed since the reduction of aromatic ring took place under the same reaction conditions. This result indicated that coordination of this compound to the NPs surface had taken place through the aromatic ring and not through the P=O function (Figure 5. 12b).

Whne triphenylphosphite was tested as substrate, no deuteration was observed, which was attributed to the smaller cone angle of this ligand, with the phenyl rings pointing away from the Ru surface (Figure 5. 12c).

In this context, we considered to examine other parameters such as the nature of the metal and of the stabilizer and study their effect on the activity and selectivity on the selective deuteration of P-containing compounds. With this purpose, we carried out a comparative study using Ru and Rh NPs stabilized by PVP or NHC ligands as catalysts in the deuteration of a number of P-based ligands.

5.2. Results and discussion

For this study, the structurally different P-containing compounds such as monodentate aryl (Figure 5. 13a), mixed aryl-alkyl and alkyl phosphines (Figure 5. 13b), diphosphines (Figure 5. 13c), N,O-arylphosphines (Figure 5. 13d) and phosphine oxides (Figure 5. 13e) were selected as substrates.

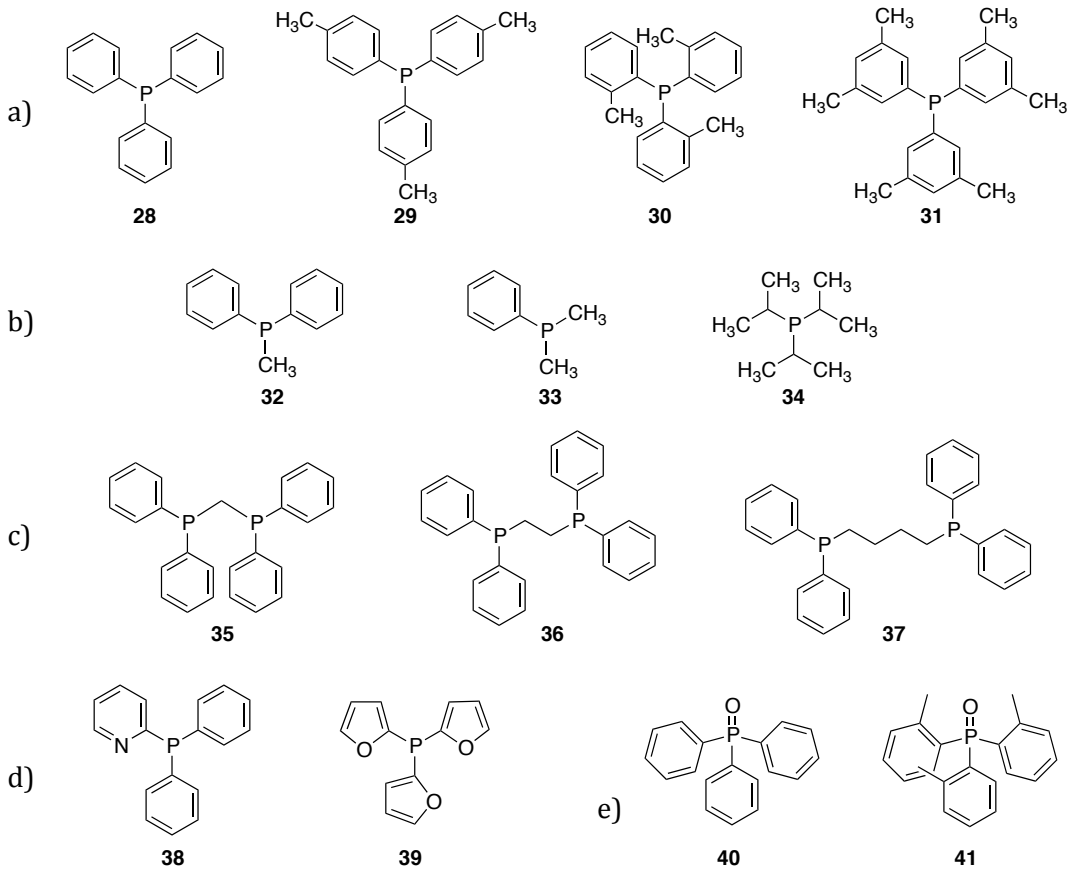

Figure 5. 13. P-containing compounds (**28-41**) studied in H/D exchange using Rh and Ru NPs stabilised by PVP or NHCs

The nanocatalysts used were **Ru@PVP**[16], **Ru@NHC**[30] and the **Rh@PVP,**[31] which were synthesised according to reported

procedures and **Rh@NHC**. These nanoparticles all exhibited small sizes (<2nm), spherical shapes and narrow size distributions. The Ru and Rh NPs presented *hcp* and *fcc* packing, respectively, with the metals in the zero oxidation state.

5.2.1. Selective deuteration of monodentate aryl phosphines

In order to study the coordination of aromatic phosphines to the surface of NPs, PPh_3 (**28**) was used as model substrate. First, the reaction was performed following the previously reported methodology using D_2 as deuterium source.[32] **Ru@PVP** were exposed to 3 bar of D_2 in solid state for 2h, after which a solution containing **28** in THF was added. Then, the reaction was left at 55°C under 2 bar of D_2 and monitored over time by NMR spectroscopic techniques.

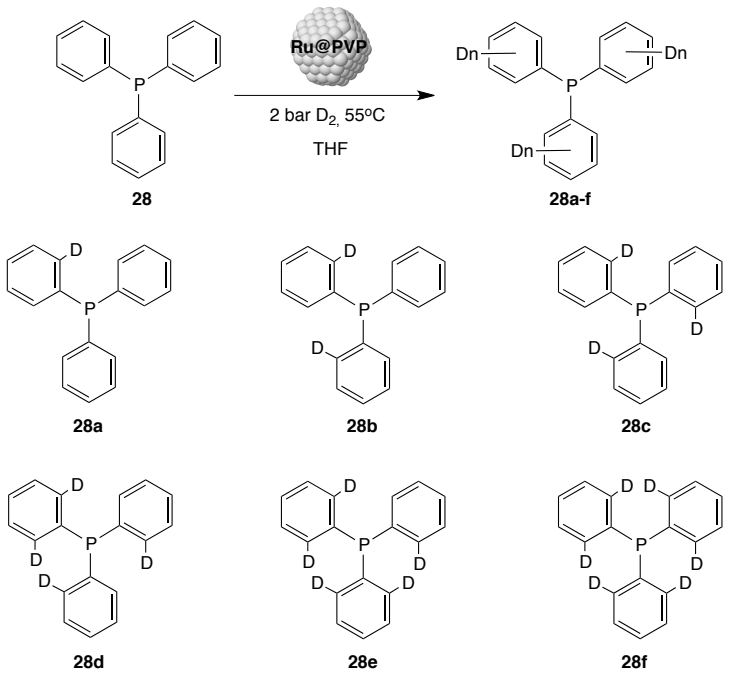

Figure 5. 14. Deuteration of PPh_3 (**28**) using **Ru@PVP**

Deuterium incorporation in an aromatic position was evidenced by the detection of a broad signal at 7.6 ppm by ^{2}D NMR (Figure S127, Supporting information). When $^{31}P\{^{1}H\}$ and $^{13}C\{^{1}H\}$ NMR spectra were recorded after different reaction times, the progressive H/D exchange of the protons at the *ortho* position of the aromatic rings was detected (formation of products **28a**-**28f**) (Figure 5. 14). Thus, when the reaction was monitored by $^{31}P\{^{1}H\}$ NMR, after 16h of reaction, 6 new resonances located between -5.5 and -6.2 ppm (Figure 5. 15b) appeared with the initial signal of the starting material **28** at -5.5 ppm (Figure 5. 15a).

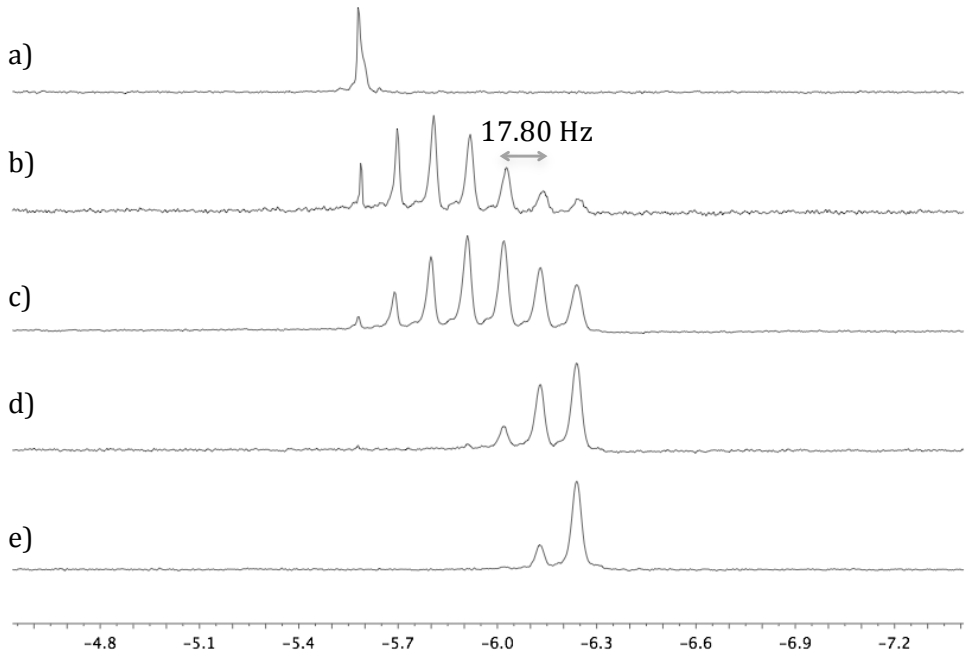

Figure 5. 15. $^{31}P\{^{1}H\}$ NMR ($CDCl_3$, 162MHz) spectra of PPh_3 (**28**) deuteration evolution using **Ru@PVP**: (a) t=0, (b) 16h, (c) 36h, and (d) 48h at 55°C and (e) 48h at 80°C

At longer reaction times, the intensity of the signals at higher fields progressively increased (Figure 5. 15b-d). These 7 signals were

attributed to **28** and to the deuteration labeled products **28a**, **28b**, **28c**, **28d**, **28e** and **28f**, respectively. When the reaction was carried out for 48h at 80°C the signal detected at -6.2 ppm corresponding to **28f** was mainly observed (Figure 5. 15e), together with a small resonance at -6.1 ppm corresponding to **28e**. It was then concluded that each added deuterium produced an isotopic shift of -0.11 ppm (-17.80 Hz) in the ^{31}P NMR. Mass spectrometry analysis of the resulting mixture of products confirmed the identity of these reaction products. Importantly, the formation of reaction products by reduction of the aromatic rings of **28** was not observed under these reaction conditions. The progressive deuteration at the *ortho* position of the aromatic rings of **28** was also observed by $^{13}C\{^{1}H\}$ NMR spectroscopy. When the mixture of products was analysed after 16h of reaction, the signal of the corresponding C2-D was detected at 134.4 ppm as a triplet of doublet ($^{2}J_{C,P}$ = 18 Hz, $^{1}J_{C,D}$ = 26 Hz) while the C2-H remained unchanged as a doublet at 134.8 ppm ($J_{C,P}$ = 19 Hz) (Figure 5. 16b).

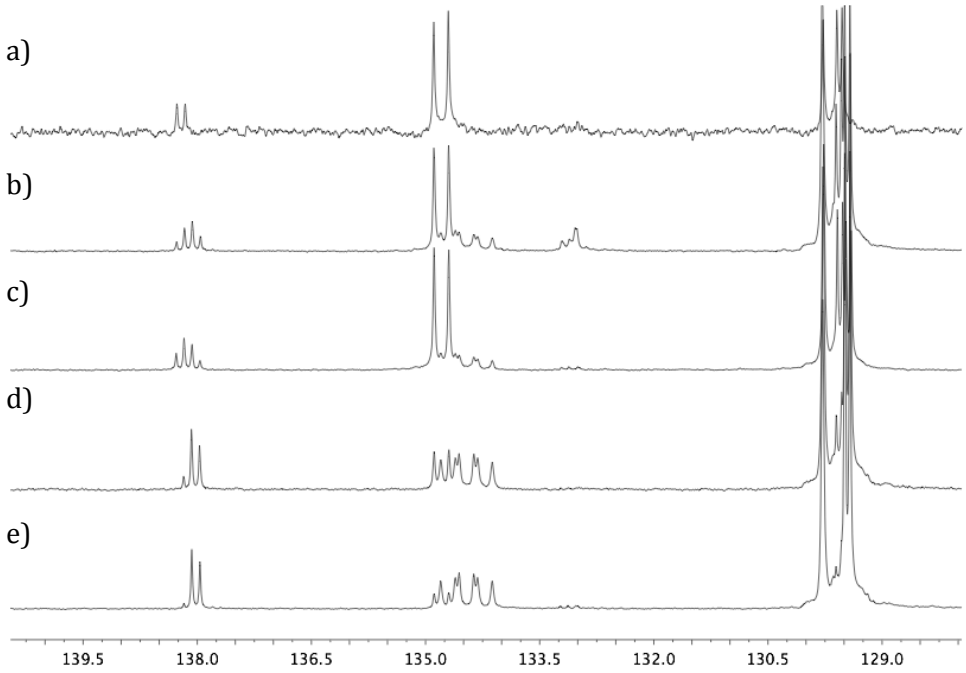

Figure 5. 16. $^{13}C\{^{1}H\}$ NMR ($CDCl_3$, 100.6MHz) spectra of PPh_3 (**28**) deuteration evolution using **Ru@PVP**: (a) t=0, (b) 16h, (c) 36h, and (d) 48h at 55°C and (e) 48h at 80°C

This observation was in agreement with the partial deuteration at the *ortho* position of the aromatic rings of **28**. The *ipso* carbon (C1) was detected at 137.3 as a multiplet, as a result of the overlap of several doublets from partial deuteration. When a $^{13}C\{^{1}H\}$ NMR spectrum was recorded after 36h and 48h of reaction at 55°C (Figure 5. 16c and d) and after 48h at 80°C (Figure 5. 16e) an increase in the intensity of the triplet of doublets signal at 134.4 ppm attributed to the C2-D was observed. This fact and the decrease of the signal detected at 134.8 ppm for the C2-H carbon determined the progressive and selective H/D exchange of the protons at the *ortho* position of the phenyl ring. Quantification of the deuterated products was performed by integration of their corresponding signals

detected by ^{31}P NMR, with a value >95% for the totally deuterated product **28f** after 48h at 80°C. The corresponding percentage of compounds in the reaction mixture, obtained by $^{31}P\{^{1}H\}$ NMR after 48h of reaction at 55°C under 2 bar of D_2 are presented in Table 5. 1. Deuteration products **28c**, **28d**, **28e** and **28f** were observed in the reaction mixture, with the hexadeuterated product **28f** as the major product (52%) (Table 5. 1, Entry 1).

To study the effect of the nature of metal and the stabilizer of the NPs, the application of Rh NPs stabilized by PVP (**Rh@PVP**) and of Ru and Rh NPs stabilized by IPr as catalyst was investigated for the deuteration of **28**. Since high contents in stabilizing ligands at the NPs surface usually decrease their activity in catalytic reactions such as hydrogenation of aromatic compounds,[33] Ru and Rh NPs stabilized using a low [IPr]/[Rh] molar ration of 0.2 (**$Ru^{0.2}$** and **$Rh^{0.2}$**) were selected as catalysts to investigate these deuteration reactions.

Table 5. 1. Selective deuteration of PPh_3 (**28**) using Ru and Rh NPs stabilized by PVP and IPr. Percentage of compounds in the reaction mixture.[a]

Entry	NPs	28 (%)[b]	28a (%)[b]	28b (%)[b]	28c (%)[b]	28d (%)[b]	28e (%)[b]	28f (%)[b]
1[c]	Ru@PVP	-	-	-	2	12	34	52
2[d]	Rh@PVP	96	3	1	-	-	-	-
3[d]	$Ru^{0.2}$	-	-	-	-	-	16	84
4[d]	$Rh^{0.2}$	13	19	23	17	13	7	8

[a] Catalytic conditions: 0.15 mmol substrate, 55°C, 2 bar D_2, 2ml THF, 48h. [b] Calculated by $^{31}P\{^{1}H\}$ NMR spectroscopy. [c] 3 mol% cat. [d] 25 mol% cat.

Deuteration of **28** with **Rh@PVP** was carried out at 55°C under 2 bar of D_2, but very low conversion was observed (Table 5. 1, Entry 2). The low solubility of these NPs in the reaction media could explain this result.

Results of deuteration of **28** with **Ru$^{0.2}$** were similar to those obtained with **Ru@PVP**. Product **28f** was formed in 84% yield, being **28e** the second major product in the reaction mixture (16%) (Table 5. 1, Entry 3). However, a higher catalyst loading of **Ru$^{0.2}$** (25 mol %) was needed in order to obtain similar deuteration rates compared to **Ru@PVP** (Table 5. 1, Entry 1 *vs.* 3), which was used in 3mol%. It can be concluded that the presence of NHC ligands at the surface of the Ru NPs hinders phosphine coordination, and thus results in a decrease in the activity of the catalyst. A high catalyst loading of 41% for the deuteration of DMAP has been previously reported using Pd NPs.[10] **Rh$^{0.2}$** were then used for the deuteration of **28**. $^{31}P\{^1H\}$ NMR showed the formation of all the expected products but exhibited a lower activity than that of **Ru$^{0.2}$** (Table 5. 1, Entry 4). Particularly, the fully deuterated product (**28f**) was formed in only 8%. It was therefore concluded that the Ru NPs used in this study (stabilized by PVP and IPr ligand) were more active than the corresponding Rh NPs in the deuteration of **28**.

Deuteration took place at the *ortho* position of the phenyl ring for all catalytic systems tested, which indicated that the coordination of substrate **28** to the surface of these NPs takes place through the P atom, presumably via a five-membered dimetallacycle (Figure 5. 17).

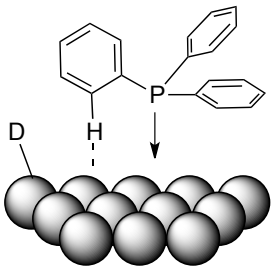

Figure 5. 17. Proposed coordination mode for PPh_3 (**28**) at the surface of Ru and Rh NPs

At this point, substrates bearing $-CH_3$ substituents in *ortho* and *para* positions of the aromatic ring were tested in this process. Thus, P(*p*-tolyl)$_3$ (**29**) was treated at 55°C under 2 bar of D_2 using **Ru@PVP**, **Ru$^{0.2}$** and **Rh$^{0.2}$** as catalysts. Exclusive deuteration at the *ortho* position of the arene rings was observed; affording compounds **29a-f** (Figure 5. 18).

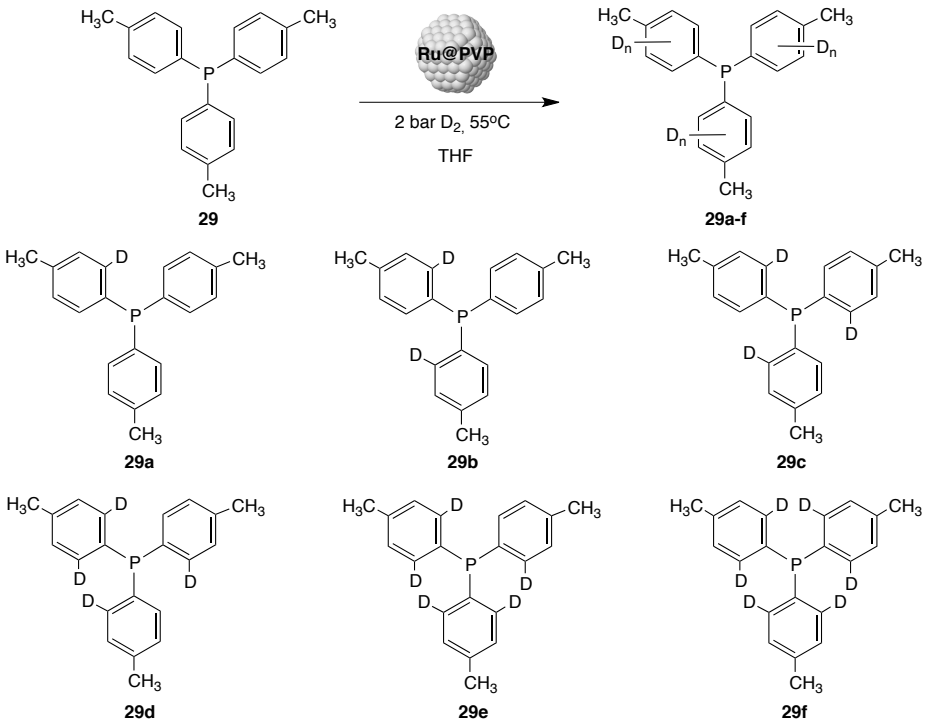

Figure 5. 18. Deuteration of P(*p*-tolyl)$_3$ (**29**) using **Ru@PVP** NPs

Each compound **29a**, **29b**, **29c**, **29d**, **29e** and **29f** showed a different signal in $^{31}P\{^{1}H\}$ NMR, separated by -0.11 ppm (-17.8 Hz), which corresponds to the isotopic shift induced by each new deuterium atom incorporated in the molecule.

When the reaction was performed using **Ru@PVP** as catalyst, the pentadeuterated product **29e** was detected as the major product of the reaction, with 38% yield (Table 5. 2, Entry 1). Thus, it was therefore deduced that using **Ru@PVP** as catalyst, the rate of deuteration of **29** was lower than that of **28**.

Table 5. 2. Selective deuteration of P(*p*-tolyl)$_3$ (**29**) using Ru and Rh NPs stabilized by PVP and IPr. Percentage of compounds in the reaction mixture.[a]

Entry	NPs	29 (%)[b]	29a (%)[b]	29b (%)[b]	29c (%)[b]	29d (%)[b]	29e (%)[b]	29f (%)[b]
1[c]	Ru@PVP	-	-	3	11	27	38	21
2[d]	$Ru^{0.2}$	-	-	-	-	1	12	87
3[d]	$Rh^{0.2}$	30	23	20	10	7	3	7

[a] Catalytic conditions: 0.15 mmol substrate, 55°C, 2 bar D_2, 2ml THF, 48h.

[b] Calculated by $^{31}P\{^{1}H\}$ NMR spectroscopy. [c] 3 mol% cat. [d] 25mol% cat.

On the other hand, when the deuteration of **29** was carried out using 25mol% of $Ru^{0.2}$, selectivities were similar to those obtained for **28** under the same reaction conditions, with 87% selectivity to **29f** (Table 5. 1, Entry 3 *vs*. Table 5. 2, Entry 2). It was therefore deduced that, in contrast with the results obtained for **Ru@PVP**, when $Ru^{0.2}$ was the catalyst, the rate of deuteration of **29** was similar to that of **28**. When $Rh^{0.2}$ was the catalyst, the results were also similar to those obtained with phosphine **28** as substrate, with a selectivity to

the hexadeuterated product **29f** clearly lower than that obtained with **Ru$^{0.2}$** (Table 5. 1, Entry 4 *vs.* Table 5. 2, Entry 3).

In summary, the presence of the *p*-Me substituent at the aromatic rings of tri-phenylphosphine only produces a small change in activity but not in selectivity since exclusive deuteration in *ortho* position was observed. This is in agreement with a coordination of these compounds to the NPs surface through the P atom (Figure 5. 17). Since **28** and **29** exhibit similar cone angles (145°),[34] the lower deuteration rate observed for **29** than for **28** in some specific cases using the same nanocatalysts was attributed to an electronic effect caused by the presence of a methyl group in the *para* position of the phenyl rings. As a general conclusion, Ru NPs (stabilized by PVP or NHC) were found to be more active than **Rh$^{0.2}$**, being **Ru@PVP** more active than **Ru$^{0.2}$**, which is in agreement with the results observed for the H/D exchange of **28**.

Next, the deuteration of an aromatic phosphine bearing a methyl group at one of the *ortho* positions of the aromatic rings P(*o*-tolyl)$_3$, (**30**) was investigated. Initially, the treatment of **30** with **Ru@PVP** under the standard reaction conditions afforded very low deuteration, based on ^{31}P and ^{2}D NMR.

Ru$^{0.2}$ NPs were then used as catalysts under the same reaction conditions, and a ^{2}D NMR analysis performed after 48h of reaction revealed the presence of a signal in the aliphatic protons region (2.39 ppm) (Figure 5. 19), which indicated that deuteration of the methyl group had taken place. Furthermore, the observation of deuterium signals at 6.81 and 7.34 ppm corresponding to C3-D and C5-D

revealed deuteration at the *meta* positions of the aromatic rings (Figure 5. 19).

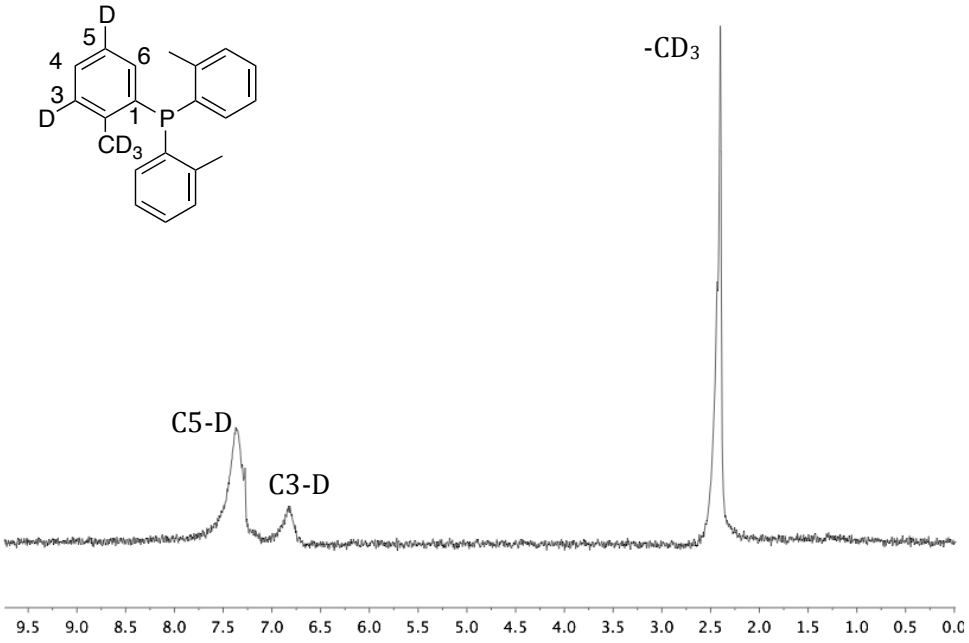

Figure 5. 19. ^{2}D NMR ($CHCl_3$, 61.49MHz) spectrum of the deuteration of P(*o*-tolyl)$_3$ (**30**) using **Ru$^{0.2}$** after 48h of reaction

In the $^{13}C\{^{1}H\}$ NMR spectrum, the detection of two triplets centred at 132.9 ($^{2}J_{C,P}$ = 25 Hz) and 128.6 ppm ($^{2}J_{C,P}$ = 24 Hz) corresponding to C3-D and C5-D close to the singlets from C3-H and C5-H, confirmed the H/D exchange at these positions (Figure 5. 20).

The formation of several deuteration products during the reaction was also noticed by the observation of various phosphorus signals by $^{31}P\{^{1}H\}$ NMR. However, the detection of the starting material **30** as the major product in the reaction mixture at -29.7 ppm suggested low deuteration rates under the tested reaction conditions.

These results were surprising since no H/D exchange in *ortho* positions of the aryl rings was detected. Additionally, an important change in activity between **Ru@PVP** and **Ru$^{0.2}$** was also observed for this substrate. The presence of NHC ligands at the NPs surface in the case of **Ru$^{0.2}$** was crucial in the reaction, possibly due to an increase in the electronic density of the metallic surface, which could favour the activation of aliphatic protons.

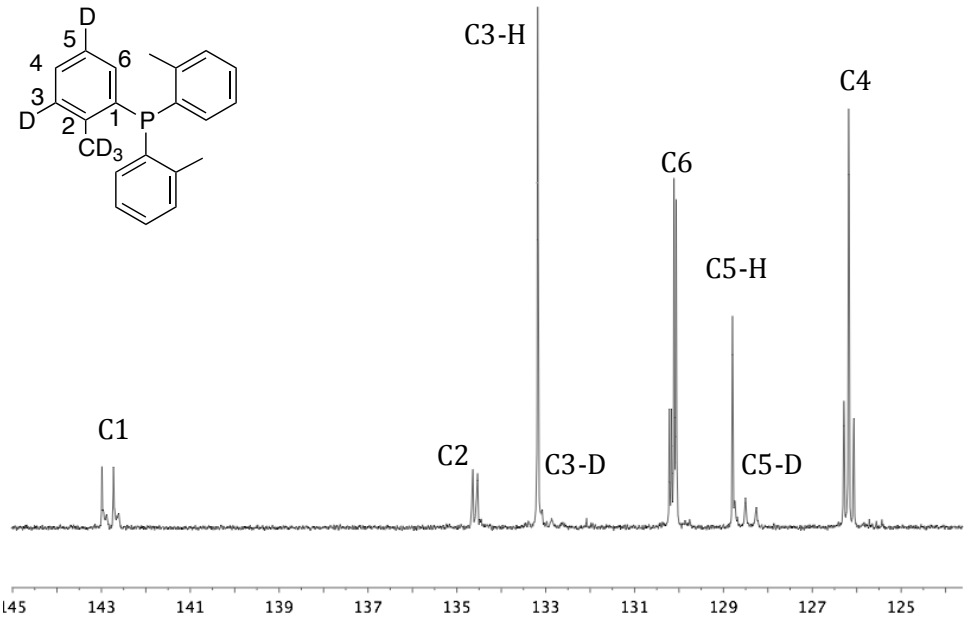

Figure 5. 20. $^{13}C\{^{1}H\}$ NMR ($CDCl_3$, 100.6MHz) spectrum of the deuteration of P(*o*-tolyl)$_3$ (**30**) using **Ru$^{0.2}$** after 48h of reaction

When the reaction was performed using **Rh$^{0.2}$** as catalyst under the same catalytic conditions the ^{2}D NMR spectrum showed signals similar than those detected when **Ru$^{0.2}$** was applied, which indicates also in this case the selective deuteration at the same aliphatic and aromatic positions (Figure 5. 21b). It was also observed that the

signal corresponding to deuteriums at the C3 position were more intense that the corresponding to deuteriums at the C5.

The ^{1}H NMR spectrum revealed the almost complete disappearance of the signal at 2.39 ppm corresponding to the $-CH_3$ group. These results indicated a very high degree of deuteration at this aliphatic position, which takes place faster when compared to aromatic protons (Figure 5. 21a).

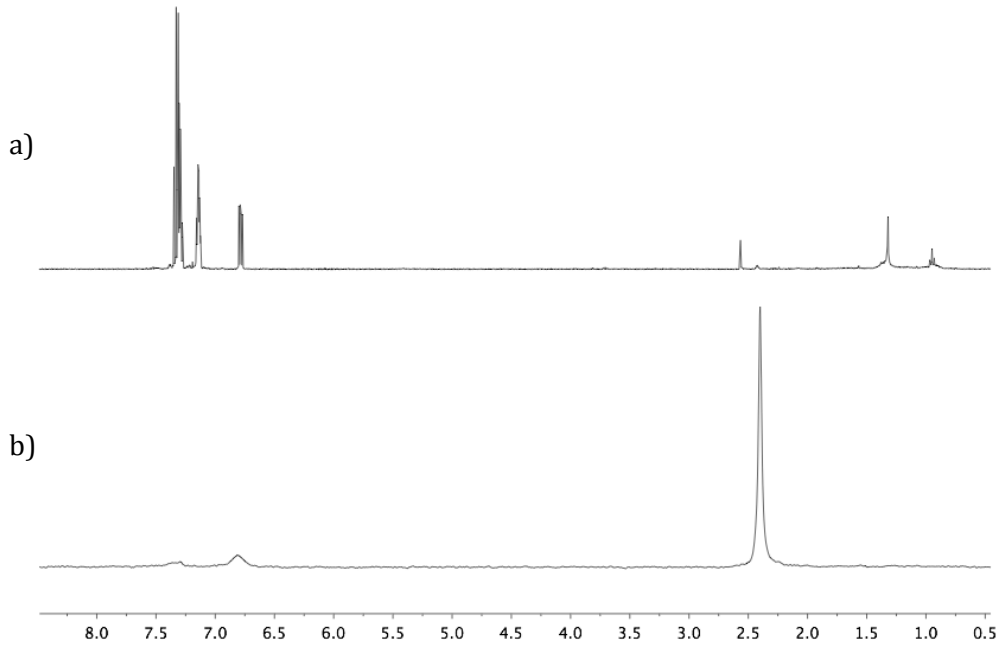

Figure 5. 21. (a) ^{1}H ($CDCl_3$, 400MHz) and (b) ^{2}D NMR ($CHCl_3$, 61.49MHz) spectra of the deuteration of P(*o*-tolyl)$_3$ (**30**) using **Rh$^{0.2}$** after 48h of reaction

These data were confirmed by $^{13}C\{^{1}H\}$ NMR via the detection of a septuplet signal at 20.68 ppm ($J_{C,D}$ = 19 Hz) arising from the coupling between the $-CH_3$ carbon and 3 directly attached deuterium atoms (Figure 5. 22, inset). As in the case of **Ru$^{0.2}$**, the detection of C3-D and

C5-D as triplet signals at 132.9 ($^2J_{C,P}$ = 25 Hz) and 128.6 ppm ($^2J_{C,P}$ = 24 Hz) confirmed deuterium incorporation at the *meta* positions of the tolyl moieties (Figure 5. 22).

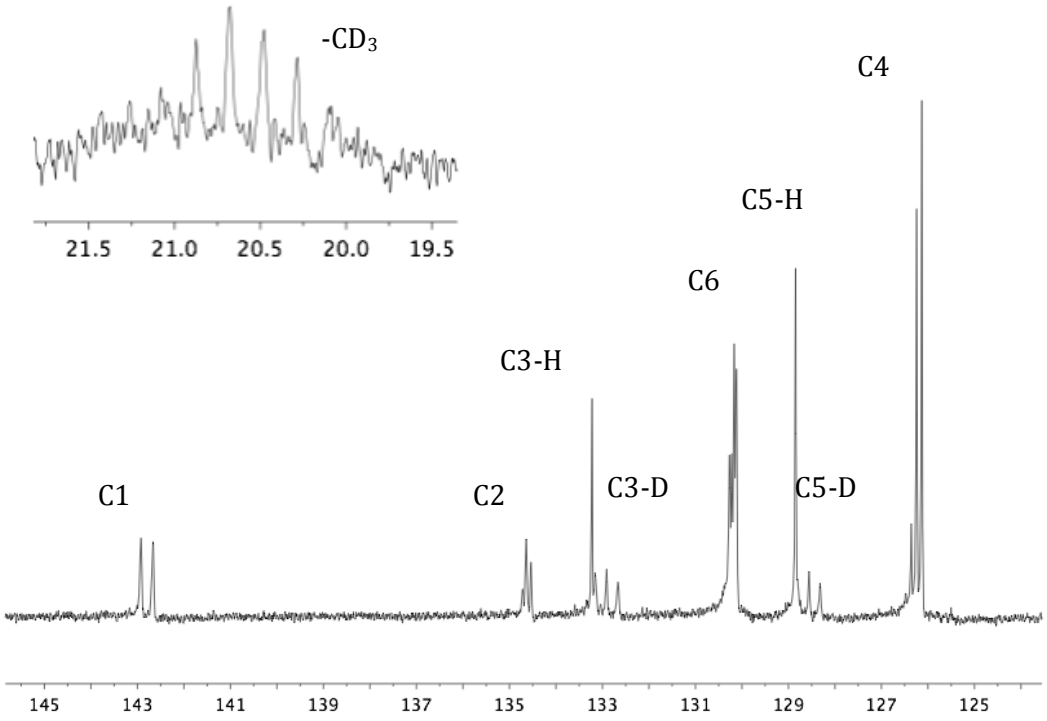

Figure 5. 22. $^{13}C\{^1H\}$ NMR ($CDCl_3$, 100.6MHz) spectrum of the deuteration of P(*o*-tolyl)$_3$ (**30**) using **Rh$^{0.2}$** after 8d of reaction

The $^{31}P\{^1H\}$ NMR spectrum of the reaction mixture recorded after 48h of reaction, showed four main signals at -29.56, -29.65, -29.74 and -29.83 ppm, with a separation of -0.09 ppm (-14.7 Hz) (**Figure 5. 23**). The fact that no phosphorus signal corresponding to the starting material **30** was detected at -29.7 ppm indicated the complete conversion of the substrate in this case and therefore a higher reaction rate compared to that of **Ru$^{0.2}$**.

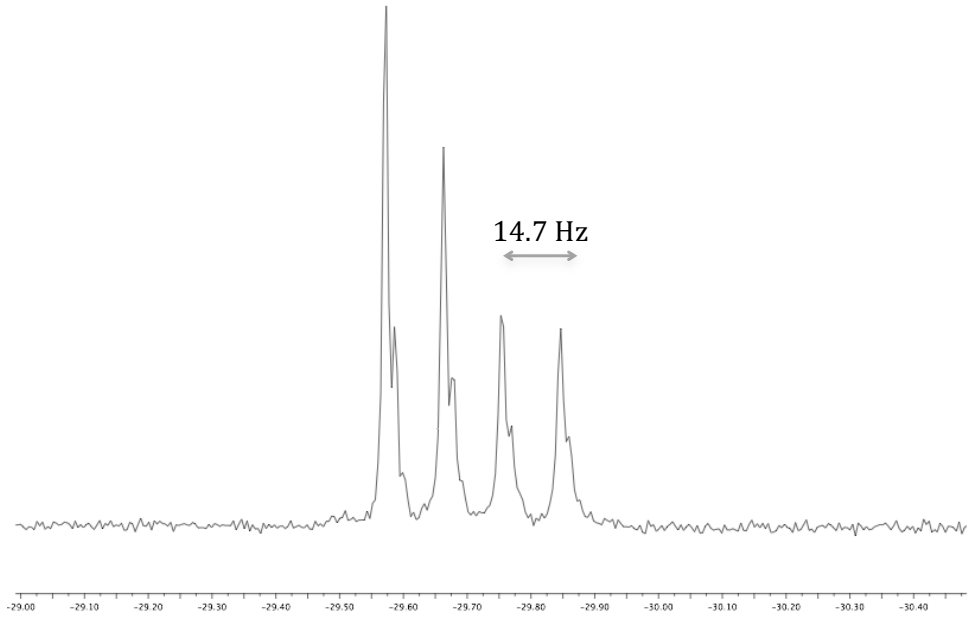

Figure 5. 23. $^{31}P\{^{1}H\}$ NMR ($CDCl_3$, 162MHz) spectrum of the deuteration of P(*o*-tolyl)$_3$ (**30**) using **Rh$^{0.2}$** after 2d at 55°C

Since the spectrum presented less signals than expected it was decided to follow the deuteration evolution during the course of the reaction. Thus, the $^{31}P\{^{1}H\}$ NMR spectra were recorded after 7h, 2d, 8d and 12d of reaction (Figure 5. 25). The $^{31}P\{^{1}H\}$ NMR spectrum obtained after 7h of reaction showed the formation of a large range of deuterated products (Figure 5. 24).

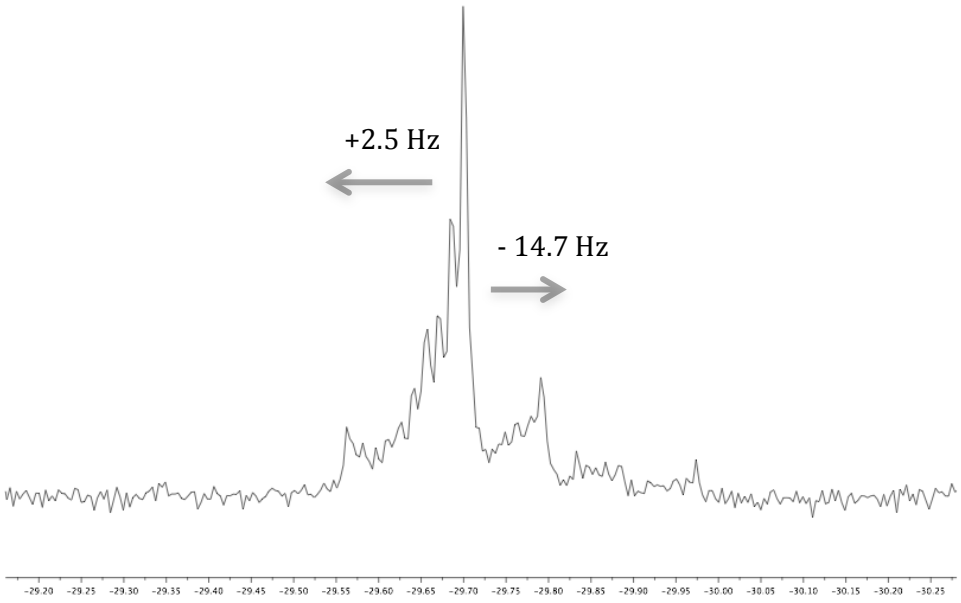

Figure 5. 24. $^{31}P\{^{1}H\}$ NMR ($CDCl_3$, 162MHz) spectrum of the deuteration of P(*o*-tolyl)$_3$ (**30**) using **Rh$^{0.2}$** after 7h at 55°C

Interestingly, and taking as reference the signal of phosphine P(*o*-tolyl)$_3$ (**30**), a difference on the sign for the isotopic shift was evidenced depending on the position where the deuteration took place. Thus, when the H/D exchange took place at the $-CH_3$, an isotopic shift of +0.015 ppm (+2.5 Hz) was detected, giving rise to the observation of 9 different products at higher chemical shifts compared to the starting material (**30**) corresponding to different deuteration degrees at the $-CH_3$ groups). At the same time, the H/D exchange at the *meta* positions of the arene rings was also detected by the observation of new signals at lower chemical shifts compared to **30**, displaying an isotopic shift of -0.09 ppm (-14.7 Hz).

The almost complete deuteration of the $-CH_3$ groups after 2 days of reaction simplified the $^{31}P\{^1H\}$ NMR spectrum, showing essentially four family of signals. The intensity of the signals at higher fields increased notably after 8 and 12 days of reaction (Figure 5. 25d and e). This evidence was attributed to the complete deuteration of the methyl groups and the progressive deuteration at the *meta* positions of the aromatic rings. The high width of the ^{31}P signals could indicate a slightly different isotopic shift depending on the *meta* position where the deuteration takes place.

The fact that the ^1H spectrum after **12d** of reaction showed approximately 66% of H/D exchange for the protons at the C3-*meta* position and 33% at the C5-*meta* position (Figure S160, Supporting information) confirmed the presence of **30b** as the major reaction product, detected at -29.83 ppm. These results were in agreement with the detection of a species with a M^+=316.3 as the main compound in the mixture by mass spectrometry (Figure S165, Supporting information).

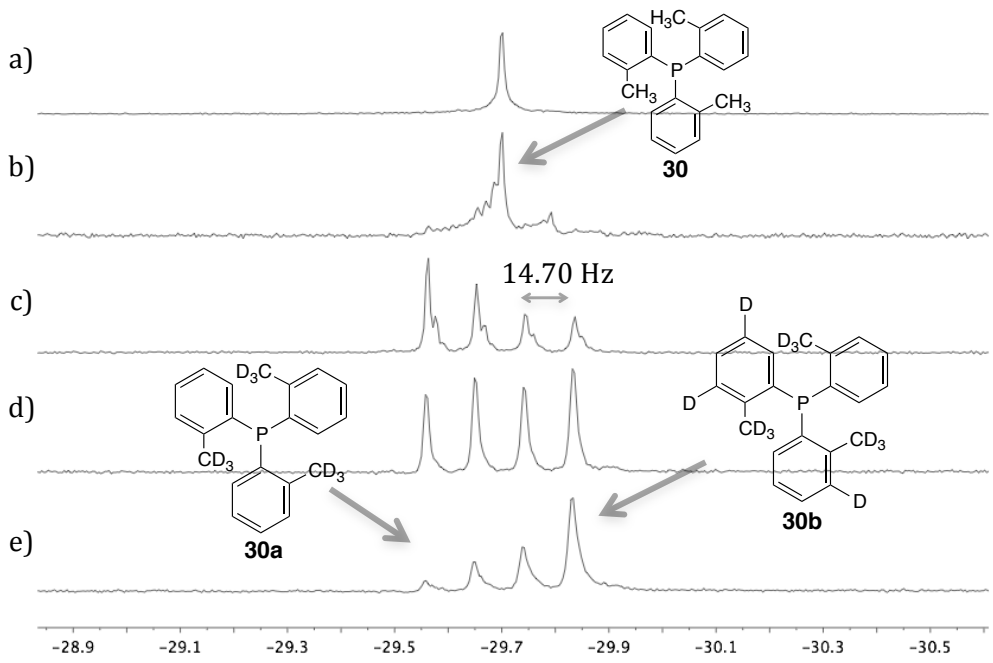

Figure 5. 25. $^{31}P\{^{1}H\}$ NMR ($CDCl_3$, 162MHz) spectra of P(*o*-tolyl)$_3$ (**30**) deuteration evolution using **Rh$^{0.2}$**: (a) t=0 (b) 7h, (c) 2 days, (d) 8 days and (e) 12 days at 55°C

The absence of H/D exchange for the protons at the C6-*ortho* position of the aromatic ring of **30** when **Ru$^{0.2}$** and **Rh$^{0.2}$** were used as catalysts and the preferred deuteration of the $-CH_3$ group and the protons at *meta* positions suggests a different coordination mode at the NPs surface compared to **28** and **29**. The cone angle of phosphine **30** (194°)[34], which is higher than 180°, must prevent the P atom to reach the NPs metallic surface and thus, having an effect on the selectivity of the deuteration reaction. One possibility based on the evidence that the H/D exchange at the protons of the $-CH_3$ groups is faster, suggested the interaction between these alkyl groups and the **Ru$^{0.2}$** and **Rh$^{0.2}$** surface. Moreover, the close proximity of the protons at the *meta* positions of the methyl group when this interaction takes

place could also explain the H/D exchange at these aromatic positions (Figure 5. 26).

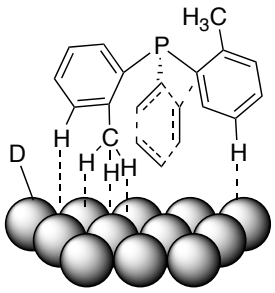

Figure 5. 26. Proposed coordination mode for P(*o*-tolyl)$_3$ (**30**) at the surface of **Ru$^{0.2}$** and **Rh$^{0.2}$**

To confirm this hypothesis, the deuteration of borane protected phosphine H_3B-P(*o*-tolyl)$_3$ (**30-BH3**) was tested. However, when the deuteration of **30-BH3** was attempted under 2 bar of D_2 at 55°C, phosphorus signals from **30** together with signals from their corresponding deuterated products (previously observed in the deuteration of **30**) were detected in the $^{31}P\{^1H\}$ NMR spectrum (Figure S167, Supporting information). These results suggested that deprotection of the phosphine borane had taken place under these reaction conditions.

The deuteration of tris(3,5-dimethylphenyl)phosphine (**31**), an aromatic phosphine bearing methyl groups in both *meta* positions, was then investigated using **Rh$^{0.2}$**. Deuterium incorporation in aromatic and aliphatic positions was confirmed by the presence of signals at 2.25 and 6.98 ppm in the ^2D NMR spectrum (Figure 5. 27).

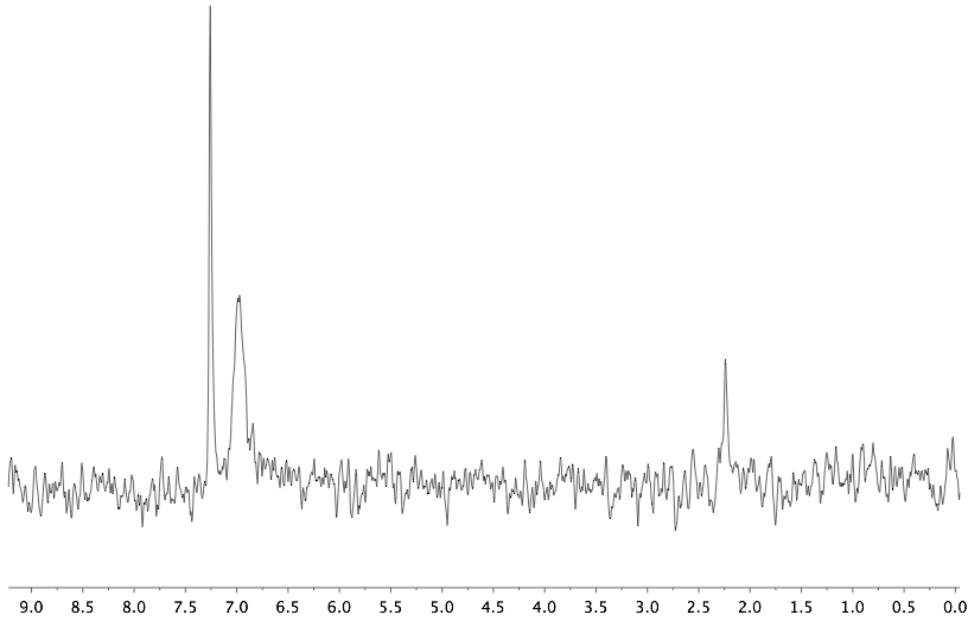

Figure 5. 27. ^{2}D NMR ($CHCl_3$, 61.49MHz) spectrum of the deuteration of tris(3,5-dimethylphenyl)phosphine (**31**) using **Rh$^{0.2}$**

However, the reaction rate was so low that mainly the phosphorus signal from the starting material was detected by $^{31}P\{^{1}H\}$ NMR (Figure S169, Supporting information) even after 8 days of reaction. The low degree of deuteration in methyl and aromatic groups did not allow the identification of the reaction products by $^{13}C\{^{1}H\}$ NMR.

With these results in hands and since both aliphatic and aromatic protons could be exchanged when the deuteration of **31** was attempted, a similar coordination mode compared to **30** was hypothesised for this substrate. However, this proposal could not be confirmed.

5.2.2. Selective deuteration of monoaryl-alkyl phosphines

Next, we focused on the study of phosphines with alkyl groups directly linked to the phosphorus atom, such as PPh_2Me (**32**) and $PPhMe_2$ (**33**).

To start with, the deuteration of PPh_2Me (**32**) was carried out using **Ru@PVP** as catalyst at 80°C under 2 bar of D_2 (Figure 5. 28) and the reaction mixture was analysed after 88h by NMR spectroscopic techniques.

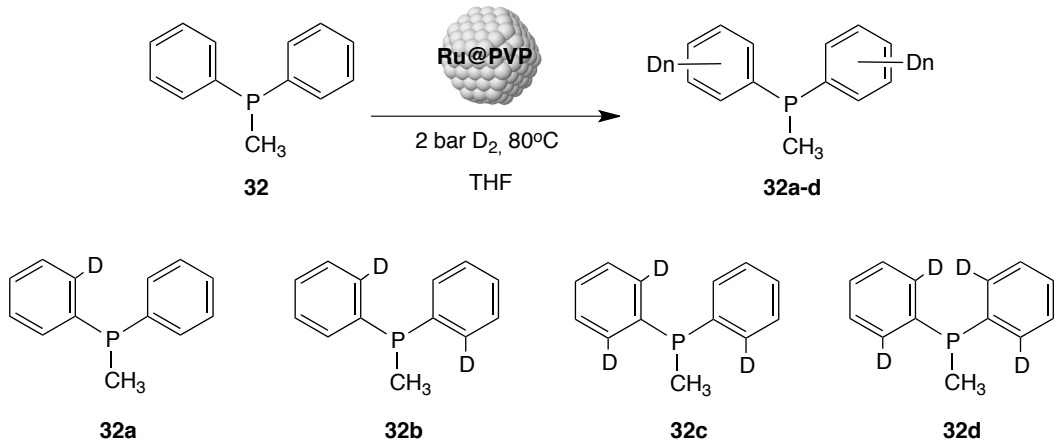

Figure 5. 28. Deuteration of PPh_2Me (**32**) using **Ru@PVP**

The detection of a single signal at -27.40 ppm by $^{31}P\{^1H\}$ NMR revealed the formation of only one reaction product. In the corresponding $^{13}C\{^1H\}$ NMR spectrum, a triplet of doublets was detected at 133.9 ppm ($^2J_{C,P}$ = 18.7 Hz, $^1J_{C,D}$ = 24.4 Hz), similar to the one observed in the deuteration of **28** and **29**, and was assigned to C2-D. This indicates the selective deuteration at the *ortho* aromatic position using **Ru@PVP**, leading to the formation of compounds

32a-d (Figure 5.28). The signal at 12.53 ppm ($^2J_{C,P}$ = 13.8 Hz) attributed to the $-CH_3$ group remained unaltered, proving that no H/D exchange took place at the methyl group. This fact was also confirmed by the detection of only an aromatic deuterium signal at 7.52 ppm in the ^{2}D NMR spectrum (Figure 5. 29a), arising from deuterium incorporation at the *ortho* positions of the aromatic rings of **32**. Based on these results, the reaction product was identified as **32d**, which is in agreement with Mass spectrometry measurements.

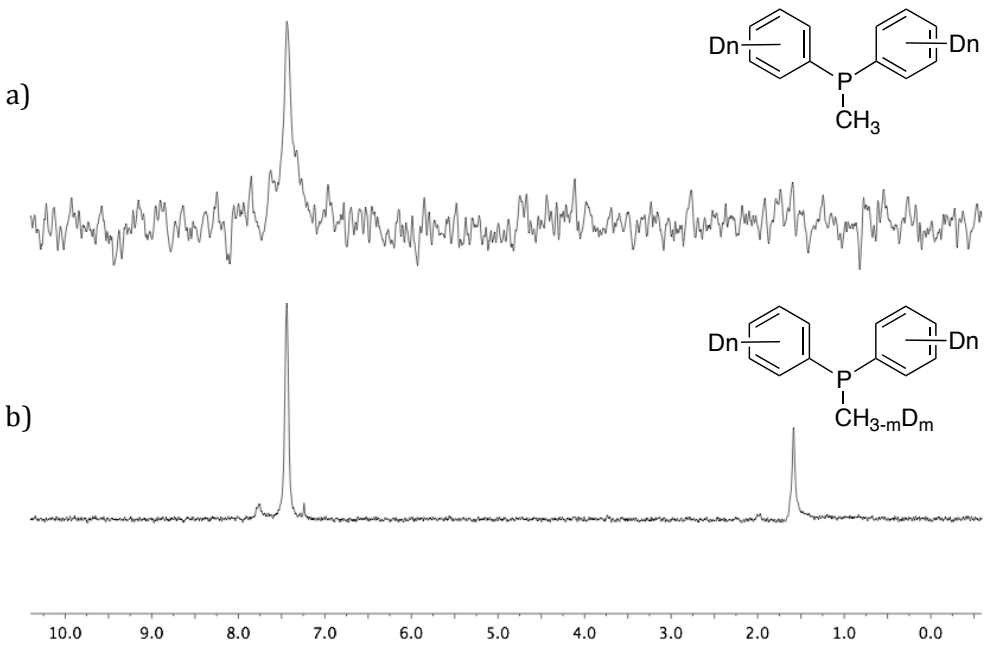

Figure 5. 29. ^{2}D NMR ($CHCl_3$, 61.49MHz) spectra of the deuteration of PPh_2Me (**32**) using (a) **Ru@PVP** and (b) **Ru$^{0.2}$**

Since the selectivity for the deuteration of **32** was similar that for **28** and **29**, it was concluded that a coordination mode through the P atom of the aryl-alkyl phosphine **32** at the **Ru@PVP** surface had

taken place (Figure 5. 17). Interestingly, this Ru nanocatalyst was not able to promote H/D exchange at the methyl groups.

The application of **Ru$^{0.2}$** and **Rh$^{0.2}$** as catalysts in this reaction was then investigated. In previous studies on the application of **Rh$^{0.2}$** as catalysts for the hydrogenation of aromatic compounds, a drop in the activity of this catalyst was observed at temperatures >60°C. In consequence, the catalytic activity of **Ru$^{0.2}$** and **Rh$^{0.2}$** towards the deuteration of **32** was carried out at 55°C.

First, H/D exchange of **32** was tested using **Ru$^{0.2}$** (Figure 5. 30) and the identification of the deuteration products in the reaction mixture was examined by ^{2}D, ^{13}C{^{1}H} and ^{31}P{^{1}H} NMR. The ^{2}D NMR spectrum recorded after 48h of reaction, showed a couple of signals at 1.60 and 7.44 ppm, indicating the deuteration at methyl and aromatic groups (Figure 5. 29b). Aromatic rings were deuterated at the *ortho* position as confirmed by the presence of a triplet of doublets at a chemical shift that was similar to that of products deuterated in *ortho* positions.

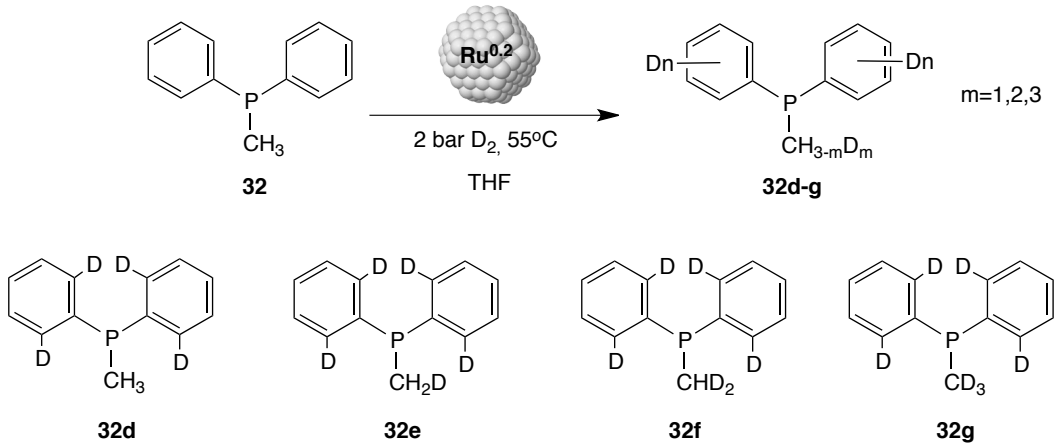

Figure 5. 30. Deuteration of PPh_2Me (**32**) using **Ru$^{0.2}$**

The 5 signals present in the $^{31}P\{^{1}H\}$ NMR spectrum at -26.92, -27.40, -27.63, -27.89 and -28.13 ppm were assigned to compounds **32** and **32d-g**. Product **32d** was detected at -27.40 ppm by $^{31}P\{^{1}H\}$ NMR, identifying the phosphorus signals from **32e**, **32f** and **32g** at -27.63, -27.89 and -28.13 ppm, respectively. The isotopic shift observed between the signals of **32d-g** was **-**0.24 ppm (-39.86 Hz) (Figure 5. 31a). No partially deuterated products at the *ortho* position of the aromatic rings were observed during this experiment.

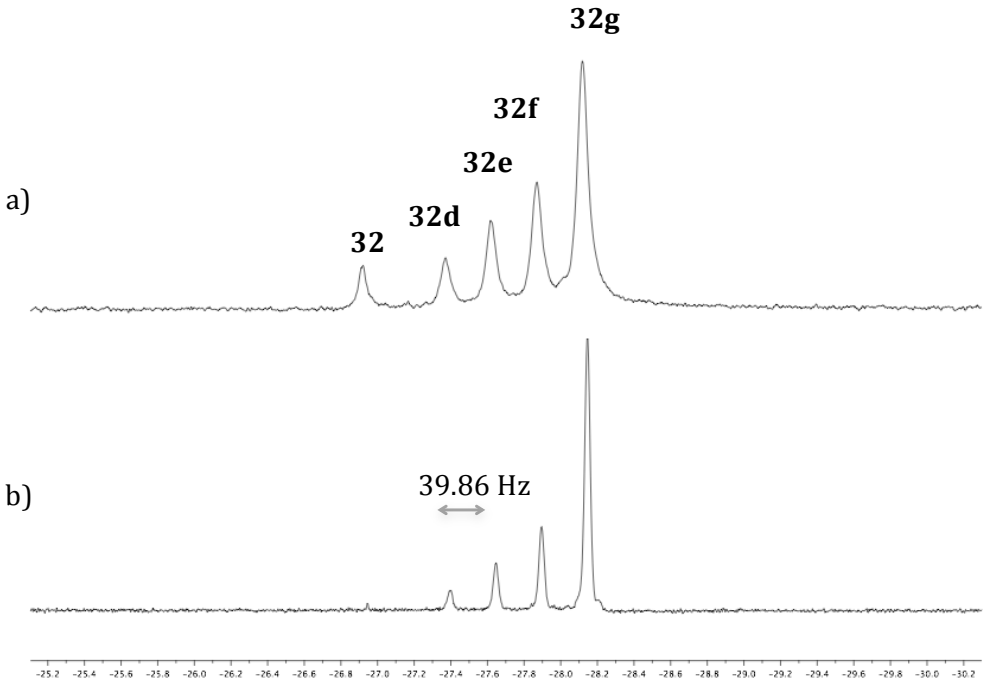

Figure 5. 31. $^{31}P\{^{1}H\}$ NMR ($CDCl_3$, 162MHz) spectra of PPh_2Me (**32**) deuteration evolution using **Ru$^{0.2}$**: (a) 48h and (b) 8 days at 55°C

The corresponding percentages of each reaction product for the deuteration of **32** were obtained by $^{31}P\{^{1}H\}$ NMR after 48h and 8 days of reaction using **Ru$^{0.2}$** as catalyst and are presented in Table 5. 3. The fact that the intensity of the phosphorus signals increased at higher fields at high reaction times indicated the progressive

deuteration of products **32d**, **32e** and **32f** towards the formation of **32g** (Figure 5. 31a *vs.* b). Product **32g** was detected as the major deuteration product in the reaction mixture in 47% yield after 48h (Table 5. 3, Entry 1), increasing up to 65% with full conversion of the starting material **32** after 8 days of reaction (Table 5. 3, Entry 2).

Table 5. 3. Selective deuteration of PPh_2Me (**32**) using **Ru$^{0.2}$**. Percentage of compounds in the reaction mixture.[a]

Entry	Time	32 (%)[b]	32d (%)[b]	32e (%)[b]	32f (%)[b]	32g (%)[b]
1	**48h**	6	9	15	23	47
2	**8 days**	-	5	10	20	65

[a]Catalytic conditions: 0.15 mmol substrate, 25 mol% cat., 55°C, 2 bar D_2, 2ml THF. [b]Calculated by $^{31}P\{^1H\}$ NMR spectroscopy.

Next, the deuteration of **32** was explored using the catalyst **Rh$^{0.2}$**. Selective deuteration at the *ortho* position of the aromatic ring and at the $-CH_3$ group was also evidenced in this case by $^{13}C\{^1H\}$ and ^2D NMR. However, the relative intensity of doublet attributed to C2-H at 132.2 ppm ($^2J_{C,P}$ = 18.48 Hz) in $^{13}C\{^1H\}$ NMR, in relation to the triplet of doublet signal assigned to C2-D suggested that the deuteration rate of aromatic rings was lower for **Rh$^{0.2}$** compared to **Ru$^{0.2}$** (Figure 5. 32).

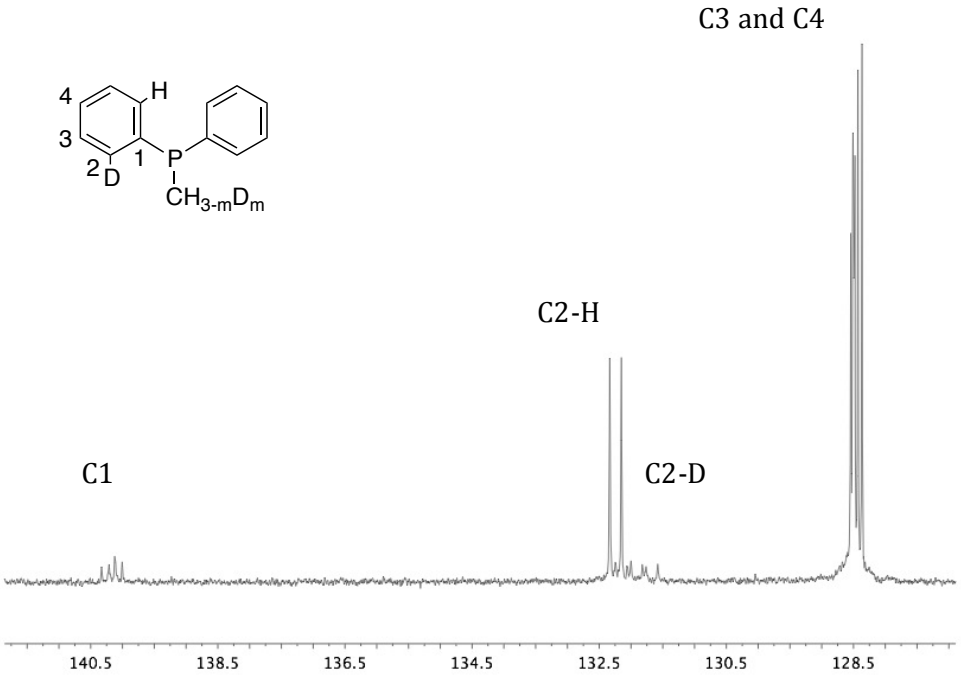

Figure 5. 32. $^{13}C\{^1H\}$ NMR ($CDCl_3$, 100.6MHz) spectrum of the deuteration of PPh_2Me (**32**) using **Ru$^{0.2}$** after 48h of reaction

The fact that the deuteration rate was also low for the $-CH_3$ moiety was confirmed by the presence of over 10 different signals in the $^{31}P\{^1H\}$ NMR spectrum of a sample extracted after 48h of reaction (Figure 5. 33a). These signals corresponds to a wide number of deuteration products that can be formed by the possible simultaneous exchange of 4 hydrogen atoms at the *ortho* position of the aromatic ring and 3 hydrogen atoms at the $-CH_3$ moiety. ^{31}P signals from the different deuteration products after H/D exchange at the *ortho* position of the aromatic ring were detected as major reaction products mainly at -27.06, -27.18, -27.29 and -27.40 ppm with an isotopic shift of -0.114 ppm (-18.55 Hz), which is the same value than that measured for the H/D exchange in the same aromatic position for **28** and **29** (-0.11 ppm, -17.80 Hz).

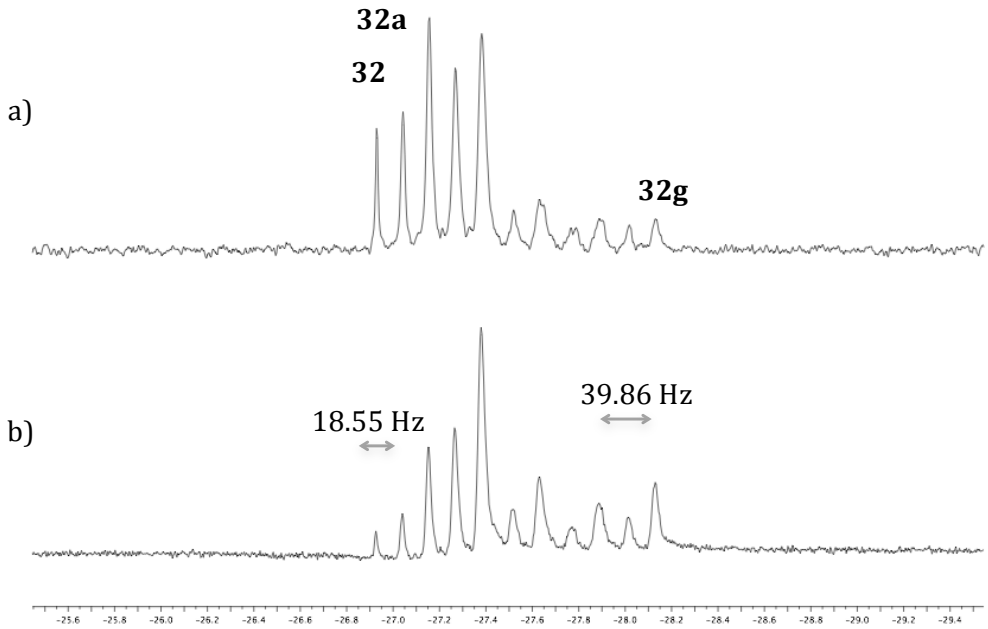

Figure 5. 33. $^{31}P\{^{1}H\}$ NMR ($CDCl_3$, 162MHz) spectra of PPh_2Me (**32**) deuteration evolution using **Rh$^{0.2}$**: (a) 48h and (b) 8 days at 55°C

Products deuterated at the $-CH_3$ group were detected at lower chemical shifts, between -27.52 and -28.13 ppm, being the ^{31}P signal at -28.18 ppm that previously assigned to the fully deuterated product **32g**. A $^{31}P\{^{1}H\}$ NMR spectrum carried out after 8 days of reaction showed an increase in the intensities of the signals at higher fields which indicates the progressive deuteration of the partially deuterated products towards the formation of **32g** (Figure 5. 33b). Quantification of the different deuteration products formed during the reaction could not be performed due to overlapping of the phosphorus signals attributed to different reaction products.

In summary, larges differences were observed in this case depending on whether the NPs were stabilized with PVP or NHCs. The **Ru@PVP** NPs did not promote deuteration at the methyl group while **Ru$^{0.2}$**

and **Rh$^{0.2}$** did. Concerning the NHC-stabilized M-NPs, **Ru$^{0.2}$** showed to be more active than **Rh$^{0.2}$**. The selectivity indicated the coordination of the phosphine through the phosphorus atom.

Different phosphines bearing alkyl moieties such as $PPhMe_2$ (**33**) and P(*i*-Pr)$_3$ (**34**) were also tested for their deuteration using **Rh$^{0.2}$** under 2 bar of D_2 and 55°C. The ^{2}D NMR spectra performed after 48 h of reaction showed signals in the aliphatic and aromatic region in the case of **33** (Figure 5. 34a), and only in the methyl region of the *i*Pr groups in the case of **34** (Figure 5. 34b). However, many signals were observed by ^{31}P NMR due to the large number of deuterated species that could be formed, and the deuteration products could not be unambiguously identified (Figures S186 an S188, Supporting information). Moreover, the difficult separation of the mixture of products from the NPs solution due to the low boiling point of these phosphines prevented the complete characterization of these products.

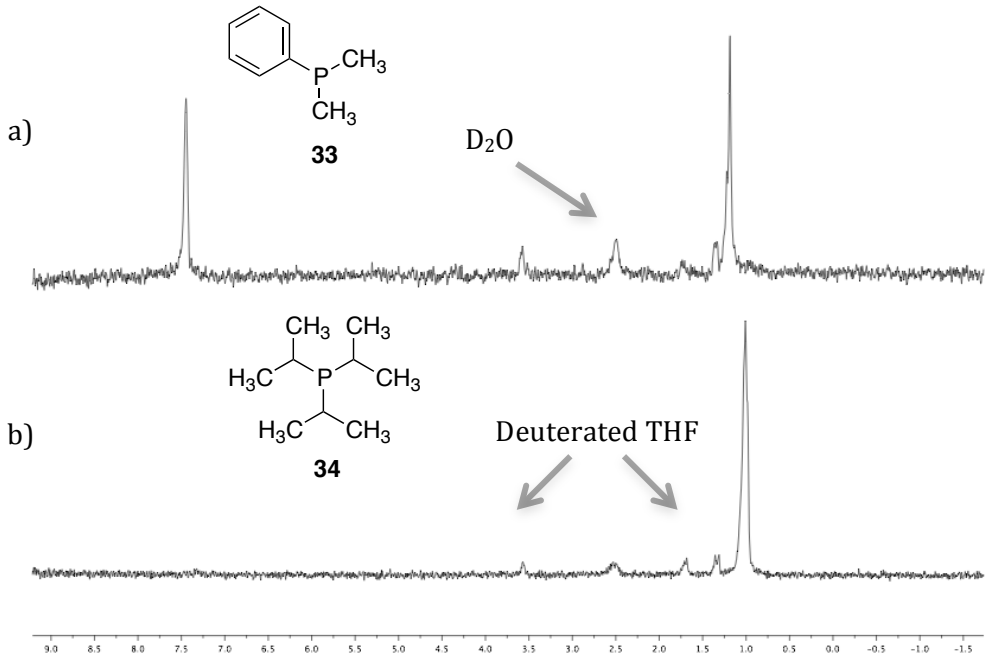

Figure 5. 34. ^{2}D NMR (THF, 61.49MHz) spectra of the deuteration of (a) $PPhMe_2$ (**33**) and (b) P(*i*-Pr)$_3$ (**34**); using **Rh$^{0.2}$**

Minor deuteration of THF used as the reaction media was also observed by the detection of signals at 1.72 and 3.58 ppm by ^{2}D NMR, which would demonstrate interaction between molecules of solvent and the surface of the Rh NPs while the deuteration of P-containing compounds took place.

5.2.3. Selective deuteration of bidentate phosphines

To start with, dppm (**35**), a diphosphine bearing a methylene carbon between the two P atoms, was studied using **Ru@PVP** and **Ru$^{0.2}$** as catalysts. However, no H/D exchange was detected after carrying out both reactions at 55°C under 2 bar of D_2, even after 8 days of reaction (Figure 5. 35a).

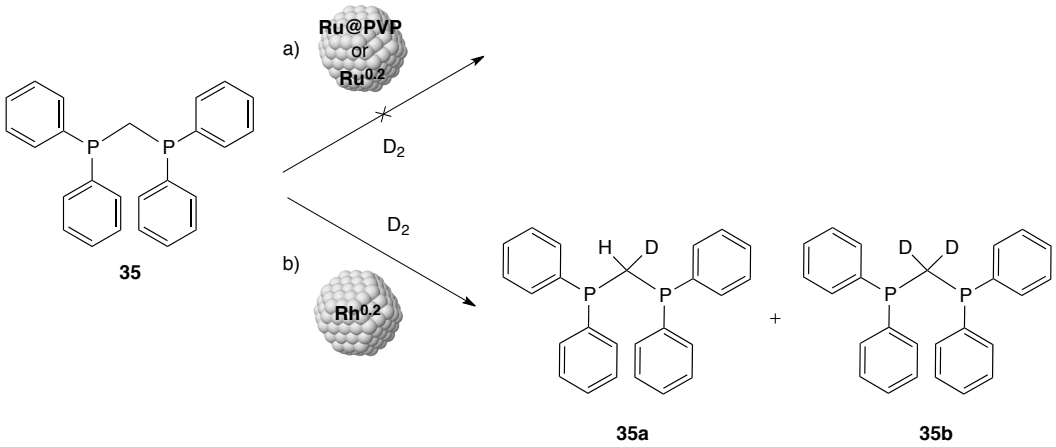

Figure 5. 35. Deuteration of dppm (**35**) using a) **Ru@PVP** and **Ru$^{0.2}$** and b) **Rh$^{0.2}$**

These results were surprising since the presence of aromatic rings close to the P atom were expected to get deuterated, similarly to the cases of the monodentate aryl phosphines **28** and **29**.

When **Rh$^{0.2}$** was tested as catalyst in the same reaction under the same reaction conditions, deuteration at the methylene group was evidenced by ^{2}D NMR via the detection of a broad signal at 2.81 ppm, (Figure 5. 36b). This evidence was corroborated by the disappearance of the corresponding signal in the ^{1}H NMR spectrum (Figure 5. 36a).

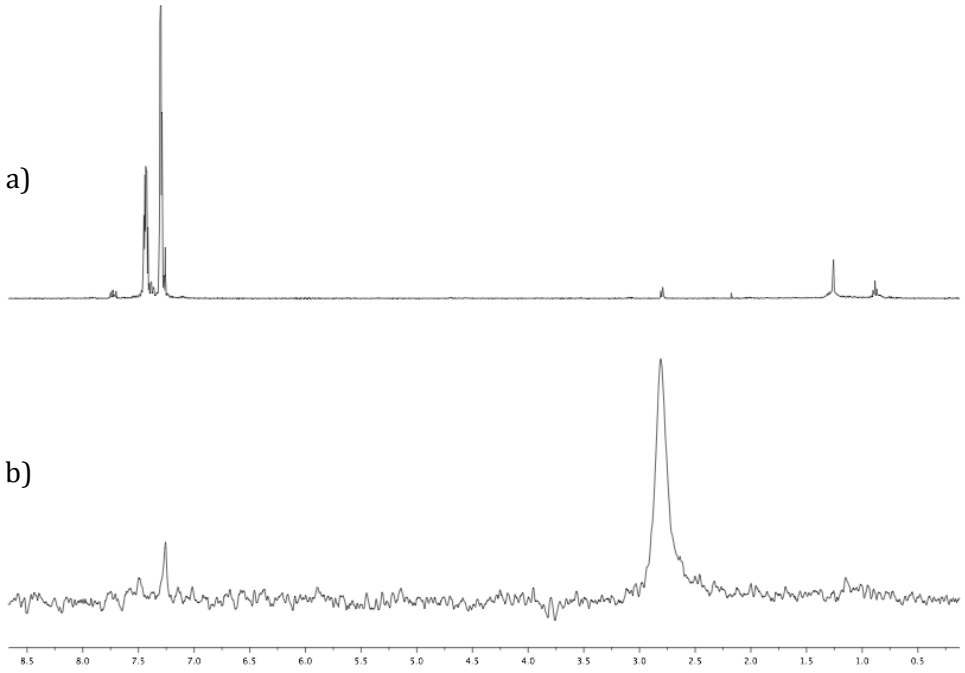

Figure 5. 36. (a) ^{1}H ($CDCl_3$, 400MHz) and (b) ^{2}D NMR ($CHCl_3$, 61.49MHz) spectra of the deuteration of dppm (**35**) using **Rh$^{0.2}$** after 48h of reaction

When the reaction mixture was analysed by ^{13}C NMR, the absence of the triplet from the methylene carbon detected at 28.16 ppm for the starting material **35** confirmed the H/D exchange at this position. Unfortunately, the expected signal attributed to the dideuterated carbon –CD_2- was not observed due to its expected high multiplicity (Figure S192, Supporting information). When a $^{31}P\{^{1}H\}$ NMR spectrum was recorded, the phosphorus signal from the starting material **35** at -22.64 ppm was detected (Figure 5. 37a) together with other two signals at -22.93 and -23.22 ppm that were assigned to the mono- and the dideuterated products **35a** and **35b** respectively (Figure 5. 35b and Figure 5. 37).

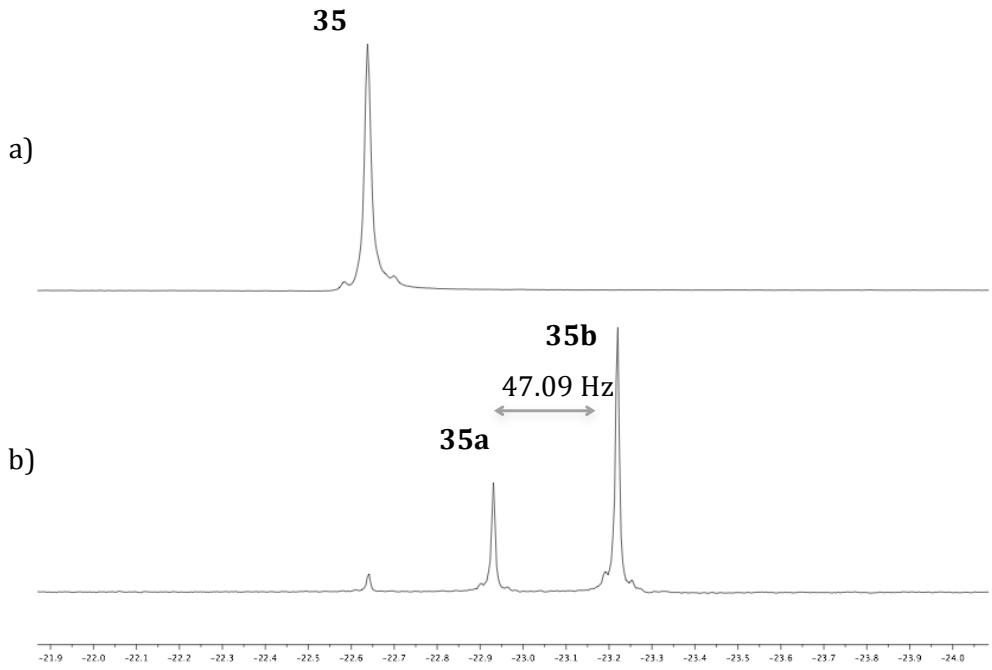

Figure 5. 37. $^{31}P\{^{1}H\}$ NMR ($CDCl_3$, 162MHz) spectra of dppm (**35**) deuteration evolution using **Rh$^{0.2}$**: (a) t=0 and (b) 48h at 55°C

The fact that an isotopic shift of 0.29 ppm (47.09 Hz) was measured between signals, which is similar to the one measured after deuterium incorporation at alkyl positions of substrate **32** (-0.24 ppm, -39.86 Hz), was in agreement with deuteratium incorporation at the methylene carbon.

The corresponding percentage of compounds in the reaction mixture after 48h and 8 days of reaction were then quantified by $^{31}P\{^{1}H\}$ NMR (Table 5. 4). An increase from 69% to 84% for the formation of product **35b** was observed when the reaction mixture was analysed after 8 days of reaction (Table 5. 4, Entries 1 *vs.* 2), in almost full conversion of **35**.

Table 5. 4. Selective deuteration of dppm (**35**) using **Rh$^{0.2}$**. Percentage of compounds in the reaction mixture.[a]

Entry	Time	35 (%)[b]	35a (%)[b]	35b (%)[b]
1	**48 h**	4	27	69
2	**8 days**	2	14	84

[a]Catalytic conditions: 0.15 mmol substrate, 25 mol% cat., 55°C, 2 bar D_2, 2ml THF. [b]Calculated by $^{31}P\{^1H\}$ NMR spectroscopy.

In terms of selectivity, the fact that **35** was selectively deuterated at the methylene carbon with no H/D exchange at aromatic positions, suggested a different coordination mode at the surface of **Rh$^{0.2}$** than the monodentate phosphines **28**, **29** and **32**. In the case of **35**, coordination through the methylene carbon is suggested (Figure 5. 38). The formation of a unstable carbene intermediate which could coordinate to the surface of metallic NPs was previously reported for indoles using **Ru@PVP** by H/D exchange experiments.[20] Such a coordination mode could be envisioned in the case of **35**.

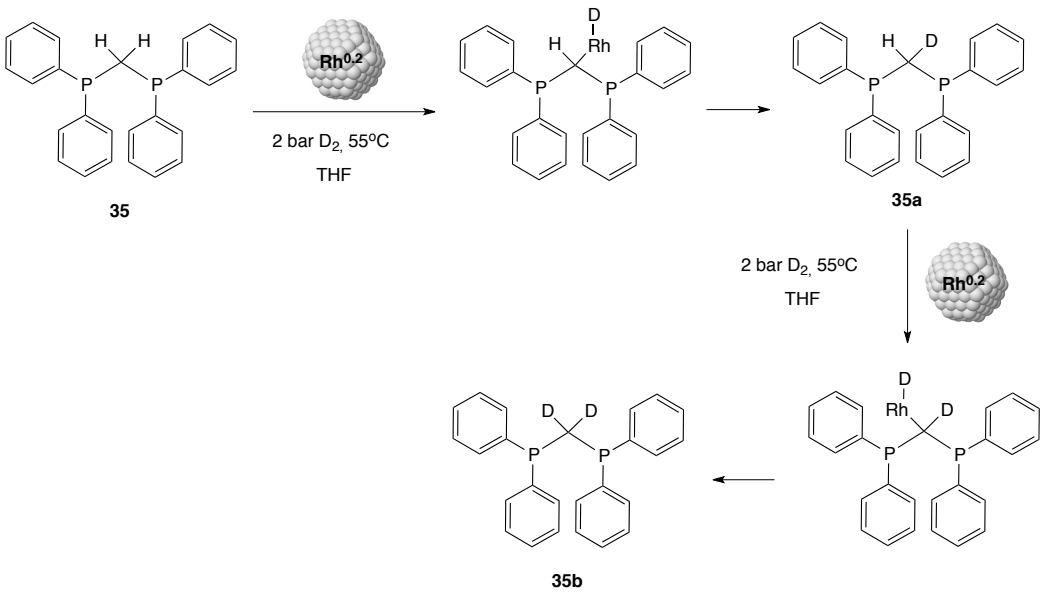

Figure 5. 38. Proposed mechanism for the deuteration of dppm (**35**) using **Rh$^{0.2}$**

In order to investigate the role of the NHC stabilizer for modulating the reactivity of the NPs, a blank experiment was performed using **Rh/C**[35] as catalyst. Thus, the deuteration of **35** was attempted in the presence of 5mol% of **Rh/C** under similar reaction conditions to those previously tested, but only deuteration of THF used as reaction media and small amounts of H_2O coming from the **Rh/C** were detected by ^{2}D NMR (Figure 5. 39).

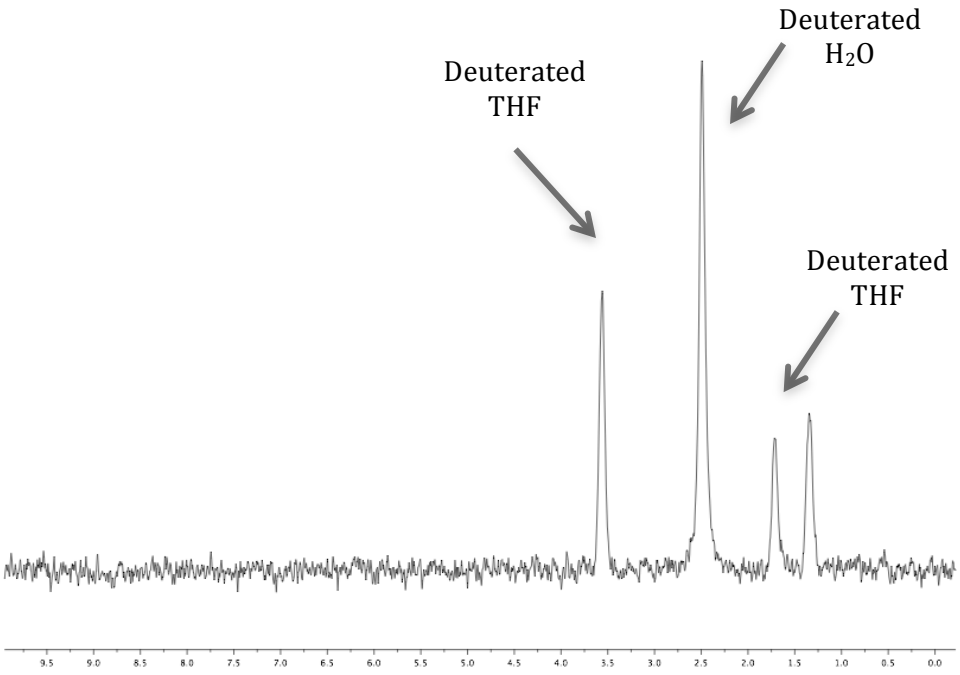

Figure 5. 39. ^{2}D NMR (THF, 61.49MHz) spectrum of the deuteration of dppm (**35**) using **Rh/C**

Since no H/D exchange was observed in this case, it was thought that the presence of NHCs at the surface of $\mathbf{Rh^{0.2}}$ could play an important role in the reaction. In this view, the presence of a greater amount of NHCs at the surface of the metallic NPs for $\mathbf{Rh^{0.2}}$ than for $\mathbf{Ru^{0.2}}$, [30] could explain the lack of activity using this latter catalyst. However, the displacement of the NHC ligands from the Ru surface caused by a strong affinity of dppm to Ru cannot be discarded either.

Next we investigated the deuteration of dppe (**36**) (bite angle 83°), containing a two carbon chain between the phosphorus atoms. In view of the previous results with dppm (**35**), these experiments were performed exclusively using $\mathbf{Ru^{0.2}}$ and $\mathbf{Rh^{0.2}}$, and under the same reaction conditions used for **35**. After 48h of the reaction the ^{2}D NMR spectrum showed only a signal in the aromatic region (7.43

ppm), for both catalysts (Figure 5. 40 and Figure S195, Supporting information).

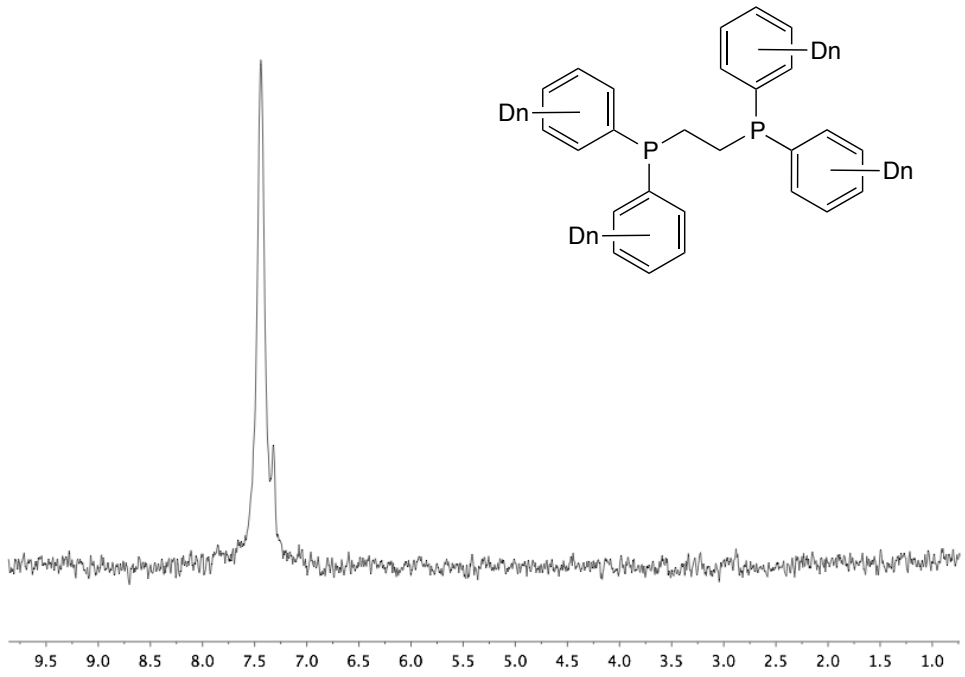

Figure 5. 40. ^{2}D NMR ($CHCl_3$, 61.49MHz) spectrum of the deuteration of dppe (**36**) using **Rh$^{0.2}$**

The $^{31}P\{^{1}H\}$ NMR spectra of the reaction crude of both catalytic tests showed several phosphorus signals at fields higher that the signal of the starting material **36** at -12.71 ppm (Figure 5. 41a). Comparing the relative intensity of the signal of the starting material with those of the deuterated products using **Ru$^{0.2}$** and **Rh$^{0.2}$** catalysts, it was concluded that deuteration progressed more rapidly with **Ru$^{0.2}$** than with **Rh$^{0.2}$** (Figure 5. 41b *vs.* c). However, the number of signals was much higher than those expected for the deuteration in the *ortho* positions of **36**, as observed for other substrates such as **28** or **29**.

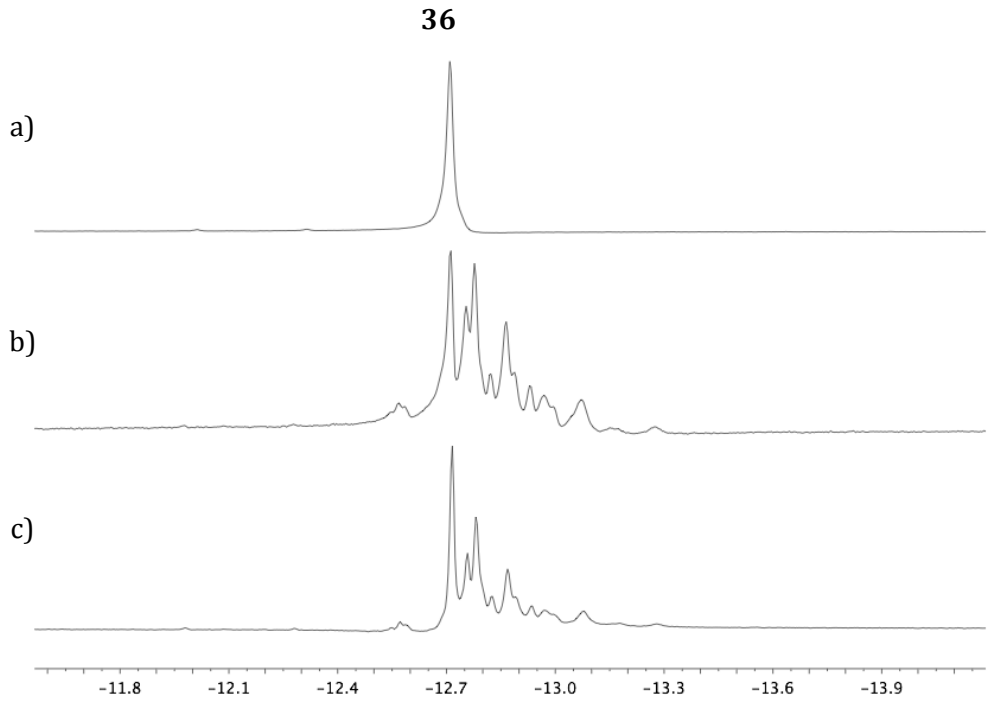

Figure 5. 41. $^{31}P\{^{1}H\}$ NMR ($CDCl_3$, 162MHz) spectra of (a) dppe (**36**) and the deuteration of **36** using (b) **Ru$^{0.2}$** and (c) **Rh$^{0.2}$** after 48h hours of reaction

Then, the $^{13}C\{^{1}H\}$ NMR spectra were analysed in order to identify the specific aromatic positions where the deuteration of **36** took place. However, both spectra showed complex carbon signals that could be due to second order effects, which made impossible the determination of the precise deuteration position for this substrate (Figures S198 and S202, Supporting information). On the other hand, the fact that H/D exchange occurred at aromatic positions and no deuterium incorporation was detected at aliphatic positions indicated a different behaviour than dppm (**35**). In view of the complexity of $^{31}P\{^{1}H\}$ and $^{13}C\{^{1}H\}$ spectra, no clear conclusions could be drawn. However, an hypothesis could be that the deuteration of **36** takes place at the *ortho* positions, as usual in aromatic rings with

the exception of P(*o*-tolyl)$_3$ (**30**). The complexity observed in those spectra could be caused by the coupling of both P atoms with the arene rings. A difference in the deuteration degree of the rings would make both P atoms inequivalent, giving rise to second order spectra. This hypothesis would involve an interaction between the NPs surface and the substrate through the phosphorus atoms.

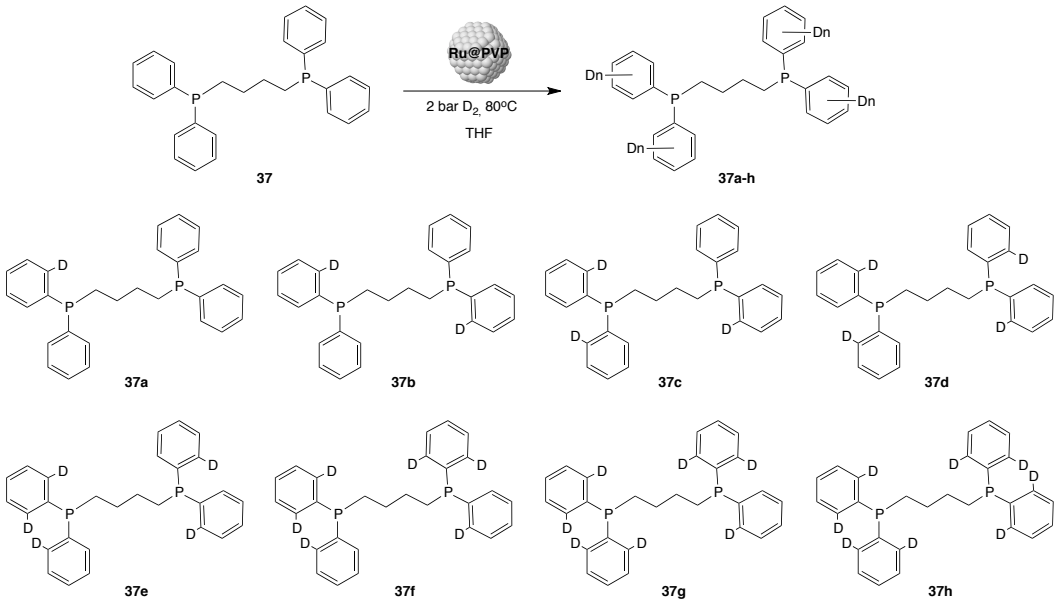

Figure 5. 42. Deuteration of dppb (**37**) using **Ru@PVP**

Given the complex spectra obtained in the study with dppe (**36**), it was decided to extend the study to dppb (**37**), a diphosphine with a longer bridge between the two P atoms. When the reaction was performed at 80°C under 2 bar of D_2 in the presence of **Ru@PVP** for 48h (Figure 5. 42), the ^{2}D {^{1}H} NMR spectrum of the reaction mixture only contained a signal at 7.42 ppm, which indicated deuteration at the aromatic ring.

The $^{13}C\{^{1}H\}$ NMR of the reaction mixture showed the characteristic triplet of doublet centred at 132.54 ppm ($^{2}J_{C,P}$ = 18.21 Hz, $^{1}J_{C,D}$ = 24.50 Hz) assigned to C2-D, close to the signal assigned to the C2-H carbon of the starting material **37**, detected as a doublet at 132.85 ppm ($J_{C,P}$ = 18.55 Hz). These results confirmed the selective deuteration of **37** in the *ortho* position of the aromatic ring, similarly to monophosphines studied with the exception of **30**. A bite angle of 97°, higher than the one of **35** (72°), was suggested (Figure 5. 43).

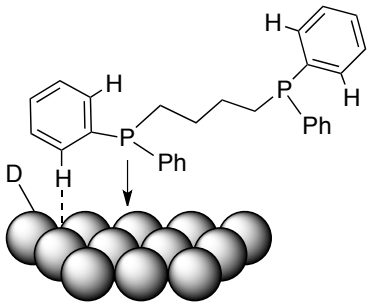

Figure 5. 43. Proposed coordination mode for dppb (**37**) at the surface of Ru and Rh NPs

Four different phosphorus signals were detected by $^{31}P\{^{1}H\}$ NMR with an isotopic shift of -0.111 ppm (-17.97 Hz) (Figure 5. 44b), similar to that for **28** and **29** (-0.11 ppm, -17.80 Hz). In the case of **28**, **29**, **32** and **35** the different signals in the ^{31}P NMR spectrum corresponded to the incorporation of a new deuterium atom in an aromatic position. In the case of **37**, since both P atoms are equivalents, it was considered that each of these 4 different phosphorus signals detected by ^{31}P NMR at -16.36, -16.47, -16.58 and -16.69 ppm, did not correspond to one product, but corresponds to the sum of the signals of the phosphorus bearing 1, 2, 3 or 4

deuterium atoms at the *ortho* position of the phenyl rings. (Figure 5. 44c).

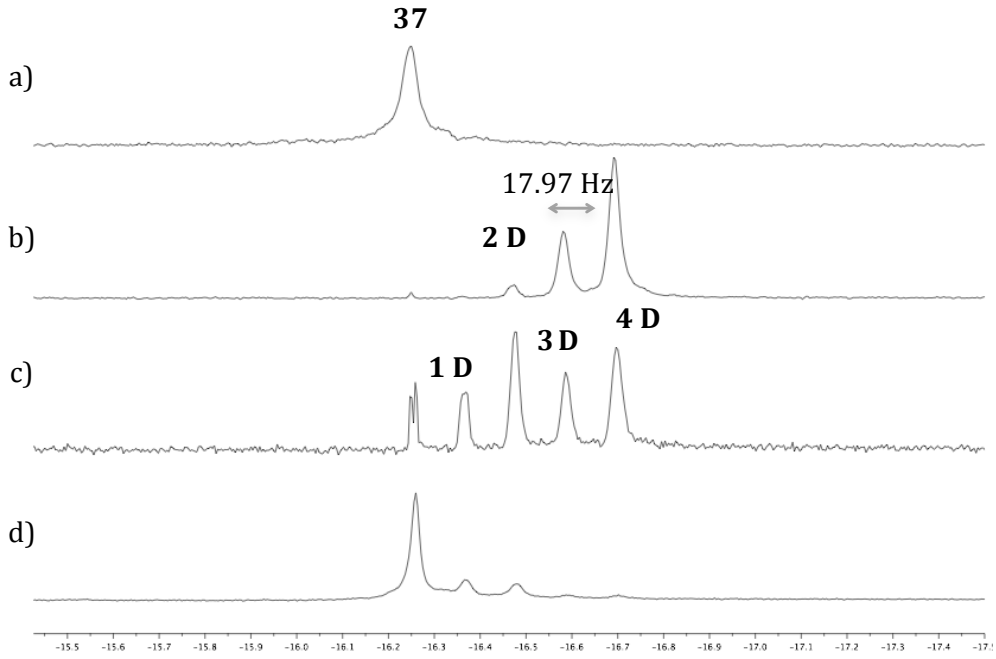

Figure 5. 44. $^{31}P\{^{1}H\}$ NMR ($CDCl_3$, 162MHz) spectra of (a) dppb (**37**) and the deuteration of **37** using (b) **Ru@PVP** at 80°C and (c) **Ru$^{0.2}$** and (d) **Rh$^{0.2}$** at 55°C; after 48h of reaction

Next, we investigated the deuteration of **37** with **Ru$^{0.2}$** and **Rh$^{0.2}$** catalysts. The reactions were conducted at 55°C under 2 bars of D_2 pressure for 48h. In both cases deuterated products obtained were similar to those obtained with **Ru@PVP**. The only difference between catalysts was the activity, with **Ru@PVP** as the most active, although this could result from the high temperature (80°C) at which the reaction was set in this case. With **Ru@PVP**, the fully deuterated compound (4 deuterium atoms at *ortho* positions of the aromatic rings linked to each P atom) was obtained in 66% yield and the yield

for the product with 3D for each PPh_2 unit was 28% (**Figure 5. 5**, Entry 1). With **Ru$^{0.2}$** as catalyst, all possible *ortho* deuterated products were detected but the fully deuterated product was present in 32%. The catalyst **Rh$^{0.2}$** (**Figure 5. 5**, Entries 2 *vs.* 3) was less active and important amounts (61%) of unaltered starting material **37** remained in the solution.

Table 5. 5. Selective deuteration of dppb (**37**) using Ru and Rh NPs stabilized by PVP and IPr. Percentages for the insertion of 0, 1, 2, 3 and 4 deuterium atoms at the *ortho* position of the aromatic rings.[a]

Entry	NPs	0 D (%)[b]	1 D (%)[b]	2 D (%)[b]	3 D (%)[b]	4 D (%)[b]
1[c]	**Ru@PVP**	0.5	0.5	5	28	66
2[d]	**Ru$^{0.2}$**	9	12	27	20	32
3[d]	**Rh$^{0.2}$**	61	16	14	4	5

[a] Catalytic conditions: 0.15 mmol substrate, 2 bar D_2, 2ml THF, 48h. [b] Calculated by $^{31}P\{^1H\}$ NMR spectroscopy. [c] 3 mol% cat. at 80°C. [d] 25 mol% cat. at 55°C

It was concluded that deuteration of dppb (**37**) takes place at the *ortho* positions of the aromatic rings, in a similar way to monophosphines **28**, **29** and **32**. In this case and given the flexibility of the linker between P atoms, this coordination to the NPs surface can be as a monophosphine or as a chelate. Finally, comparing the results obtained for dppm (**35**), dppe (**36**) and dppb (**37**), it can be concluded that dppm is the exception showing a completely different behaviour, since aromatics were not deuterated while H/D exchange at the methylene group took place. This was explained by the particular activation of C-H between 2 P atoms within the P-CH_2-P group, and/or the possibility of a carbene formation. We consider

that dppe behaves similarly to dppb and that the complexity of spectra are due to second order effects.

Deuteration of bidentate phosphine-heterocycles

Finally, the deuteration of bidentate phosphine-heterocycles such as PPh_2py (**38**) and $P(furyl)_3$ (**39**), containing different heteroatoms in their structure with similar P-N and P-O distances compared to the P-P distance of **35**, was attempted (Figure 5. 45).

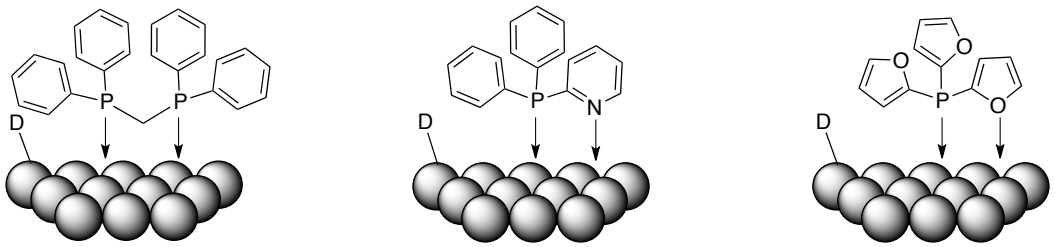

Figure 5. 45. Proposed coordination mode for bidentate P-containing compounds dppm (**35**), PPh_2py (**38**) and $P(furyl)_3$ (**39**) using Rh and Ru NPs stabilised by PVP or NHCs

Regardless of whether **Ru@PVP**, **$Ru^{0.2}$** or **$Rh^{0.2}$** was used as catalyst at 55°C under 2 bar of D_2, no deuterated products were obtained. These results are similar to those obtained for **35** using **Ru@PVP** and **$Ru^{0.2}$**. We considered in that case, the coordination strength of the substrates to the NPs surface could be the responsible for the lack of activity. Similarly, in the case of **38** and **39**, the coordination could take place through the P and the heteroatom (N or O). Indeed, a reported value of 68°[36] for the bite angle of **38**, which is similar to the bite angle reported for **35** (72°), supported this hypothesis. Besides, since no protons are present at the carbon between the P

and the corresponding heteroatom (N or O) in the case of **38** and **39**, similar deuteration selectivities to that obtained for **35** using **Rh$^{0.2}$** was not possible.

5.2.4. Selective deuteration of phosphine oxides

The coordination of phosphine oxides at the NPs surface was investigated by deuteration of O=PPh_3 (**40**) and O=P(*o*-tolyl)$_3$ (**41**), two phosphine oxide derivatives of phosphines PPh_3 (**28**) and P(*o*-tolyl)$_3$ (**30**).

The H/D exchange of **40** using **Ru@PVP** as catalyst was first attempted under 2 bar D_2 at 55°C (Figure 5. 46), and the products formed during the reaction were analysed by NMR spectroscopy after 36h of reaction. The $^{31}P\{^1H\}$ NMR spectrum showed signals at 45.6 and 51.4 ppm corresponding to O=PCy_2Ph (**40b**) and O=PCy_3 (**40c**) respectively, which indicated the reduction of the phenyl rings of the starting material **40** under these reaction conditions (Figure 5. 47a).

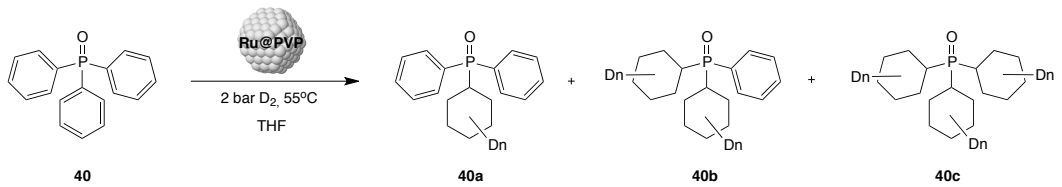

Figure 5. 46. Deuteration of O=PPh_3 (**40**) using **Ru@PVP**

This was confirmed by the detection of several aliphatic deuterium signals between 0.8-2.25 ppm (Figure S215, Supporting information) in the corresponding ^{2}D NMR spectrum. When the reaction time and the temperature were decreased to avoid reduction of **40**, GC-MS

analysis of the reaction mixture again revealed the formation of these reduction products (Figure S217, Supporting information).

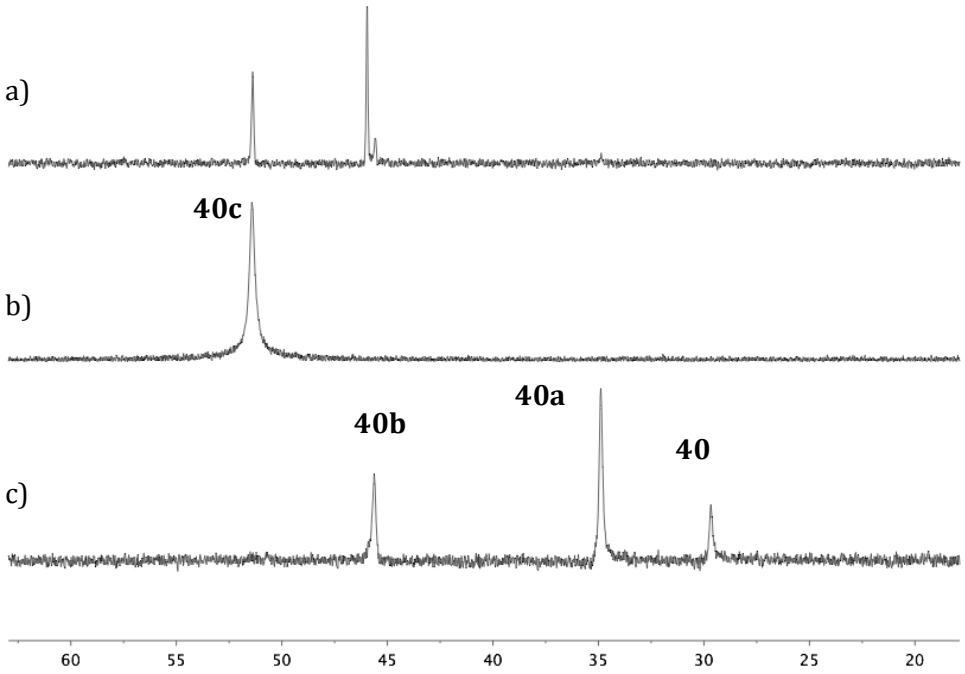

Figure 5. 47. $^{31}P\{^{1}H\}$ NMR (THF-d^8, 162MHz) spectra of the deuteration of $O=PPh_3$ (**40**) using (a) **Ru@PVP**, (b) **Ru$^{0.2}$** and (c) **Rh$^{0.2}$**

Taking into account the results obtained using **40** as substrate, it was concluded that reduction of the aromatic rings in the case of **40** should be due to the coordination of the phosphine oxide **40** to the surface of the Ru NPs through the phenyl rings, thus favouring their reduction (Figure 5. 48).

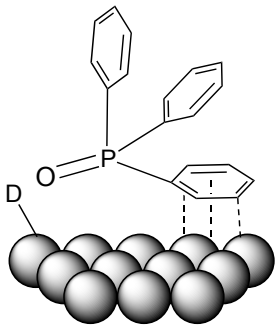

Figure 5. 48. Proposed coordination mode for $O=PPh_3$ (**40**) at the surface of Ru and Rh NPs

The effect of the metal and the presence of NHC ligands at the surface of the Rh and Ru NPs were then evaluated.

When the deuteration of **40** was carried out under the same reaction conditions, using $\mathbf{Ru^{0.2}}$ as catalyst, the reduction of the aromatic rings was also observed. This was evidenced by the detection of similar broad aliphatic deuterium signals by ^{2}D NMR compared to the ones observed using **Ru@PVP**. Besides, only the detection of a signal centred at 51.4 ppm by $^{31}P\{^{1}H\}$ NMR attributed to **40c**, revealed in this case the complete reduction of the starting material **40** (Figure 5. 47b). The fact that higher yields for the reduction of **40** were achieved using $\mathbf{Ru^{0.2}}$ as catalysts could be attributed to the application of these nanocatalysts in higher catalyst loadings compared to **Ru@PVP**, which would result in higher reaction rates for the reduction reaction.

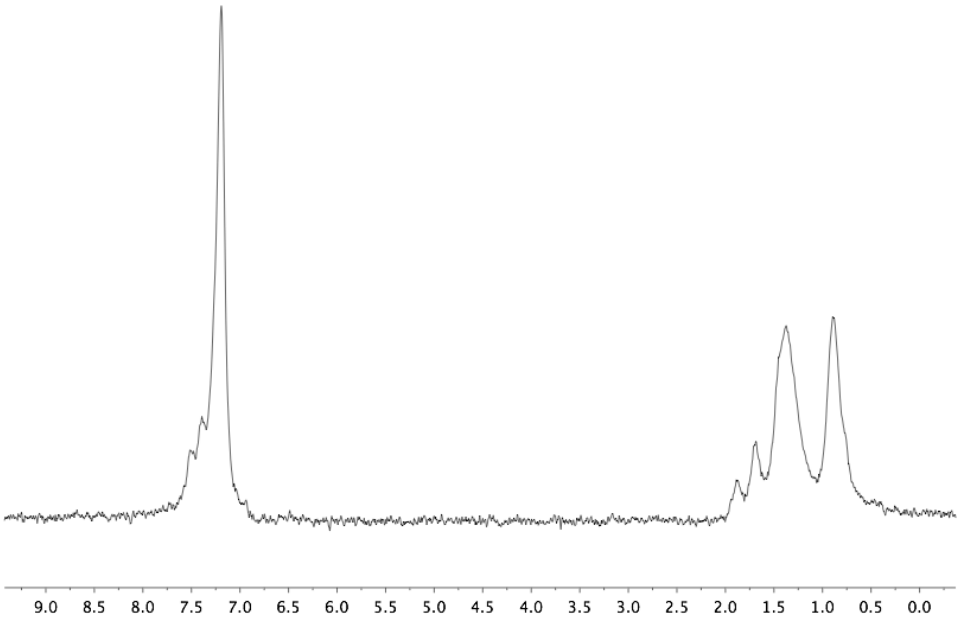

Figure 5. 49. ^{2}D NMR ($CHCl_3$, 61.49MHz) spectra of the deuteration of $O{=}PPh_3$ (**40**) using **Rh$^{0.2}$** after 48h of reaction

Similar results were also obtained when **Rh$^{0.2}$** was used as catalyst, however, the detection of signals from $O{=}PCyPh_2$ (**40a**), **40b** and **40c** suggested even lower reaction rates for the reduction of the aromatic rings of **40** using this Rh nanocatalyst (Figure 5. 47c). Indeed, deuterium exchange at aromatic positions prior to reduction of the aromatic rings for **40** could be observed in this case by the detection of a broad signal at 7.2 ppm by ^{2}D NMR (Figure 5. 49). GC-MS analysis of the reaction mixture obtained using both, **Ru$^{0.2}$** and **Rh$^{0.2}$**, confirmed the formation of these reduction products (Figures S220 and 223, Supporting information).

In summary, the presence of NHC ligands at the NPs surface of Ru and Rh NPs did not have an effect on the coordination mode of $O{=}PPh_3$ (**40**) at the NPs surface, which takes place through π-

interactions of the phenyl rings, leading to the reduction of the aromatic rings of the phosphine oxide **40**.

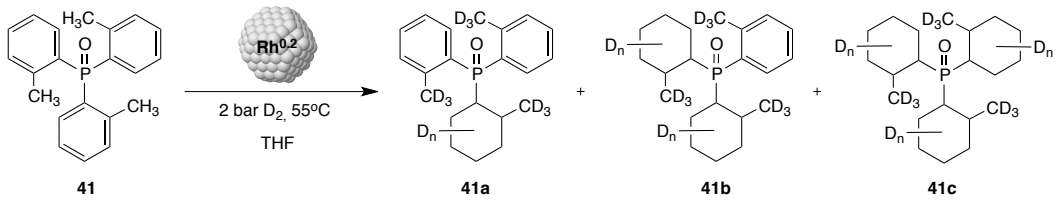

Figure 5. 50. Deuteration of O=P(*o*-tolyl)$_3$ (**41**) using **Rh$^{0.2}$**

The effect of the presence of a methyl group at the *ortho* position of the aromatic ring of O=P(*o*-tolyl)$_3$ (**41**) was then studied. Indeed, since in the case of the corresponding aromatic phosphine **30** a difference in selectivity compared to PPh$_3$ (**28**) was observed using **Rh$^{0.2}$** as catalyst, the H/D exchange of **41** was attempted using this catalytic system (Figure 5. 50). In this case, apart from the appearance of some deuterium signals by ^{2}D NMR between 0.8-2.35 ppm arising from the reduction of the aromatic rings, sharper signals between 2.45 and 2.86 ppm were also detected and suggested deuterium incorporation at –CH$_3$ positions (Figure 5. 51). H/D exchange at aromatic positions prior to the arene reduction was observed by the detection of deuterium signals at 7.2 ppm by ^{2}D NMR (previously observed for the deuteration of **40** using the same catalyst). The detection of several signals by ^{31}P NMR at similar chemical shifts compared to those observed for **40a**, **40b** and **40c**, which appeared at higher frequencies compared to the starting material **41** (37.16 ppm), also confirmed the reduction of the

aromatic rings of the phosphine oxide **41** (Figure 225, Supporting information).

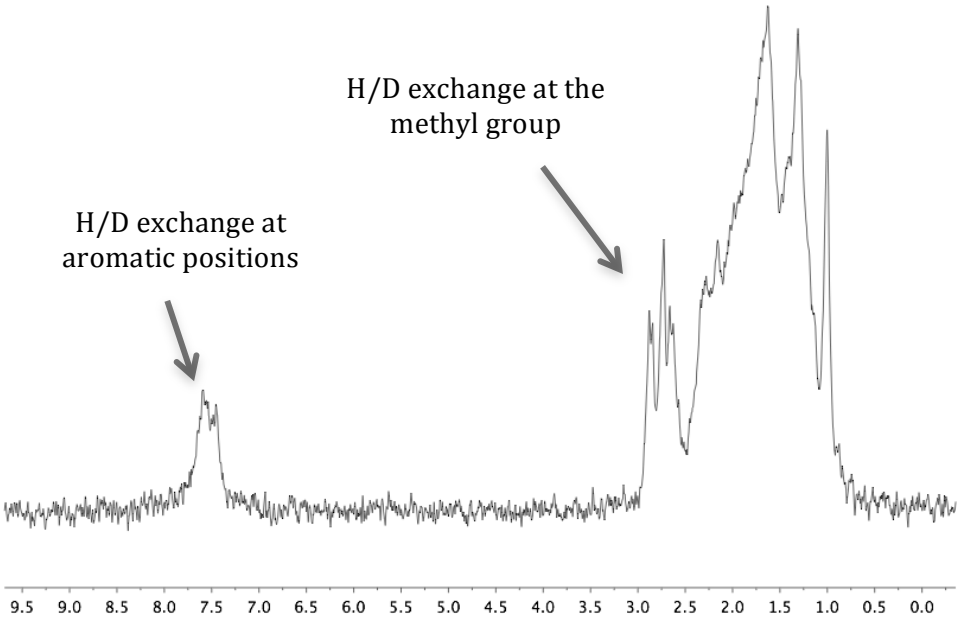

Figure 5. 51. ^{2}D NMR ($CHCl_3$, 61.49MHz) spectrum of the deuteration of O=P(*o*-tolyl)$_3$ (**41**) using **Rh$^{0.2}$** after 48h of reaction

As in the case of **40** the reduction of the aromatic rings was attributed to their coordination at the surface of the corresponding Rh and Ru NPs through π-interactions. On the other hand, the H/D exchange at $-CH_3$ positions of **41** also indicated the interaction between these alkyl moieties and the Rh surface, which would confirm our previous assumption based on the proposed coordination modes for **30** and **31** at the surface of Ru and Rh NPs stabilized by NHC ligands.

5.3. Conclusions

The general conclusions that can be drawn from the results described in this chapter are that the nature of the metal and the properties of the stabilizers at the nanocalyst surface clearly influence the selectivity of the H/D exchange process when P-containing compounds are used as substrates.

The affinity between Ru and phosphorus favours the P-coordination at the Ru NPs surface while in the case of Rh, the weaker M-P coordination lead to the deuteration of alkyl groups more readily.

Furthermore, the distinct selectivities obtained in some cases using nanocatalysts bearing NHC ligands compared to those provided using PVP-stabilized NPs clearly evidenced a modification of the surface properties of these catalysts by these stabilizing agents which could be electronic in nature.

A decrease in the activity for **Ru$^{0.2}$** and **Rh$^{0.2}$** compared to **Ru@PVP** was attributed to the presence of ligand at the surface of the NPs, which could prevent the substrate to coordinate to the metallic surface and thus reducing the H/D exchange reaction rate. Besides, **Ru$^{0.2}$** showed to be generally more active than **Rh$^{0.2}$** for the deuteration of P-containing compounds. **Rh@PVP** showed to b almost inactive due to solubility issues.

Furthermore, the fact that deuteration of the several P-containing molecules could be achieved using **Ru@PVP**, **Ru$^{0.2}$** and **Rh$^{0.2}$** showed the high efficiency of these nanocatalysts to perform C-H activation.

Next, conclusions on the coordination mode of the different P-containing molecules at the surface of the corresponding Ru or Rh NPs (stabilized by PVP or NHCs) will be exposed here depending on the substrate structure:

Aryl phosphines:

*Deuteration of PPh_3 (**28**) and P(p-tolyl)$_3$ (**29**):*

- **Ru@PVP**: *ortho* position of the aromatic ring
- **Ru$^{0.2}$**: *ortho* position of the aromatic ring
- **Rh$^{0.2}$**: *ortho* position of the aromatic ring

Coordination of **28** and **29** to the NPs surface of **Ru@PVP**, **Ru$^{0.2}$** and **Rh$^{0.2}$** through the P atom.

*Deuteration of P(o-tolyl)$_3$ (**30**):*

- **Ru@PVP**: *no deuteration*
- **Ru$^{0.2}$**: *meta* position of the aromatic ring and methyl group
- **Rh$^{0.2}$**: *meta* position of the aromatic ring and methyl group

-Coordination of **30** to the NPs surface of **Ru$^{0.2}$** and **Rh$^{0.2}$** through the $-CH_3$ moiety

-**Rh$^{0.2}$** more active than **Ru$^{0.2}$**

*Deuteration of tris(3,5-dimethylphenyl)phosphine (**31**):*

- **Rh$^{0.2}$**: *aromatic and aliphatic* position

-Coordination of **31** to the NPs surface of **Rh$^{0.2}$** through the $-CH_3$ moiety

Aryl-alkyl phosphines:

*Deuteration of PPh_2Me (**32**):*

- **Ru@PVP**: *ortho* position of the aromatic ring
- **$Ru^{0.2}$**: *ortho* position of the aromatic ring and methyl group
- **$Rh^{0.2}$**: *ortho* position of the aromatic ring and methyl group

-Coordination of **32** to the NPs surface of **Ru@PVP**, **$Ru^{0.2}$** and **$Rh^{0.2}$** through the P atom

*Deuteration of $PPhMe_2$ (**33**) and $PiPr_3$ (**34**):*

- **$Rh^{0.2}$**: *aromatic and aliphatic* position for **33**; *aliphatic* position for **34**

-Coordination of **33** and **34** to the NPs surface of **$Rh^{0.2}$** through the P atom

Bidentate phosphines:

*Deuteration of dppm (**35**):*

- **Ru@PVP**: *no deuteration*
- **$Ru^{0.2}$**: *no deuteration*
- **$Rh^{0.2}$**: *methylenic position*

-Coordination of **35** to the NPs surface of **$Rh^{0.2}$** through the methylenic carbon

*Deuteration of dppe (**36**):*

- **$Rh^{0.2}$**: *aromatic position*

-Coordination of **36** to the NPs surface of **$Rh^{0.2}$** through the P atom

*Deuteration of dppb (**37**):*

- **Ru@PVP**: *ortho* position of the aromatic ring
- **Ru$^{0.2}$**: *ortho* position of the aromatic ring
- **Rh$^{0.2}$**: *ortho* position of the aromatic ring

-Coordination of **37** to the NPs surface of **Ru@PVP**, **Ru$^{0.2}$** and **Rh$^{0.2}$** through the P atom

*Deuteration of PPh_2py (**38**) and $P(furyl)_3$ (**39**):*

- **Ru@PVP**: *no deuteration*
- **Ru$^{0.2}$**: *no deuteration*
- **Rh$^{0.2}$**: *no deuteration*

-Coordination as a chelate to the NPs surface of **Ru@PVP**, **Ru$^{0.2}$** and **Rh$^{0.2}$**.

Phosphine oxides:

*Deuteration of $O=PPh_3$ (**40**):*

- **Ru@PVP**: *reduction of the aromatic rings*
- **Ru$^{0.2}$**: *reduction of the aromatic rings*
- **Rh$^{0.2}$**: *reduction of the aromatic rings*

-Coordination of **40** to the NPs surface of **Ru@PVP**, **Ru$^{0.2}$** and **Rh$^{0.2}$** through π-interaction of the arene rings

*Deuteration of $O=P(o\text{-}tolyl)_3$ (**41**):*

- **Rh$^{0.2}$**: *reduction of the aromatic rings / deuteration at the methyl groups*

-Coordination of **41** to the NPs surface of $\mathbf{Rh^{0.2}}$ through π-interaction of the arene rings and through the $-CH_3$ moiety.

5.4. Experimental part

General procedures

All operations were carried out using standard Schlenk tubes, Fischer-Porter bottle techniques or in a glove-box under argon atmosphere. The chemicals were purchased from Sigma-Aldrich and used without further purification. THF and pentane were dried over sodium/benzophenone, distilled and then thoroughly degassed before use by three freeze- pump cycles.

General procedure for the H/D exchange reactions

A 100 ml Fischer-porter glassware was charged in a dry-box with the desired **Ru@PVP** (3mol%), **Rh@PVP** (25mol%), **$Rh^{0.2}$** (25mol%) or **$Ru^{0.2}$** (25mol%) and a magnetic stirrer. The Fischer-Porter was left under vacuum for 5 minutes and then it was pressurized under 3 bar of D_2 gas during 2 hours. Next a solution of the substrate (0.15 mmol) in degassed THF (2 ml) was added under argon. The reaction was stirred under 2 bar of D_2 under the required temperatures and time. Then the solution was cooled down to room temperature, the solvent was removed, deuterated products were extracted using pentane and evaporated to dryness. In the case of compounds with low boiling points, direct NMR analysis was performed without isolation of the reaction products.

Synthesis of substrates

Synthesis of H_3B-P(*o*-tolyl)$_3$ (**30-BH3**)[37]:

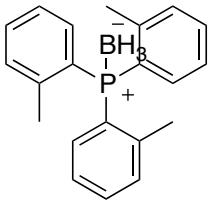

To a solution of P(*o*-tolyl)$_3$ (200mg, 0.657 mmol) in dried THF (2ml) a solution of BH_3·THF (1.65 ml, 1.6425 mmol) was added at -78°C with stirring. The reaction was stirred overnight at room temperature. All volatiles were removed in vacuum and the resulting residue was dissolved in CH_2Cl_2 with subsequent filtration over silica. The product was obtained as a white solid after removing the solvent. (Yield: 173 mg, 83%). **^{1}H-NMR** ($CDCl_3$, 400MHz, δ in ppm): δ = 7.42 (t, 3H, -$CH_{arom,meta3}$-, J= 6.84 Hz), 7.33 (dd, 3H, -$CH_{arom,meta5}$-, J= 7.71 Hz, J= 4.13 Hz), 7.14 (t, 3H, -$CH_{arom,ortho}$-, J= 6.74 Hz), 6.98 (dd, 3H, -$CH_{arom,para}$-, J= 11.3 Hz, J= 8.58 Hz), 2.41 (s, 9H, -CH_3). **^{31}P{^{1}H} NMR** ($CDCl_3$, 162MHz, δ in ppm): δ = 22.69. **^{11}B{^{1}H}-NMR** (C_6D_6, 128MHz, δ in ppm): δ = -31.56 (s).

Synthesis of O=P(*o*-tolyl)$_3$ (**41**)[38]:

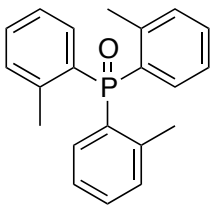

P(*o*-tolyl)$_3$ (200mg, 0.657 mmol) was dissolved in 9 ml of Toluene in an Schlenk flask and the solution was cooled to 0°C. Then, H_2O_2 (0.65ml, 6.57 mmol) were added dropwise with stirring. The reaction was stirred overnight at room temperature. Then, the toluene phase was transferred into a round bottom flask with a metal cannula, the aqueous phase was washed with toluene (3x2 ml) and all organic phases were combined. The resulting solution was stirred for 4h in the presence of molecular sieves. After retrieving the

molecular sieves, the solvent was removed in vacuum to obtain the product as a white crystalline solid. (Yield: 179 mg, 85%). **^{1}H-NMR** ($CDCl_3$, 400MHz, δ in ppm): δ = 7.42 (t, 3H, -$CH_{arom,meta3}$-, J= 7.46 Hz), 7.31 (dd, 3H, -$CH_{arom,meta5}$-, J= 7.01 Hz, J= 4.17 Hz), 7.16 (t, 3H, -$CH_{arom,ortho}$-, J= 6.59 Hz), 7.09 (dd, 3H, -$CH_{arom,para}$-, J= 11.5 Hz, J= 8.72 Hz), 2.49 (s, 9H, -CH_3). **^{31}P{^{1}H} NMR** ($CDCl_3$, 162MHz, δ in ppm): δ = 37.16.

General characterization techniques

Nuclear Magnetic Resonance (NMR):

^{1}H, ^{2}D, ^{13}C, ^{31}P spectra were recorded on a Varian® Mercury VX 400 (400 MHz, 61.49 MHz, 100.6 MHz, 162 MHz respectively). Chemical shift values for ^{1}H and ^{13}C were referred to internal $SiMe_4$ (0.0ppm) and for ^{31}P was referred to H_3PO_4 (85% solution in THF, 0 ppm). Chemical shifts are reported in parts per million (ppm) and coupling constants are reported in Hertz (Hz).

Gas Chromatography – Mass Spectrometry (GC-MS):

The structure of the different deuteration reaction products was determined by GC-FID on an Agilent Technologies 7890A spectrometer, with an achiral HP-5 column (30m x 0.25mm x 0.25μm). The method used consists in an initial isotherm period at 80°C for 2 min followed by a 15°C/min ramp to 280°C and a hold time of 20 min, with a flow of 1.3ml/min.

5.5. References

[1] a) P. B. Arockiam, C. Bruneau, P. H. Dixneuf, *Chem. Rev.* **2012**, *112*, 5879-5918. b) I. A. I. Mkhalid, J. H. Barnard, T. B. Marder, J. M. Murphy, J. F. Hartwig, *Chem. Rev.* **2010**, *110*, 890-931. c) A. E. Shilov, G. B. Shulpin, *Chem. Rev.* **1997**, *97*, 2879-2932. d) S.-Y. Zhang, F.-M. Zhang, Y.-Q. Tu, *Chem. Soc. Rev.* **2011**, 40, 1937-1949. e) G. Song, F. Wang, X. Li, *Chem. Soc. Rev.* **2012**, *41*, 3651-3678. f) K. M. Engle, T.-S. Mei, M. Wasa, J.-Q. Yu, *Acc. Chem. Res.* **2012**, 45, 788-802.

[2] a) R. H. Crabtree, *J. Organomet. Chem.* **2004**, *689*, 4083-4091. b) R. A. Periana, G. Bhalla, W. J. Tenn, K. J. H. Young, X. X. Liu, O. Mironov, Cj. Jones, V. R. Ziatdinov, *J. Mol. Catal. A.* **2004**, *220*, 7-25. c) X. Ribas, R. Xifra, T. Parella, A. Poater, M. Sola, A. Llobet, *Angew. Chem. Int Ed.* **2006**, *45*, 2941-2944.

[3] D. M. Marcus, K. A. McLachlan, M. A. Wildman, J. O. Ehresmann, P. W. Kletnieks, J. F. Haw, *Angew. Chem. Int. Ed.* **2006**, *45*, 3133-3136.

[4] J. Atzrodt, V. Derdau, *J. Labelled Compd. Radiopharm.* **2010**, *53*, 674-685.

[5] J. Atzrodt, V. Dernau, T. Fey, J. Zimmermann, *Angew. Chem. Int. Ed.* **2007**, *46*, 7744-7765.

[6] L. Neubert, D. Michalik, S. Bähn, S. Imm, H. Neumann, J. Atzrodt, V. Derdau, W. Holla, M. Beller, *J. Am. Chem. Soc.* **2012**, *134*, 12239-12244.

[7] B. Gröll, M. Schnürch, M. D. Mihovilovic, *J. Org. Chem.* **2012**, *77*, 4432-4437.

[8] V. Derdau, J. Atzrodt, J. Zimmermann, C. Kroll, F. Brückner, *Chem. Eur. J.* **2009**, *15*, 10397-10404.

[9] D. Pla, M. Gómez, *ACS Catal.* **2016**, 3537-3552.

[10] J. A. Sullivan, K. A. Flanagan, H. Hain, *Catal. Today* **2008**, *139*, 154-160.

[11] K. A. Flanagan, J. A. Sullivan, H. Müeller-Bunz, *Langmuir* **2007**, *23*, 12508-12520.

[12] K. A. Guy, J. R. Shapley, *Organometallics* **2009**, *28*, 4020-4027.

[13] K. Philippot, B. Chaudret, *C. R. Chemie* **2003**, *6*, 1019-1034.

[14] T. Pery, K. Pelzer, G. Buntkowsky, K. Philippot, H.-H. Limbach, B. Chaudret, *ChemPhysChem*, **2005**, *6*, 605-607.

[15] J. García-Antón, M. Rosa Axet, S. Jansat, K. Philippot, B. Chaudret, T. Pery, G. Buntkowsky,H-H. Limbach, *Angew. Chem.* **2008**, *120*, 2104-2108.

[16] F. Novio, K. Philippot, B. Chaudret, *Catal. Lett.* **2010**, *140*, 1-7.

[17] I. Favier, S. Massou, E. Teuma, K. Philippot, B. Chaudret, M. Gómez, *Chem. Commun.* **2008**, 3296-3298.

[18] E. Rafter, T. Gutmann, F. Löw, G. Buntkowsky, K. Philippot, B. Chaudret, P. W. N. M. van Leeuwen, *Catal. Sci. Technol.* **2013**, *3*, 595-599.

[19] T. Gutmann, I. del Rosal, B. Chaudret, R. Poteau, H.-H. Limbach, G. Buntkowsky, *ChemPhysChem* **2013**, *14*, 3026-3033.

[20] G. Pieters, . Taglang, E. Bonnefille, T. Gutmann, C. Puente, J.-C. Berthet, C. Dugave, B. Chaudret, B. Rousseau, *Angew. Chem. Int. Ed.* **2014**, *53*, 230-234.

[21] P. Lara, K. Philippot, B. Chaudret, *ChemCatChem* **2013**, 5, 28-45.

[22] C. Taglang, L. M. Martínez-Prieto, I. del Rosal, L. Maron, R. Poteau, K. Philippot, B. Chaudret, S. Perato, A. S. Lone, C. Puente, C. Dugave, B. Rousseau, G. Pieters, *Angew. Chem. Int. Ed.* **2015**, *54*, 10474-10477.

[23] L. M Martínez-Prieto, E. A. Baquero, G. Pieters, J. C. Flores, E. de Jesús, C. Nayral, F. Delpech, P. W. N. M. van Leeuwen, G. Lippens, B. Chaudret, *Chem. Commun.*, 2017, *53*, 5850-5853.

[24] J. Llop, A. Gual, E. Mercadé, C. Claver, C. Godard, *Catal. Sci. Technol.* **2013**, *3*, 2828-2833.

[25] J. Ll. Castelbou, P. Blondeau, C. Claver, C. Godard, *RSC Adv.* **2015**, *5*, 97036-97043.

[26] J. Ll. Castelbou, E. Bresó-Femenia, P. Blondeau, B. Chaudret, S. Castillón, C. Claver, C. Godard, *ChemCatChem* **2014**, *6*, 3160-3168.

[27] A. Gual, C. Godard, K. Philippot, B. Chaudret, A. Denicourt-Nowicki, A. Roucoux, S. Castillón, C. Claver, *ChemSusChem* **2009**, *2*, 769-779.

[28] M. R. Axet, S. Castillón, C. Claver, K. Philippot, P. Lecante, B. Chaudret, *Eur. J. Inorg. Chem.* **2008**, *22*, 3460-3466.

[29] E. Bresó-Femenia, C. Godard, C. Claver, B. Chaudret, S. Castillón, *Chem. Commun.* **2015**, *51*, 16342-16345.

[30] P. Lara, O. Rivada-Wheelaghan, S. Conejero, R. Poteau, K. Philippot, B. Chaudret, *Angew. Chem. Int. Ed.* **2011**, *50*, 12080-12084.

[31] M. Ibrahim, R. Poreddy, K. Philippot, A. Riisager, E. J. Garcia-Suarez, *Dalton Trans.* **2016**, *45*, 19368-19373.

[32] G. Pieters, C. Taglang, E. Bonnefille, T. Gutmann, C. Puente, J.-C. Berthet, C. Dugave, B. Chaudret, B. Rousseau, *Angew. Chem. Int. Ed.* **2014**, *53*, 230-234.

[33] D. Gonzalez-Galvez, P. Lara, O. Rivada-Wheelaghan, S. Conejero, B. Chaudret, K. Philippot, P. W. N. M. van Leeuwen *Catal. Sci. Technol.* **2013**, *3*, 99-105

[34] C. A. Tolman, *Chem. Rev.* **1977**, *77*, 313–348.

[35] S. C. Schou, *J. Label. Compd. Radiopharm* **2009**, *52*, 376-381.

[36] P. Kumar, A. K. Singh, M. Yadav, P.-Z. Li, S. K. Singh, Q. Xu, D. S. Pandey, *Inorg. Chim. Acta* **2011**, *368*, 124-131.

[37] F. Dornhaus, M. Bolte, H.-W. Lerner, M. Wagner, *Eur. J. Inorg. Chem.* **2006**, 1777-1785.

[38] C. R. Hilliard, N. Bhuvanesh, J. A. Gladysz, J. Blümel, *Dalton Trans.* **2012**, *41*, 1742-1754.

Chapter 6

General conclusions

6. 1. General conclusions

From the study on the synthesis and characterization of Rh NPs stabilized by IPr performed in **Chapter 3**, the following conclusions have been extracted:

-This synthetic method allows the formation of well disperse, spherical and non-oxidized Rh NPs with fcc packing structure, with mean diameters between 1.26 - 1.68 nm.

-TEM analysis of freshly synthesised Rh NPs showed a decrease in the mean diameter of the NPs at higher [IPr]/[Rh] molar ratios.

- An increase in the [IPr]/[Rh] molar ratio from 0.2 to 0.4 showed an increase in the amount of ligand present at the surface of the NPs from 21.5 to 37 wt%; with decrease in the hydride/Rh_s molar ratio from 0.58 to 0.39.

-The presence of stabilizing ligand at the Rh NPs surface was evidenced by IR and solution/solid-state NMR spectroscopy.

-High CO pressure experiments in solution-state showed:

1) The decoordination of strongly coordinated protonated species from the Rh surface of the NPs.

2) The strong binding of the NHC ligand IPr at the surface of the NPs by the formation of Rh-NHC species.

-CO adsorption-IR spectroscopy showed the availability of faces, edges and apexes for **$Rh^{0.2}$**, **$Rh^{0.4}$** and **$Rh^{0.6}$**, being the edges and apexes less available at high [IPr]/[Rh] molar ratios of 0.4 and 0.6.

-The presence of a carbene and protonated imidazolium species at the surface of the Rh NPs was detected by solution-state NMR spectroscopy.

-CO adsorption-CP MAS NMR spectroscopy showed the availability of faces, edges and apexes for **Rh$^{0.2}$**, **Rh$^{0.4}$** and **Rh$^{0.6}$**, having more stabilizing ligand located the edges and apexes of the Rh NPs at high [IPr]/[Rh] molar ratios of 0.4 and 0.6.

-The fact that static CO species were detected at the faces of the NPs, suggested coordination of the protonated imidazolium species at these sites of the Rh NPs.

The formed Rh NPs has been applied in the selective hydrogenation of different substrates bearing aromatic moieties (**Chapter 4**). From this study, the following conclusions have been extracted:

Selective hydrogenation of aromatic ketones:

-Lower activities were in general obtained for the reduction of aromatic ketones using **Rh$^{0.4}$** and **Rh$^{0.6}$** compared to **Rh$^{0.2}$** due to the presence of excess of ligand in the surface of the Rh NPs.

-The lack of reduction of alkyl ketones as such as **1a**, **2a** and **3a** indicate interaction between the corresponding aromatic ketones and the Rh NPs surface through the arene ring. This fact was confirmed by an increase in the selectivity up to 91% towards the formation of **3a** when **3** was used as substrate.

-The presence of bulky groups close to the ketone group, substrates **4** and **5** decreased the selectivity towards the arene ring reduction

(products **4a** and **5a**) due to an effect on the coordination of the aromatic ring to the surface of the NPs in a flat way, necessary for its reduction.

-In general, the presence of electron-donating substituents in the *ortho* position of the aromatic ring (**6** and **7**) produced a decrease in the activity of the reaction, achieving moderate lower selectivities towards the reduction of the aromatic ring.

-The presence of both, electron-donating or electron-withdrawing substituents in the *para* position of the aromatic ring (**8** and **9**) produced a strong decrease in the selectivity towards the reduction of the aromatic ring.

Hydrogenation of phenol derivatives:

- Selectivities up to 79% for the formation of cyclohexanone (**11a**) or 100% towards cyclohexanol (**11b**) could be achieved using $\mathbf{Rh^{0.2}}$ depending on the reaction conditions.

-The effect of the presence of high amounts of ligand at the NPs surface showed to have a detrimental effect on the activity and selectivity towards the formation of **11a**.

-The application of $\mathbf{Ru^{0.2}}$ for the reduction of **11** gave rise to lower activities and selectivities towards the formation of **11a**.

-The presence of $-CH_3$ groups in the *ortho* (**12** and **14**) and *para* (**13**) position of the aromatic ring decreased the reduction reaction rate due to an effect on the coordination of the aromatic ring to the surface of the NPs in a flat way, necessary for its reduction.

-The possible coordination of **15** and **16** in a chelating mode to the NPs surface produced an increase on the selectivity of the reaction towards the formation of cyclohexane-1,2-diol (**15b**) and 2-methoxycyclohexanol (**16b**).

-An increase in the electronic density of the aromatic ring for the reduction of nitrobenzene (**17**) along with the strong coordination of the aniline product (**17b**) gave rise to full selectivity towards the reduction of the nitro group.

Hydrogenation of N-heterocyclic compounds:

-**Rh$^{0.2}$** and **Rh$^{0.4}$** were able to reduce pyridine rings (**18**) with high efficiency at 30°C under 20 bar of H_2.

- The effect of the presence of high amounts of ligand at the NPs surface showed to have a detrimental effect on the activity and selectivity towards the reduction of pyridine rings (**19** and **21**).

-The presence of $-CH_3$ groups in the *ortho* position of the pyridine ring (**19** and **20**) decreased the reaction rate due to an increase in the steric hindrance close to the N atom, which coordinates to the NPs surface before reduction of the aromatic ring.

-The presence of $-CH_3$ and $-CF_3$ groups in the *para* position of the pyridine ring (**21** and **22**) also decreased the hydrogenation reaction rate, which suggests an effect of tis groups on the coordination of the aromatic ring to the surface of the NPs in a flat way, necessary for its reduction.

-Pyridine derivatives bearing ketone group in the *ortho* position of the aromatic ring (**23** and **24**) were hydrogenated much faster than

pyridine (**18**), to form the totally reduced compound as the only reaction product (**23d**) in the case of **23**; and the β-enaminone (**24a**) as the major reaction product in the case of **24** in 78% selectivity under 5 bar of H_2.

-The formation of piperidine (**18a**) was observed to poison the NPs surface by hydrogenation experiments using 1:1 pyridine (**18**):benzene (**25**) mixtures.

-The presence of a phenyl ring in the *ortho* position of the aromatic ring have an effect on the hydrogenation reaction rate due to an increase in the steric hindrance close to the N atom.

-For the reduction of **26** and **27**: Moderate to high selectivities towards the reduction of the pyridine ring for the formation of compounds **26a** and **27a** up to 65 and 89% could be obtained respectively when performing the reaction at 30°C under 20 bar of H_2.

-The totally reduction products (**26c** and **27c**) for the hydrogenation of **26** and **27** could be obtained as the only reaction product at 60°C under 20 bar of H_2 after 48 and 24h of reaction, respectively.

From the study regarding the application of Ru and Rh NPs in the selective deuteration of P-containing ligands carried out in **Chapter 5**, the following conclusions have been extracted:

-Deuteration of the several P-containing molecules using **Ru@PVP**, $\mathbf{Ru^{0.2}}$ and $\mathbf{Rh^{0.2}}$ showed the high efficiency of these nanocatalysts to perform C-H activation.

-A decrease in the activity for **Ru$^{0.2}$** and **Rh$^{0.2}$** compared to **Ru@PVP** was attributed to the presence of ligand at the surface of the NPs, which could prevent the substrate to coordinate to the metallic surface and thus reduce the H/D exchange reaction rate.

-The coordination mode of various P-based ligands at the surface of the corresponding Ru or Rh NPs (stabilized by PVP or NHCs) was proposed based on the selective H/D exchange at different positions:

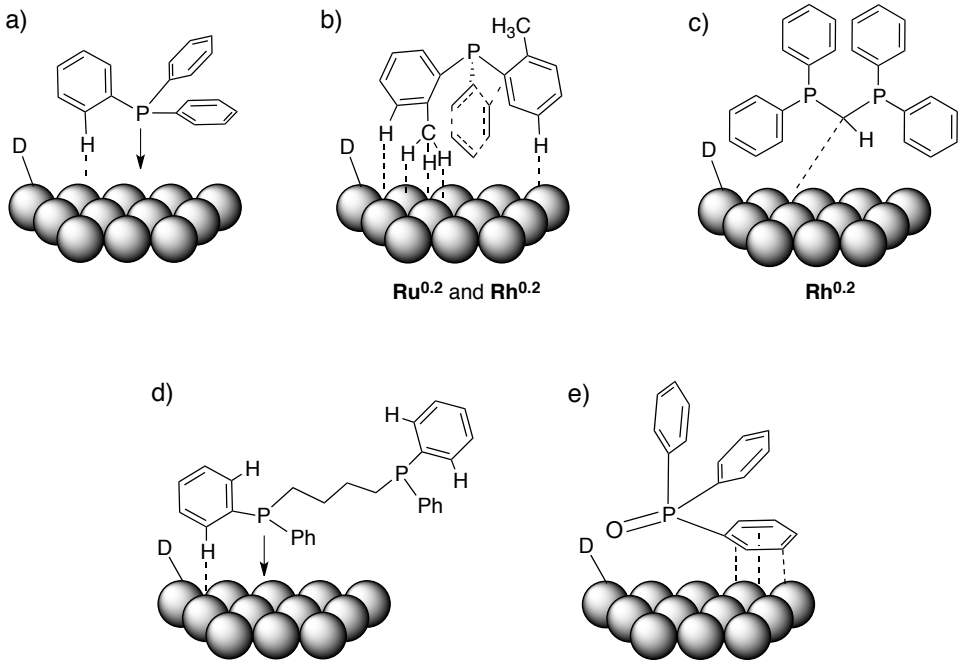

Figure 6. 1. Proposed coordination modes of P-based ligands at the NPs surface of Ru and Rh NPs

- Aromatic phosphines **28**, **29** and **32** coordinate to the NPs surface of **Ru@PVP**, **Ru$^{0.2}$** and **Rh$^{0.2}$** through the P atom. (Figure 6. 1a).
- P(*o*-tolyl)$_3$ (**30**) coordinates to the NPs surface of **Ru$^{0.2}$** and **Rh$^{0.2}$** through the –CH$_3$ group (Figure 6. 1b).

- Diphosphine dppm (**35**) coordinates to the NPs surface of **Rh$^{0.2}$** through the methylenic carbon (Figure 6. 1c).
- Diphosphine dppb (**37**) coordinate to the NPs surface of **Ru@PVP**, **Ru$^{0.2}$** and **Rh$^{0.2}$** through the P atom (Figure 6. 1d).
- Phosphine oxides coordinate to the NPs surface of **Ru@PVP**, **Ru$^{0.2}$** and **Rh$^{0.2}$** through the arene ring (Figure 6. 1e).

Chapter 7

Appendices

7.1. Congresses and scientific meetings

2014

-VI Journées Franco-Catalanes de Chimie Moléculaire, Laboratoire Trans-Pyrénéen: de la Molécule aux Matériaux, 27-28th January 2104, Toulouse, France.

Attendance

-GEQO XXXII meeting (Grupo Especializado de Química Organometálica), September 17th-19th 2014, Tarragona, Spain
Poster contribution: "Synthesis and characterization of Rh nanoparticles stabilized by NHC ligands and their application in selective hydrogenation reactions."

2015

-GEQO XXXIII meeting (Grupo Especializado de Química Organometálica), May 14th 2015, Madrid, Spain
Attendance

-18th IUPAC International symposium, OMCOS 18 (Organometallic Chemistry directed towards Organic Synthesis), June 28th-July 2nd 2015, Sitges, Spain

Poster contribution: "Synthesis and surface study of Rh nanoparticles stabilized by NHC ligands and their application in selective catalysis."

2016

-VII Journées Franco-Catalanes "Hetero-elements and Coordination Chemistry: from Concepts to Applications" 1st HA3C meeting, 26th-27th January 2016, Toulouse, France

Oral communication: "NHC-stabilized Rh nanoparticles: Synthesis, characterization and application in H/D exchange processes using P-donor ligands as substrates."

-GEQO XXXIV congress, (Grupo Especializado de Química Organometálica), 7th-9th September 2016, Girona, Spain

Poster contribution: "NHC-stabilized Rh nanoparticles: Surface study and effect on the H/D exchange reaction of phosphorus and oxygen containing compounds."

7.2. Stages

-June-March 2015: stage in Laboratoire de Physique et Chimie des Nano-Objects (LPCNO) in Institut National des Sciences Appliqués (INSA), Toulouse, France.

-April 2016: short stage in Laboratoire de Physique et Chimie des Nano-Objects (LPCNO) in Institut National des Sciences Appliqués (INSA), Toulouse, France.

7.3. Publications based on the content of the thesis

-"NHC-stabilized Rh nanoparticles: Surface study and application in the catalytic hydrogenation of aromatic substrates" – Submitted to Journal of Catalysis (15/03/2017). Status: Under review.

-"Selective Catalytic Deuteration of Phosphorus Ligands using Ruthenium and Rhodium Nanoparticles: A comparative study" – Status: Under preparation